GEORGE C. MARSHALL SPACE FLIGHT CENTER
HUNTSVILLE, ALABAMA

(NASA-TM-X-57140) PROCEEDINGS OF THE CONFERENCE ON PROPELLANT TANK PRESSURIZATION AND STRATIFICATION, VOLUME 2 (NASA)

N75-71719
THRU
N75-71730
Unclas
00/98 07320

PROCEEDINGS OF THE CONFERENCE ON PROPELLANT TANK PRESSURIZATION AND STRATIFICATION

January 20, 21, 1965

VOLUME II
of
TWO VOLUMES

National Aeronautics and Space Administration

NASA

REPRODUCED BY
NATIONAL TECHNICAL
INFORMATION SERVICE
U.S. DEPARTMENT OF COMMERCE
SPRINGFIELD, VA. 22161

FC - Form 454 (Revised September 1961)

GEORGE C. MARSHALL SPACE FLIGHT CENTER

PROCEEDINGS OF THE CONFERENCE ON PROPELLANT TANK PRESSURIZATION AND STRATIFICATION

January 20, 21, 1965

Volume II
of
Two Volumes

PROPULSION DIVISION
PROPULSION AND VEHICLE ENGINEERING LABORATORY

TABLE OF CONTENTS
FOR VOLUME II

SESSION III

	Page
A Theoretical Model for Predicting Thermal Stratification and Self Pressurization of a Fluid Container R. W. ARNETT and D. R. MILLHISER Institute for Material Research, National Bureau of Standards	1
Investigation of Stratification Reduction Techniques B. D. NEFF Martin Company	21
Stratification Reduction by Means of Bubble Pumps D. C. PEDREYRA Martin Company	43
Experimental Investigation of the Effects of Baffles on Natural Convection Flow and on Stratification G. C. ULIET and J. J. BROGAN Lockheed Missiles and Space Company	61
Transient Laminar Free Convection Heat and Mass Transfer in Two-Dimensional Closed Containers Containing Distributed Heat Source HUSSEIN Z. BARAKAT University of Michigan	87
Transient, Laminar, Free-Convection Heat and Mass Transfer in Closed, Partially Filled, Liquid Containers DR. JOHN A. CLARK and HUSSEIN Z. BARAKAT University of Michigan	119

SESSION IV

A Hypothesis for Helium Adsorption/Desorption in Slush Hydrogen CLARENCE A. SCHALLA Lockheed Missiles and Space Company	191
Selecting Liquid Level Transducers for Cryogenic Service D. A. BURGESON National Bureau of Standards	205

Preceding page blank

TABLE OF CONTENTS (CONCLUDED)

Page

Analytical and Experimental Study of Stratification in Standard and Reduced Gravity Fields
E. Y. HARPER, S. E. HURD, A. M. LEVY and D. M. TELLEP
Lockheed Missiles and Space Company 207

Orbital Tests to Investigate Thermal Behavior of Cryogens Under Weightlessness
J. C. ELIZALDE
TRW Space Technology Labs 245

Static and Dynamic Behavior of the Liquid-Vapor Interface During Weightlessness
E. W. OTTO
NASA/Lewis Research Center 281

Zero Gravity Liquid Propellant Control by Dielectrophoresis
J. B. BLACKMON
Douglas Aircraft Company 355

TABLE OF CONTENTS
FOR VOLUME I

	Page
FOREWORD	1
CHAIRMEN AND COMMITTEES	2
SESSION I	
Analytical Investigation of Some Important Parameters in the Pressurized Liquid Hydrogen Tank Outflow Problem WILLIAM A. ROUDEBUSH and DAVID A. MANDELL NASA/Lewis Research Center	3
Experimental and Analytical Studies of Cryogenic Propellant Tank Pressurization M. E. NEIN, NASA/George C. Marshall Space Flight Center J. F. THOMPSON, JR., Mississippi State University	29
Fast Response Thermocouple for the Measurement of Temperatures in Cryogenic Gases C. C. ROBINSON, A. R. LOWRIE, and T. BIELAWSKI Beech Aircraft Corporation	55
Propellant Tank Pressurization by Internal Combustion PAUL A. FRIEDMAN and RICHARD J. KENNY Martin Company	69
A Cryogenic Helium Pressurization System for the Lunar Excursion Module J. C. SMITHSON and W. R. SCOTT NASA/Manned Spacecraft Center	109
Bulk Liquid Interfacial Mass Transfer with Variable Ullage Pressure; Dimensionless Mass Transfer Alignment Chart for Suddenly Pressurized Liquid-Vapor Systems JOHN R. O'LOUGHLIN, Consultant to The Boeing Company, Associate Professor of Mechanical Engineering, Tulane University	125
SESSION II	
Thermal Analysis and Description of Liquid Hydrogen Tank Fluid Line Fittings JOSEPH M. FOWLER The Boeing Company	157

TABLE OF CONTENTS

	Page
Thermal Design of Cryogenic Heat Exchangers for Space Vehicle Pressurization Systems J. H. HARGIS, Brown Engineering Company, Inc. H. A. STOKES, Chrysler Corporation.....	189
Weight Optimization of a Gas Generator/Heat Exchanger Subsystem During the Initial Design of a Pressurization System: Two Computer Programs DR. W. A. MUTH, Martin Company.....	215
Digital Computer Analysis of Pneumatic Pressure Regulator Dynamics JAMES G. ABSALOM, Rocketdyne Division North American Aviation, Inc.....	245
Servomechanism Approach to Facility Tank Pressurization SANFORD M. GOLDSTEIN and KURT J. SCHURMAN Rocketdyne Division, North American Aviation, Inc.....	297
Cryogenic Storage of Helium for Propellant Tank Pressurization J. S. TYLER, AiResearch Manufacturing Company.....	327

X64-13023

A THEORETICAL MODEL FOR PREDICTING THERMAL STRATIFICATION AND SELF PRESSURIZATION OF A FLUID CONTAINER

by

R. W. Arnett and D. R. Millhiser

Institute for Material Research
National Bureau of Standards
Boulder, Colorado

ABSTRACT

13023

Thermal stratification and self-pressurization of cryogenic propellant tanks are of concern to many people in the astro-space and missile industries. A procedure, based upon the Von Karman integral method, is presented for analytically determining both the liquid thermal stratification and the extent of the associated self-pressurization. Both conical and cylindrical geometrys are treated.

Author

*A THEORETICAL MODEL FOR PREDICTING THERMAL STRATIFICATION AND SELF PRESSURIZATION OF A FLUID CONTAINER

Methods for analyzing thermal stratification of cryogenic propellants have been studied by several investigators in recent years [Robbins and Rogers, 1964], [Schmidt, et al, 1961], [Schwind and Vliet, 1964], [Scott, et al, 1960], [Tatom, et al, 1964], [Tellep and Harper, 1963]. Most of these analyses have been aimed primarily at the temperature distribution within and the volume occupied by the thermally stratified layer. Some have touched on the effect of this thermal stratification on the ullage pressure [Tellep and Harper, 1963], but no intensive attack has been reported on this phase of the problem.

As a part of consultation work on the Centaur project for NASA-Lewis Research Center, the Cryogenics Division of National Bureau of Standards has undertaken an analysis which could be used with a geometry approximating that of the Centaur liquid hydrogen tank. The expressions obtained as a result of this analysis can be applied to other geometries with only slight modification of procedure. Numerical solutions of the equations involve numerical integration and/or iteration. These computations are most efficiently performed by a digital computer.

The configuration used to approximate the Centaur shape is shown in Figure 1. Since the approximate shape included a conical nose which contained liquid under some operating conditions, the basic analysis was conducted using this shape. Reduction of the resulting equation to reflect a purely cylindrical shape is readily accomplished. The approach used is based upon the classical approximate integral analysis developed by Von Karman [1946] as modified by Eckert and Jackson [1951]. Development of the equations was based upon the more detailed model shown in Figure 2.

* This work supported by NASA-Lewis Research Center, Cleveland, Ohio.

A free convection turbulent boundary layer was assumed with temperature and velocity variations through the layer patterned after Eckert and Jackson [1951], i. e.,

$$\theta = \theta_w\left[1-\left(\frac{y}{\delta}\right)^{\frac{1}{7}}\right]$$

and

$$u = U\left(\frac{y}{\delta}\right)^{\frac{1}{7}}\left(1-\frac{y}{\delta}\right)^{4}.$$

The approach used was to equate the vertical component of the change in momentum flow through the element to the vertical forces acting on the element. An identity in x results from this procedure consisting of:

$$\left[2\pi \cos^2\gamma \frac{\partial}{\partial x}\int_0^\delta \rho u^2 (R-y)\,dy\right]dx$$
$$\equiv 2\pi g\beta\int_0^\delta \rho\theta\,(R-y)\,dy\,dx - 2\pi R\,\tau_w\,dx\,. \qquad (1)$$

Substitution for the wall shear stress is made by means of the Blasius correlation [Eckert and Drake, 1959, p. 143].

$$\tau_w = 0.0228\,\rho U^2\left(\frac{\nu}{U\delta\cos\gamma}\right)^{\frac{1}{4}}. \qquad (2)$$

Temperature differences experienced between the wall and the bulk fluid are small for the cases considered here, therefore $\rho/\rho_B \cong 1$, if the application of this assumption to arithmetical differences is avoided. The arithmetic difference has been taken care of by the introduction of the volumetric coefficient of expansion, β.

Evaluation of the integrals in (1) and substitution for τ_W gives

$$\cos^2\gamma \frac{\partial}{\partial x}\left[0.05232\, R U^2 \delta \left(1 - \frac{\delta}{8R}\right)\right] \equiv \tfrac{1}{8} g\beta R \theta_W \delta \left(1 - \frac{4\delta}{15R}\right) - 0.0228\, R U^2 \left(\frac{\nu}{U\delta\cos\gamma}\right)^{\frac{1}{4}}. \tag{1a}$$

For the application intended here, a moderately well insulated tank is assumed, and it is found that the dominating thermal resistance is formed by the insulation so that the heat flux to the tank is essentially constant. The assumption of constant heat flux and the combination of the Blasius correlation with the Reynolds analogy [Eckert and Drake, 1959, p. 203] together with a Prandtl number correction due to Colburn [Jakob, 1949, Eckert and Drake, 1959, p. 324] results in

$$\cos^2\gamma \frac{\partial}{\partial x}\left[0.05232\, R U^2 \delta \left(1 - \frac{\delta}{8R}\right)\right] \equiv \frac{g\beta g_W A^{\frac{2}{3}} \delta R}{0.1824 c\, \rho_B U}\left(\frac{U\delta\cos\gamma}{\nu}\right)^{\frac{1}{4}}\left(1 - \frac{4\delta}{15R}\right) - 0.0228\, R U^2 \left(\frac{\nu}{U\delta\cos\gamma}\right)^{\frac{1}{4}}. \tag{1b}$$

It is now assumed that the equivalent velocity and the boundary layer thickness are of exponential form as given by

$$U = C_1 x^m$$

and

$$\delta = C_2 x^n.$$

When this substitution is made and the differentiation performed, the identity

$$0.05232\, C_1^2 C_2 (2m+n) R x^{2m+n-1}\left[1+\frac{1}{2m+n}\frac{x}{R}\frac{\partial R}{\partial x}-\frac{C_2(2m+2n)}{8(2m+n)}\frac{x^n}{R}\right]\cos^2\gamma$$

$$=\frac{g\beta q_w}{0.1824\, c\,\rho_B \nu^{\frac{1}{4}}} C_2^{\frac{5}{4}} C_1^{-\frac{3}{4}} x^{\frac{5n-3m}{4}} R\cos^{\frac{1}{2}}\gamma\left(1-C_2\frac{4}{15}\frac{x^n}{R}\right)$$

$$-0.0228\frac{\nu^{\frac{1}{4}}}{\cos^{\frac{1}{4}}\gamma} C_1^{\frac{7}{4}} C_2^{-\frac{1}{4}} R x^{\frac{7m-n}{4}} \qquad (1c)$$

is obtained.

Comparison of this expression with that of previous investigators [Morse, 1962] who used a semi-infinite vertical flat plate model reveals that the terms involving the ratio x^n/R result from the circular shape configuration while the term incorporating $\partial R/\partial x$ enters because of the conical shape.

Since this expression is an identity with x as the variable, there must be equality of the exponents of x. When these equalities are written for either a vertical flat plate or cylindrical configuration, the values for m and n are obtainable and consistent with values of 3/7 and 5/7 respectively. When the term resulting from the conical shape is included, the answer is undefined. As a result, the expressions developed in this paper do not fully reflect the effect of the conical shape.

To obtain a value for the constants C_1 and C_2, a second equation is developed based upon a thermal energy balance. Change in thermal energy through the fluid element is equated to thermal energy input with the following identity resulting:

$$\left[2\pi c\,\rho_B \cos r \frac{\partial}{\partial x}\int_0^{\delta} \theta u (R-y)\,dy\right]dx$$

$$\equiv 2\pi R q_w \frac{dx}{\cos r} \,. \tag{3}$$

Upon evaluating the integral, substituting for θ_w , U and δ , and performing the differentiation, this becomes

$$\frac{1.6066\, C_1^{\frac{1}{7}} C_2^{\frac{5}{7}} Pr^{\frac{2}{3}} \cos^{\frac{9}{7}} r}{\nu^{\frac{1}{7}}} x^{\frac{m+5n}{4}} \left\{\left[\frac{1}{R}\frac{\partial R}{\partial x} - 0.1307\, C_2 n \frac{x^{n-1}}{R}\right]\right.$$

$$\left. + \left(\frac{m+5n}{4}\right)\left(\frac{1}{x}\right)\left[1 - 0.1307\, C_2 \frac{x^n}{R}\right]\right\} \equiv 1 \,. \tag{3a}$$

Again, a check of the exponents reveals consistency except in the case of a conical shape.

Inserting values for m and n and solving (1c) and (3a) simultaneously for C_1 and C_2 yields the following expressions:

$$C_1 = \frac{[K_1 K_2]^{\frac{5}{14}}}{K_7 K_6^{\frac{1}{14}}}\left[\frac{K_4}{K_3} + Pr^{\frac{2}{3}}\frac{K_6}{K_5}\right]^{-\frac{5}{14}}\left[\frac{g\beta q_w}{c\,\rho_B}\right]^{\frac{5}{14}}\left[\frac{Pr^{\frac{4}{21}}}{\nu^{\frac{1}{14}}\cos^{\frac{11}{14}} r}\right] \tag{4a}$$

and

$$C_2 = \left[\frac{1}{K_1 K_2 K_6^{11}}\right]^{\frac{1}{14}}\left[\frac{c\,\rho_B \nu^3}{g\beta q_w Pr^8 \cos^{23} r}\right]^{\frac{1}{14}}\left[\frac{K_4}{K_3} + Pr^{\frac{2}{3}}\frac{K_6}{K_5}\right]^{\frac{1}{14}} , \tag{4b}$$

where

$$K_1 = 22.735$$
$$K_2 = 1 - 0.2667\, C_2 \frac{x^n}{R}$$
$$K_3 = 539.86$$
$$K_4 = 1 + \frac{x}{R}\frac{\partial R}{\partial x} - 0.1818\, C_2 \frac{x^n}{R}$$
$$K_5 = 1211.7$$
$$K_6 = 1 + \frac{x}{R}\frac{\partial R}{\partial x} - 0.2239\, C_2 \frac{x^n}{R}$$
$$K_7 = 6.6624 \quad .$$

An iteration procedure will permit determination of C_2 , although a good first approximation can be obtained by assuming a vertical flat plate geometry, thus making K_2, K_4 and K_6 equal to 1.

Either of the above methods may be used to determine the constants, thus providing a description of the boundary layer growth.

Using the developed expressions for the boundary layer, a growth rate for the thermally stratified layer is now determined as

$$\frac{\partial \Delta}{\partial t} = \frac{1}{A_\Delta - A_{\delta\Delta}} \left(\frac{\partial V}{\partial t}\right)_\Delta \quad . \tag{5}$$

Evaluating A_Δ, $A_{\delta\Delta}$ and $(\partial V/\partial t)_\Delta$ gives an expression for growth rate as

$$\frac{\partial \Delta}{\partial t} = \frac{0.2928\, U_\Delta \delta_\Delta \cos\gamma}{R_\Delta - \delta_\Delta\left(2 - \frac{\delta_\Delta}{R_\Delta}\right)}\left[1 - 0.1860\, \frac{\delta_\Delta}{R_\Delta}\right] . \tag{5a}$$

A numerical integration may now be used to produce a relation between Δ and t .

STRATIFIED LAYER TEMPERATURE GRADIENT

To derive an analytical expression for the temperature gradient in the thermally stratified layer, it is assumed that the boundary layer decays completely in traversing the layer. This action is mathematically expressed as

$$\delta_\ell = \delta_\Delta \left(1 - \frac{z}{\Delta}\right)^r$$

and

$$U_\ell = U_\Delta \left(1 - \frac{z}{\Delta}\right)^p,$$

where δ_Δ and U_Δ are the boundary layer thickness and equivalent velocities at the bottom of the layer. (See Figure 3).

An identical procedure to that previously used for setting up a momentum equation is employed with the result that p and r are determined to have values of 3/7 and 5/7 respectively.

Establishment of an energy equation proceeds along identical lines but requires the addition of a term representing energy transport across the inner face of the element. After evaluating integrals, substituting for θ_w, U_ℓ and δ_ℓ, and performing any required differentiations, a differential equation in $\theta_{B\ell}$ and Z is obtained. Since it appears simpler to solve the equation by numerical integration, the equation is arranged with this in mind and is given as

$$\frac{\partial \theta_{B\ell}}{\partial Z} = \left[\frac{0.8307\, q_w}{c\rho_B U_\Delta \delta_\Delta \cos^2\gamma}\right] \left\{ \frac{1 - \left[\frac{1.6086\, Pr^{\frac{3}{7}} U_\Delta^{\frac{4}{7}} \delta_\Delta^{\frac{5}{7}} \cos^{\frac{2}{7}}\gamma}{\nu^{\frac{4}{7}} \Delta}\right] \left[0.2239 \frac{\delta_\Delta}{R}\left(1 - \frac{z}{\Delta}\right)^{\frac{5}{7}} - 1 + \left(1 - \frac{z}{\Delta}\right)\frac{\Delta}{R}\frac{\partial R}{\partial Z}\right]}{\left(1 - \frac{z}{\Delta}\right)^{\frac{3}{7}}\left[1 - 0.1861 \frac{\delta_\Delta}{R}\left(1 - \frac{z}{\Delta}\right)^{\frac{5}{7}}\right]} \right\} \quad (6)$$

The above equation enables us to define a vertical temperature pattern in the stratified layer in the absence of vaporization or condensation at the surface.

ULLAGE SPACE TEMPERATURE GRADIENT

The approach utilized above can be applied to the ullage space when modified to reflect variable wall heat flux. Experimental evidence [Maxson, 1963] shows that significant temperature increases can occur in the ullage space under pressurized conditions. As a result, the wall heat transfer rate will change due to a significant increase in the inner wall temperature. It then becomes necessary to describe wall heat flux as a function of temperature difference. This is accomplished by assuming a simple linear relation, i. e.,

$$q_w = \Omega(T_a - T_\ell) = \Omega\theta_{a\ell} .$$

Since $\theta_{a\ell} \doteq \theta_a - \theta_{B\ell}$, we have $q_w = \Omega(\theta_a - \theta_{B\ell})$. Substitution of this term for q_w and development of the equation yields the differential equation

$$\frac{\partial\theta_{B\ell}}{\partial z}\left\{\left[\frac{A^{\frac{2}{3}}\Omega U_\Delta^{\frac{1}{4}}\delta_\Delta^{\frac{5}{4}}\cos^{\frac{1}{4}}\gamma}{0.0228\, c\rho_B \nu^{\frac{1}{4}}}\right]\left[0.004785\frac{\delta_\Delta}{R}\left(1-\frac{z}{\Delta}\right)^{\frac{12}{7}} - 0.03663\left(1-\frac{z}{\Delta}\right)\right]\right.$$
$$\left. + U_\Delta\delta_\Delta\left[0.1464\left(1-\frac{z}{\Delta}\right)^{\frac{8}{7}} - 0.02724\frac{\delta_\Delta}{R}\left(1-\frac{z}{\Delta}\right)^{\frac{12}{7}}\right]\right\}$$
$$+(\theta_a-\theta_{B\ell})\left\{\left[\frac{A^{\frac{2}{3}}\Omega U_\Delta^{\frac{1}{4}}\delta_\Delta^{\frac{5}{4}}\cos^{\frac{1}{4}}\gamma}{0.0228\, c\rho_B \nu^{\frac{1}{4}}\Delta}\right]\left[0.03663\frac{\Delta}{R}\left(1-\frac{z}{\Delta}\right)\frac{\partial R}{\partial z} - 0.03663\right.\right. \quad (7)$$
$$\left.\left. + 0.004785\left(\frac{12}{7}\right)\frac{\delta_\Delta}{R}\left(1-\frac{z}{\Delta}\right)^{\frac{5}{7}}\right] - \frac{\Omega}{c\rho_B\cos^2\gamma}\right\} \equiv 0 .$$

Solution of this equation requires a combined iteration and numerical integration procedure.

PRESSURIZATION COMPUTATIONS

In order to use the above developed equations to predict pressurization rates, it is necessary to couple the results for the ullage space and the liquid phase. To accomplish this we look at a differential volume element described by

$$dV = \pi R^2 d\psi .$$

Note that the variable ψ introduced here is a variable over the entire height of the ullage space regardless of whether the ullage stratified layer has occupied the entire ullage space, (Figure 1). The mass contained in this element is then given by

$$dM = \pi \rho R^2 d\psi ,$$

and the total mass by

$$M = \pi \int_0^h \rho R^2 d\psi . \tag{8}$$

The fluid mass density, ρ , is a function of the local temperature and pressure, while R is a function of ψ .

Since equation (7) will provide information on θ_{Bl} as a function of z , and therefore of ψ , the total mass may be determined from

$$M = \pi \int_0^h \rho(\theta_{Bl}, P_s)\left[R_s - \psi \tan\gamma\right]^2 d\psi , \tag{8a}$$

where ψ includes the region below the stratified vapor layer as well as the layer where a thermal gradient exists. A combined iteration and numerical integration procedure must be used. A pressure is assumed and the expression numerically integrated until the computed mass compares with the known mass from initial conditions or a previous step. The pressure obtained from this procedure has a matching saturation temperature which is compared with the liquid surface temperature determined earlier from the thermal analysis of the stratified liquid layer. If a satisfactory match is not made, then vaporization of liquid or condensation of gas is permitted to bring the liquid surface temperature into equilibrium with the computed pressure. The different temperature patterns which result from liquid temperature greater than saturation temperature and liquid temperature less than saturation temperature are shown in Figure (4a) and (4b) respectively. The mass vaporized is added to the initial ullage mass (determined by assuming saturated gas to fill the ullage at the beginning of pressurization) and the new mass used in the next step. Computation of the mass vaporized, DM_v, is accomplished by use of the equation

$$DM_V = \frac{\pi}{L_V} \int_0^{Z_1} \kappa_l \rho_B (\theta_l - \theta_s) R^2 dz_1 \quad , \tag{9}$$

where Z_l is measured from the liquid surface downward and L_v represents the latent heat of vaporization.

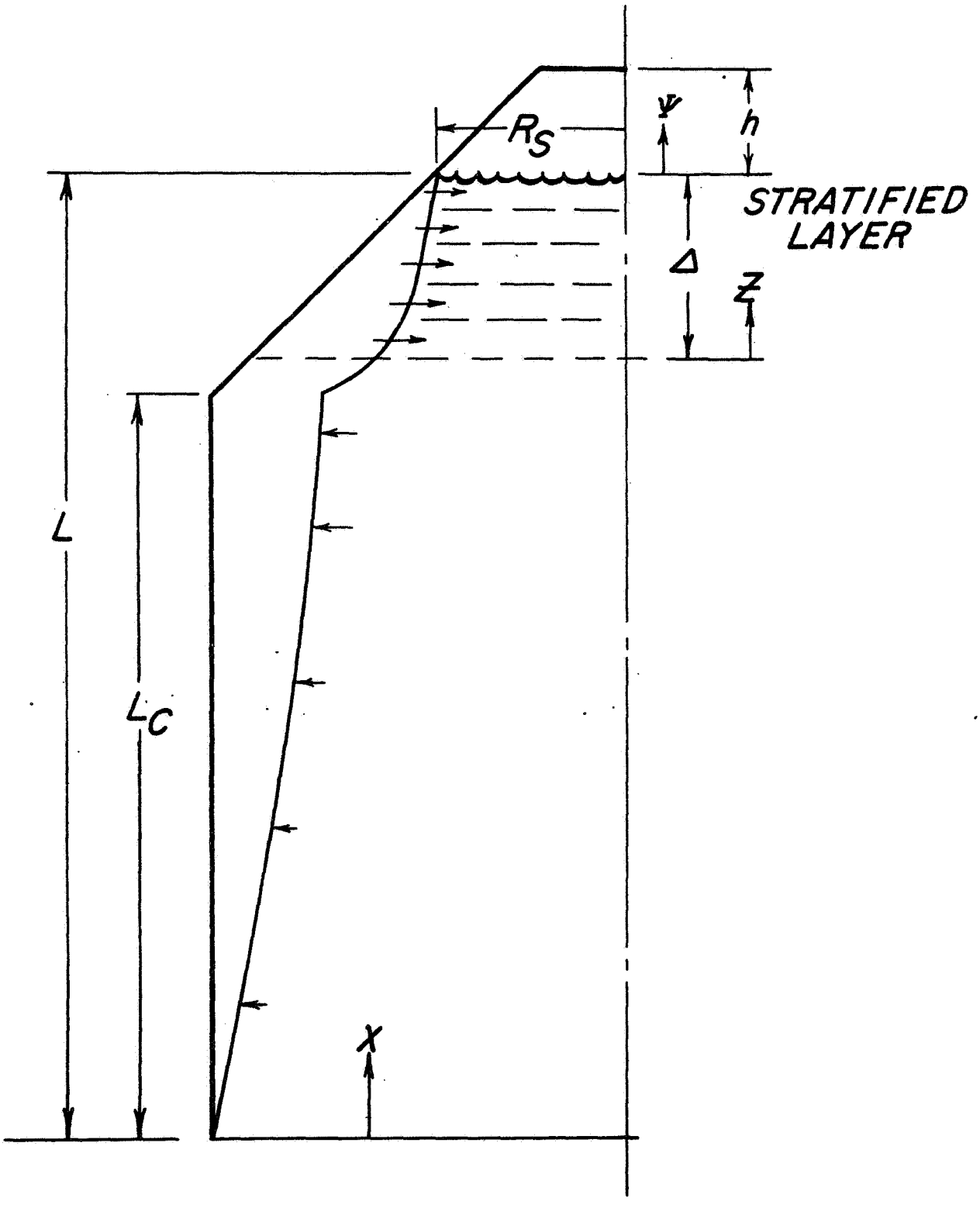


Figure 1. Assumed Geometry

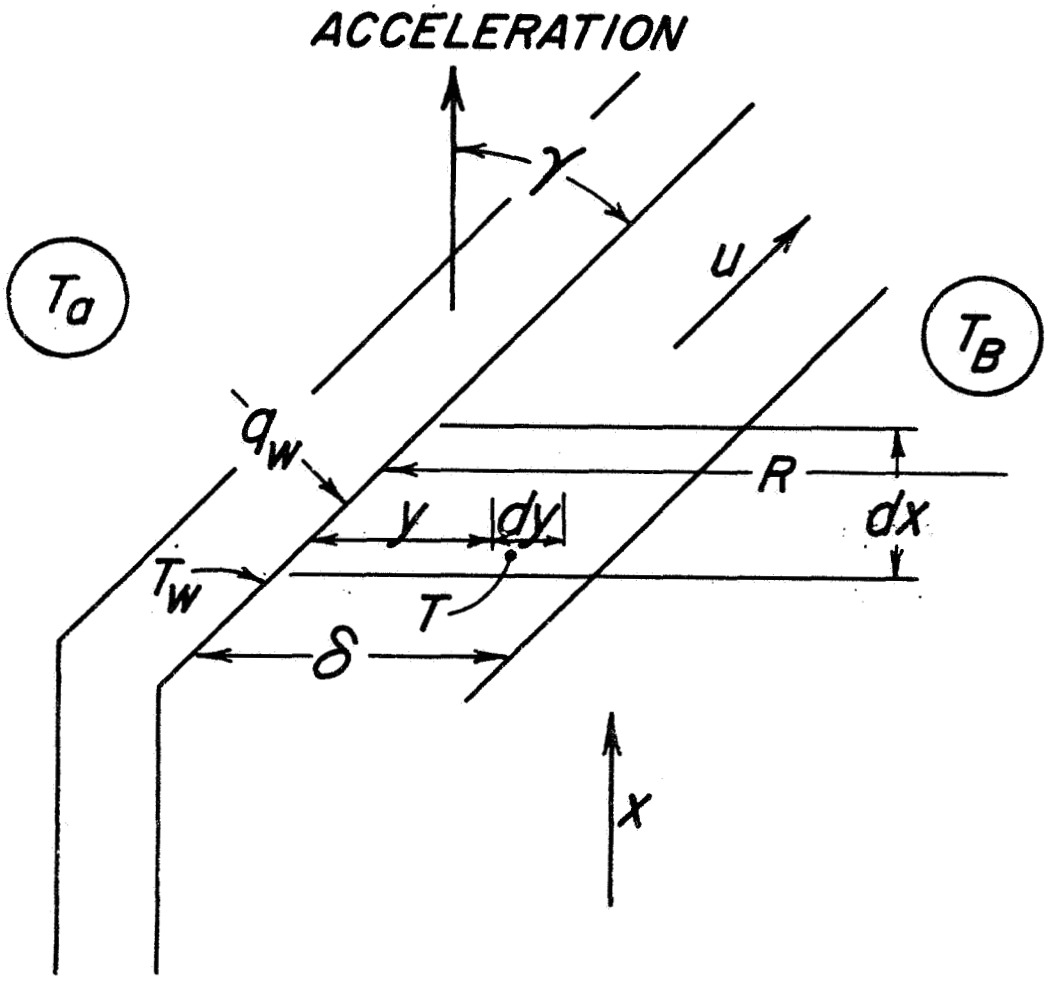


Figure 2. Element Considered For Boundary Layer Growth

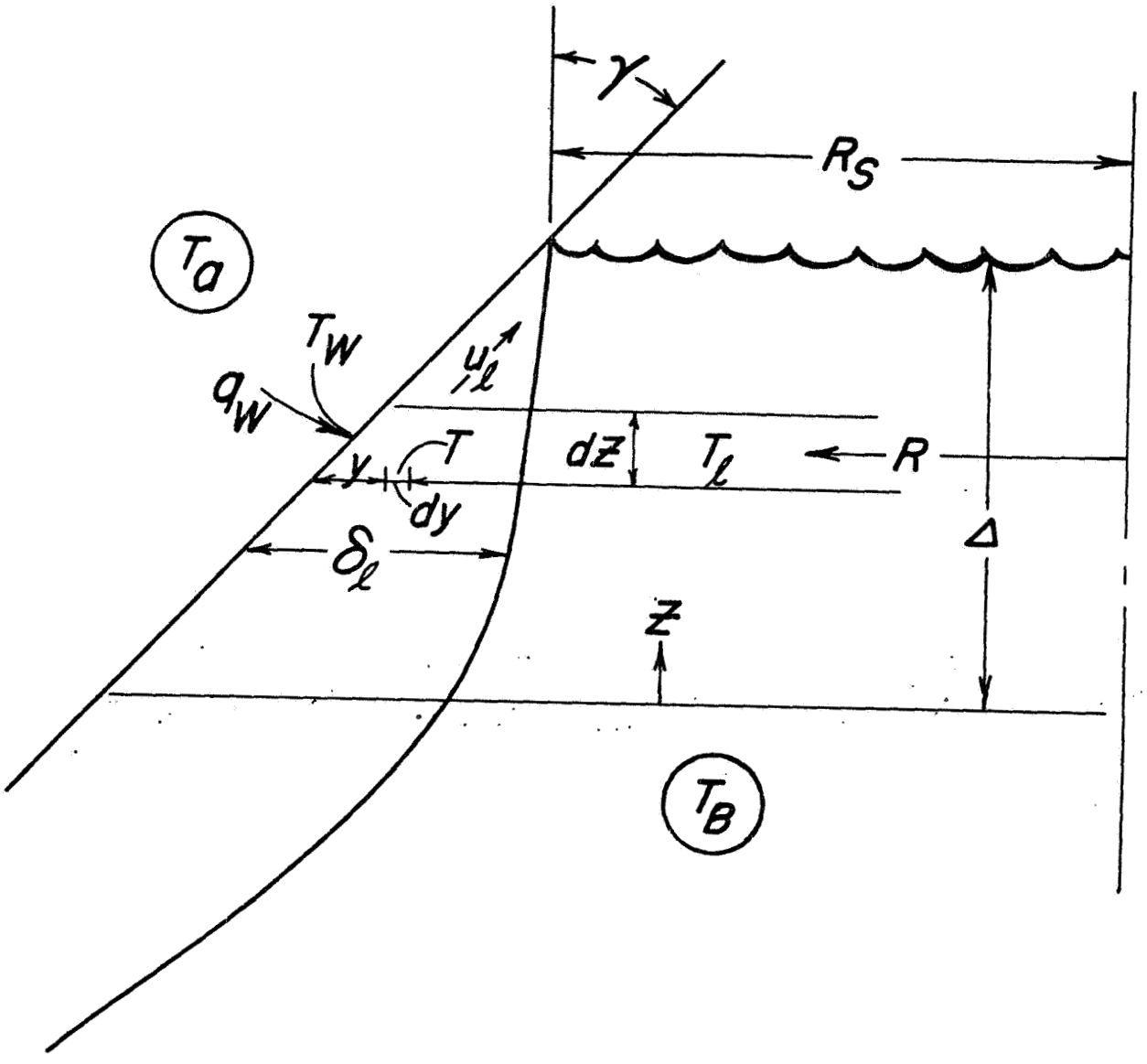
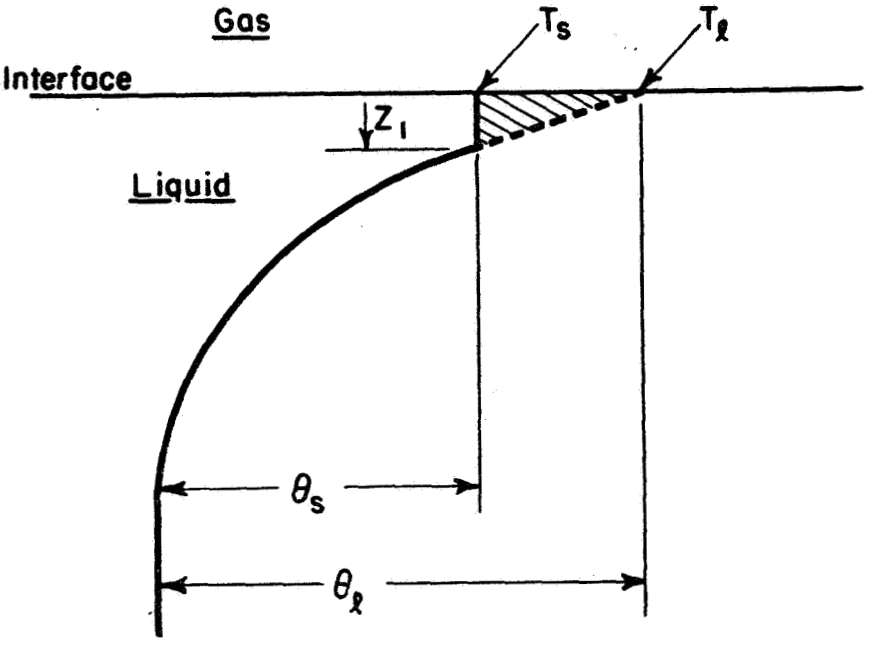
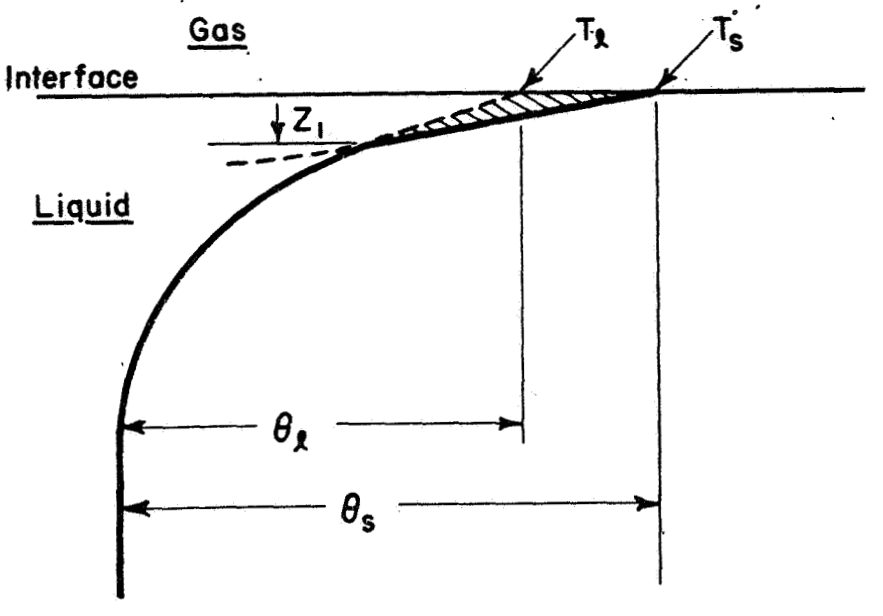


Figure 3. Element Considered For Boundary Layer Decay



(a) Evaporation



(b) Condensation

Figure 4. Interface Temperature Adjustment

Nomenclature

A - cross section area

C_1, C_2, m, n, r, p - derived constants

c - specific heat

G_{RL} - modified Grashof number,

g - acceleration

h - vapor space height

K - substitutional term

k - thermal conductivity

L - liquid depth

L_c - length of cylindrical tank

M - mass

P_r - Prandtl number

q - unit area heat flux

R - tank radius

R_s - radius at the liquid surface

T - absolute temperature

t - time

u - local velocity in boundary layer

U - equivalent free stream velocity

V - volume

x - vertical distance in tank

y - horizontal distance from tank wall

Z - vertical distance from bottom of stratified layer

β - volumetric coefficient of thermal expansion

γ - half angle of conical nose

Δ - stratified layer thickness

δ - boundary layer thickness

θ - temperature difference, $T - T_B$.

$\theta_a = T_a - T_B$

$\theta_{al} = T_a - T_l$

$\theta_{Bl} = T_l - T_B$

$\theta_W = T_W - T_B$

μ - dynamic viscosity

ν - kinematic viscosity

ρ - fluid mass density

τ - viscous shear stress

ψ - vertical distance in ullage space

Ω - overall tank wall heat transfer coefficient

Subscripts

a - ambient conditions (external to tank)

B - at bulk fluid condition

l - in stratified layer

n - in the conical nose

W - at tank wall

S - in the ullage space

Δ - at bottom of stratified layer

δ - pertaining to boundary layer

References

Eckert, E. R. G., and R. M. Drake, Jr. (1959). Heat and mass transfer, second edition (McGraw-Hill Book Co., Inc., New York).

Eckert, E. R. G., and T. W. Jackson (1951). Analysis of turbulent free convection boundary layer on flat plate, National Advisory Committee for Aeronautics Report No. 1015.

Jakob, Max (1949). Heat transfer, Vol. 1, p. 520 (John Wiley and Sons, New York).

Maxson, J. G. (1963). Centaur fuel boiloff valve lockup test and nose fairing skirt seal and heater evaluation, General Dynamics/ Astronautics Report No. 55B 3029-1, 33.

Morse, F. H. (August 1962). Informal notes concerning the natural convection boundary layer in the RIFT tank, Lockheed Missiles and Space Co. FM 42.

Robbins, J. H., and A. C. Rogers, Jr. (1964). An analysis on predicting thermal stratification in liquid hydrogen, presented at the First AIAA Meeting, Washington, D. C., June 29-July 2, 1964, AIAA Paper No. 64-426.

Schmidt, A. F., J. R. Purcell, W. A. Wilson, and R. V. Smith (April-June 1961). An experimental study concerning pressurization and stratification of liquid hydrogen, J. Research NBS 65C (Eng. and Inst.), No. 2, 81-87.

Schwind, R. G., and G. C. Vliet (1964). Observations and interpretations of natural convection and stratification in vessels, Proc. 1964 Heat Transfer and Fluid Mech. Inst., Warren H. Giedt and Salomon Levy, editors, pp. 52-68 (Stanford University Press).

Scott, L. E., R. F. Robbins, D. B. Mann, and B. W. Birmingham (Jan-March 1960). Temperature stratification in a nonventing liquid helium dewar, J. Research NBS 64C (Eng. and Inst.), No. 1, 19-23.

Tatom, J. W., W. H. Brown, L. H. Knight, and E. F. Coxe (1964). Analysis of thermal stratification of liquid hydrogen in rocket propellant tanks, Advances in Cryogenic Engineering, K. D. Timmerhaus, editor, 9, 265-272.

Tellep, D. M., and E. Y. Harper (Aug. 1963). Approximate analysis of propellant stratification, AIAA Journal 1, No. 8, 1954-1956.

Von Karman, Th. (Sept. 1946). On laminar and turbulent friction, National Advisory Committee for Aeronautics Tech. Memo No. 1092.

INVESTIGATION OF STRATIFICATION REDUCTION TECHNIQUES

by
B. D. Neff
Martin-Marietta Corporation
Martin Company-Denver Division
Denver, Colorado

I. INTRODUCTION

For a pump fed flow system, the head required to suppress cavitation is the net positive suction head (NPSH), which is the difference between total head and vapor head at the pump inlet. In missile boosters using cryogenic propellants, vapor pressure is usually a significant portion of the total pressure. Liquid vapor pressure will increase in a non-uniform manner due to temperature stratification resulting from ground hold and flight aerodynamic heating of the subcooled cryogenic fluid. The upper propellant layers usually show a large increase in vapor pressure, while the lower layers show little or no increase (Reference 1). Therefore, the system operating pressure is often determined by the NPSH requirement at stage burnout when the warmest propellant is being consumed. If the total heat input to the propellant were uniformly distributed within the fluid, a minimum increase in the vapor pressure would result, requiring a minimum total pressure and tankage weight for a given NPSH. Therefore, effective methods for reducing stratification are required.

This report describes a program, largely experimental, in which three different techniques for reducing stratification were evaluated; a) bottom heating, b) mixing by means of a bubble-lift pump, and c) baffles. The test apparatus employed was a small transparent tank for non-cryogenic fluids and a 4 foot diameter x 6 foot long vacuum jacketed tank for tests with cryogenic fluids. The apparatus and experimental program are briefly described in Section II, the results and conclusions in Sections III and IV, respectively.

II. EXPERIMENTAL PROGRAM

The first portion (Phase A) of this program included approximately 70 tests with water which provided a preliminary evaluation of the effect of wall-bottom heating, bottom geometry, and various baffle configurations. Data included thermocouple temperature measurements and some photographic recording of flow patterns within a transparent test vessel. The test vessel was heated by hot water poured into another transparent tank surrounding it. Small glass microspheres (Emerson and Cummings Inc. Ecco-spheres S-1) of graded densities were immersed in the water test fluid, and were illuminated by a planar light source to provide a means of observing the fluid motion. Photographs of the flow fields within the test vessel were then obtained at several time increments during the test, as shown in Figure 1.

The second portion (Phase B) of the program utilized a 4 foot diameter by 6 foot tall test vessel, which is enclosed in a 6 foot diameter by 9 foot tall vacuum chamber. This test vessel was designed specifically for liquid hydrogen propellant feed and pressurization system tests (Reference 1). Side-wall heating is accomplished with a heat chamber consisting of four low absorptivity aluminum reflectors installed within the vacuum annulus which contain four rows of infrared quartz lamps. Liquid temperature measurements throughout the vessel were obtained by means of thermistors to an accuracy of $\pm 0.15^{\circ}R$. The thermistors were calibrated each day of test by recording all sensor outputs during a continuous venting from high saturation pressure and temperature down to ambient.

The four foot diameter test apparatus was modified as required for each of the three stratification reduction techniques evaluated, as shown in Figure 2. Figure 2a shows the false bottom that was installed to simulate a

convex-inward hemispherical dome. It contained an electrical resistance heater capable of producing varying heat inputs. Sixteen liquid hydrogen tests and 13 liquid nitrogen tests were run with this configuration. Wall heating rates were varied from 0.26 BTU/ft^{2}sec to 0.02 BTU/ft^{2}sec, and bottom heating rates were varied from 0.042 to 0.013 BTU/ft^{2}sec. The same bottom configuration (Figure 2b) was retained for the 9 liquid hydrogen tests and 9 liquid nitrogen tests in which the bubble lift pump was evaluated. Bubble pumping rates were similar to those used on the wall-bottom heating tests. Four baffle configurations were evaluated, as shown schematically on Figure 2c. These consisted of a single conical downward baffle with three different hole sizes, and a three baffle configuration with the intermediate baffle hole size. Four different wall heating rates were run on each configuration.

III. RESULTS

The stratification process, based on the Phase A photographs and temperature measurements, is visualized to be similar to that shown on Figure 3 at the start of heating. With wall heating of a subcooled fluid, flow starts near the wall, continuing upward to the surface where a large annular vortex forms at the wall-surface intersection. The large annular vortex near the wall creates a general downward flow in the center of the tank, penetrating the quiescent fluid to greater depths as time progresses, until fluid motion in macroscopic eddies is observable throughout the heated volume. The time required to obtain this general fluid motion and vortex intensity is some function of the wall heating rates.

The the Phase A photographs, the fluid near the tank bottom was essentially quiescent until penetrated by the central descending flow. Temperature measurements taken during this start transient indicated that the energy in the fluid was distributed non-uniformly in the upper regions of the volume, without any heating occurring where the central flow pattern had not penetrated. After the macroscopic eddy motion was observed throughout the wall-heated portion of the test vessel, the temperature-volume profile did not change in shape, but the temperature increased uniformly with time at each longitudinal location throughout the volume. The test fluid did not approach saturation in the Phase A tests, therefore, photographic data of the fluid motion as saturation was approached was not obtained. A typical set of photographs of the stratifying process at different run times is shown on Figure 1.

The processes described above can be illustrated by height (or volume) vs temperature profiles, plotted for different test times as shown on Figure 4. This data was obtained from a test with liquid hydrogen which approached saturation near the end of testing. The start transient of region 1 on Figure 4 shows the temperature or sensible energy distribution in the fluid to be limited to the upper parts of the volume. As time progressed, the fluid near the bottom of the test vessel experienced a temperature rise, indicating general bulk motion, and a fixed volume-temperature profile shape resulted during the "quasi-steady state" of region 2. Finally, as the fluid temperature approached saturation, the volume-temperature profile shape again changed slightly in the lower portions of the volume, as shown in region 3.

In order to evaluate the relative effectiveness of the different stratification reduction techniques employed, it was necessary to devise a suitable measure of stratification intensity. The method used divided the fluid volume-temperature profile into two distinct parts defined as the bulk and the stratified areas, which are proportional to heat content. The ratio of the heat input to the stratified fluid (Q_S), to the heat input to the bulk fluid (Q_B), then becomes a useful measure of stratification intensity; i.e., the greater value of Q_S/Q_B, the greater the amount of stratification.

The appropriate values of Q_S and Q_B are obtained by first plotting the temperature-volume profile for the desired time increment, and then dividing the area bounded by the profile into two parts as shown on Figure 5a. Assuming constant fluid properties for each time increment, the area bounded by the volume-temperature profile will be proportional to the sensible energy gain of the fluid. By dividing each volume-temperature profile at the point

where the temperature gradient (dT/dV) approaches zero at about 17.5 ft^3 volume, (Figure 5a), two areas are obtained; one proportional to sensible energy gain in the bulk (Q_B), and the other proportional to the energy gain in the stratified layer (Q_S). Since the volume-temperature profile curve shape is approximately constant following the initial transients, the sensible energy rise of the bulk fluid (Q_B) becomes a nearly linear function of the total heat input, in the "quasi-steady state" region on Figure 5b.

The performance of bubble pumping and baffles as stratification reduction devices is evaluated by comparing the value of Q_S/Q_B for wall and bottom heating alone, with that obtained when these additional devices are used. For consistency, the comparisons are made for equal values of total heat content (Q_T) within the fluid for each of the variables considered. A typical log-log plot of Q_S/Q_B vs Q_T is shown on Figure 6a. Since some bottom heating was always present, a ratio of bottom to wall heat inputs (Q_b/Q_W) was also used for cross plotting of Q_S/Q_B vs Q_T data as shown in Figure 6b.

Typical volume-temperature data from a wall-bottom heating test using the Phase B test vessel (Figure 2a) are shown on Figure 4. Three test data plots of stratification intensity (Q_S/Q_B) versus the ratio of bottom to wall heat input (Q_b/Q_W) are shown in Figure 6b. It is seen that the stratification intensity is reduced as the wall heating rate is reduced and/or the bottom heating rate is increased. The stratification reduction obtained for Q_b/Q_W greater than 0.1, and wall heating rates less than 0.05 $BTU/ft^2 sec$, was enough to reduce the maximum temperature of the fluid to less than that without bottom heating. In these ranges of wall heating rates and Q_b/Q_W, increased bottom heating was an effective stratification reduction device, even though the total heat input to the fluid was greater.

Equations 1 and 2 shown on Figure 7 are empirical expressions for the stratification intensity derived from the wall-bottom heating test results, relating Q_S/Q_B as a function of Q_T, Q_b and Q_W. Equation 2 requires the use of Figure 7e for determination of the coefficient a_2.

A typical volume-temperature profile obtained from the bubble pump test configuration (Figure 2b) with constant wall heating is shown in Figure 8. It is evident in comparing Figures 8a and 4, that bubble pumping had a significant effect on the volume-temperature profile. The pumping, however, was accomplished using ambient temperature helium gas, which resulted in a significant increase in the total heat gain of the fluid. Unfortunately, the increased sensible energy gain from the pumping gas overshadowed the stratification reduction effect obtained with the pumped fluid. For values of total heat content (Q_T) equal to those of the wall-bottom heating tests, the stratification intensity was reduced, but a considerable part of this total heat gain came from the pumping gas. Increasing the bottom heating rate was less effective in reducing stratification for the bubble pump tests than for the tests with wall-bottom heating only. On one test in this series, the tank top pressure was reduced to 15 psig, resulting in a significant improvement in bubble pump performance (Reference 2). The liquid level for this test was also lower, and the net result was significantly lower values of stratification intensity (Figure 8b).

Results of one of the tests of a specific baffle configuration (Figure 2c), showing pronounced effect on stratification, are shown on Figure 9. In general, baffles were more effective in reducing stratification at short times, as the wall heating rate was increased, and as the baffle hole size was reduced to restrict fluid circulation (Figures 10a and 10b). Bottom heating had an additive effect to that of the baffles in reducing the stratification intensity.

Three baffles were more effective in reducing stratification than a single baffle of the same hole size. These observations were arrived at by a comparison of baffle test data with the equation 1 and 2 predictions.

Typical fluid temperature data obtained during outflow for the multiple baffle configuration is shown on Figures 11a and 11b. The corresponding volume-temperature profiles prior to outflow are superimposed on the outflow temperature curves, showing that some fluid heating continued during outflow, and that some fluid mixing occurred.

IV. CONCLUSIONS

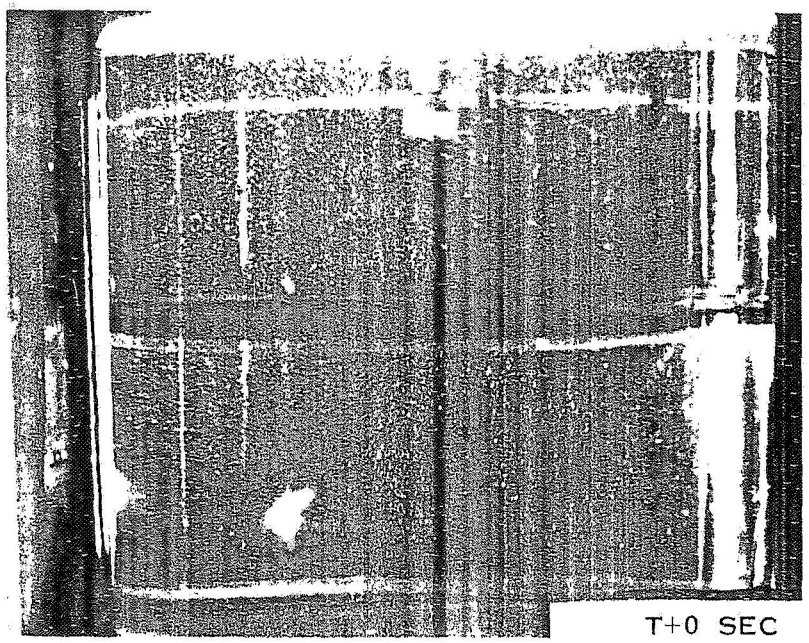
1. Stratification intensity generally is reduced by a reduction in wall heating rates and/or an increase in bottom heating rates.
2. Fluid mixing by means of a bubble-lift pump will reduce the stratification intensity, but in the majority of the tests conducted, the heating effect of the ambient temperature pumping gas overshadowed the desired beneficial effect. The use of bottom heating in addition to bubble pumping did not significantly improve the stratification reduction effect.
3. Baffles are effective in reducing stratification for short heating times, for relatively high wall and bottom heating rates, and when the baffle hole size is relatively small.

REFERENCES

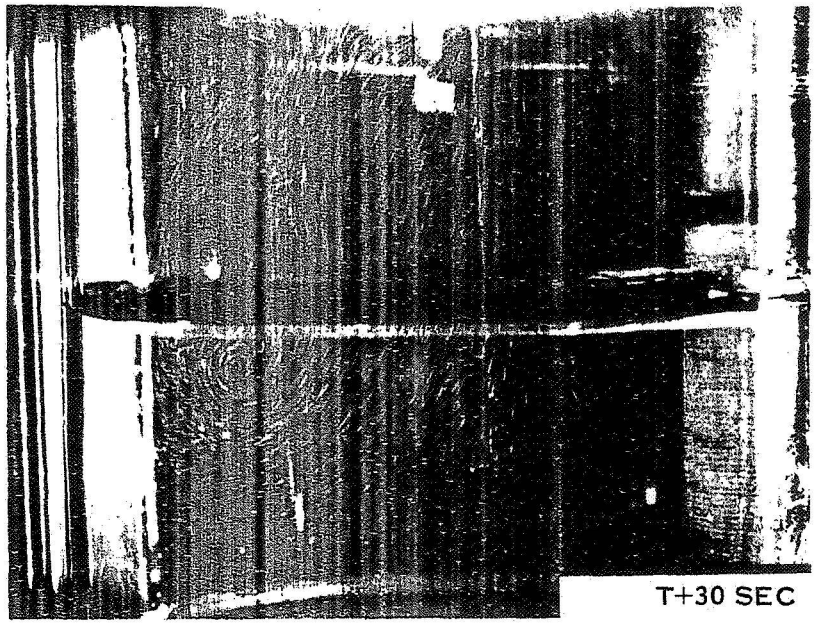
1. Bailey, T. E., et al., "Analytical and Experimental Determination of Liquid Hydrogen Temperature Stratification, Final Report," April 1963, NASA Contract NAS8-5046, Martin Company, Denver, Colorado, NASA-CR-63-5.

2. Pedreyra, D. C., "Bubble Lift Pump," Section Report 0560-64-18, September 1964, Martin Company, Denver, Colorado.

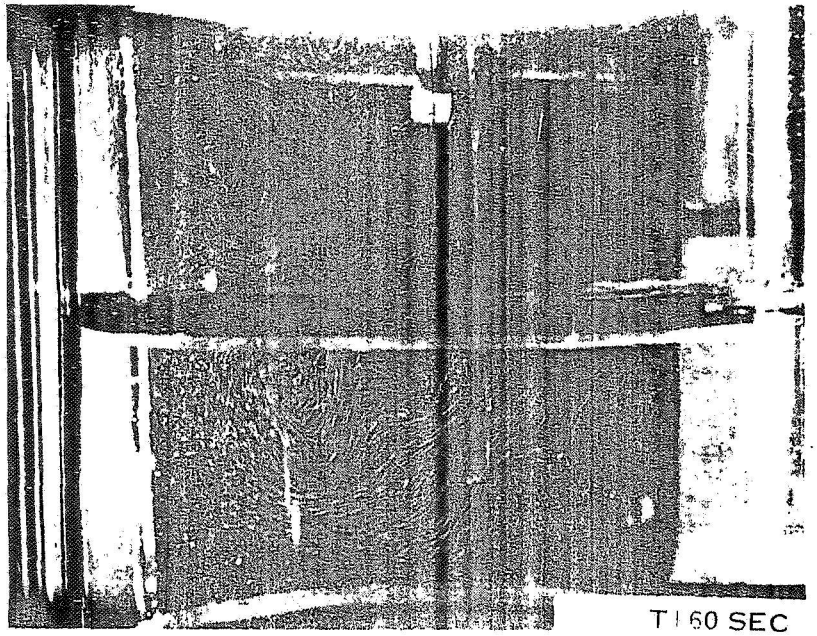
PHASE A WATER TESTS WITH MICROSPHERES



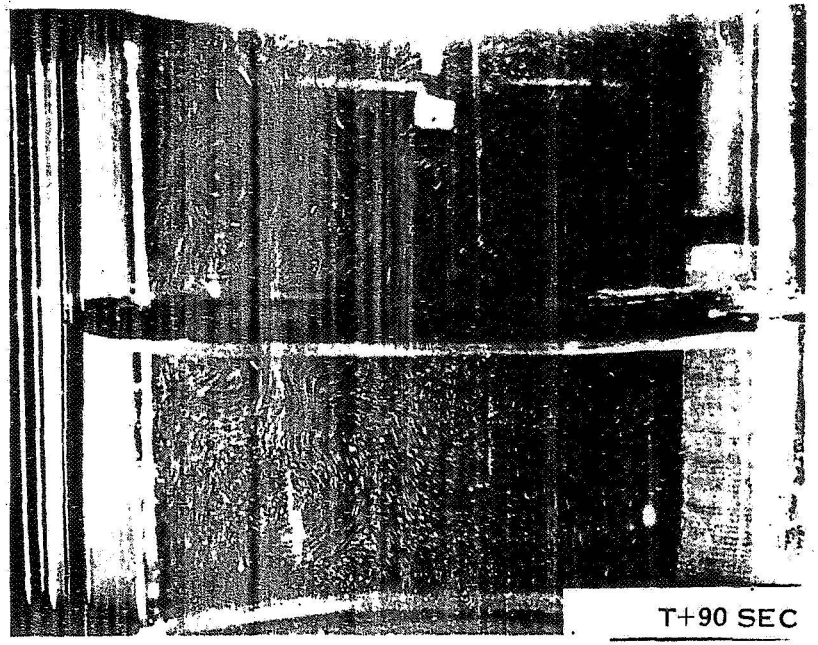
T+0 SEC



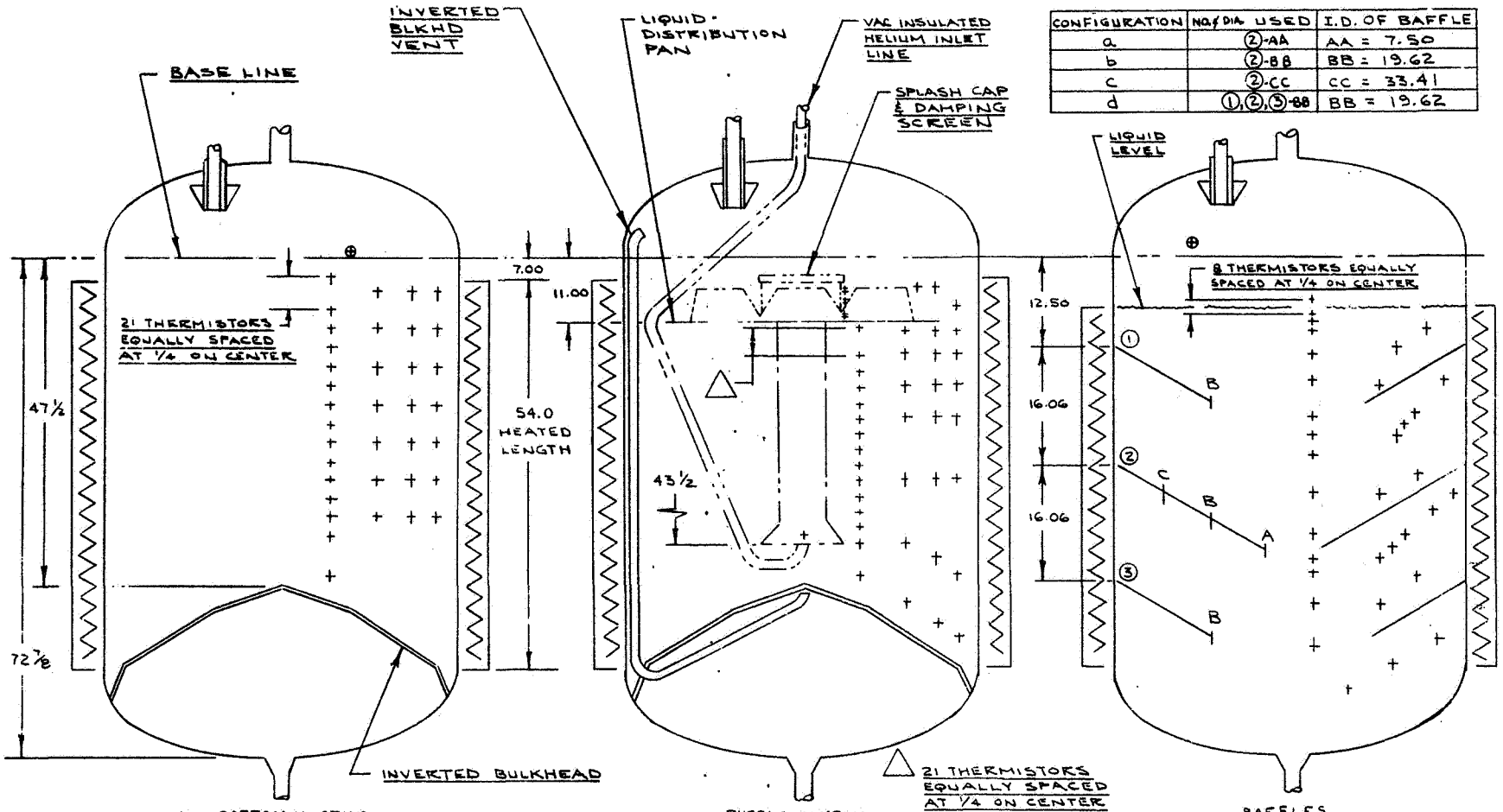
T+30 SEC



T+60 SEC



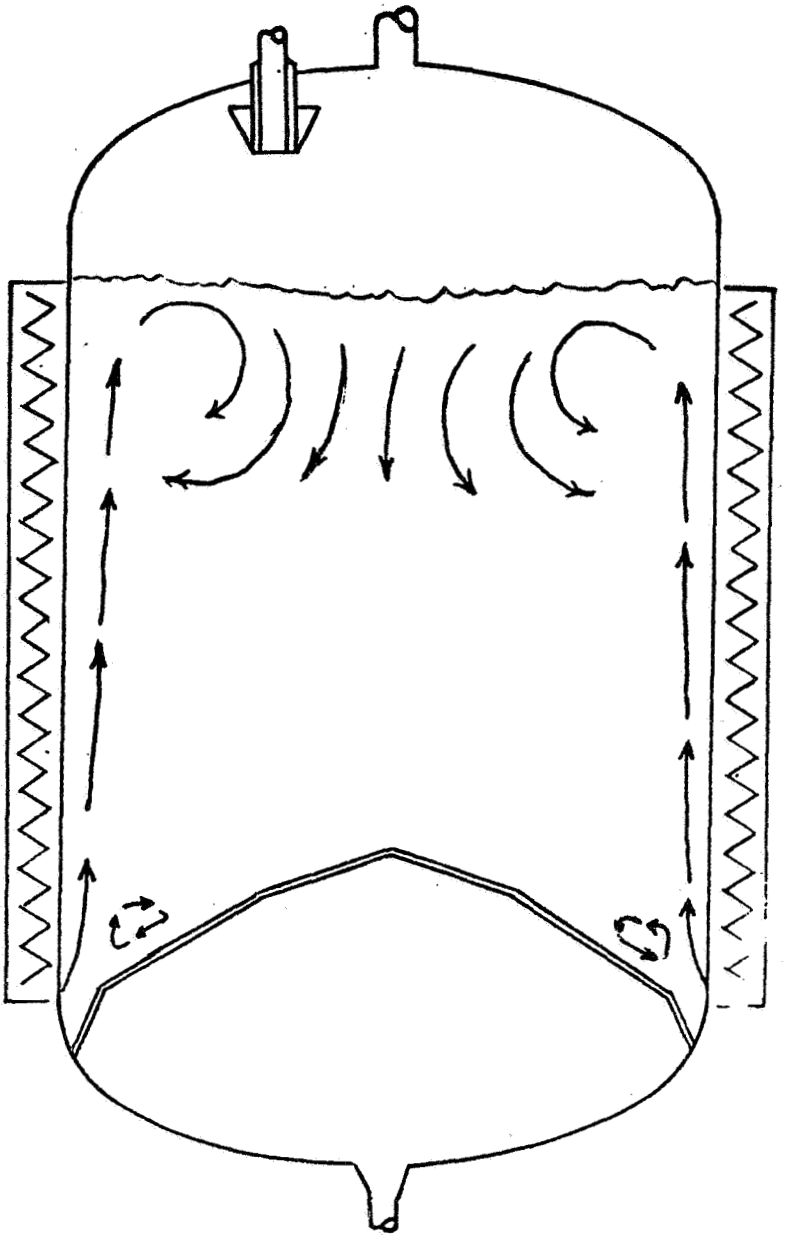
T+90 SEC



CONFIGURATION	NO. & DIA. USED	I.D. OF BAFFLE
a	②-AA	AA = 7.50
b	②-BB	BB = 19.62
c	②-CC	CC = 33.41
d	①,②,③-BB	BB = 19.62

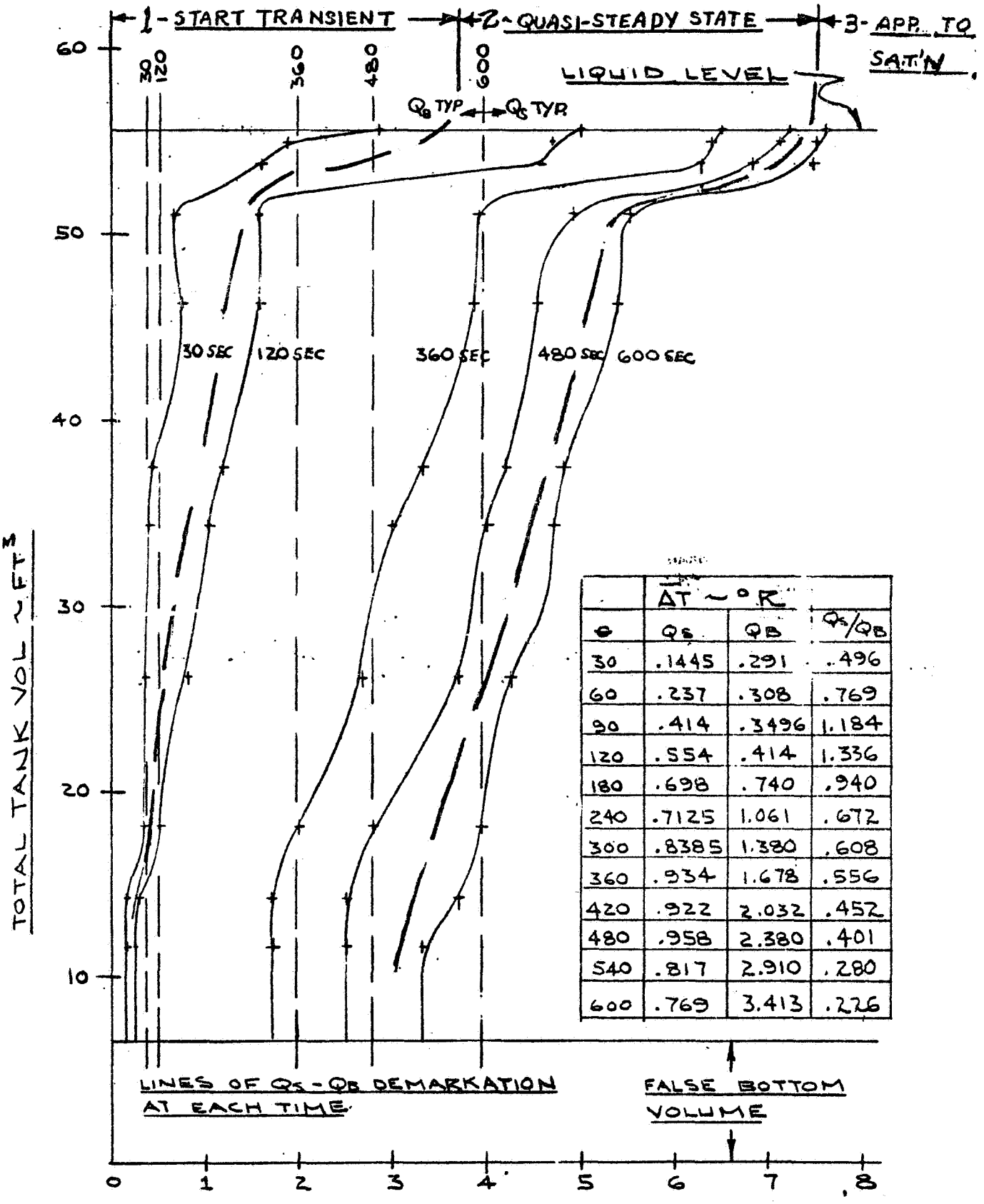
LEGEND
⊕ GAS ULLAGE T/C
+ THERMISTORS

TEST CONFIGURATIONS FIG 2



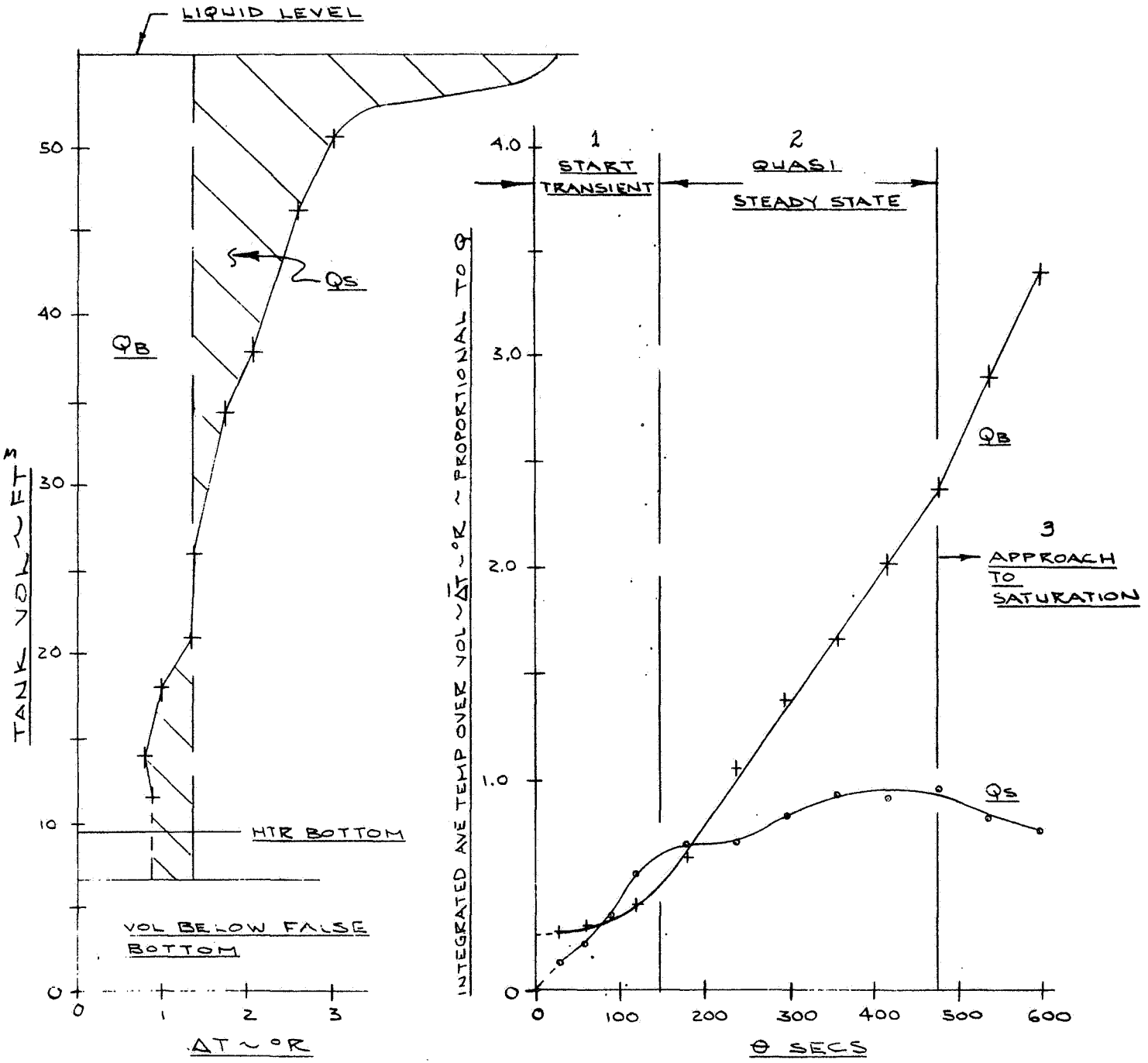
STRATIFYING FLOW PROCESS

FIG 3.



	$\overline{\Delta T}$ ~ °R		
Θ	Q_S	Q_B	Q_S/Q_B
30	.1445	.291	.496
60	.237	.308	.769
90	.414	.3496	1.184
120	.554	.414	1.336
180	.698	.740	.940
240	.7125	1.061	.672
300	.8385	1.380	.608
360	.934	1.678	.556
420	.922	2.032	.452
480	.958	2.380	.401
540	.817	2.910	.280
600	.769	3.413	.226

FIG 4 ~ TYP WALL-BOTTOM HTG. DATA



Qs & QB DETERMINATION

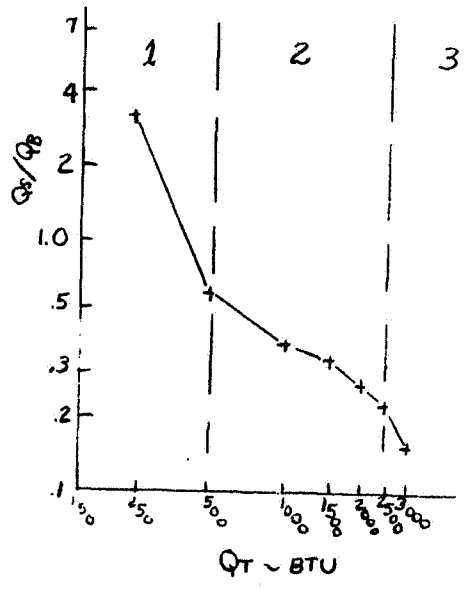


FIG 6a

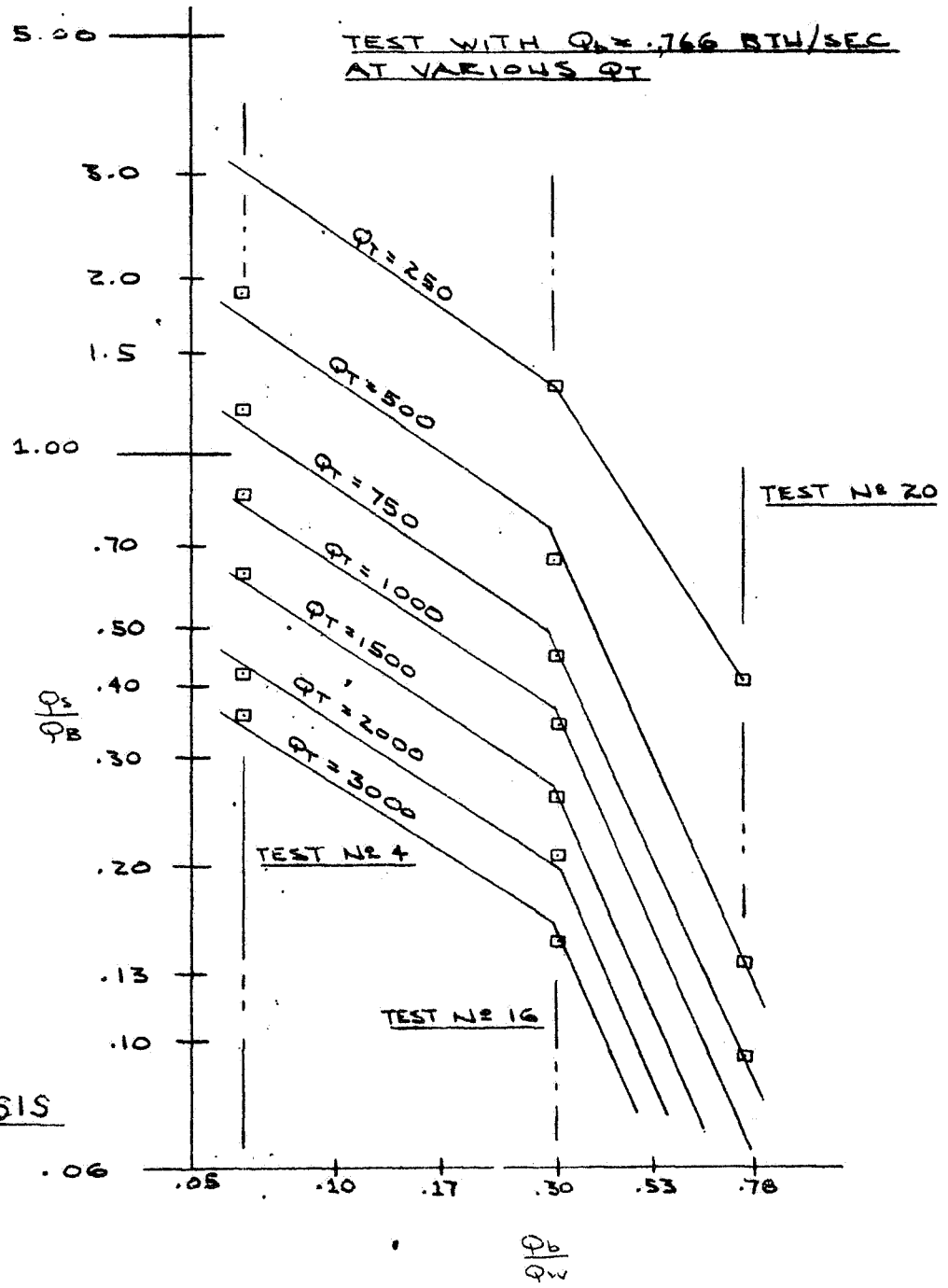


FIG 6b

TYPICAL DATA ANALYSIS

FIGURE 6

$\dot{Q}_s/\dot{Q}_B = a_1\left(\frac{\dot{Q}_b}{\dot{Q}_w}\right)^{b_1}$ FOR FIGS

FOR $\dot{Q}_w < 2.55$ BTU/SEC; $a_1 = \left\{.0173\left[1.06\times10^{5}\right]\dot{Q}_b{}^{.515}\dot{Q}_T{}^{-.286\dot{Q}_b+.515}\right\}$, $b_1 = -1.8$

EQN 1: $\dot{Q}_s/\dot{Q}_B = .0173\left[1.06\times10^{5}\right]\dot{Q}_b{}^{.515}\dot{Q}_T{}^{-.286\dot{Q}_b+.515}\left[\dot{Q}_b/\dot{Q}_w\right]^{-1.8}$

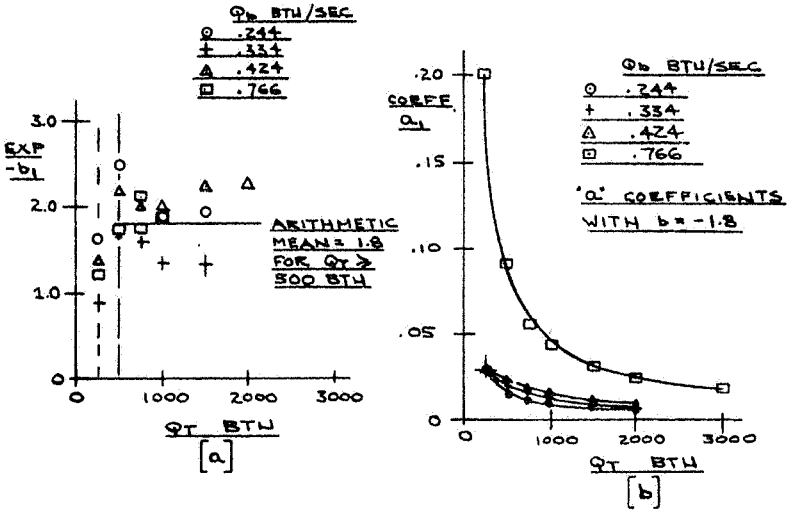
OR, "a" & "b" ARE DEFINED BELOW

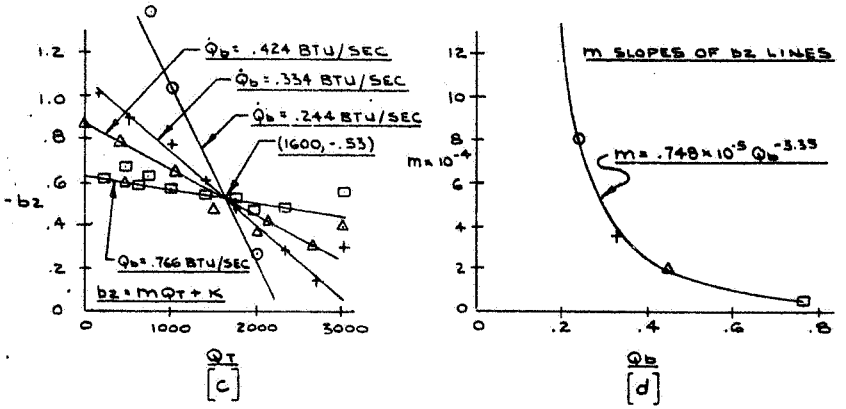
FOR 12 BTU/SEC > $\dot{Q}_w$ > 2.55 BTU/SEC FROM FIGS

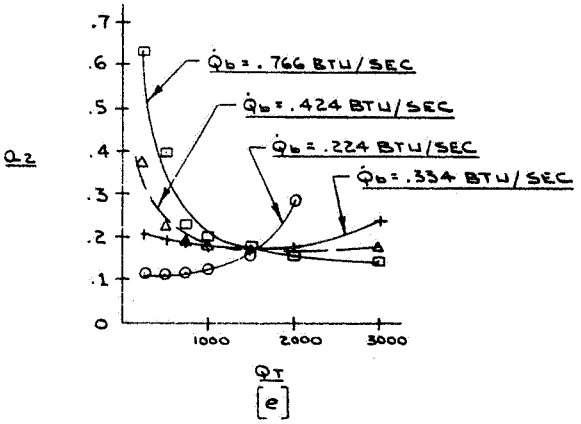
EQN 2: $\dot{Q}_s/\dot{Q}_B = a_2\left(\dot{Q}_s/\dot{Q}_b\right)^{bz}$

WHERE $bz = .748\times10^{-5}\dot{Q}_b{}^{-3.35}\left[\dot{Q}_T - 1600\right] - .53$ "SHOWN BELOW"

& a_2 MAY BE OBTAINED FROM FIG "C" BELOW







EMPIRICAL EQUATIONS FOR WALL-BOTTOM HEATING FIG 7

TEST Nº 31

Q_W = 2.82 BTU/SEC

Q_b = .244 BTU/SEC

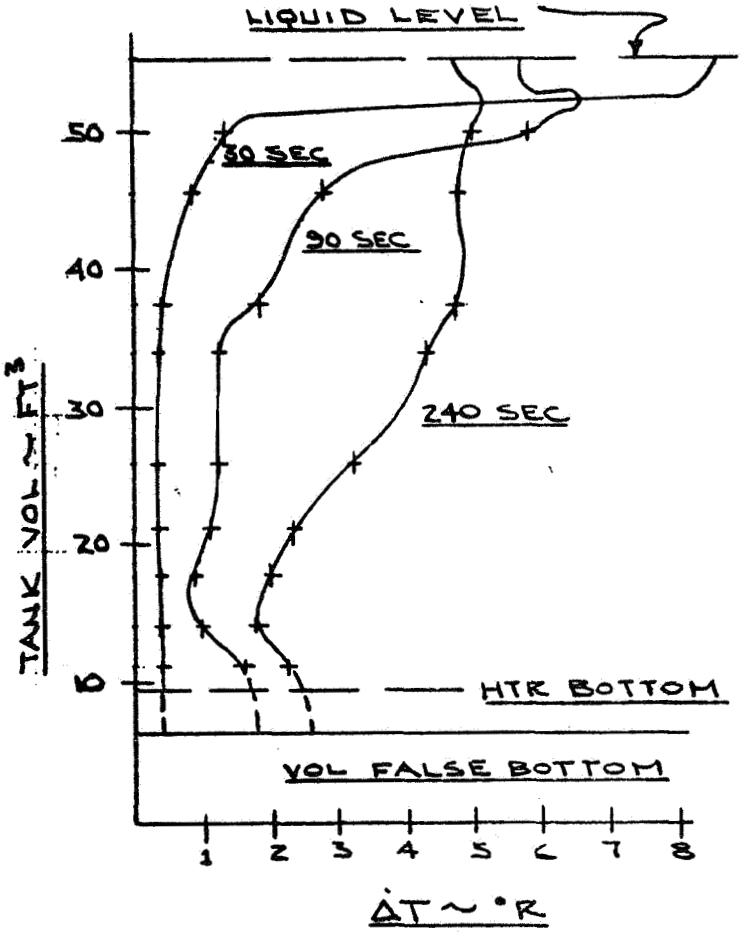
Q_{HE} = 1.84 BTU/SEC

$\dot{M}$ = .1 CFS

Q_b/Q_W = .087

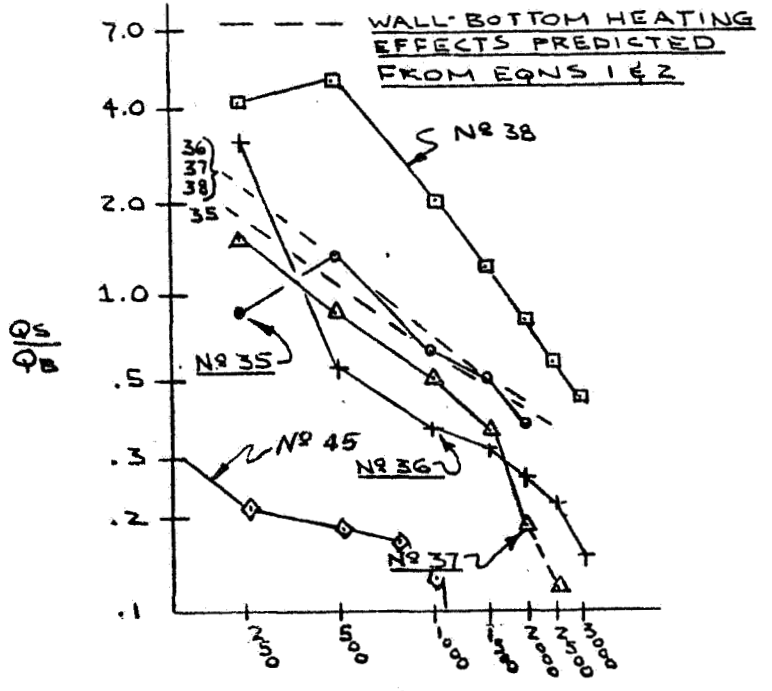
Q_{HE}/Q_W = .653

TEST Nº	Q_W BTU/SEC	Q_b/Q_W	M	Q_{HE}/Q_W	Q_T BTU/SEC	θ SEC @ Q_T = 988	SYM
35	2.5	.097	0	0	4.00	247	o
36	2.83	.086	.05	.392	5.49	180	+
37	2.82	.087	.10	.653	6.44	153	Δ
38	2.84	.086	.135	.820	8.23	120	□
45	?.86	.085	.05	.48	-	-	◇



(a)

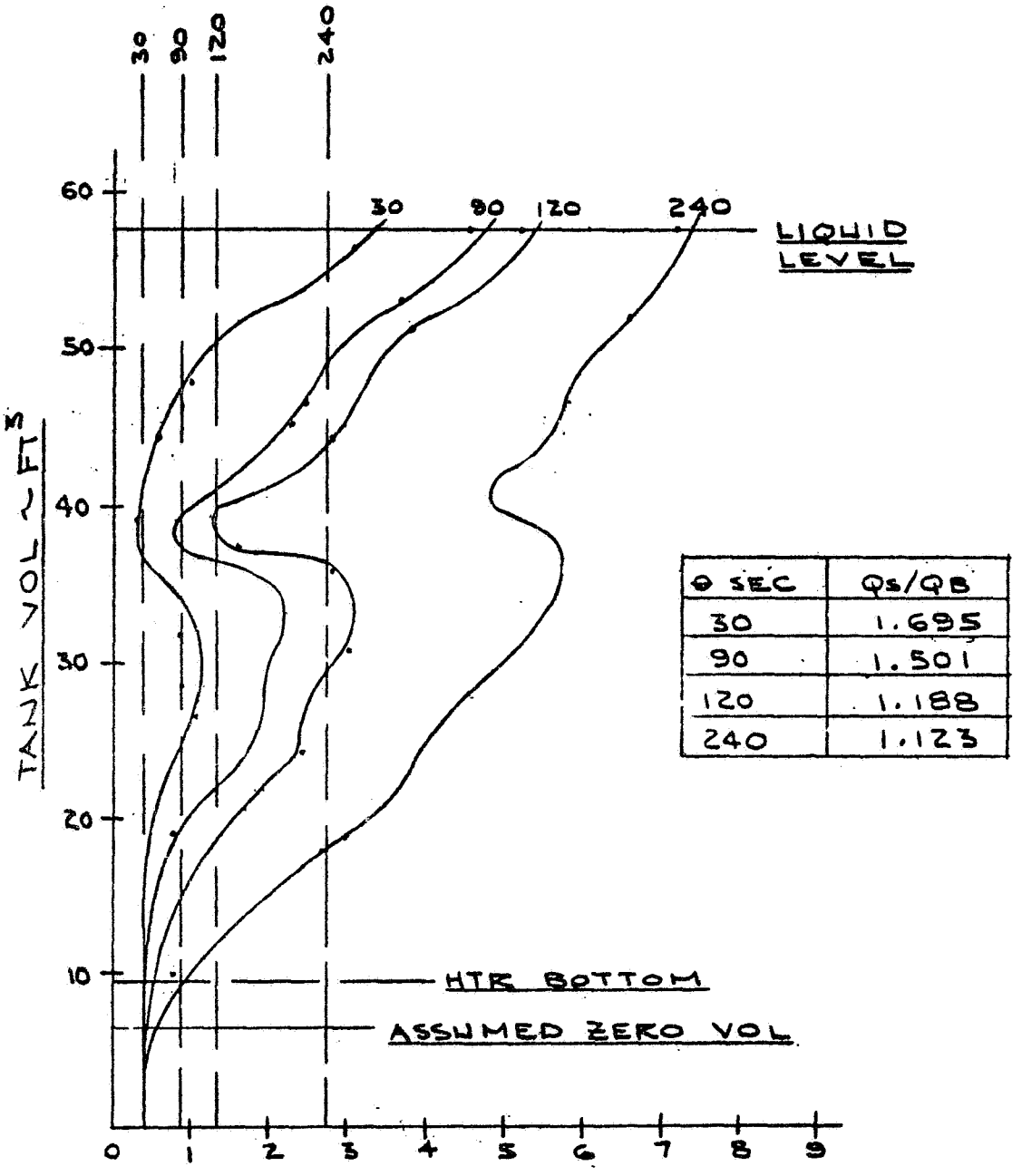
TYP BUBBLE PUMP TEST RESULTS



(b)

FIG 8

TEST Nº 62
SINGLE CONICAL BAFFLE
INCLINED 30° DOWN
7.5" BAFFLE HOLE DIA
$\hat{\tau}_z = .841$
$Q_W = 8.1$ BTU / SEC



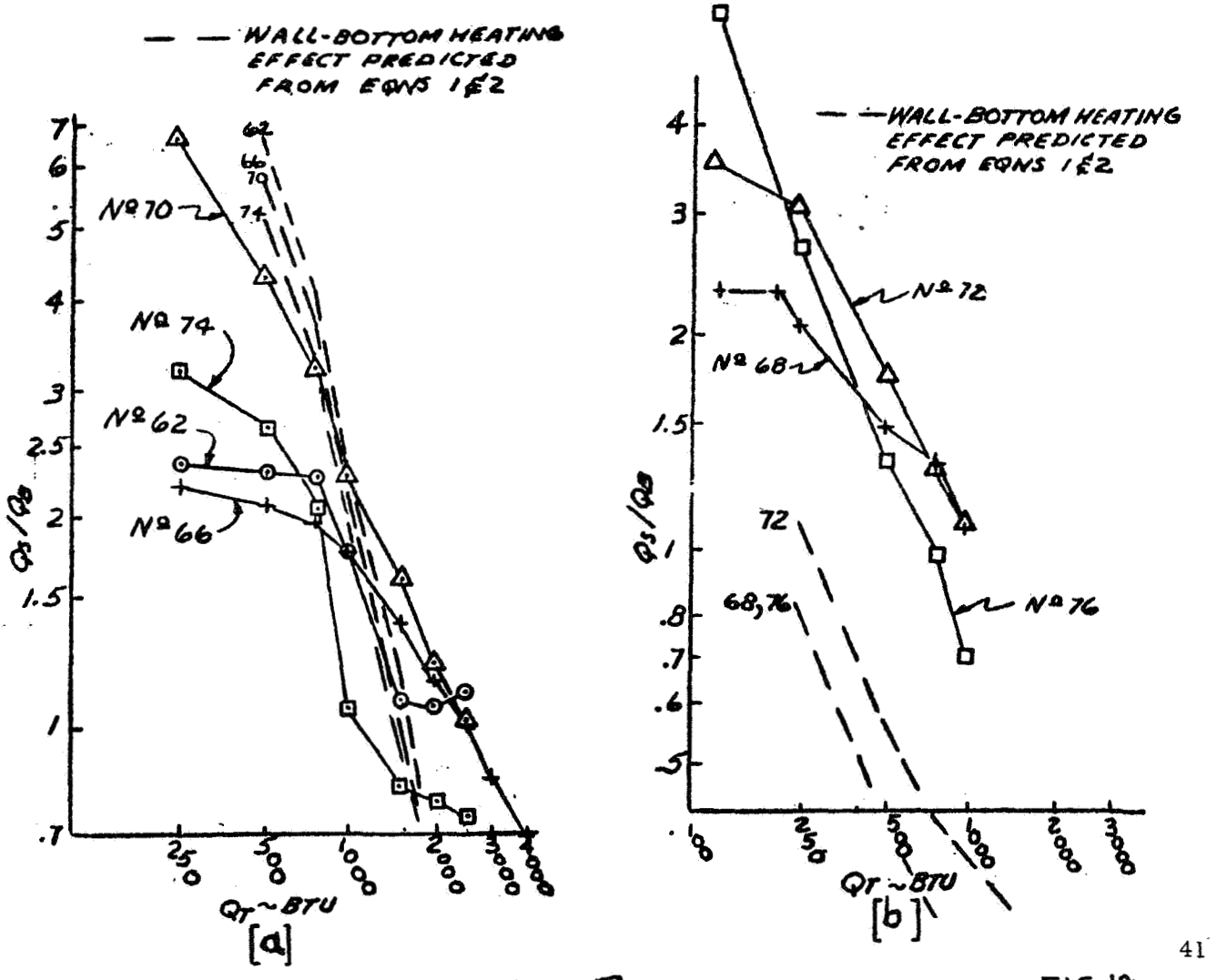
θ SEC	Qs/QB
30	1.695
90	1.501
120	1.188
240	1.123

TYP BAFFLE TEST
Δ VOL ~ TEMP PROFILES

FIG 9

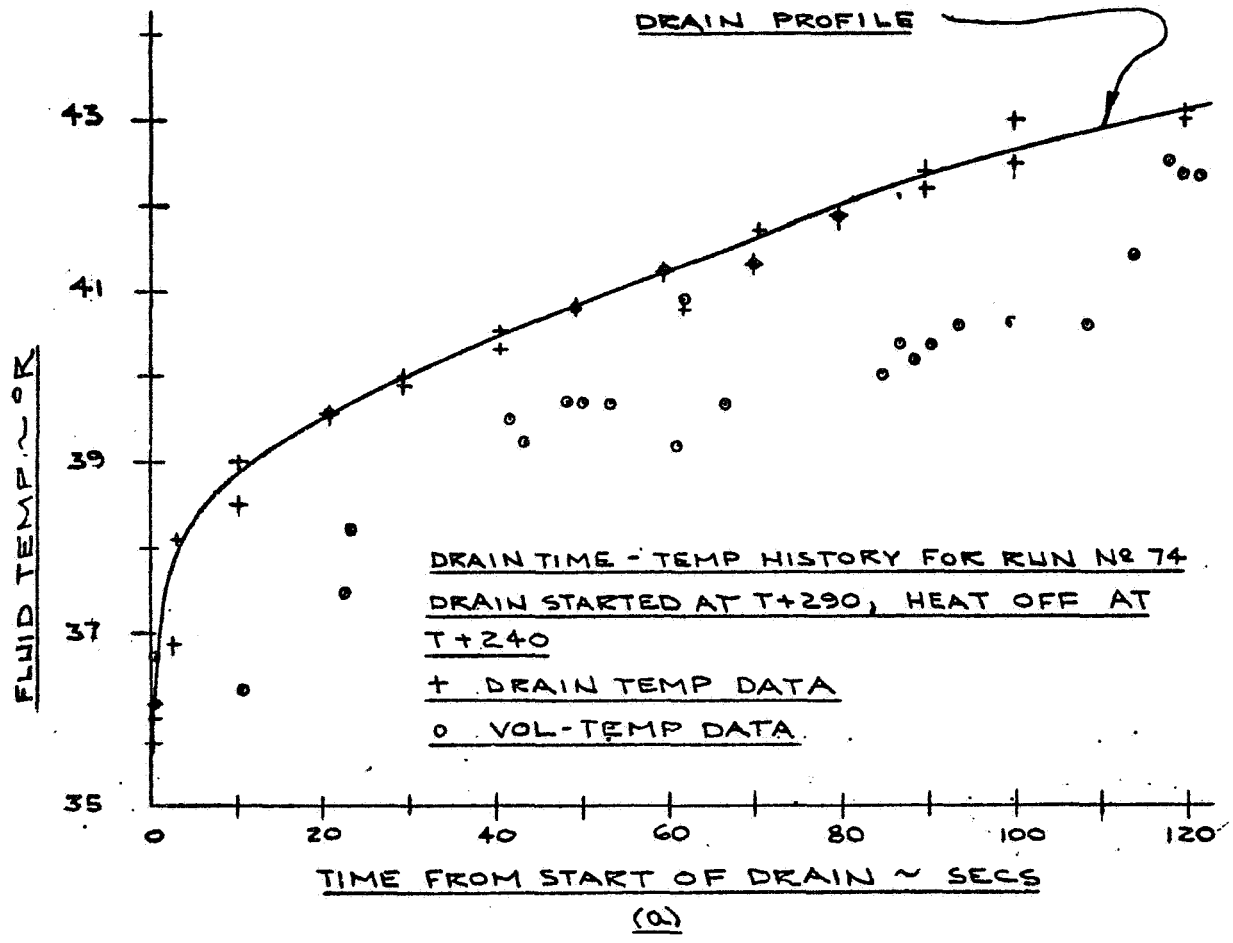
TEST Nº	Qw BTU/SEC	Qb/Qw	Nº BAFFLES	θ SECS @ Qr=240 BTU	BAFFLE HOLE DIA	π_2	SYM
62	8.1	.0301	1	240	7.5	.841	⊙
66	7.4	.0330	1	280	19.6	.582	+
70	7.4	.0332	1	250	33.4	.283	△
74	7.1	.0343	3	342	19.6	.582	⊡

TEST Nº	Qw BTU/SEC	Qb/Qw	Nº BAFFLES	BAFFLE HOLE DIA	π_2	SYM
68	1.51	.162	1	19.6	.582	+
72	1.82	.134	1	33.4	.283	△
76	1.53	.160	3	19.6	.582	⊡
77	1.56	.153	0	48	0	◇

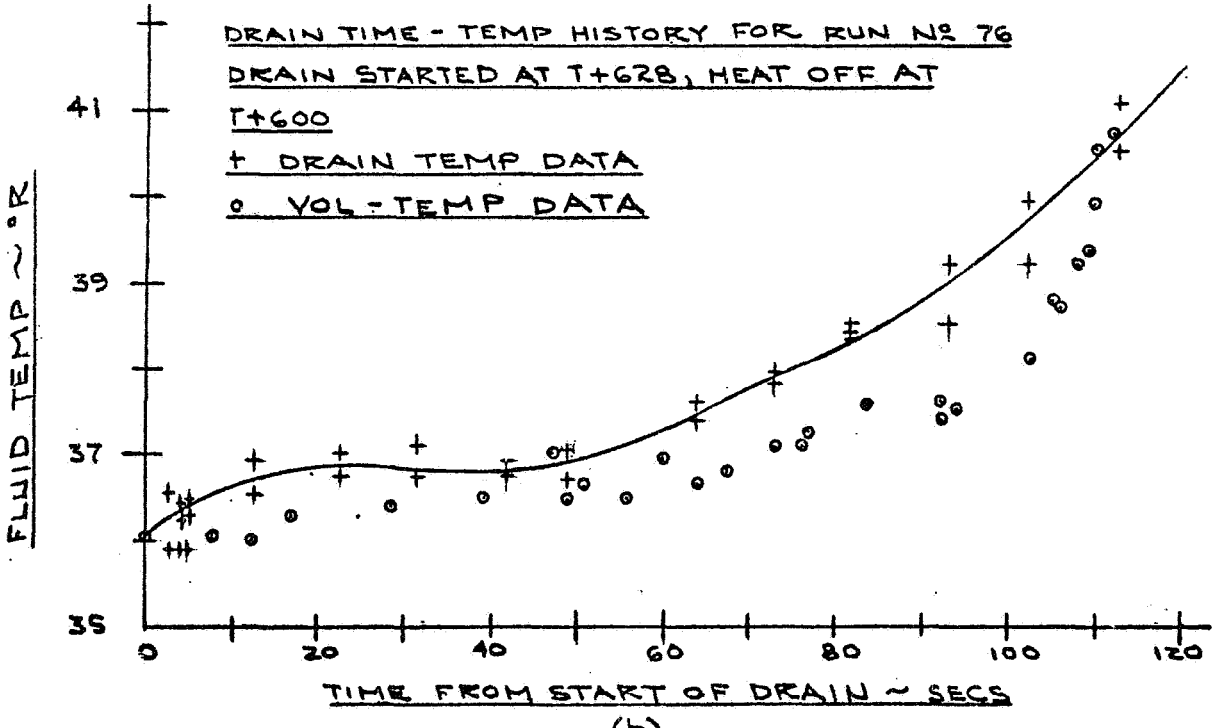


BAFFLE TEST RESULTS.

FIG 10


DRAIN PROFILE
43
41
39
37
35
FLUID TEMP ~ °K
0
20
40
60
80
100
120
TIME FROM START OF DRAIN ~ SECS
DRAIN TIME - TEMP HISTORY FOR RUN Nº 74
DRAIN STARTED AT T+290, HEAT OFF AT T+240
+ DRAIN TEMP DATA
o VOL-TEMP DATA

(a)


DRAIN TIME - TEMP HISTORY FOR RUN Nº 76
DRAIN STARTED AT T+628, HEAT OFF AT T+600
+ DRAIN TEMP DATA
o VOL - TEMP DATA
41
39
37
35
FLUID TEMP ~ °K
0
20
40
60
80
100
120
TIME FROM START OF DRAIN ~ SECS

(b)

FIG 11

STRATIFICATION REDUCTION BY MEANS OF BUBBLE PUMPS

by
D. C. Pedreyra
Martin-Marietta Corporation
Martin Company-Denver Division
Denver, Colorado

INTRODUCTION

Liquid temperature stratification in rocket vehicle cryogenic propellant tanks is usually undesirable because the hot liquid cannot be used unless the propellant tank pressure is increased to meet the minimum net positive suction head requirements of the engine pump. Therefore, to minimize tank pressure and vehicle weight it is necessary to mix the hot and cold liquids. Since any mixing apparatus must be adaptable to flight vehicles, simplicity and reliability are prime considerations. A properly designed bubble-lift-pump appeared to have promise of accomplishing the desired mixing action. A bubble-lift-pump achieves pumping action through the bouyancy of fluid whose density is reduced by injecting gas into the fluid.

During the execution of a NASA contract, NAS8-5208, a study of cryogenic propellants stratification reduction, a bubble-lift-pump was installed and operated in both liquid nitrogen and liquid hydrogen tanks. Since adequate bubble-pump design information was not available in the literature, it was necessary to study cryogenic bubble-pump characteristics with a sub-scale model before designing the full-scale pump. This paper describes the design and testing of the sub-scale bubble-lift-pump, as well as the pump used in the stratification reduction investigation. The effectiveness of the bubble-lift-pump as a stratification reduction device is discussed in a separate paper (Reference 1).

TECHNICAL DISCUSSION

At the outset a literature search failed to uncover previous theoretical or experimental work that could be used directly to design the bubble-lift-pump. Most of the previous work on bubble-lift-pumps has been concerned with air bubbles used to pump water in very long tubes. A typical example is the work of Nicklin (Reference 2). The airlift pump theory of Nicklin does not consider heat nor mass transfer between the bubble and the liquid. Since a bubble-lift-pump used with liquid hydrogen or liquid oxygen could involve considerable heat transfer (depending on the gas injection temperature), and a considerable amount of mass transfer due to the high liquid vapor pressure, these factors cannot be ignored.

Another factor that precludes direct application of Nicklin's work in the design of a bubble-lift-pump for this particular application in the assumption that the velocity of the gas relative to the liquid is constant throughout the length of the tube at

$$V_{\infty} = .35\sqrt{gD} \qquad (1)$$

where g is the acceleration of gravity and D is the diameter of the tube. Reference 3 indicates that the velocity of a given bubble relative to liquid is

$$V_b = V_{\infty}\left[1 + 8 \exp\left(-1.06\, L_s/D\right)\right] \qquad (2)$$

where V_{∞} is the fully developed velocity described in equation (1), L_s is the length of the liquid slug between the bubble and the preceding bubble, and D is the diameter of the tube. Equation (2) was derived

emperically from data obtained in an experimental program and shows that if the distance between bubbles is less than about 8 diameters, the bubble velocity is greater than the fully developed velocity given in equation (1). Since the performance of a bubble-pump is a function of velocity of the gas relative to the liquid this variation in gas velocity must be accounted for in any theoretical model that attempts to describe the performance.

Other experiments reported in Reference 3 indicate that the entrance effects in developing flow can extend for as much as 20 tube diameters from the entrance. The length to diameter ratios (L/D) of the bubble pumps used in the stratification program were considerable less than 20, indicating that the flow would not be fully developed before the bubble had traversed the entire length of the tube. For very long tubes with $L/D \gg 20$, the assumption that the gas velocity is described by equation (1) will not seriously limit the theoretical analysis.

The sub-scale pump was designed and tested to investigate the effects of heat and mass transfer, inlet gas momentum, and bubble velocity on the performance of the pump, and thereby determine the feasibility of using a bubble-lift-pump in the stratification reduction program.

SUB-SCALE PUMP

The sub-scale pump consisted of a 3 inch diameter tube 28 inches long flared at the lower end, and a gas injection tube installed in the lower end. The pump length was set by the size of the tank in which the pump was tested. The pump diameter was dictated by available tube sizes and the need for a length to diameter ratio similar to that of

the full-scale pump. Since it was necessary to measure liquid flow rate, a trough with a V-notch weir was attached to the upper end of the tube. Figure 1 shows the sub-scale pump with weir trough attached to the lid of the test dewar. Gas is introduced thru eigher a 0.040 inch or 0.25 inch orifice. The purpose of the two different sizes is to permit investigation of the effect of initial gas momentum on the performance of the pump.

Liquid levels in the trough and in the dewar were measured with thermistor point level sensors. The row of dewar level sensors with protective coverings can be seen in Figure 1. A square edge orifice flow section was used to measure the gas flow rate.

After the data from the first few tests with liquid nitrogen proved to be questionable, the pump was operated with water so that the flow issuing from the top of the riser could be visually observed. It was discovered that the liquid issuing from the riser was agitated so violently that a portion of it was being thrown clear of the trough, therefore, precluding an acurate liquid flow rate measurement through the weir. To correct this condition, a splash cap was installed over the pump riser tube, and a screen baffle installed upstream of the weir to provide uniform flow through the weir.

Initially the pump was tested with water at two different temperatures to determine the effects of liquid vapor pressure on pump performance. Then the pump was operated in both liquid nitrogen, and liquid hydrogen with ambient temperature helium injected through the 0.25 inch orifice. Finally the pump was operated in both liquid nitrogen and liquid hydrogen with helium injected through the 0.040 inch orifice. The data from these tests is given in Table I. The feasibility of a cryogenic liquid

bubble-lift-pump was demonstrated with the sub-scale pump; therefore, the full-scale pump was designed accordingly.

FULL-SCALE PUMP

The bubble-pump installed in the stratification reduction test tank shown in Figure 2 is 32 ½ inches long, 6 inches in diameter, and flared at the lower end. The diameter was selected so that at a flow rate of 0.5 ft^3/sec, the average liquid velocity would be low enough that the friction losses are negligible. The arbitrarily chosen flow rate of 0.5 ft^3/sec will circulate all the liquid in the stratification reduction test tank in two minutes. The length was dictated by the size of the test tank.

The liquid flow rate was measured with the six 60° V-notch weirs in the circular weir tray. The peculiar shape of the weir tray was dictated by the need to distribute the liquid uniformly at the periphery of a 4 ft. diameter tank. The liquid level sensors in the weir tray are located to sense the liquid levels for liquid flow rates of 0.05, 0.1, and 0.4 ft^3/sec which is the estimated range of flow rates to effect mixing in the stratification reduction tests. The liquid level in the tank is sensed by a series of level sensors placed ½ inch apart, starting 1 inch below the bottom of the weir tray and extending for 5 inches. A 0.040 inch diameter orifice was used in the end of the gas supply line located at the bottom of the riser tube.

Prior to installation of the pump in the test tank, the weirs were calibrated with water. This was accomplished by supplying facility water to the weir tray to the desired level, and weighting the water issuing from the weirs in a catch tank.

After the weirs had been calibrated, the gas supply line to the

bottom of the riser tube was installed, and the pump operated with water to determine the effectiveness of the riser tube splash cap (Figure 2) in maintaining uniform weir flow. Additional baffling was incorporated in the splash cap after these tests. Finally, the pump was tested with liquid nitrogen as shown in Figure 3. At the conclusion of these calibration and checkout tests, the bubble-pump was installed in the test tank. The full-scale pump test data is given in Table II.

DATA EVALUATION

In order for the data of Tables I and II to be of use in designing the pump for a full-scale flight vehicle some method of correlation must be utilized. The best method of correlation is a theoretical model that accurately describes the performance. As mentioned before, however, an adequate theoretical model apparently does not exist. Therefore, it was necessary to develop an emperical correlation. After considering a variety of different parameters, it was concluded that the dimensionless groups shown in Figure 4 provide the best correlation. These groups include the important parameters that would be expected to influence the performance of the pump. The diameter of the tube is incorporated in the liquid velocity factor of the abscissa. The band of data shown in Figure 4 encompasses all the sub-scale pump data points except for the tests in which hydrogen was pumped with helium injected through the 0.040 inch orifice. This was to be expected, since the momentum transfer from the high velocity helium gas to the liquid hydrogen in the riser tube would be a significant factor. Converting the momentum transfer to equivalent height of pumped liquid

$$h_m = \frac{\dot{m}V}{g_c \rho A},$$

where h_m = equivalent height of pumped liquid

$\dot{m}$ = weight gas flow rate

V_g = velocity of gas in injector

ρ = density of liquid

A = cross sectional area of riser tube

the resulting head (0.18 ft. for the sub-scale data of Figure 4) is significant when compared to the pump lift height (0.49 ft.). Adjustment of the data points in Figure 4 to include the momentum effects was not attempted due to the lack of sufficient data.

To convert the gas weight flow rates of Tables I and II to the volumetric flow rate G used in the dimensionless group of Figure 4, the gas density must be known. This gas density is a function of both the heat transfer from the bubble to the liquid, and the mass transfer rate of liquid vapor into the bubble. Accurate prediction of the gas density as a function of location in the riser tube is very difficult. To simplify the problem the gas density was estimated by assuming simple free convection from the bubble surface to the gas within the bubble, zero mass transfer, and a uniform spherical bubble whose diameter is 2/3 the diameter of the tube. The assumption of free convecti should not seriously limit the analysis since there are no forced convection currents within the bubble. However, the assumption of zero mass transfer will introduce an error, but it may not be of major significance because the error will be essentially the same for all gas flow rate calculations, and would only result in an upward or downward displacement of Figure 4 by the same amount. The assumption of constant bubble size is justified by the fact that although the volume

of the bubble tends to decrease due to the temperature drop, its size will increase due to the coalescence of bubbles as they rise in the tube. Using the above assumptions together with the simplified gas velocity obtained from equation (1) it was determined that the gas would not reach the liquid temperature before it had traversed the entire length of the riser tube. Isc, the gas cooling rate for the conditions of interest is relatively independent of the liquid properties; i.e. liquid nitrogen or liquid hydrogen. In view of the foregoing, the density of the gas in the riser tube was assumed to be constant, and equal to the calculated value at the vertical mid-point of the tube. The gas densities that were actually used for each calculation are given in Tables I and II, along with other pertinent data used to calculate the dimensionless groups of Figure 4.

The full scale data does not appear to correlate with the dimensionless groups shown in Figure 4. There are two possible explanations for the scatter of data. First, the tank liquid level measurements for the full-scale pump were taken at ½ inch increments, which can introduce a 10% error in lift height. Secondly, the actual level to which the liquid rises inside the splash cap of the riser is unknown. The effective lift height of the liquid is greater than the level in the weir tray, but the amount of this difference is not known. The weir tray liquid level was used as the lift height because no better measurement was available. Since the sub-scale data seemed to correlate fairly well, the failure of the full scale data to correlate is thought to be due to the low quality of the data not the inadequacy of the correlation.

In spite of the experimental errors and differences in length-to diameter ratios, the correlation shown in Figure 4 could be used for preliminary design of cryogenic bubble-lift-pumps. Development of a theoretical model which includes the effects of mass transfer, heat transfer, and variable bubble velocity should yield a more precise design tool than the emperical correlation shown here, but the additional effort required was not justified in the program. A demonstration of the feasibility of a bubble-lift-pump for stratification reduction was the prime consideration, not the optimization of bubble-lift-pump design.

CONCLUSIONS

The performance of cryogenic liquid bubble-lift-pumps of small L/D is difficult to predict due to the complication of mass transfer, heat transfer and variable bubble velocity. Tests of two different sizes of pumps indicate that a bubble-lift-pump can be used satisfactorily to pump a cryogenic liquid, and that preliminary design and performance predictions can be accomplished with the aid of the correlation presented in Figure 4.

REFERENCES

1. Neff, B. D. "Experimental Studies of Stratification Reduction" Section Report 0560-64-19, September 1964, Martin Company, Denver, Colorado.

2. Nicklin, D. J. "The Air-lift Pump: Theory and Optimisation" Transaction of the Institution of Chemical Engineers, Vol. 41, 1963.

3. Moissis, R., Griffith, P. "Entrance Effects in a Developing Slug Flow", Tech Report No. 18, M.I.T., June 1960.

TABLE I

SUB-SCALE BUBBLE PUMP TEST DATA

Liquid	Gas	Injector Size Inches	Lift Height h Inches	Liquid Flow Rate ft^3/sec	Gas Flow Rate lb/sec	Average Density of Gas in Riser lb/ft^3	Average Volumetric Gas Flow Rate in Riser ft^3/sec	Liquid Vapor Pressure psia
127°F Water	Nitrogen	0.25	4.44	0.0073	0.00119	0.053	0.0227	2.05
			6.38	0.0385	0.00457		0.0871	
			5.69	0.0232	0.00283		0.0538	
			6.44	0.0385	0.00490		0.0932	
			4.65	0.0425	0.00339		0.0645	
			2.94	0.0089	0.00067		0.0127	
			4.89	0.0450	0.00381		0.0450	
183°F Water			2.88	0.0073	0.00030	0.048	0.0063	8.02
			4.31	0.0271	0.00108		0.0225	
			5.13	0.0450	0.00212		0.0441	
			3.28	0.0097	0.00042		0.0086	
			5.06	0.0400	0.00205		0.0426	
			4.94	0.0089	0.00079		0.0164	
			6.22	0.0278	0.00172		0.0357	
			5.19	0.0089	0.00090		0.0187	
			6.48	0.0285	0.00200		0.0415	
Nitrogen	Helium	0.040	4.39	0.0089	0.00017	0.022	0.0077	12.00
			5.88	0.0089	0.00047		0.0214	
			6.34	0.0089	0.00053		0.0238	
			5.60	0.0465	0.00101		0.0458	
			5.86	0.0465	0.00122		0.0554	
			6.11	0.0465	0.00123		0.0568	
			6.36	0.0465	0.00133		0.0604	
			4.39	0.0089	0.00039		0.0177	
Hydrogen			5.60	0.0465	0.00042		0.0191	
			5.86	0.0465	0.00048		0.0217	
			6.11	0.0465	0.00050		0.0229	
			4.39	0.0089	0.00025		0.0114	
			6.86	0.0465	0.00045		0.0202	
			5.39	0.0089	0.00030		0.0137	
			4.89	0.0089	0.00033		0.0150	
Nitrogen	Helium	0.25	5.39	0.0089	0.00033		0.0149	
			5.64	0.0089	0.00036		0.0165	
			5.60	0.0465	0.00108		0.0491	
			6.36	0.0465	0.00130		0.0588	
			6.61	0.0465	0.00151		0.0684	
			6.86	0.0465	0.00157		0.0710	
			4.89	0.0089	0.00043		0.0194	
			5.14	0.0089	0.00045		0.0204	
Hydrogen			7.36	0.0465	0.00150		0.0681	
			5.89	0.0089	0.00065		0.0295	
			6.86	0.0465	0.00133		0.0602	
			7.36	0.0465	0.00147		0.0668	
			7.61	0.0465	0.00157		0.0711	
			6.14	0.0089	0.00068		0.0306	
			6.14	0.0089	0.00072		0.0326	

NOTE: Test vessel pressure 11.7 psia for all tests.

TABLE II

FULL-SCALE BUBBLE PUMP TEST DATA

Liquid	Tank Pressure P lb/in^2 Abs.	Liquid Vapor Pressure P_v lb/in^2 Abs.	Lift Height h in.	Gas Flow Rate m lb/sec	Average Gas Density in Riser ρ_g lb/ft^3	Average Volumetric Gas Flow Rate in Riser G ft^3/sec	Volumetric Liquid Flow Rate $_3$LQ ft^3/sec
Hydrogen	41.7	12.0	5.28	0.00342	0.084	0.0407	0.05
	41.7	17.5	4.28	0.00234	0.084	0.0278	0.05
	41.7	23.7	3.78	0.00160	0.084	0.0191	0.05
	41.7	14.7	4.77	0.00335	0.084	0.0399	0.10
	41.7	19.3	4.27	0.00285	0.084	0.0340	0.10
	41.7	13.8	5.28	0.00329	0.084	0.0392	0.05
	41.7	17.0	3.78	0.00215	0.084	0.0256	0.05
	41.7	21.1	2.78	0.00167	0.084	0.0199	0.05
	41.7	15.2	3.78	0.00217	0.084	0.0258	0.05
	41.7	23.3	2.78	0.00135	0.084	0.0161	0.05
	41.7	13.8	3.78	0.00125	0.084	0.0149	0.05
	41.7	15.2	3.53	0.00155	0.084	0.0185	0.05
	41.7	18.1	2.78	0.00155	0.084	0.0185	0.05
Nitrogen	41.7	19.9	3.78	0.00260	0.084	0.0309	0.05
	41.7	25.7	2.78	0.00196	0.084	0.0137	0.05
	26.7	13.3	4.27	0.00296	0.054	0.0548	0.1
	26.7	16.4	4.27	0.00228	0.054	0.0421	0.1
	26.7	12.5	3.78	0.00222	0.054	0.0411	0.05
	26.7	13.0	3.78	0.00203	0.054	0.0376	0.05
	26.7	14.3	3.78	0.00138	0.054	0.0255	0.05
	26.7	15.6	3.78	0.00110	0.054	0.0204	0.05
	26.7	15.5	3.78	0.00095	0.054	0.0175	0.05
	26.7	18.7	3.78	0.00053	0.054	0.0096	0.05
	26.7	13.4	3.78	0.00148	0.054	0.0274	0.05
	26.7	15.9	3.78	0.00108	0.054	0.0200	0.05

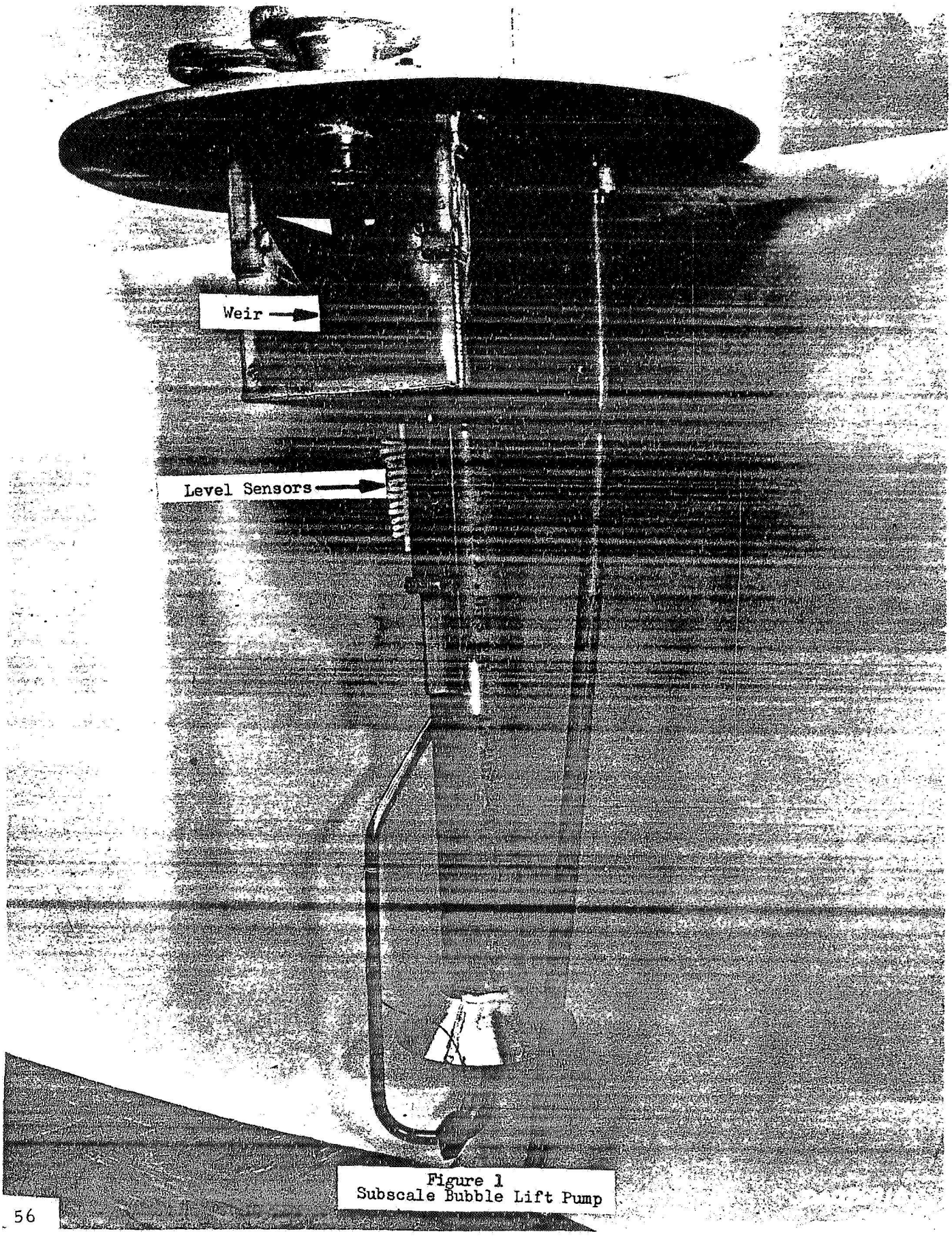


Figure 1
Subscale Bubble Lift Pump

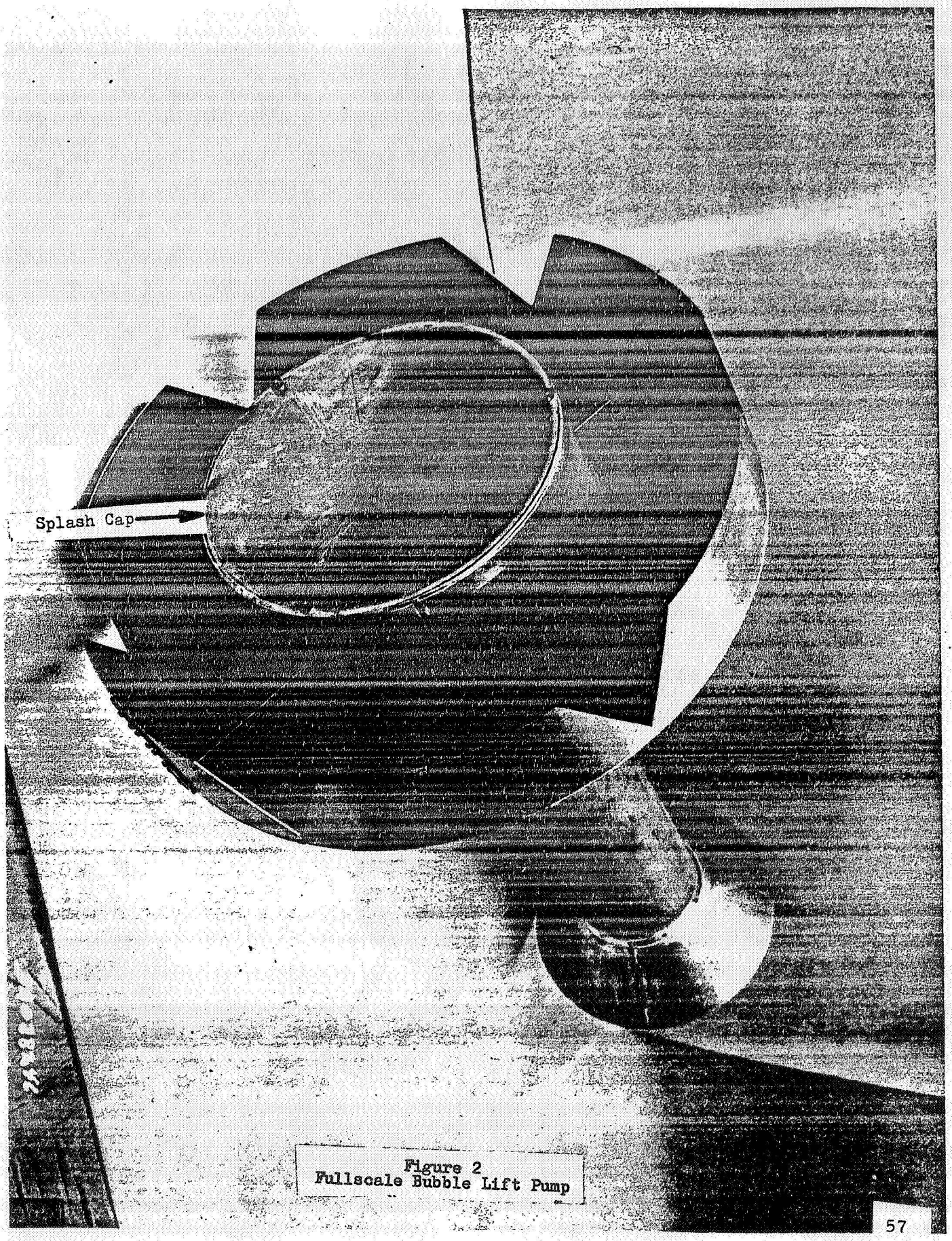


Figure 2
Fullscale Bubble Lift Pump

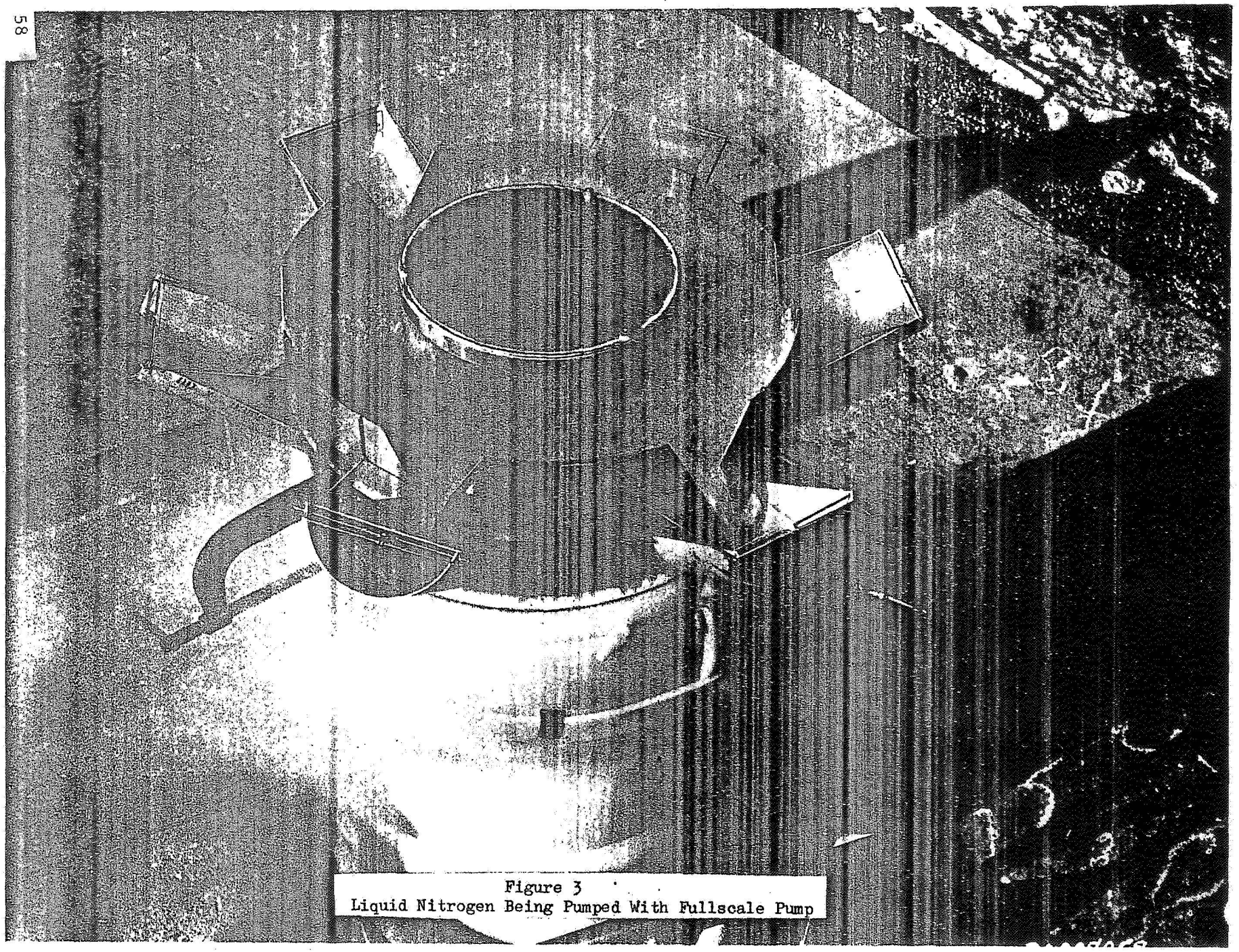


Figure 3
Liquid Nitrogen Being Pumped With Fullscale Pump

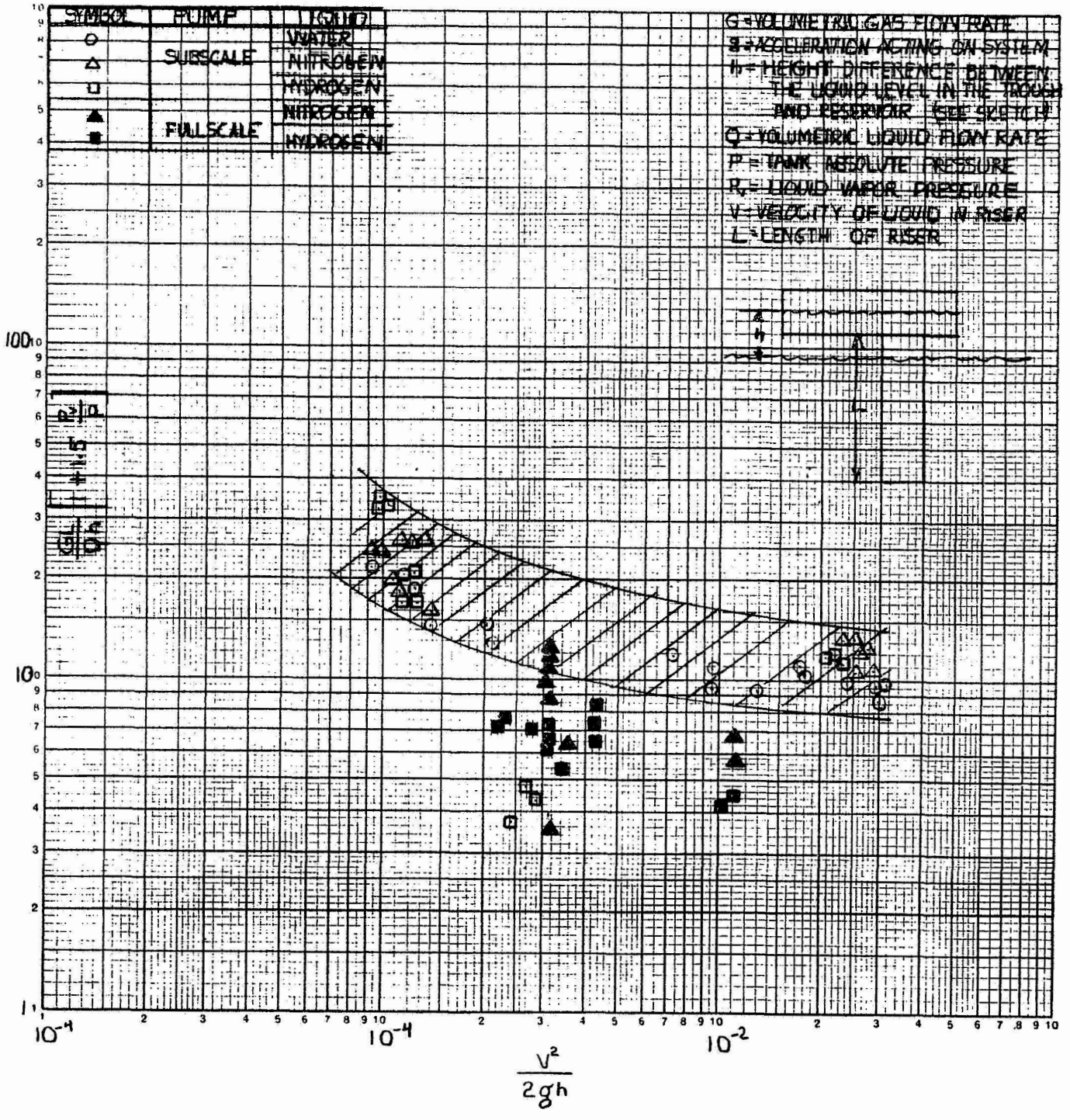


FIGURE 4 BUBBLE PUMP TEST DATA CORRELATION

EXPERIMENTAL INVESTIGATION OF THE EFFECTS OF BAFFLES ON NATURAL CONVECTION FLOW AND ON STRATIFICATION

by
C. C. Vliet and J. J. Brogan
Lockheed Missiles and Space Co.
Pala Alto, California

Preceding page blank

EXPERIMENTAL INVESTIGATION OF THE EFFECTS OF BAFFLES ON NATURAL CONVECTION FLOW AND ON STRATIFICATION#

G. C. Vliet* and J. J. Brogan**
Lockheed Missiles and Space Co., Palo Alto, Calif.

Abstract:

13026

The results of a study on the effect of baffles on natural convection flow and on stratification are presented. This study, which is expected to be applicable to cryogenics, was performed with water rather than a cryogen in a two-dimensional vessel to facilitate optical methods for determining the nature of the flow. Visual studies using a Schlieren apparatus and temperature measurements using thermocouples were performed. Two geometries: a vessel with only heated vertical walls and a vessel with a heated vertical wall and a heated inclined bottom, were considered.

Baffles on heated vertical walls were only partially effective in reducing stratification. The effectiveness decreases with time and increases with the number and size of baffles. The Schlieren studies showed that initially the baffles effectively divert the natural convection flow but later the flow reattaches to the wall above the baffle making the baffle ineffective.

In the inclined plate studies significant stratification results only when the ratio of bottom to wall heat flux is less than or equal to 1, but when this ratio is 2 or greater there is little stratification. Schlieren studies indicate that baffles on the bottom have a pronounced effect on the natural convection flow but there is little effect on the ultimate stratification.

Author

#This work was supported by NAS 8-5600.

* Research Scientist - Aerospace Sciences Laboratory

** Head, Cryogenic Propulsion Systems
Large Space Vehicle Program.

EXPERIMENTAL INVESTIGATION OF THE EFFECT OF BAFFLES ON NATURAL CONVECTION FLOW AND ON STRATIFICATION

G. C. Vliet and J. J. Brogan
Lockheed Missiles and Space Co., Palo Alto, Calif.

I. INTRODUCTION

The thermal energy absorption by liquid propellants of space vehicles results in a weight penalty which occurs from either* a loss of vaporized propellant or an increase in tank weight required to contain the warmer propellant. The magnitude of the latter penalty increases with the severity of the liquid propellant temperature variation. Various methods for predicting stratification have been developed (Refs. 1 & 2) and it is a logical next step to examine and evaluate methods of reducing stratification.

Various methods, both active and passive, have been proposed to reduce stratification and one of these, a passive method, is the use of anti-stratification baffles. An experimental study has been conducted to determine the effect of baffles on natural convection flow and on stratification. These studies include the use of the Schlieren and shadowgraph techniques to visualize and assist in interpreting the natural convection flow, and also actual temperature measurement using thermocouples to determine the magnitude of stratification. These studies were performed in a small two-dimensional laboratory scale apparatus using water as the test fluid. It was not the intent nor was it possible to scale the fluid dynamics of these tests to the typically large space vessels containing cryogenic fluids but rather to gain a greater understanding of the effects of baffles with the intention that they may later be applied to a large space vessel if proved attractive. The use of water, although not a cryogenic fluid, in the small two-dimensional vessel permitted numerous geometry and test conditions to be investigated easily.

II. EXPERIMENTAL APPARATUS

The experimental tests were performed in a glass tank 15 inches high, 12 inches wide and 6 inches deep (depth of field). Within this vessel, 6 inch wide electrical resistance heater plates** (uniform heat flux) were positioned to obtain the desired geometry. In the first series of tests (Vertical Plate Tests) two vertical $10\frac{1}{2}$ high plates were positioned 6 inches apart to form the two-dimensional vessel shown in Figure 1(a). Baffles 6 inches long and of various widths were placed horizontally against each of the heater plates. In the second series (Inclined Plate Tests) one 8 inch high plate was placed vertically above the top end of a 6 inch long inclined plate, the bottom end of which was against one end

*Actually an optimum weight penalty may be obtained by a combination of venting plus increasing tank weight to withstand the additional pressure rise.

**One mil stainless steel shim stock was used as the resistance heating element.

of the tank. See Figure 1(b). This configuration formed one-half of a two-dimensional vessel with a wedge shaped heated bottom. In the inclined plate tests, baffles were placed on the heated inclined plate. In each series of tests the tank was filled with water to the top(s) of the heated vertical plate(s) and d.c. power supplies were used to resistively heat the plates.

Temperature measurements were made with a probe of 12 copper-constantan thermocouples and a precision 6 channel microvolt recorder. In the vertical plate tests the thermocouple probe was positioned vertically in the center of the vessel. In the inclined plate tests the thermocouple probe was positioned vertically midway between the glass walls and approximately 1/3 the distance (2 inches) up the inclined plate as shown in Figure 1(b). The visual observations were made using both the Schlieren and shadowgraph techniques using a mercury lamp as a light source.

III. EXPERIMENTAL RESULTS & DISCUSSION

The initiation of stratification in these laboratory tests is somewhat differe than most cases encountered with a cryogenic propellant. Ordinarily the vessel containing the cryogenic liquid is vented prior to stratification and a natural convection boundary layer flow is established at the time the vent is closed and stratification begins. In these laboratory tests the liquid is initially stagnant and stratification begins with the heating of the wall whic has an inherent transient associated with it. It is felt, however, that the effect of this initial transient is quickly erased as stratification progresse

A. Vertical Plate Tests

1. Temperature Profile Measurements:

Vertical temperature profiles were measured in the absence of baffles and for the several baffle configurations listed below:

(1) One baffle at mid-height on each wall ($\frac{1}{4}$, $\frac{1}{2}$, 1 and 2" wide baffle)

(2) Two baffles on each wall dividing plate in thirds ($\frac{1}{2}$, $\frac{1}{4}$, 1 and 2" wide baffles)

(3) 5 Staggered 1" baffles (2 on one wall and 3 on the other).

(4) Combination of one 1" and one 2" baffle on each wall.

(5) Two curved baffles on each wall (1" radius).

These tests were performed with water and for wall heat fluxes in the range 0.5 to 1.0 Btu/ft^2 hr which corresponds to a modified Rayleigh number of $\sim 10^{12}$.

The vertical temperature distribution for the test without baffles is presented in Figure 2 with time the parameter. It is seen that before the stratified region reaches the bottom, the second derivative of temperature is positive whereas later it becomes negative.

The vertical temperature distributions for four specific baffle configurations are compared to the case without baffles in Figures 2 and 3 with time the parameter. Figure 2 for one baffle at the mid-point of each wall, and Figure 3 for two baffles on each wall show only the cases of $\frac{1}{4}$ inch and 2 inch baffles. The profiles of all the remaining cases measured are not presented because they are similar to and fall within the range of these four cases presented herein.

In comparing the temperature profiles in the presence of baffles to the profiles in the absence of baffles in Figure 2 and 3 it is seen that the temperature profiles are not seriously altered by the presence of baffles. The baffles have their greatest effect in causing energy to be mixed into the lower regions of liquid initially. Later the effect is less pronounced. Even at early stages of stratification the surface temperature is little affected by baffles because the temperature gradient near the surface generally steepens with baffles present, apparently due to the shorter boundary layer run with the baffle present.

2. Baffle Effectiveness:

Considering that it is desirable to maintain as nearly a uniform liquid temperature as possible, a measure of the severity of stratification is the temperature moment about the bottom of the vessel:

$$M_T = \int_0^H (T-T_i)x\,dx$$

Where $T \triangleq$ liquid temperature; $T_i \triangleq$ initial uniform liquid temperature; $x \triangleq$ axial height and H is the tank height. However, to compare the effectiveness of a baffle this temperature moment will be first made dimensionless with respect to the uniformly mixed case:

$$M_T^* = \frac{M_T - \frac{1}{2}\bar{T}H^2}{\frac{1}{2}\bar{T}H^2}$$

where $\bar{T} \triangleq$ the average liquid temperature. The baffle effectiveness parameter will be based on a comparison of the dimensionless temperature moment with a baffle to the dimensionless temperature moment without a baffle:

$$E = 1 - (M_T^*/M_{T_n}^*)$$

which on rearrangement becomes:

$$E = \frac{M_{T_n} - M_T\,(\bar{T}_n/T)}{M_{T_n} - \frac{1}{2}\bar{T}_nH^2}$$

where the subscript "n" refers to the "no" baffle case.

This parameter has the following significance:

(1) when zero, the baffle is completely ineffective.

(2) when 1.0, the baffle results in a uniform temperature (i.e. completely effective)

(3) if asymptotic temperature shapes are approached with and without a baffle, then the parameter also approaches an asymptotic value.

(4) if negative the baffle is deleterious (this is unlikely).

The baffle effectiveness is plotted in Figure 4 only for the case of two baffles of various sizes on each wall. This figure shows that wall baffles are only moderately effective in reducing stratification. In the early stages they are most effective but the effectiveness decreases with time, appearing to approach an asymptote. For the case of one baffle on each wall the asymptote was approached much quicker and was smaller in magnitude. Even the best configurations indicate an effectiveness of only 20 percent at later stages. In general the effectiveness increases with number and size of baffles, the best configuration tested being two 2" baffles on each wall.

An empirical correlation of the baffle effectiveness for the cases of one or two baffles of various sizes on each wall is shown in Figure 5. This correlation suggests:

$$E = 0.25\left[1 + 2.2e^{-0.15\,\theta/N}\right]\left(\frac{B}{W}\right)^{0.5}(N)^{0.5}$$

where N = no. of baffles, B/W is the ratio of baffle width to tank width and θ is measured in minutes.

3. Visual Studies:

A series of Schlierin movies were taken showing the nature of the natural convection flow in the absence of baffles and in the presence of several sizes of wall baffles. In Figures 6 through 8 the field is 8 inches diameter showing the top 7 inches of the vessel. The liquid surface is near the top, a heated vertical wall is seen on either side and the baffles used in Figures 7 and 8 are against the wall near the bottom of the field. The light areas represent regions of positive temperature gradient in the vertical direction.

In the absence of baffles (Figure 6) the stratification process is seen to initiate with a rather large surface flow from each plate which meets at the vessel center and forms a downward moving warm plume. The plume is quickly arrested by buoyant effects and then spreads out to form a thermally stratified layer. Following this initial transient, stratification progresses in a smoother manner

as the stratified layer grows with the supply at its base of warm boundary layer liquid. The rather thick boundary layer on entering and traversing the stratified region is observed to thin considerably as it gives up mass to the stratified region. The stratified layer continues to grow in thickness until it reaches the bottom of the vessel. A more detailed description of the mechanism of stratification appears in Reference (3).

The reason for the relatively low effectiveness of wall baffles is better understood from the Schlierin movies for $\frac{1}{2}$ inch baffles shown in Figure 7 and 2 inch baffles in Figure 8. The interpretations of the flow phenomena in the presence of baffles as observed in the Schlierin studies are illustrated in the sketches of Figure 9. In the initial stages of stratification the boundary layer below the baffle on encountering the baffle is effectively diverted, causing it to flow out into the bulk liquid where it mixes as it flows upward, as shown in Figures 9(a). The result is that initially a significant portion of this warm boundary layer liquid is mixed into the cooler bulk liquid. However, as the stratified layer near the surface grows due to the boundary layer flow above the uppermost baffle, the height to which the ejected boundary layer liquid will rise decreases as illustrated in Figure 9(b), since it is arrested by the warmer stratified layer. As the stratified layer nears the baffle, the natural convection flow from the baffle is drawn in toward the vertical wall above the baffle due to entrainment by the boundary layer forming on the wall above the baffle. At this point, the natural convection flow is soon no longer ejected by the baffle but rather flows around the baffle, reattaches to the wall and flows upward as shown in Figure 9(c). In general, the stratification progresses toward the bottom of the vessel making successive baffles ineffective as each baffle is approached, and the temperature profile created in the vessel results in a thin, slowly moving boundary layer. There is progressively less effect of the baffle on the flow, as the degree of turbulence observed immediately above the baffle decreases with time. The boundary layer flows around the baffle and attaches to the wall with little apparent mass or energy exchange with the bulk liquid.

In general the larger the baffle the longer it takes for the flow to reattach to the wall. For the $\frac{1}{4}$ inch baffles the reattachment occurred almost immediately while for the $\frac{1}{2}$ and 1 inch baffles reattachment took approximately 3 and 6 minutes respectively and for the 2 inch baffles the flow didn't reattach over the 10 to 15 minutes duration of the test. However, even in this latter case there was only a small effect of the baffle on the ultimate temperature profiles as is seen in Figure 3.

Curved baffles were also found to be quite ineffective in reducing stratification. Instead of turning the boundary layer and ejecting it downward the under portion of the baffle merely fills with warm liquid which thereafter acts like a flat baffle and the boundary layer moves horizontally outward. At later times the boundary layer reattaches to the wall above the baffle as in the case of a flat baffle. A curved baffle is apparently ineffective in turning the boundary layer flow downward since much of the kinetic energy in the boundary layer is lost in viscous shear.

Similar results are anticipated in larger vessels if the baffles are scaled to vessel dimensions. The time scale will necessarily change since stratification rate is a function of vessel dimensions, Reference (4).

B. Inclined Plate Tests

1. Effect of Plate Inclination:

The major portion of the inclined plate tests were performed for an inclination of 45 degrees with the horizontal, however a few tests were made at varying plate inclination to determine this effect on stratification. The measured temperature profiles for bottom plate inclinations of 45, 22, 11, and 0 degrees with the horizontal are plotted in Figure 10 in non-dimensional form since the heights of the vessels varied among the tests. The vertical height is made dimensionless with the liquid height and the temperature difference is made dimensionless with the difference between the surface and initial temperature. The profiles shown in Figure 10 are all for the case where the bottom and wall heat fluxes are the same and equal to 0.9 Btu/ft^2 sec and at 20 minutes after start of heating. Note that in the case of the zero inclination, two heated vertical $10\frac{1}{2}$ inch walls, separated by an 8 inch heated bottom, were used as compared to the other three cases. It is seen that as the plate angle decreases the temperature measurements show an increasing tendency toward profiles which are composed of a uniform temperature region below and a stratified layer above. The non-dimensional profiles for the 22 and 11 degree inclinations are essentially the same as the case of horizontal bottom. The case of 45 degree inclination is seen to deviate from this shape somewhat.

Visual studies using both the Schlieren and shadowgraph show that there is definite natural convection flow "along" the inclined heated plate but that the thickness of the flow increases with decreasing angle until when horizontal the energy flux through the bottom simply mixes into the lower portion of the liquid causing it to have an essentially uniform temperature. The ratio of the depth of this uniform temperature region to the liquid height is approximately equal to the ratio of energy entering the bottom to the total energy entering the vessel.

2. Effect of Heat Flux Ratio:

For the case of a 45° inclined bottom the ratio q* of bottom heat flux to wall heat flux was varied from 0.5 to 5 to determine its effect on stratification. Figure 11 compares the measured temperature profiles for the three heat flux ratios, $q^* = 0.5$; 1.0 and 2.0. There is essentially no stratification for $q^* = 2.0$ (and greater) and the degree of stratification becomes increasingly important as the ratio decreases.

The lack of stratification for q* equal to 2.0 and greater is apparently due to the large entrainment of liquid from the bottom into the boundary layer on the inclined bottom resulting in a low average temperature of the boundary layer when it reaches the surface. This effectivity represents a rapid recirculation rate of the liquid resulting in a small temperature difference from top to bottom. Anderson (5) shows temperature profiles for a similar geometry but with radiant heating of the liquid in the lower region of the vessel. The profiles exhibit a uniform temperature in the lower portion and a stratified layer above. For these tests the ratio of the total energy absorbed due to radiant heating to total wall heating was varied from approximately 0.4 to 1.7. A stratified layer was observed in all cases but became less pronounced as the ratio increased.

3. Effect of Heat Flux Level:

Tests were conducted for similar heat flux ratios but for heat fluxes one order of magnitude less, and it was found that the same conclusions on the effect of heat flux ratio could be drawn. This suggests that the relative absence of stratification for $q^* \geq 2.0$ is not due to the heat flux magnitude, at least in this range.

4. Effect of Baffles Placed on Inclined Plate:

Since there was observed to be little stratification for heat flux ratios of 2.0 or greater there is little to be gained by using baffles under such conditions. The experimental measurements presented in this section on the effect of baffles are for the case of a 45 degree bottom and for the case where stratification was significant without baffles, namely, for $q^* \simeq 1.0$.

Several tests were performed for $q^* \simeq 1.0$ using baffles in an attempt to reduce stratification. Two of these cases:

(i) two 1 inch baffles perpendicular to the inclined bottom,
(ii) two $\frac{1}{2}$ inch baffles perpendicular to the inclined bottom,

are compared to the case of no baffles in Figure 12 at three times (10, 20 and 30 minutes) after start of heating. The heat rates are seen to be approximately the same but not identical in the three cases as is evident by the areas under the profiles.

The baffles are seen to have very little effect on the ultimate stratification as is evident from Figure 12. The small effect they do have is to create a more uniform temperature region near the bottom of the vessel than for the case without baffles. This is similar to the case of a heated horizontal bottom and heated vertical wall as in Figure 10 where the two very distinct regions are evident. A similar conclusion resulted for the various tests performed with other baffle configurations on the bottom.

5. Visual Studies:

The effect of baffles on the natural convection flow along the heated inclined bottom was studied with both the Schlieren and shadowgraph methods.

It was felt that to be effective in reducing stratification the baffle should divert the natural convection flow along the inclined surface out into the bulk liquid. Shadowgraph pictures presented in Figure 13 show how well this is accomplished by various baffle sizes and orientations. All cases are for $q''_b = 4\ q''_w = 2.4$ Btu/ft^2 sec.* and a 45° inclined bottom. Figure 13(a) shows the flow in the absence of baffles while Figures 13(b), 13(c), and 13(d) for $\frac{1}{2}$ and 1 inch baffles respectively show the influence of baffle size on the flow for the case of two baffles perpendicular to the inclined wall. It is seen that the baffle must be greater than $\frac{1}{2}$ inch to effectively divert the flow. Since the boundary layer thickness appears to be between $\frac{1}{2}$ and 1 inch these pictures indicate that the baffle must be at least as high as the boundary layer thickness to effectively divert the flow. Three 1 inch perpendicular baffles shown in Figure 13(e) appear to be less effective. It was found that baffles placed perpendicular to the flow were more effective than vertical baffles as seen by comparing Figures 13(c) and 13(f).

It should be noted that although the visual studies indicate certain baffle sizes and orientations to be quite effective in diverting the flow outward into the bulk liquid, the temperature measurements indicate that this is not effective in reducing stratification. That similar profiles result with and without baffles in the bottom is interpreted in the following manner: with baffles in the bottom a boundary layer forms on the vertical walls creating the usual stratified region and the energy entering the bottom is mixed by turbulent action into the unstratified fluid, similar to the case of a heated flat bottomed vessel. In the absence of baffles there is a gross fluid circulation in the vessel due to the natural convection flow along the heated inclined bottom of the vessel. However, the average temperature increase of this fluid is small (due to the large circulation rate) and the circulation is therefore confined to the region below the stratified fluid which is formed by fluid of higher average temperatures in the boundary layer near the vertical wall. A similar temperature profile therefore results with the minor difference that in the latter case there is a very shallow temperature gradient in the "unstratified" region.

Similar results are expected in larger vessels but additional tests on larger scale vessels are advised. Furthermore, baffles in the bottom of a draining vessel may have merit and should be investigated.

---

*A similar flow field was observed for the case where $q^* = 1.0$.

CONCLUSIONS

Baffles on heated vertical surfaces are found to be only moderately effective in reducing stratification, and mainly early in time. Their effectiveness decreases with time and increases both with number and size of baffles. The degree of stratification in vessels with heated bottoms is a function of the ratio of bottom to wall heat fluxes, decreasing as this ratio increases. Baffles on inclined bottom surfaces of heated vessels effectively alter the fluid dynamics but are found to be ineffective in reducing stratification. When baffles are scaled to vessel dimensions similar results are expected in larger vessels, however the time scale will be different since stratification rate is a function of vessel size. Similar stratification reduction tests in larger vessels for confirmation of these conclusions as well as an investigation of the influence of baffles in the bottom of draining vessels are recommended.

REFERENCES:

1. "Stratified Layer Flow Model - A Numerical Approach to Temperature Stratification in Liquids Contained in Heated Vessels," G. C. Vliet, LMSC Report No. 8-30-63-4; November, 1963. (Also co-authored with J. J. Brogan, T. S. Sheppard, F. H. Morse, and F. L. Hines, Jr. of Spacecraft and Rockets, Vol. 1, No. 6, p. 666, Nov.-Dec. 1964.

2. "Approximate Analysis of Propellant Stratification", D. M. Tellep and E. Y. Harper, AIAA Jr. V. 1, n. 8, p. 1954, August 1963.

3. "Flow Visualization and Interpretive Studies of Natural Convection Phenomenon", R. G. Schwind and G. C. Vliet, Proceedings of the 1964 Heat Transfer and Fluid Mechanics Institute, Berkeley, California, p. 51, June, 1964.

4. J. H. Chin, "Dimensional Analysis for Non-Draining Cylindrical Propellant Tank", Lockheed Missiles and Space Company Report No. 802337, Sept. 1962.

5. "Experimental Investigation of the Behavior of a Confined Fluid Subjected to Non-Uniform Source and Wall Heating," B. H. Anderson and M. J. Kolar; NASA TN-D-2079, November 1963.

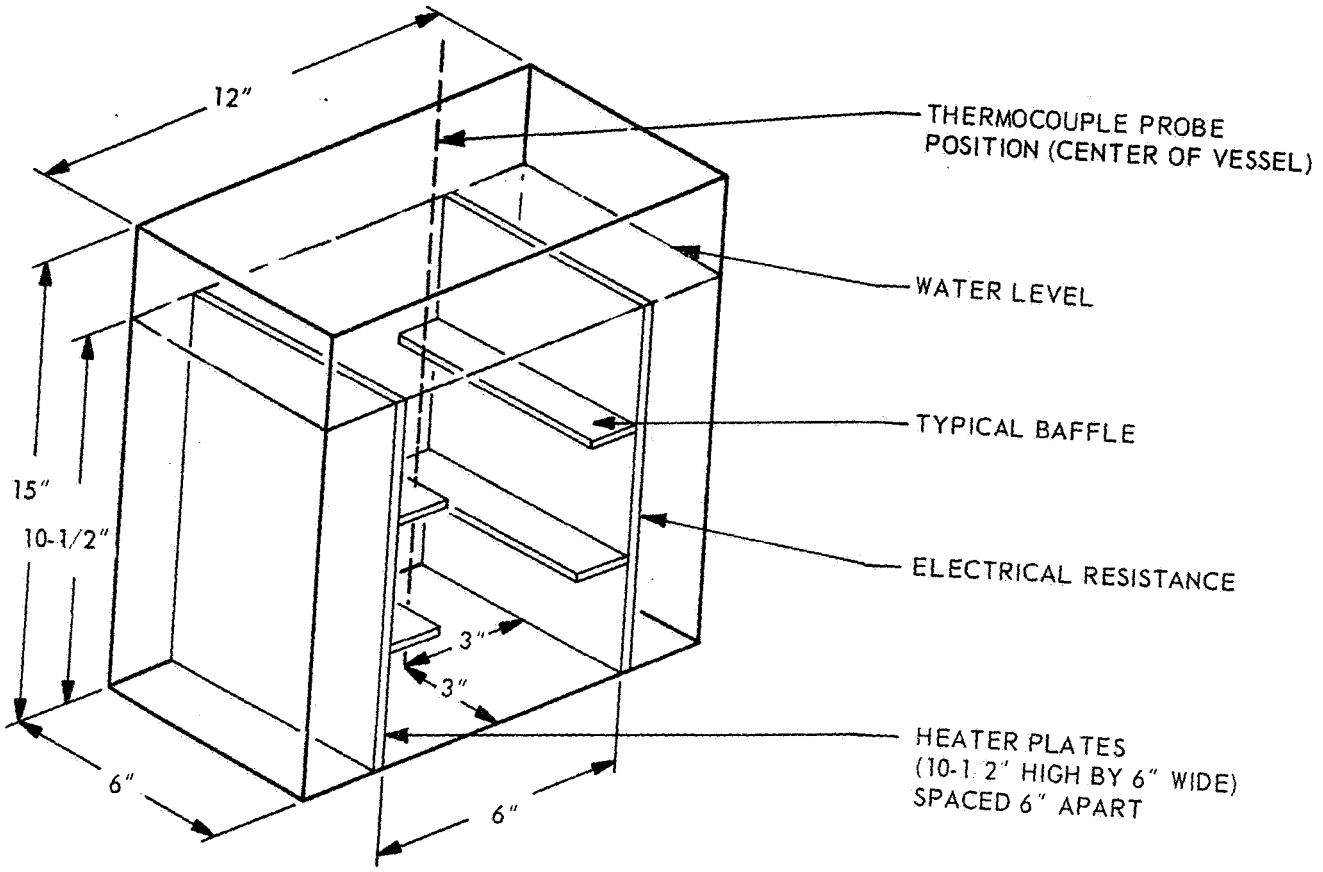


FIGURE 1(a) VERTICAL PLATE TESTS

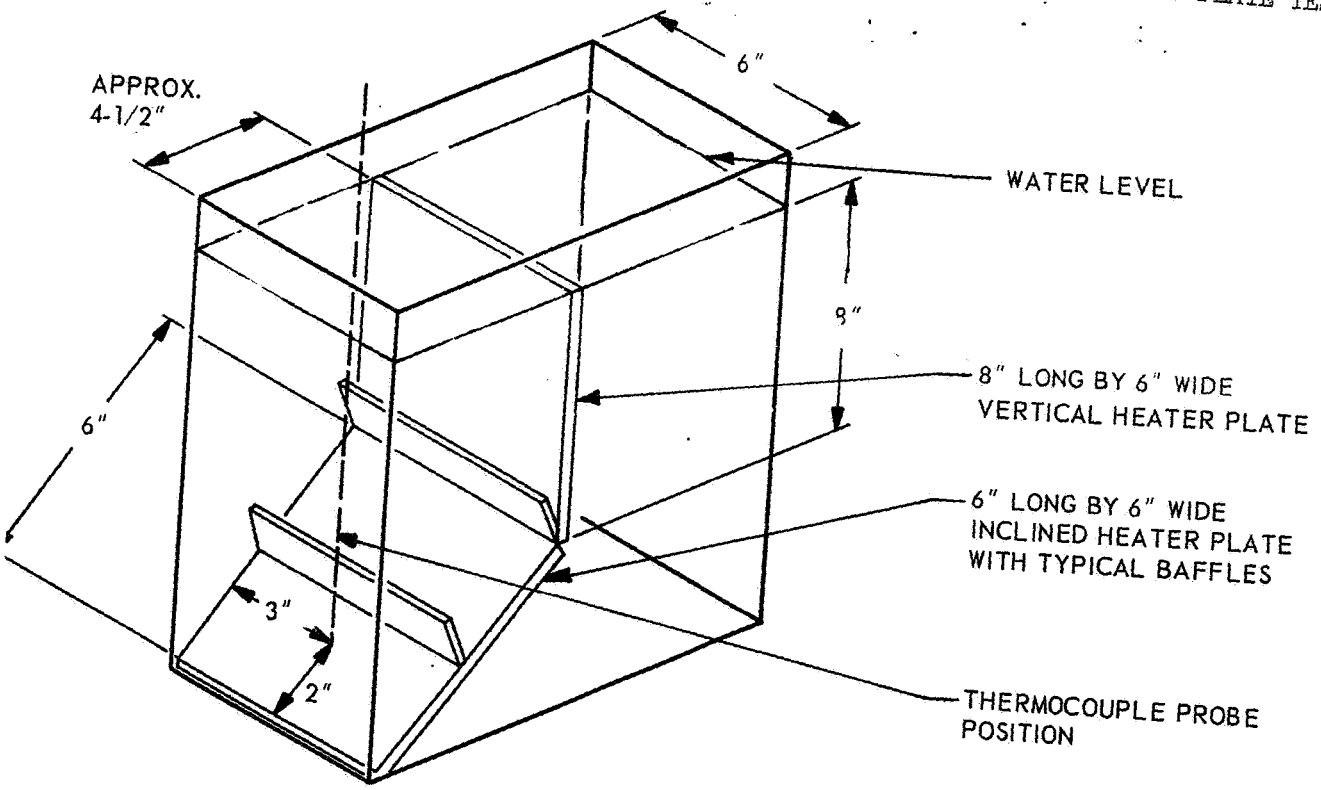


FIGURE 1(b) INCLINED PLATE TESTS

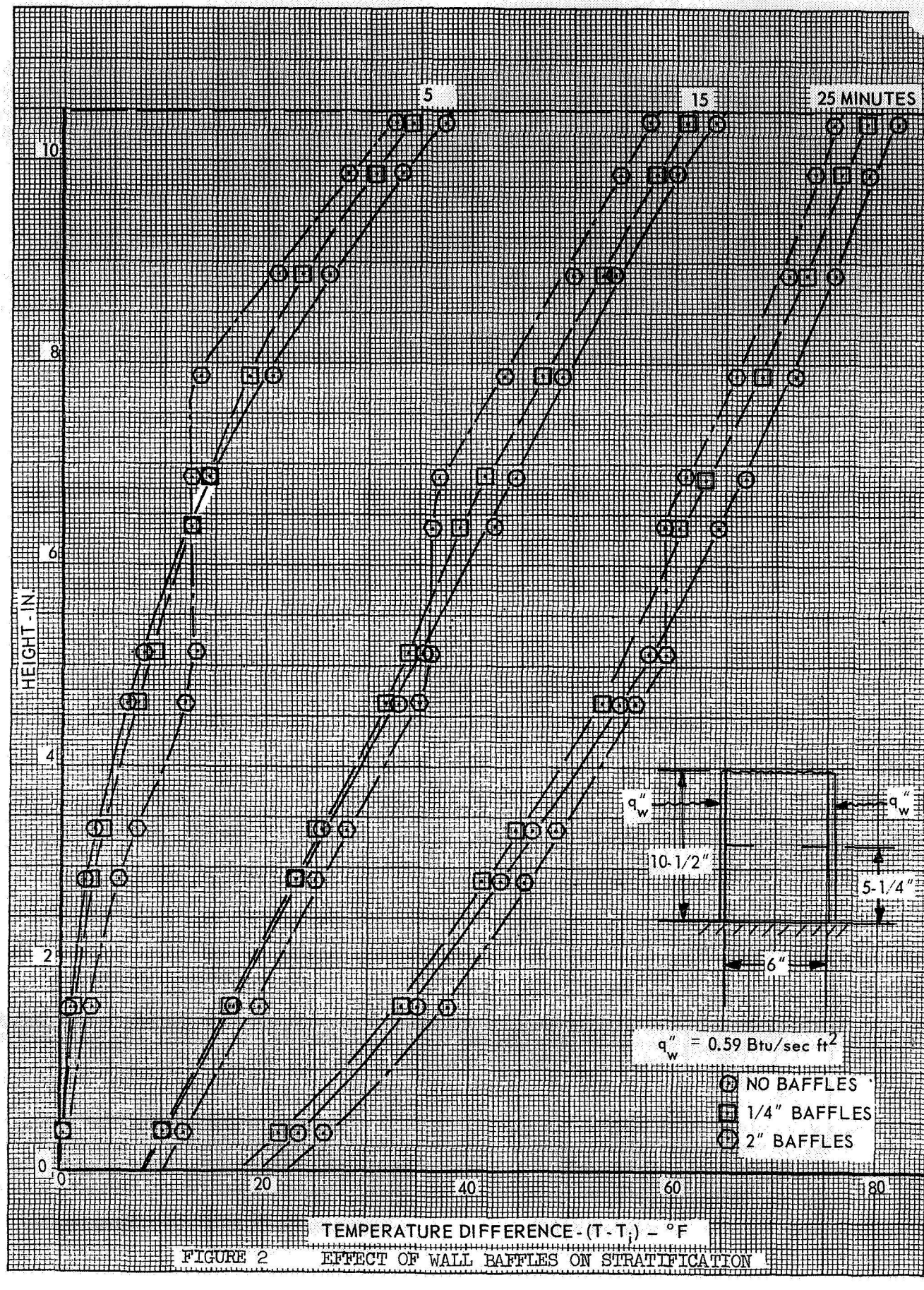


FIGURE 2 EFFECT OF WALL BAFFLES ON STRATIFICATION

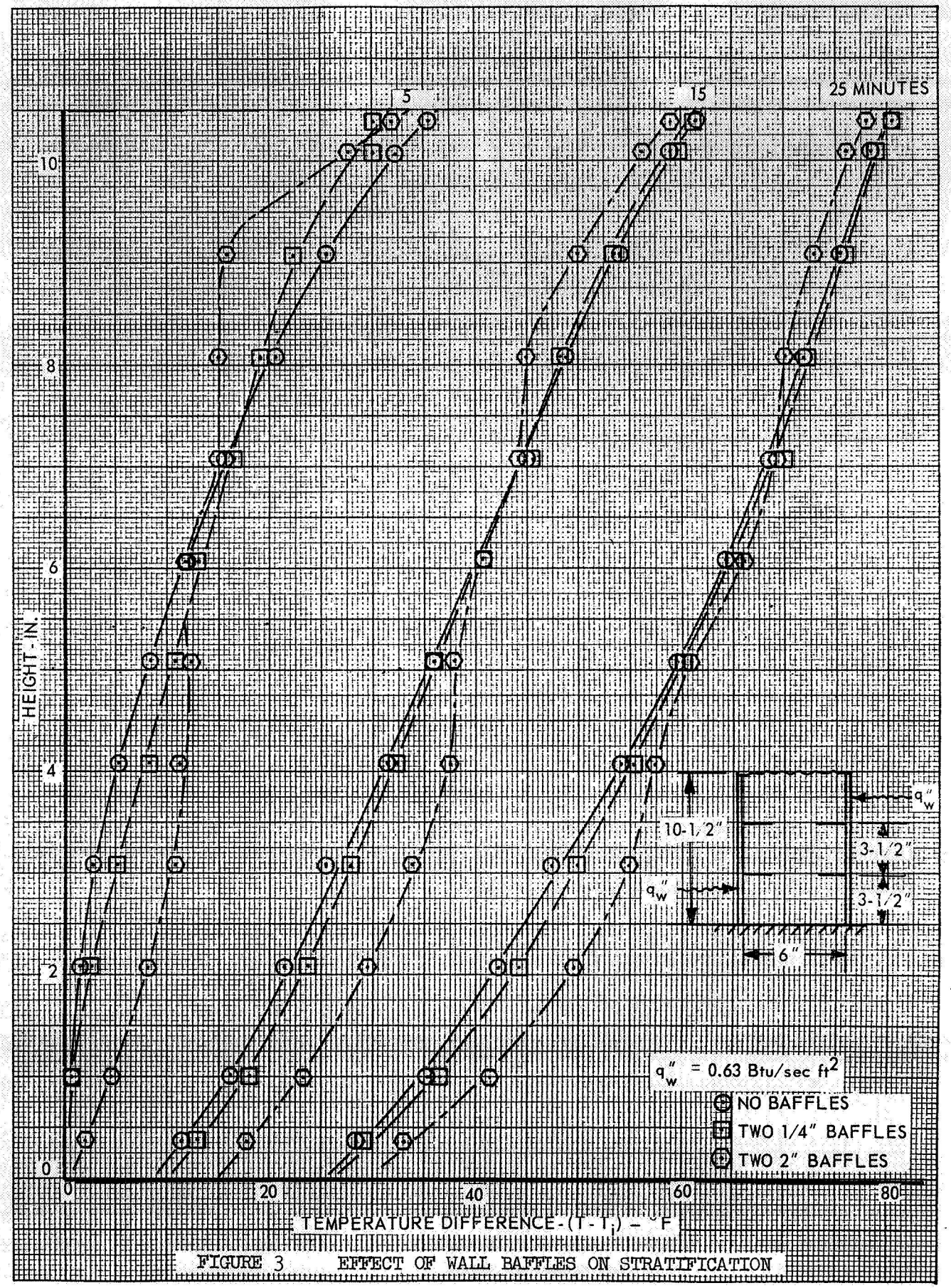


FIGURE 3 EFFECT OF WALL BAFFLES ON STRATIFICATION

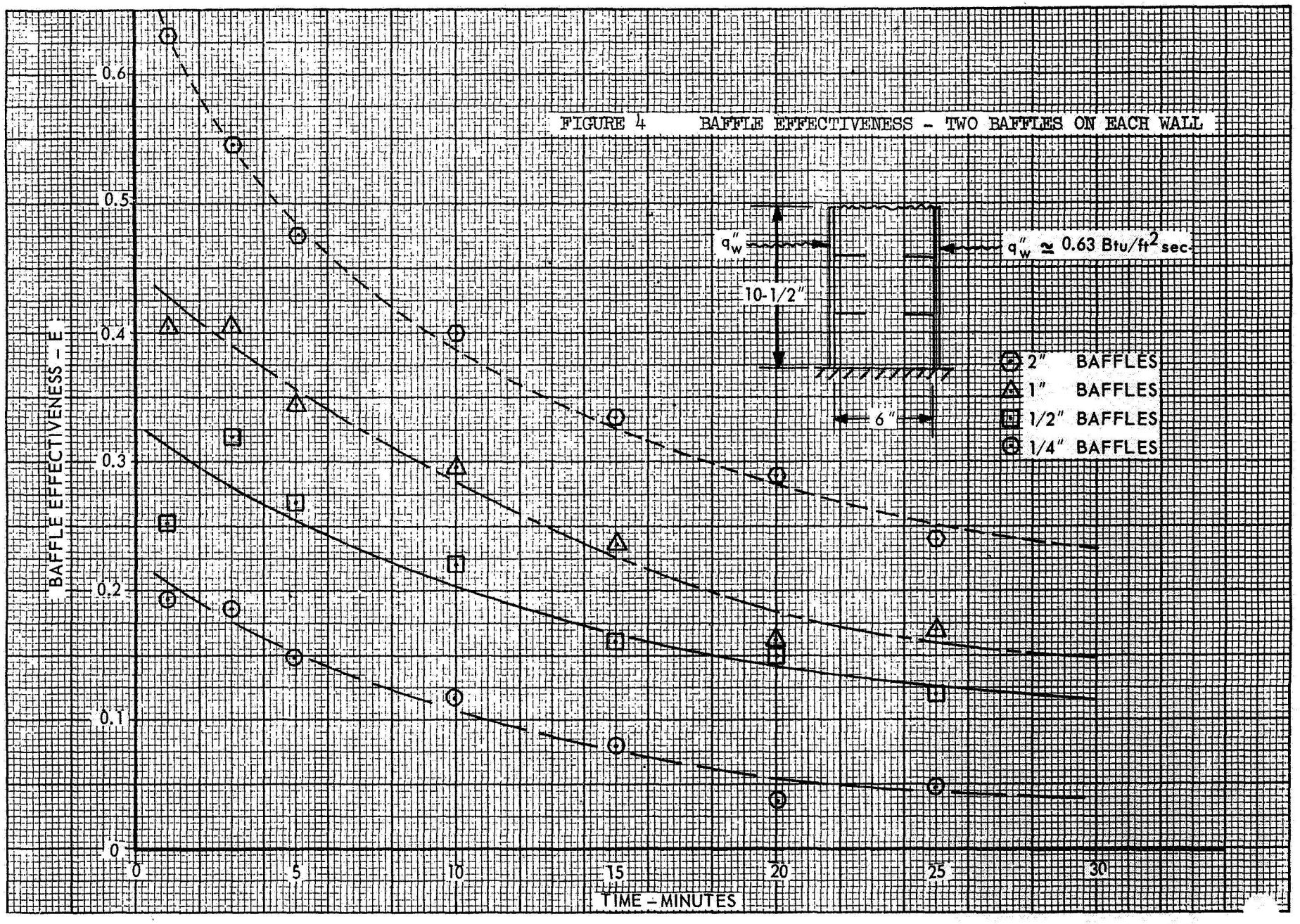


FIGURE 4 BAFFLE EFFECTIVENESS - TWO BAFFLES ON EACH WALL

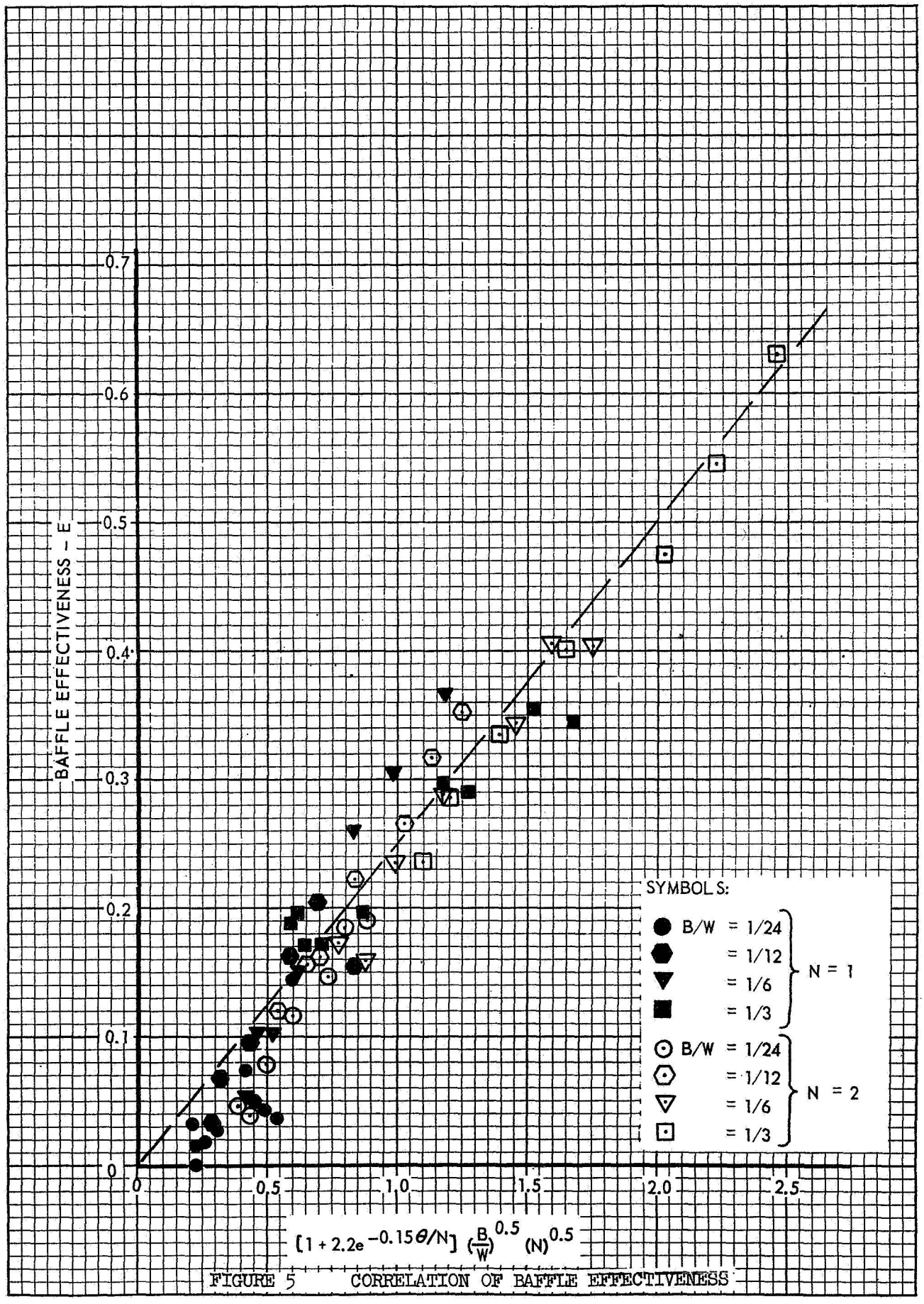


FIGURE 5 CORRELATION OF BAFFLE EFFECTIVENESS

FIGURE 6

SCHLIEREN PHOTOGRAPHS FOR STRATIFICATIO. WITHOUT WALL BAFFLES. $q''_w \simeq 1.0$ BTU/FT^{2}SEC.

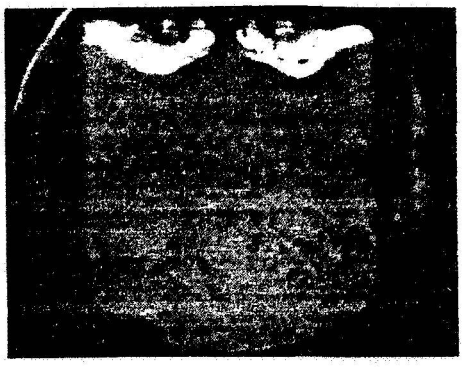


FIG. 6(a) - 20 SEC.

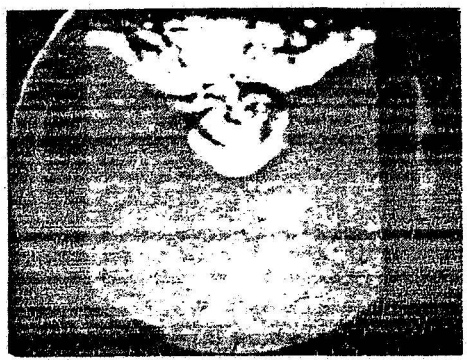


FIG. 6(b) - 27 SEC.

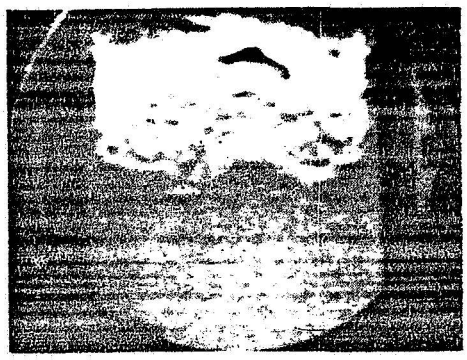


FIG. 6(c) - 40 SEC.

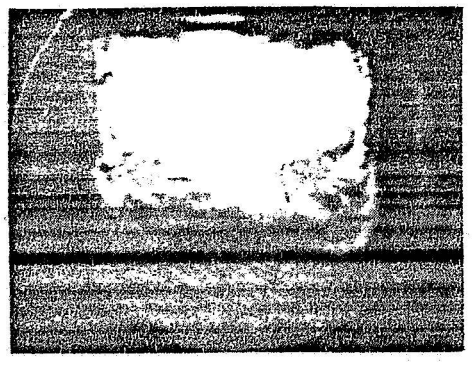


FIG. 6(d) - 1 MIN.

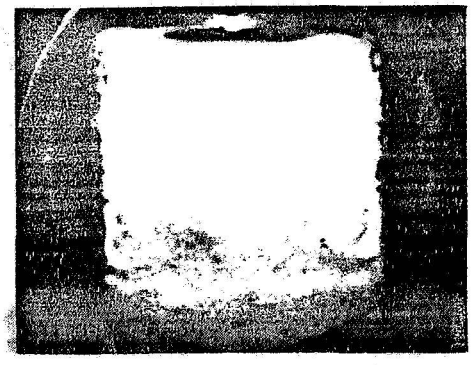


FIG. 6(e) - 1½ MIN.

FIGURE 7

SCHLIEREN PHOTOGRAPHS FOR STRATIFICATION WITH $\frac{1}{2}$ INCH WALL BAFFLE. $q''_w \simeq 1.0$ BTU/FT^2-SEC.

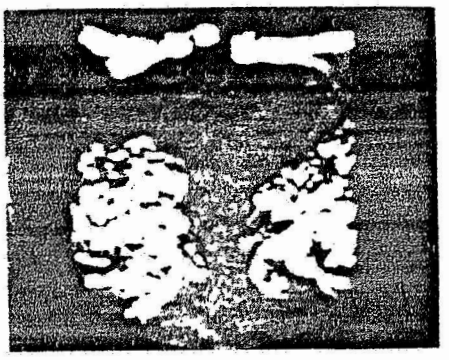


FIG. 7(a) - 20 SEC.

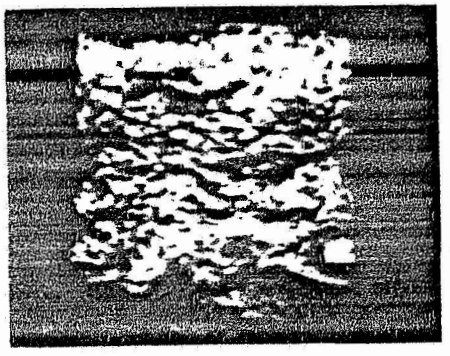


FIG. 7(b) - 40 SEC.

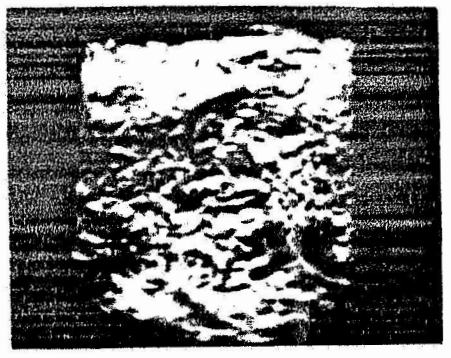


FIG. 7(c) - 1 MIN.

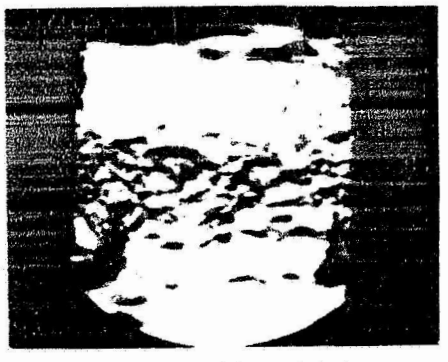


FIG. 7(d) - 2 MIN.



FIG. 7(e) - $2\frac{1}{2}$ MIN.

FIGURE 8

SCHLIEREN PHOTOGRAPHS FOR STRATIFICATION WITH 2 INCH WALL BAFFLE $q''_w \simeq 1.0$ BTU/FT^{2}SEC.



FIG. 8(a) - 1 MIN.

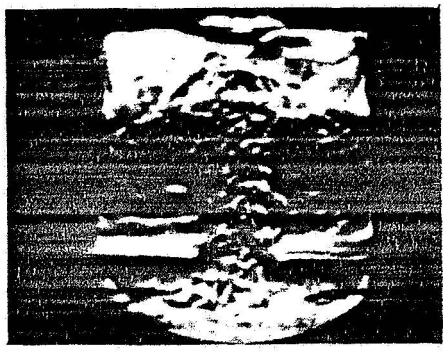


FIG. 8(b) - 2 MIN.

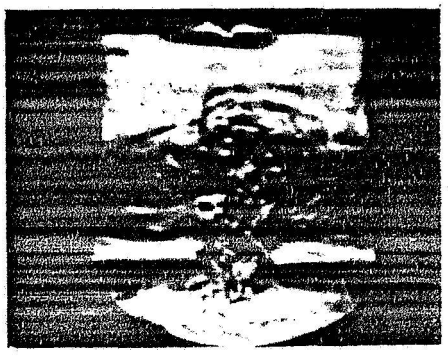


FIG. 8(c) - 3 MIN.

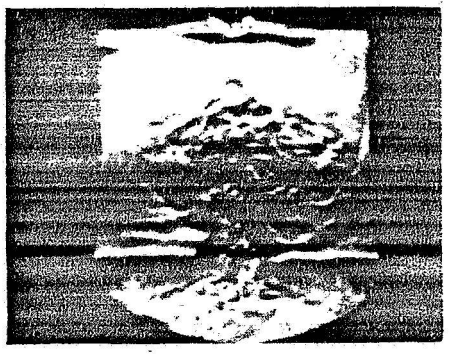


FIG. 8(d) - 4 MIN.

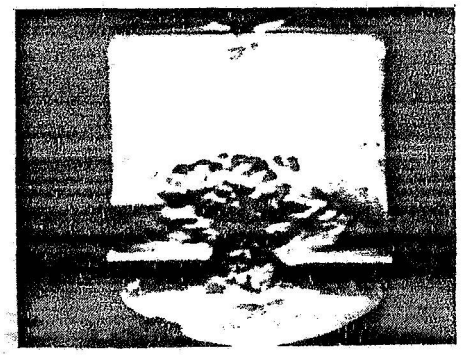


FIG. 8(e) - 10 MIN.

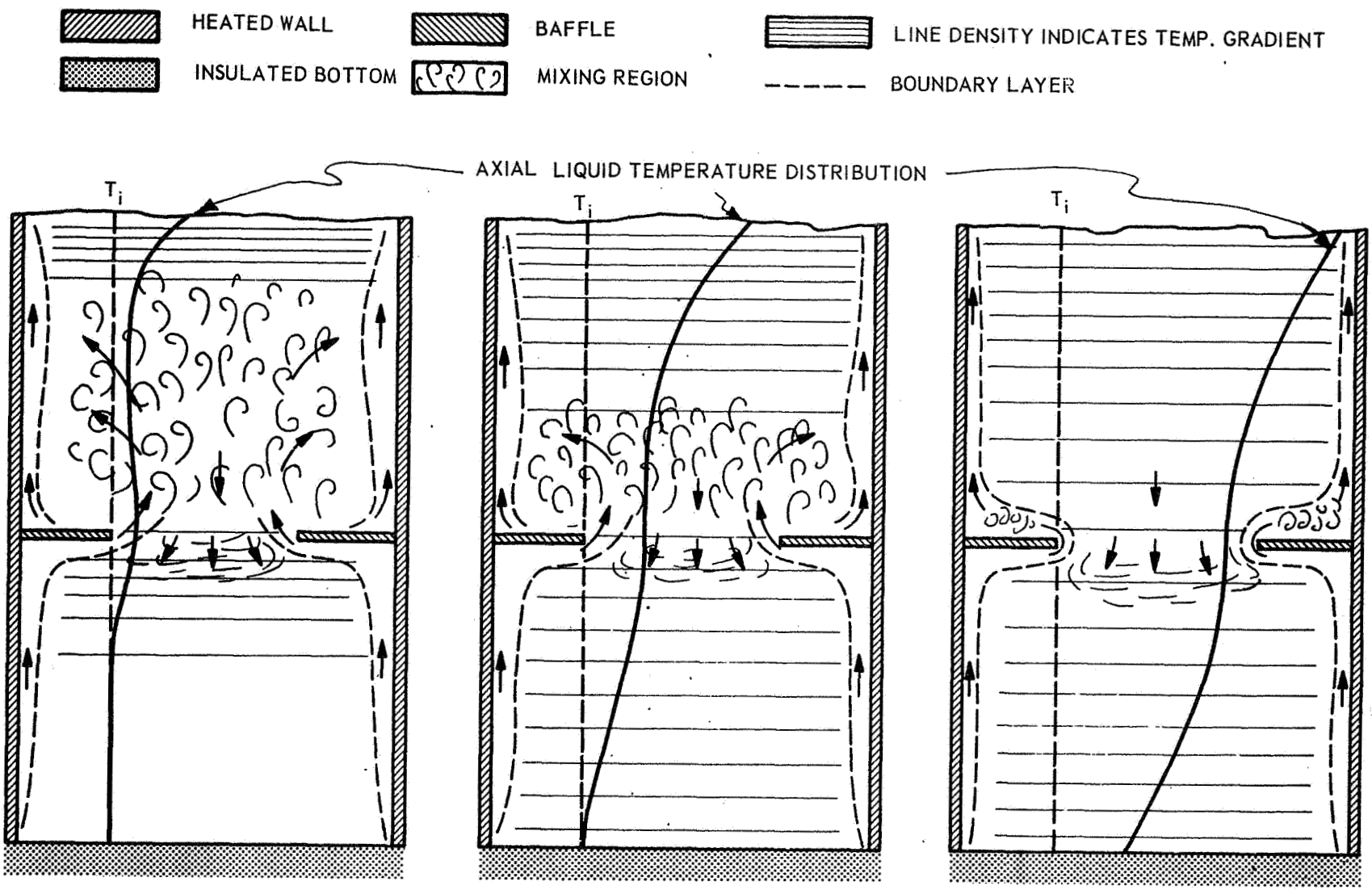
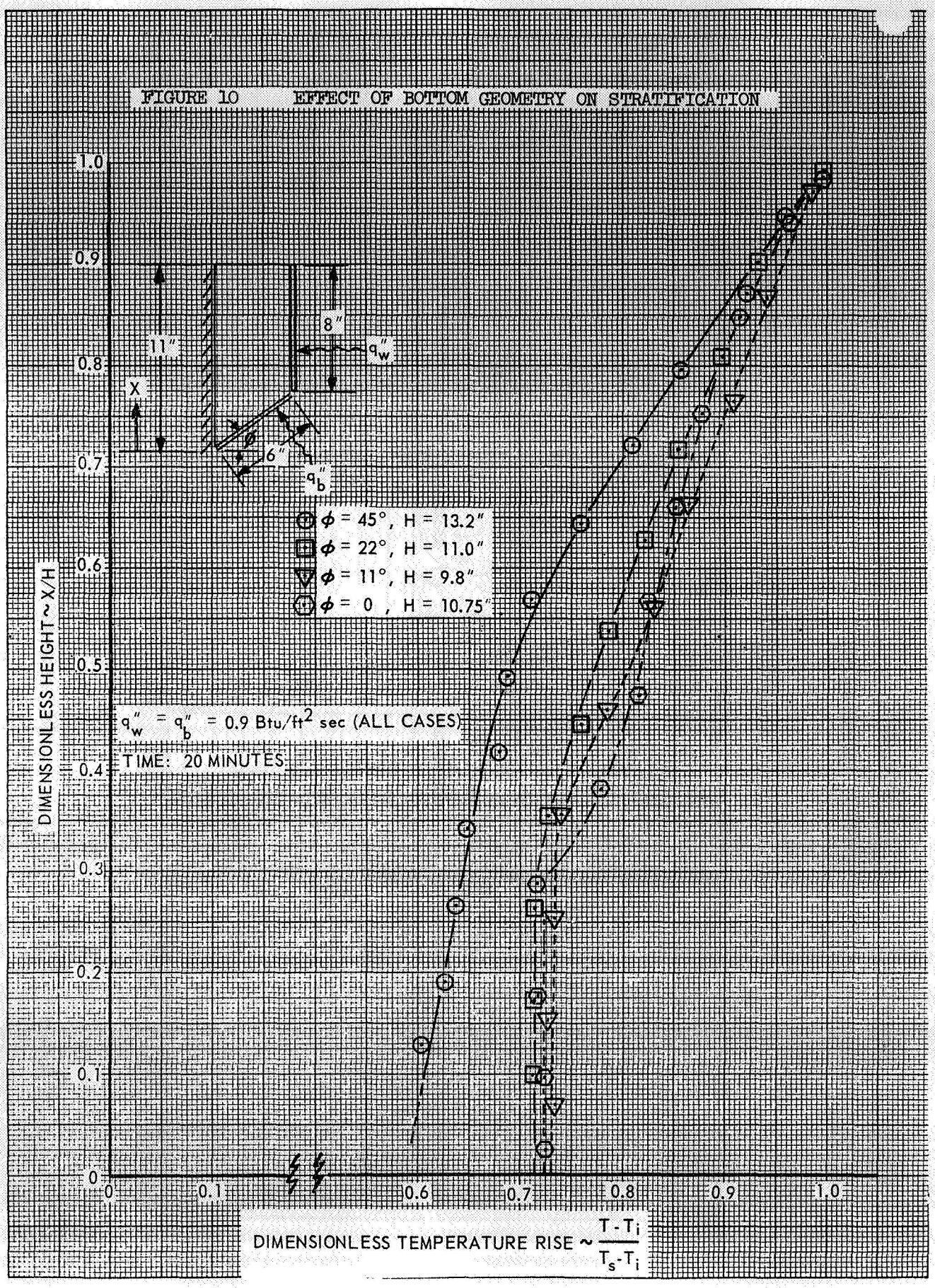


FIGURE 9 - EFFECT OF WALL BAFFLES ON NATURAL CONVECTION FLOW & STRATIFICATION

FIGURE 10 EFFECT OF BOTTOM GEOMETRY ON STRATIFICATION



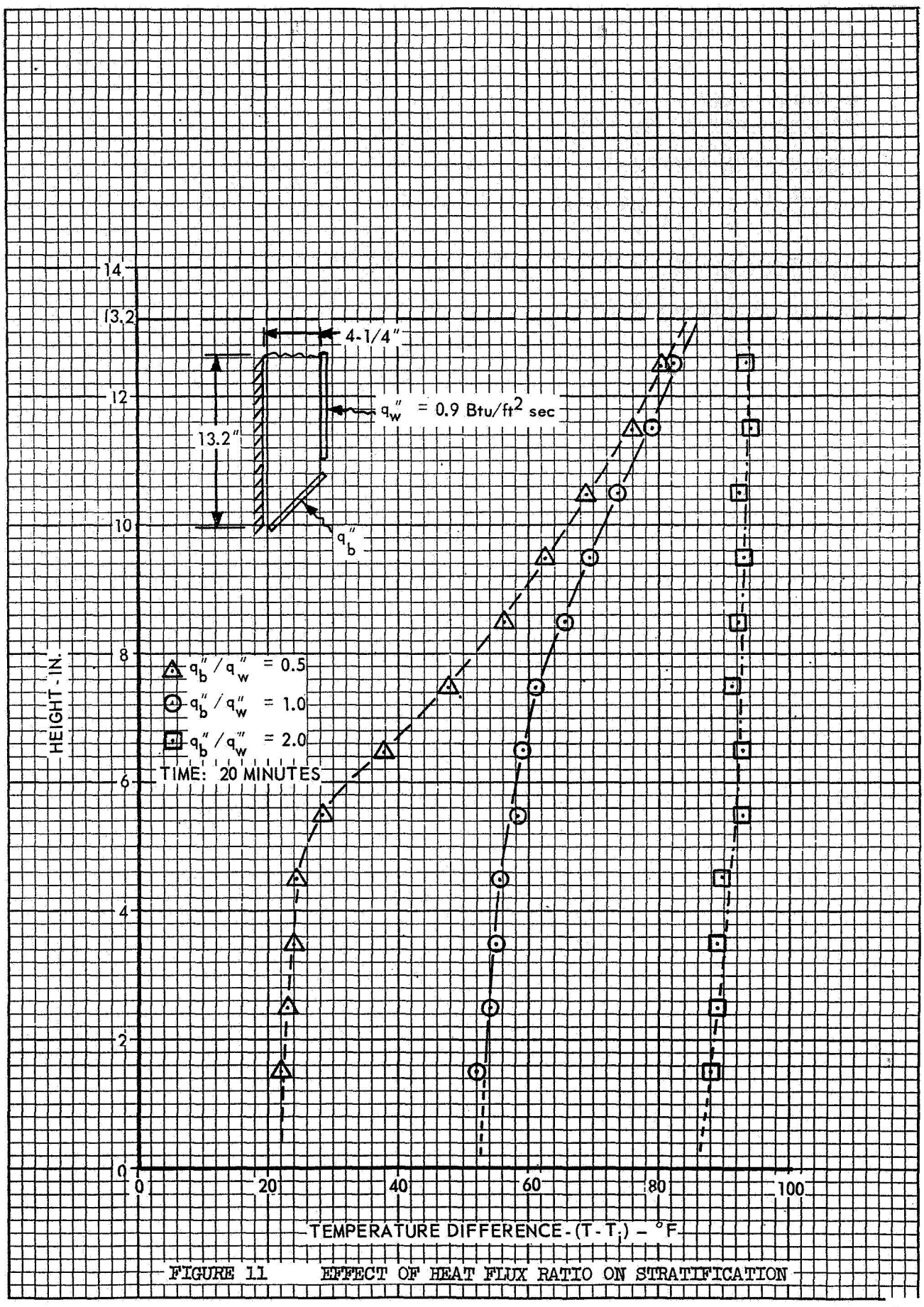


FIGURE 11 EFFECT OF HEAT FLUX RATIO ON STRATIFICATION

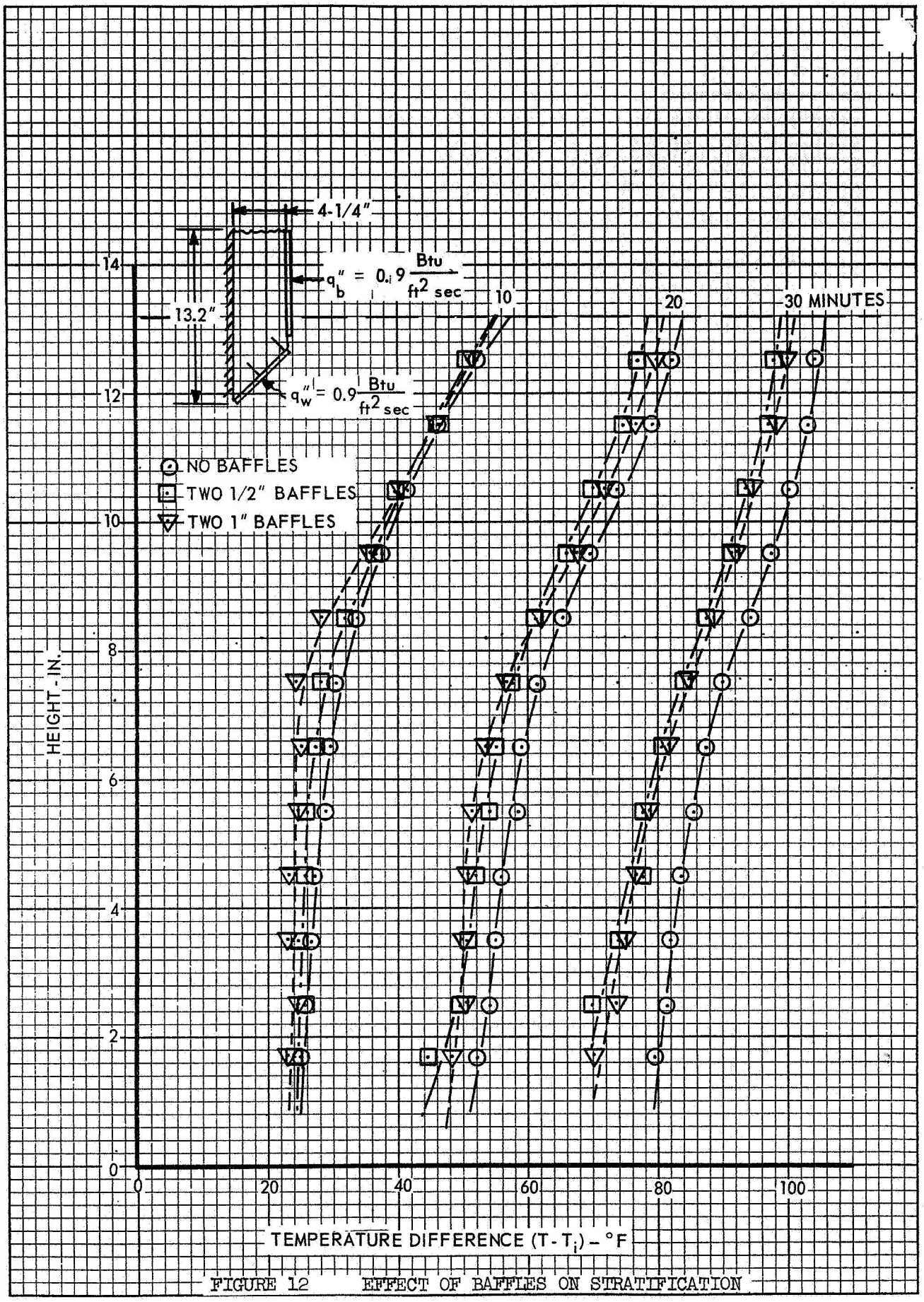


FIGURE 12 EFFECT OF BAFFLES ON STRATIFICATION

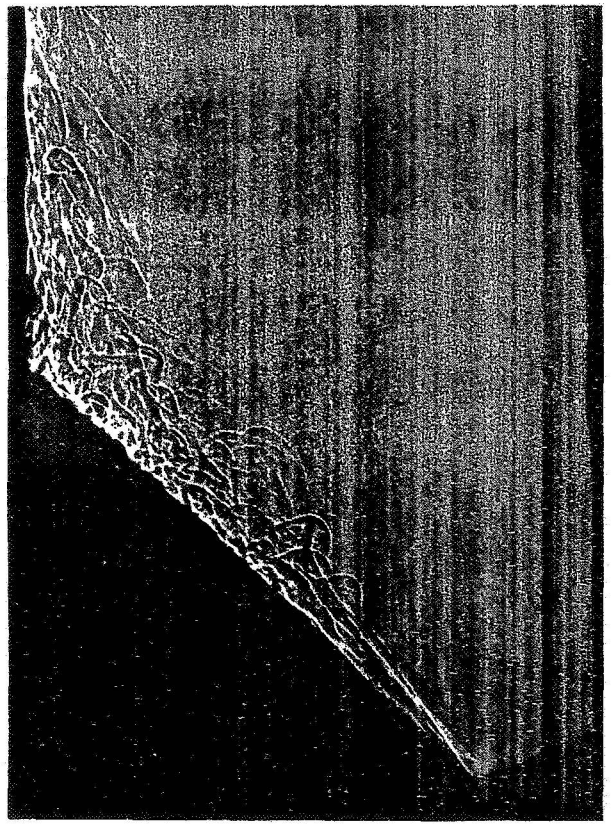


FIGURE 13(a)

NO BAFFLES

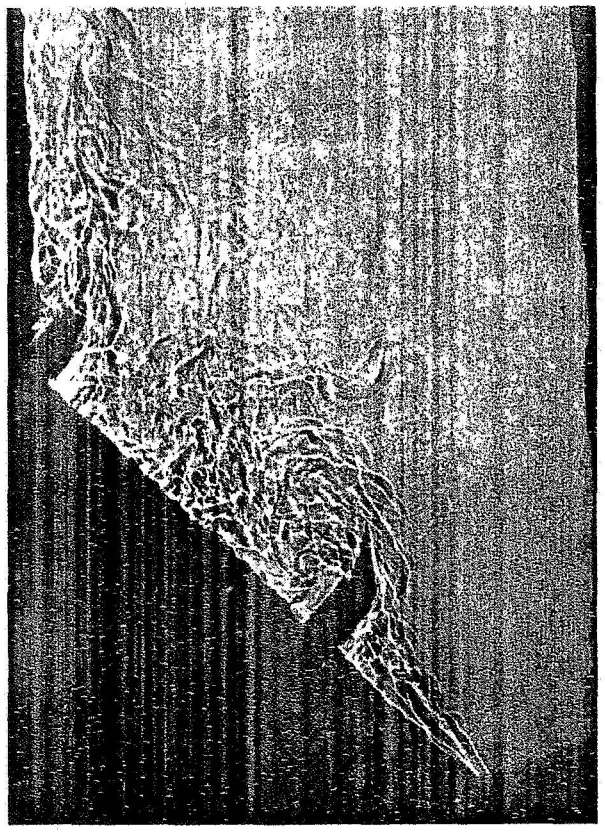


FIGURE 13(b)

TWO $\frac{1}{2}$ INCH
PERPENDICULAR BAFFLES

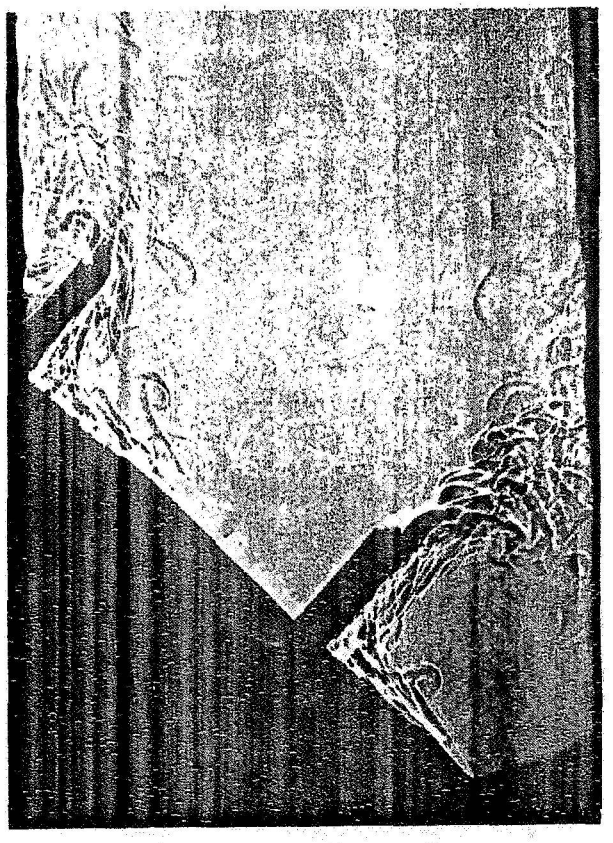


FIGURE 13(c)

TWO 1 INCH
PERPENDICULAR BAFFLES

FIGURE 13 - SHADOWGRAPH PHOTOGRAPHS OF FLOW WITH BAFFLES ON INCLINED PLATE
(All photographs for 45 degree plate with $q''_b = .4q''_w = 2.4$ Btu/ft.^{2}sec.)

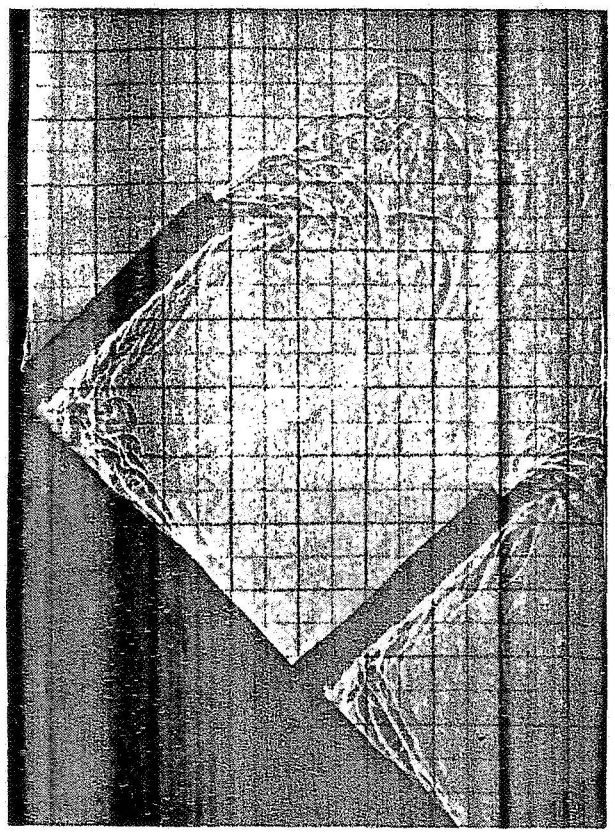


FIGURE 13(d)

TWO 2 INCH
PERPENDICULAR BAFFLES

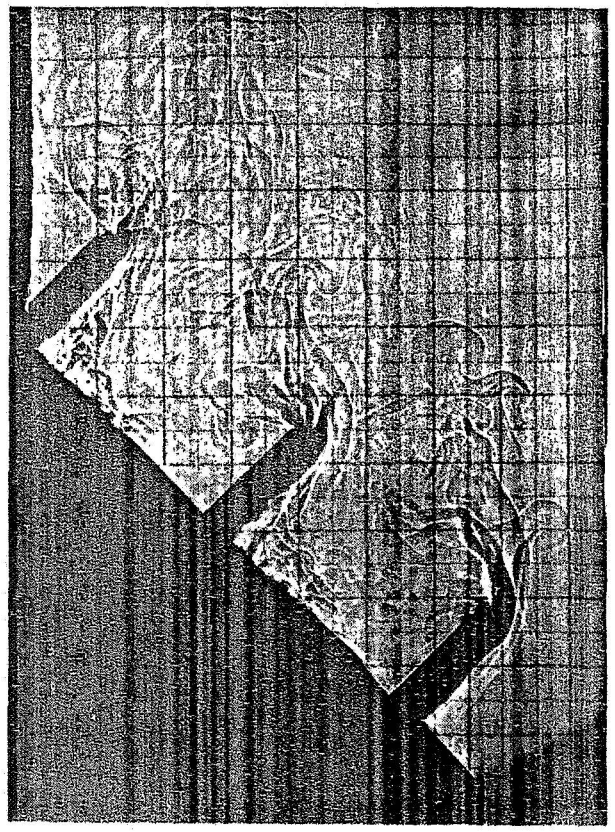


FIGURE 13(e)

THREE 1 INCH
PERPENDICULAR BAFFLES

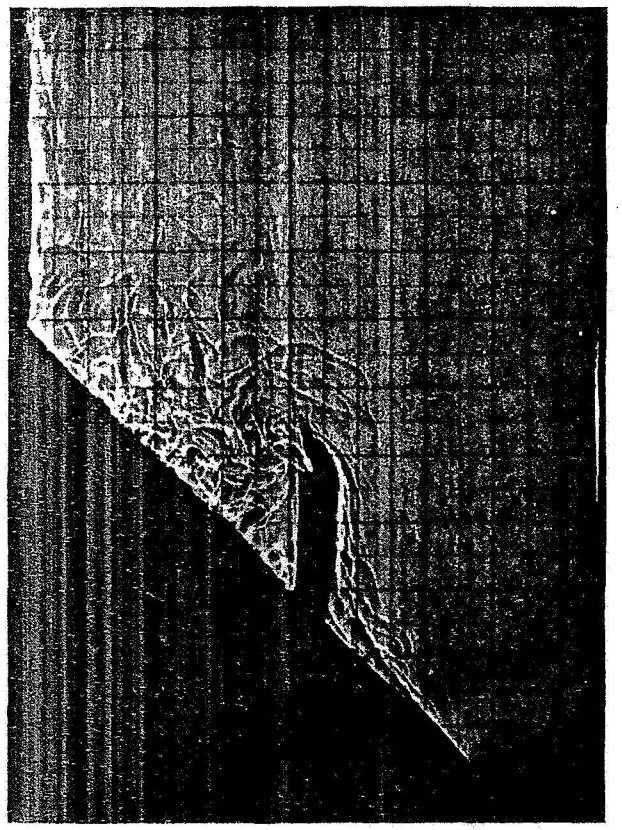


FIGURE 13(f)

ONE 1 INCH
VERTICAL BAFFLE

FIGURE 13 (Cont'd) - SHADOWGRAPH PHOTOGRAPHS OF FLOW WITH BAFFLES ON INCLINED PLATE
(All photographs for 45 degree plate with $q''_b = 4q''_w = 2.4$ Btu/ft.^{2}sec.)

TRANSIENT LAMINAR FREE CONVECTION HEAT AND MASS TRANSFER IN TWO-DIMENSIONAL CLOSED CONTAINERS CONTAINING DISTRIBUTED HEAT SOURCE

by
Hussein Z. Barakat
University of Michigan
Ann Arbor, Michigan

Reproduced from best available copy.

"Transient Laminar Free Convection Heat and Mass Transfer in Two-Dimensional Closed Containers Containing Distributed Heat Source" [1]

by

Hussein Z. Barakat[2]

Abstract

13027

The transient laminar free convection heat and mass transfer in two-dimensional rectangular containers containing volume heat sources is studied. The momentum and the continuity equations are coupled to obtain the vorticity transport equation, which is integrated numerically using the finite-difference approximation. Results of the calculations show that for small Rayleigh's numbers the steady state is reached through smooth velocity and temperature transients. For large Rayleigh's numbers velocity and temperature oscillations were predicted after a period of time from the beginning of the transients.

Author

---

1. A publication from the Heat Transfer Laboratory, Department of Mechanical Engineering, University of Michigan, Ann Arbor, Michigan.

2. Graduate Student, Department of Mechanical Engineering, University of Michigan, Ann Arbor, Michigan

Introduction

In recent years the natural convection heat and mass transport in vessels containing distributed heat sources received considerable interest owing to its importance in connection with nuclear reactors.

Up to the present time, exact solutions exist only for some simple models such as the case where heat is generated between two vertical flat plates whose height and length are large compared to their separation, or the case of an infinitely long cylinderical containers with internal heat generation (1). However, approximate solutions for containers with finite length exist. In such solutions some assumptions regarding the flow and the temperature distribution patterns are necessary. These assumptions, which are necessary due to the complexity of the problem, may or may not be realistic. A typical approximate solution is that obtained by Hammitt (2). Some aspects of such approximate methods, their shortcomings and the validity of the simplifying assumptions will be discussed later.

Our task is to examine the nature of the flow and of the temperature distribution, without resorting to any simplifying assumptions regarding the behavior of the flow pattern or the temperature distribution.

The method of finite-difference approximation has been chosen to obtain the temperature and velocity distributions. The use of this method will enable us to exmmine the nature of the velocity and temperature transients that take place, as well as the steady state solutions. It should be mentioned that it has been established that the method of finite-difference approximation yields

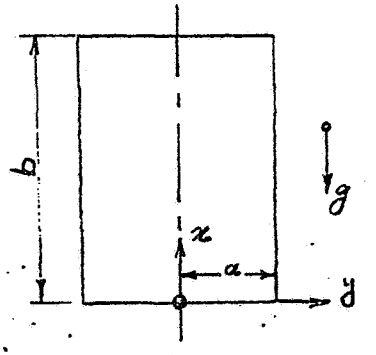
solutions which agree satisfactorily with exact solutions, provided that provisions are made for the stability, consistency and convergence problems (3,4). The examination of the stability, consistency and convergence questions is beyond the scope of this paper. However, the reader is referred to references 3,4, and 5 where these points are thoroughly discussed.

The geometry of the container and the corner and end effects make the assumption of boundary layer flow invalid. This is particularly true for small length to radius ratios, where the end effec cannot be neglected. For this reason, the full Navier-Stokes equations were used. In such cases the concept of boundary layer and boundary layer thickness as applied to flow over flat surface cannot be applied. However, in this paper the term "boundary layer thickness" is used to identify the distance from the tank walls at which the velocity component parallel to the wall is eq to zero.

Reproduced from best available copy.

Analytical Model

A two dimensional rectangular container of width, 2 a and height b, which is filled with a fluid containing a uniformly distributed heat source, is considered. The bottom and top of the container are assumed to be insulated. The container is initially at a temperature T_o. Beginning from this condition, heat is suddenly generated at a uniform rate q''' BTU/hr-cu.ft. The walls of the container are assumed to be kept at the initial temperature T_o. The x and y axes are located as shown in the Figure. Neglecting pressure terms and the dissipation function in the energy equation and assuming constant fluid properties except in the body force term, the differential equations describing the phenomena are:



The x- momentum equation

$$\rho\left(\frac{\partial u}{\partial t} + u\frac{\partial u}{\partial x} + v\frac{\partial u}{\partial y}\right) = -\rho g - \frac{\partial P}{\partial x} + \mu\left(\frac{\partial^2 u}{\partial x^2} + \frac{\partial^2 u}{\partial y^2}\right) \qquad (1)$$

The y- momentum equation

$$\rho\left(\frac{\partial v}{\partial t} + u\frac{\partial v}{\partial x} + v\frac{\partial v}{\partial y}\right) = -\frac{\partial P}{\partial y} + \mu\left[\frac{\partial^2 v}{\partial x^2} + \frac{\partial^2 v}{\partial y^2}\right] \qquad (2)$$

The Energy equation

$$\frac{\partial T}{\partial \tau} + u\frac{\partial T}{\partial x} + v\frac{\partial T}{\partial y} = \frac{q'''}{\rho c_p} + \alpha\left(\frac{\partial^2 T}{\partial x^2} + \frac{\partial^2 T}{\partial y^2}\right) \qquad (3)$$

The Continuity equation

$$\frac{\partial u}{\partial x} + \frac{\partial v}{\partial y} = 0 \qquad (4)$$

Boundary Conditions:

(a) Velocity boundary conditions

The no slip condition at the tank walls gives:

$$u(0,y,t) = u(b,y,t) = u(x,a,t) = 0$$

$$v(0,y,t) = v(b,y,t) = v(x,a,t) = 0$$

From the geometric symmetry with respect to the y-axis, the following boundary conditions are obtained:

$$\frac{\partial u}{\partial y}(x,0,t) = 0$$

$$v(x,0,t) = 0$$

(b) Thermal boundary conditions:

$$T(x,a,t) = T_0$$

$$\frac{\partial T}{\partial y}(x,0,t) = 0$$

$$\frac{\partial T}{\partial x}(0,y,t) = \frac{\partial T}{\partial x}(b,y,t) = 0$$

Initial Conditions

$$T(x,y,0) = T_0$$

$$u(x,y,0) = v(x,y,0) = 0$$

Reduction of the governing differential equations:

The method of solution used here follows that of reference (3). The reader is referred to that reference for a complete discussion of this method. Only a brief description of the computational procedure will be given.

Equations (1) to (4) can be put in a form which is suitable for finite-difference computation as follows:

Differentiating the x-momentum equation w.r.t.y and the y-momentum equation w.r.t.x and combining both equations to eliminate the pressure terms, taking into consideration that the fluid properties are assumed to be constant, except in the body force term, the following differential equation is obtained:

$$\rho\frac{\partial}{\partial t}\left(\frac{\partial u}{\partial y}-\frac{\partial v}{\partial x}\right)+u\frac{\partial}{\partial x}\left(\frac{\partial u}{\partial y}-\frac{\partial v}{\partial x}\right)+v\frac{\partial}{\partial y}\left(\frac{\partial u}{\partial y}-\frac{\partial v}{\partial x}\right)=-g\frac{\partial \rho}{\partial y}+$$

$$\mu\left[\frac{\partial^2}{\partial x^2}\left(\frac{\partial u}{\partial y}-\frac{\partial v}{\partial x}\right)+\frac{\partial^2}{\partial y^2}\left(\frac{\partial u}{\partial y}-\frac{\partial v}{\partial x}\right)\right] \qquad (5)$$

Since the pressure variations are small, then density changes will be largely due to temperature changes. Accordingly, the density ρ could be closely approximated by:

$$\rho=\rho_0\left(1+\beta(T_0-T)\right) \qquad (6)$$

where ρ_0 and T_0 are reference density and temperature which are the initial values in this case. β is the coefficient of thermal expansion.

At this point it may be expedient to introduce the following substitutions to transform the differential equations into the non-dimensionalized form:

$$u = \frac{\alpha b}{a^2} U \quad ; \quad v = \frac{\alpha}{a} V \quad ; \quad T - T_0 = \frac{\nu \alpha b}{\beta g a^4} \theta$$

$$t = \frac{a^2}{\alpha} \tau \quad ; \quad x = b X \quad ; \quad y = a Y$$

$$U = \frac{\partial \psi}{\partial Y} \quad ; \quad V = -\frac{\partial \psi}{\partial X} \tag{7}$$

where ψ is the stream function.

Substituting (6) and (7) in (3) and (5), the following equations are obtained:

$$\frac{\partial}{\partial \tau}\left(\frac{a^2}{b^2}\frac{\partial^2 \psi}{\partial X^2} + \frac{\partial^2 \psi}{\partial Y^2}\right) + \frac{\partial \psi}{\partial Y} \cdot \frac{\partial}{\partial X}\left(\frac{a^2}{b^2}\frac{\partial^2 \psi}{\partial X^2} + \frac{\partial^2 \psi}{\partial Y^2}\right) -$$

$$\frac{\partial \psi}{\partial X} \cdot \frac{\partial}{\partial Y}\left(\frac{a^2}{b^2}\frac{\partial^2 \psi}{\partial X^2} + \frac{\partial^2 \psi}{\partial Y^2}\right) = Pr\left[\frac{\partial \theta}{\partial Y} + \frac{a^2}{b^2}\frac{\partial^2}{\partial X^2}\left(\frac{a^2}{b^2}\frac{\partial^2 \psi}{\partial X^2} + \frac{\partial^2 \psi}{\partial Y^2}\right) + \right. \tag{8}$$

$$\left. \frac{\partial^2}{\partial Y^2}\left(\frac{a^2}{b^2}\frac{\partial^2 \psi}{\partial X^2} + \frac{\partial^2 \psi}{\partial Y^2}\right)\right]$$

$$\frac{\partial \theta}{\partial \tau} + \frac{\partial \psi}{\partial Y} \cdot \frac{\partial \theta}{\partial X} - \frac{\partial \psi}{\partial X} \cdot \frac{\partial \theta}{\partial Y} = Q + \frac{a^2}{b^2}\frac{\partial^2 \theta}{\partial X^2} + \frac{\partial^2 \theta}{\partial Y^2} \tag{9}$$

where $Q = (g''' \beta g a^6)/(K \nu \alpha b)$

Equation (8) can be written in the following form:

$$\frac{\partial w}{\partial \tau} + U\frac{\partial w}{\partial X} + V\frac{\partial w}{\partial Y} = Pr\left[\frac{\partial \beta}{\partial Y} + \frac{a^2}{b^2}\frac{\partial^2 w}{\partial X^2} + \frac{\partial^2 w}{\partial Y^2}\right] \tag{10}$$

where

$$\omega = \frac{a^2}{b^2}\frac{\partial^2\psi}{\partial x^2} + \frac{\partial^2\psi}{\partial y^2} \qquad (11)$$

By the above transformation equations 1,2,3 and 4 in u, v and T are replaced by equations (9), (10) and (11) in θ, ω and ψ. The form of the latter system of equations is more suitable for solution by Finite-difference approximation.

Boundary Conditions

The velocity boundary conditions given before give rise to the following boundary conditions for the stream function and the vorticity ω.

$$\psi(0,y,\tau) = \psi(1,y,\tau) = \psi(x,0,\tau) = \psi(x,1,\tau) = 0$$

$$\omega(x,0,\tau) = 0$$

Three more boundary conditions for the vorticity at the wall, bottom and top of the container are required. It turned out to be difficult to find an explicit expression for the vorticity at these locations. Fortunately the method of solution enables us to evaluate the vorticity at the solid boundary after each time step, to be used in determining the vorticity inside the domain of interest at the next step as will be explained later.

The boundary conditions of the dimensionless temperature θ, can be expressed as follows:

$$\theta(x,1,\tau) = 0$$

$$\frac{\partial\theta}{\partial x}(0,y,\tau) = \frac{\partial\theta}{\partial x}(1,y,\tau) = \frac{\partial\theta}{\partial y}(x,0,\tau) = 0$$

and the initial conditions become:

$$\theta(x,y,0) = \psi(x,y,0) = \omega(x,y,0) = 0$$

Finite-difference equations, stability requirement:

Using Taylor's series expansion the partial differential equations (9), (10) and (11) are approximated by finite-difference equations as follows:

1- The time derivative is represented by forward differences according to the following:

$$\frac{\partial f}{\partial t} = \frac{f(\tau+\Delta\tau) - f(\tau)}{\Delta\tau} \qquad (12)$$

2- The nonlinear terms $U\frac{\partial\theta}{\partial X}$, $V\frac{\partial\theta}{\partial Y}$, $U\frac{\partial\omega}{\partial X}$ and $V\frac{\partial\omega}{\partial Y}$ are linearized by considering U and V to be known and taken equal to their values at the past time increments. The derivatives $\frac{\partial\theta}{\partial X}$ $\frac{\partial\theta}{\partial Y}$, $\frac{\partial\omega}{\partial X}$ and $\frac{\partial\omega}{\partial Y}$ are approximated by forward differences if the coefficient velocity component is negative and are represented by backward-differences if the coefficient velocity is positive. For example, if $U \geqslant 0$, then:

$$\left(\frac{\partial f}{\partial X}\right) = \frac{f(x,y) - f(x-\Delta x, y)}{\Delta X} \qquad (13)$$

if $U \leqslant 0$, then

$$\frac{\partial f}{\partial X} = \frac{f(x+\Delta x, y) - f(x,y)}{\Delta X} \qquad (14)$$

where the function f in this case stands for either θ or w.

Similar formulae can be written for $\frac{\partial f}{\partial y}$ depending upon the sign of the velocity component V at the particular nodal point considered.

3- The second order derivatives are approximated according to the following equation:

$$\frac{\partial^2 f}{\partial x^2} = \frac{f(x+\Delta x, y) - 2f(x,y) + f(x-\Delta x, y)}{(\Delta x)^2} \qquad (15)$$

Similar expression can be written for $\frac{\partial^2 f}{\partial y^2}$. Accordingly each of equation (9), (10) and (11) can be replaced by a system of linear algebraic equations. Implicit finite-differences are used to approximate the partial derivatives $\frac{\partial \theta}{\partial x}$, $\frac{\partial \theta}{\partial y}$, $\frac{\partial^2 \theta}{\partial x^2}$ and $\frac{\partial^2 \theta}{\partial y^2}$. In such a representation the values of the variables on the right-hand side of (13), (14) and (15) are taken at the advanced time level $\tau+\Delta\tau$. The resulting set of algebraic equations are solved using the Gauss-Seidel iterative method. On the otherhand, explicit differences were used to approximate the derivatives $\frac{\partial w}{\partial x}$, $\frac{\partial w}{\partial y}$, $\frac{\partial^2 w}{\partial x^2}$, and $\frac{\partial^2 w}{\partial y^2}$. In this case the values of the variables on the right-hand side of (13), (14) and (15) are taken equal to those at the time level τ , which are known. In this case the vorticity can be calculated explicitly at each nodal point. The finite-difference approximation procedure used in the energy equation could have been used in the vorticity equation or vice-versa, but the procedure of solving the vorticity equation chosen in this paper is more convenient, because of the difficulties

encountered in obtaining the required boundary conditions for the vorticity at the solid boundaries, as it was discussed before.

The above described procedure of representing the terms $U\frac{\partial \Gamma}{\partial X}$ and $V\frac{\partial \Gamma}{\partial Y}$ is necessary in order that the computational procedure used be stable. The value of the time increment used in the calculation should satisfy the stability requirement imposed by the computational procedure used in solving the vorticity equation. According to the stability analysis of reference (3) the time increment should be taken such that the following inequality is satisfied at all nodal points,

$$\Delta\tau \leqslant 1 \Big/ \left(\frac{a^2}{b^2}\frac{Pr}{(\Delta X)^2} + \frac{Pr}{(\Delta Y)^2} + \frac{|U_{i,j}|}{\Delta X} + \frac{|V_{i,j}|}{\Delta Y} \right) \qquad (16)$$

No limitations on the time increment are imposed by the computational procedure used to calculate the temperature distribution.

The reader is referred to reference (3) for more discussions of stability and convergence.

According to the above discussions, the system of partial-differential equations (9), (10) and (11) can be approximated by finite-differences as follows, for the case when $U \geqslant 0$, $V \geqslant 0$

$$\frac{\theta'_{i,j} - \theta_{i,j}}{\Delta\tau} + U_{i,j}\frac{\theta'_{i,j} - \theta'_{i-1,j}}{\Delta X} + V_{i,j}\frac{\theta'_{i,j} - \theta'_{i,j-1}}{\Delta Y} = Q +$$

$$\frac{a^2}{b^2}\frac{\theta'_{i+1,j} - 2\theta'_{i,j} + \theta'_{i-1,j}}{(\Delta X)^2} + \frac{\theta'_{i,j+1} - 2\theta'_{i,j} + \theta'_{i,j-1}}{(\Delta Y)^2} \qquad (17)$$

$$\frac{\omega'_{i,j} - \omega_{i,j}}{\Delta\tau} + U\frac{\omega_{i,j} - \omega_{i-1,j}}{\Delta X} + V\frac{\omega_{i,j} - \omega_{i,j-1}}{\Delta Y} = Pr\frac{\theta'_{i,j+1} - \theta'_{i,j-1}}{2(\Delta Y)} +$$

$$Pr\left[\frac{a^2}{b^2}\frac{\omega_{i+1,j} - 2\omega_{i,j} + \omega_{i-1,j}}{(\Delta X)^2} + \frac{\omega_{i,j+1} - 2\omega_{i,j} + \omega_{i,j-1}}{(\Delta Y)^2}\right] \tag{18}$$

$$\omega_{i,j} = \frac{a^2}{b^2}\frac{\psi_{i+1,j} - 2\psi_{i,j} + \psi_{i-1,j}}{(\Delta X)^2} + \frac{\psi_{i,j+1} - 2\psi_{i,j} + \psi_{i,j-1}}{(\Delta Y)^2} \tag{19}$$

The prime refers to the value of the variables at time level $(\tau + \Delta\tau)$ and the unprimed variables correspond to those at the time level τ .

The Procedure of Calculation is as follows:

1) Equation (17) is solved for the temperature distribution, using Gauss-Seidel Method of iteration.

2) The calculated values of θ' are used in equation (18) and the vorticity ω is calculated at each interior nodal point.

3) Equation (19) is used to calculate the stream function at each interior nodal point. The block-Iterative method, as explained by reference (6), is used for this purpose because it is more efficient than other iterative methods.

4) The calculated values of Ψ at the interior nodal points are used to evaluate the vorticity at the solid boundaries according to equation (11). Taylor's series expansion is used

to obtain expressions for the vorticity at the solid boundaries in terms of the stream function at the neighboring points. For example at $X=0$, the vorticity at the bottom can be calculated according to:

$$\omega_{x=0,y} = \frac{a^2}{b^2} \cdot \frac{8\psi(\Delta x, y) - \psi(2\Delta x, y)}{2(\Delta x)^2}$$

Similar expressions can be obtained for the vorticity at the other solid boundaries.

Discussion of Results

Calculations were carried on for two levels of heat generation Q equal to 10^4 and 10^6. The Grashoff number based on the container height and the maximum difference between the centreline and the wall temperatures are 3.5×10^6 and 1.05×10^7, respectively, while those based on half the width are 7×10^3 and 1.6×10^5, respectively. The value of Prandtl number equal to four and a = 0.5 foot were used in both runs. The ratio a/b was taken equal to 0.125 and 0.25, respectively. The velocity and temperature distribution at different axial positions and different times for the first case are shown in Figures (1), (2) and (3), while those for the second run are shown in Figures (4), (5), (6) and (7).

The results obtained in both cases show that the velocity distribution is not of the boundary layer type. On the contrary the boundary layer fills a large portion of the cross-section of the container. The shape of the velocity profiles obtained agrees with that obtained experimentally by Wilkie and Fisher, (7). However, it is not in agreement with the shape of the velocity profile postulate by Lighthill and used by Hammitt, in which it is assumed that a core

of constant velocity moves upward at a lower velocity, while the fluid moves downward in a small region near the boundary at higher velocities. However, such a flow pattern takes place only at small values of time as shown in Figure (9-b). The same conclusion could be reached by examining Figure (6), where the velocities near the boundary are higher than those at the center line for small values of time.

The shape of the radial temperature distribution obtained also agrees with those of Wilkie and Fisher and also with those obtained experimentally by Hammitt. Large temperature gradients exist near the wall particularly for high Grashoff numbers. The temperature near the center line is lower than that near the walls outside the boundary layer. This is particularly noticable for high Grashoff numbers where high velocities exist. This means that near the center line more heat is removed by convection than is being generated.

The results obtained for the velocity and temperature distribution show that, except near the end regions, the boundary layer and the shape of the velocity profile became very rapidly established.

It is very interesting to notice that for low Grashoff numbers, a time steady flow pattern has been reached through smooth velocity and temperature transients, Figure (3). On the other hand, for high Grashoff numbers, the velocity and temperature begin to oscillate as shown in Figures (6) and (7). The fact that the amplitudes of the oscillations are bounded and remain unappreciably changed over

a long period of time, suggests that this oscillatory phenomenon is a natural stability phenomenon and that it is not a mathematical stability problem. This conclusion is supported by the fact that the amplitude of these oscillations are larger near the center line, where the shear stress is zero, and smaller near the walls, while it is negligible at the corners where the damping effect of the wall shear stresses is appreciable as shown in Figure (6).

The oscillatory phenomena can be explained by examining the nature of heat transfer mechanisms in free convection. Initially and for short periods after the introduction of the transients, conduction is the dominant mechanism of heat transfer. This would lead to large transverse temperature gradients. The existance of large temperature gradients will accelerate the velocity transients. For large Rayleigh's numbers, greater velocity response rates and higher velocities are expected. In such case, the natural convection effects will become appreciable after a short period from introducing the transients. The result of these effects will be a decrease in the transverse temperature gradients due to heat transfer by free convection from high temperature to low temperature regions. The decrease in the transverse temperature gradients would lead to a decrease in the velocity. The decrease in velocity means less heat transfer from the hot to the cold fluid regions, which will result in higher transverse temperature gradients.

The above described thermal and velocity interactions result in a cyclic increase and decrease in velocity and temperature.

In the case of small Rayleigh's number conduction accounts for

_arger percent of the heat transfer across the container, also the magnitude of the velocities will be small. Both of these factors account for the absence of oscillations for small Rayleigh's numbers.

Such oscillatory transients were predicted analytically by Zeiberg (8) for transient free convection in a heat generating fluid confined between two infinite parallel plates.

In his analysis of natural convection in long containers having a volume heat source, Woodrow (1) suggests that, in the regions not near the ends, a uniform vertical temperature gradient exists. His prediction was confirmed by the experimental results of reference (7). The same conclusion could be reached by examining the results obtained by the author. In Figure (8) the axial temperature distribution at constant values of y equal to 0.5 and 0.9 shows that such constant axial temperature gradients exist.

The author was unable to make comparison between the experimental and theoretical values of the velocities and temperatures because of the unavailability of the first. For the latter reason, calculations were made using a somewhat rough grid size, using $\Delta x = \Delta Y = 0.1$. The results of the calculations using a rough grid will give qualitative information about the nature of the temperature and velocity transients as well as the shape of the velocity and temperature profiles, since their magnitudes are usually affected by the grid sizes, but the flow pattern usually remains the same, Figure (9-a). Should the absolute magnitudes

of the temperature, or any related function, be of interest, then calculations should be carried out using smaller grid sizes.

Finally, an interesting question regarding whether the shape of the velocity distribution near the boundary could be fairly predicted by this method and to what extent, is examined. If the boundary layer thickness, although speaking about boundary layer flows in this case is not correct, is large compared to the grid size, then the shape of the velocity in the boundary layer near the wall could be fairly predicted. This will be true particularly for low Grashoff numbers and for large values of time, as shown in Figure (1). On the other hand, if that thickness is smaller than the chosen grid size, then that grid size would not give an accurate prediction of the shape of the velocity distribution near the wall. Smaller grid sizes should be used in such cases. This is the case where the Grashoff number is high, Figure (4-b). A close examination of Figure (4-a) shows that near the end regions there the boundary layer is thicker, the shape of the velocity profile near the wall is fairly predicted for high Grashoff numbers and small values of time. Figure (4-b) shows that for high Grashoff numbers, the results of calculations using rough grid size do not predict the shape of the velocity profile near the wall because the boundary layer thickness near the middle section of the tank height is small compared to that near the end regions. From Figures (9-a) and (9-b) it is clear that the smaller grid sizes give a better prediction of the velocity distribution near the wall, even at small time.

Acknowledgement

The author wishes to express his sincere gratitude to Professor John A. Clark, Professor of Mechanical Engineering, Professor -In- Charge, Heat Transfer Laboratory, University of Michigan. This work has been completed under his supervision and without his guidance and encouragement it would not have been done. The author is grateful to Professor R. C. F. Bartels the Director of the Computing Center and the staff of the computing center, University of Michigan for the machine-time that was made available to the author on the I.B.M. 7090 machine.

Reproduced from best available copy.

References

1. J. Woodrow, "Free Convection in Heat Generating Fluid (Laminar Flow)", 1953, A.E.R.E. E/R 1267.

2. F.G. Hammitt, "Heat and Mass Transfer in Closed Vertical, Cylinderical Vessels with Internal Heat Sources", PhD thesis, University of Michigan, 1957.

3. John A. Clark and H.Z. Barakat, "Transient Laminar Free Convection Heat and Mass Transfer in Closed Partially Filled Liquid Containers", Tech. Report No. 1, NACA Contract No. NAS-8-825. Huntsville, Alabama.

4. R.D. Richtmeyer, "Difference Methods for Initial Value Problem" Interscience Publication, 1957.

5. J. Hellums, "Finite-Difference Computation of Natural Convection Heat Transfer", PhD thesis, University of Michigan, 1960.

6. John Todd, "Survey of Numerical Analysis", McGraw-Hill, 1962, Chapter 11.

7. D. Wilkie and S.A. Fisher, "Natural Convection in Liquid Containing a Distributed Heat Source", International Developments in Heat Transfer, Part V."

8. Zeiberg, S.L. and Muller, W.K. "Transient, Laminar, Combined Fr and Forced Convection in a Duct", Journal of Heat Transfer, ASME Transactions, Series C, May 1962

NOMENCLATURE

a	half the width of the container
b	the initial height or the liquid
C_p	constant pressure specific heat, BTU/lbm $^{\circ}$F
Gr	Grashoff number = $g\beta(T_s - T_o)a^3/\nu^2$
g	the acceleration of gravity, ft/sec^2
k	thermal conductivity, BTU/hr ft $^{\circ}$F
p	pressure
Pr	Prandtl number = ν/α
Ra	Rayleigh number, (GrPr)
q'''	Heat generation, BTU/hr/ft^3
Q	Dimensionless heat generation term
T	temp R
t	time, sec.
u	x-component of the velocity, ft/sec
v	y-component of the velocity, ft/sec
U	dimensionless x-component of the velocity
V	dimensionless y-component of the velocity
x	axial distance, ft
X	dimensionless x
y	transverse, or normal distance measured from center line, ft
y	dimensionless y
w =	$\frac{a^2}{b^2}\frac{\partial^2\psi}{\partial x^2} + \frac{\partial^2\psi}{\partial y^2}$
α	thermal diffusivity, ft^2/sec
β	coefficient of thermal expansion

ρ density, lbm/ft^3

μ viscosity, lbm/ft-sec

ν kinematic viscosity, ft^2/sec

τ dimensionless time

θ dimensionless temperature

ψ stream function

Subscripts

i,j denotes position in the space grid

o denotes initial conditions

w wall

Superscript

n denotes the time level, $\tau = n \cdot \Delta\tau$

( )' refers to time level $\tau+\Delta\tau$

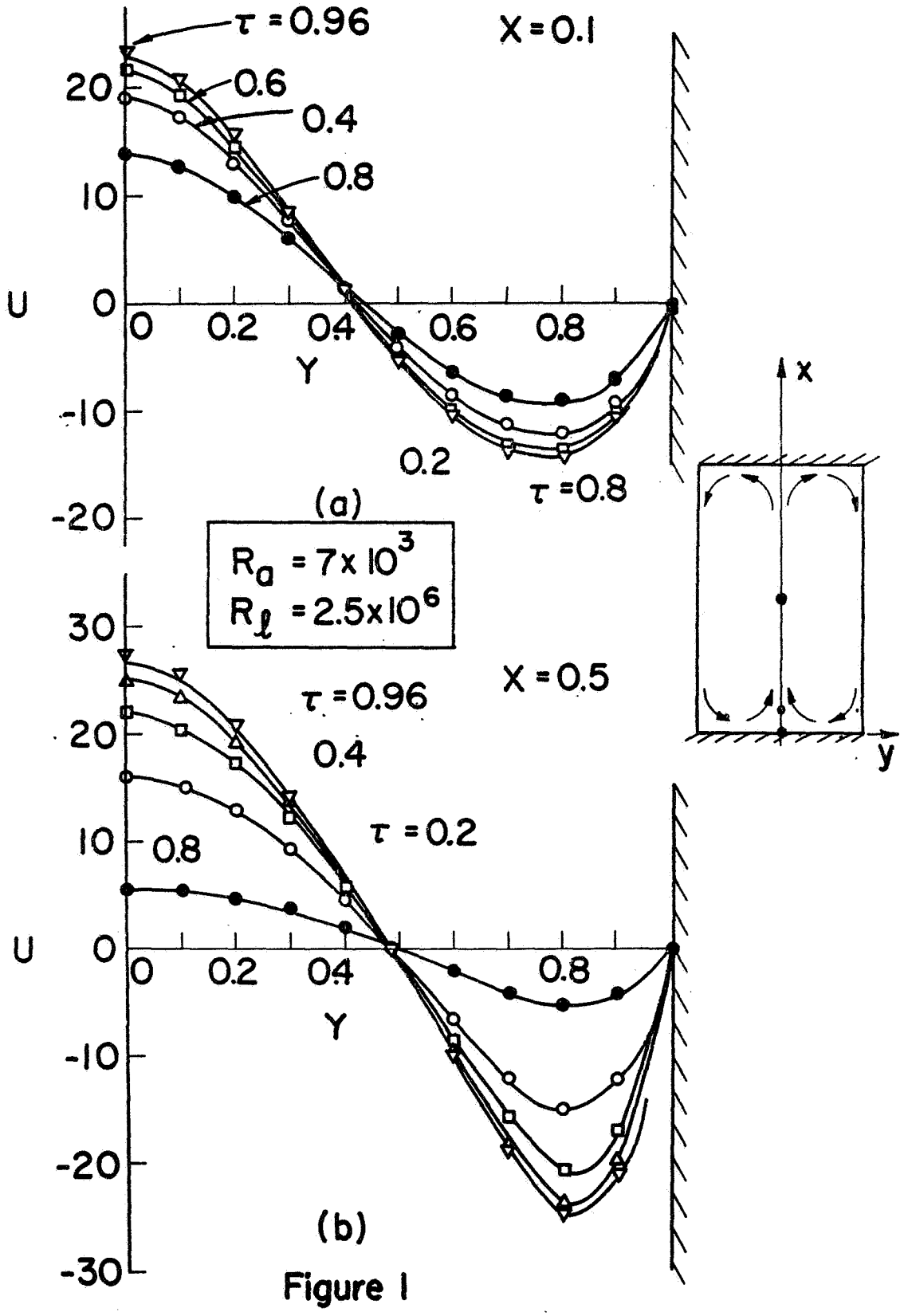


Figure 1

VELOCITY DISTRIBUTION ACROSS CONTAINER FOR THE LOW RAYLEIGH'S NUMBER

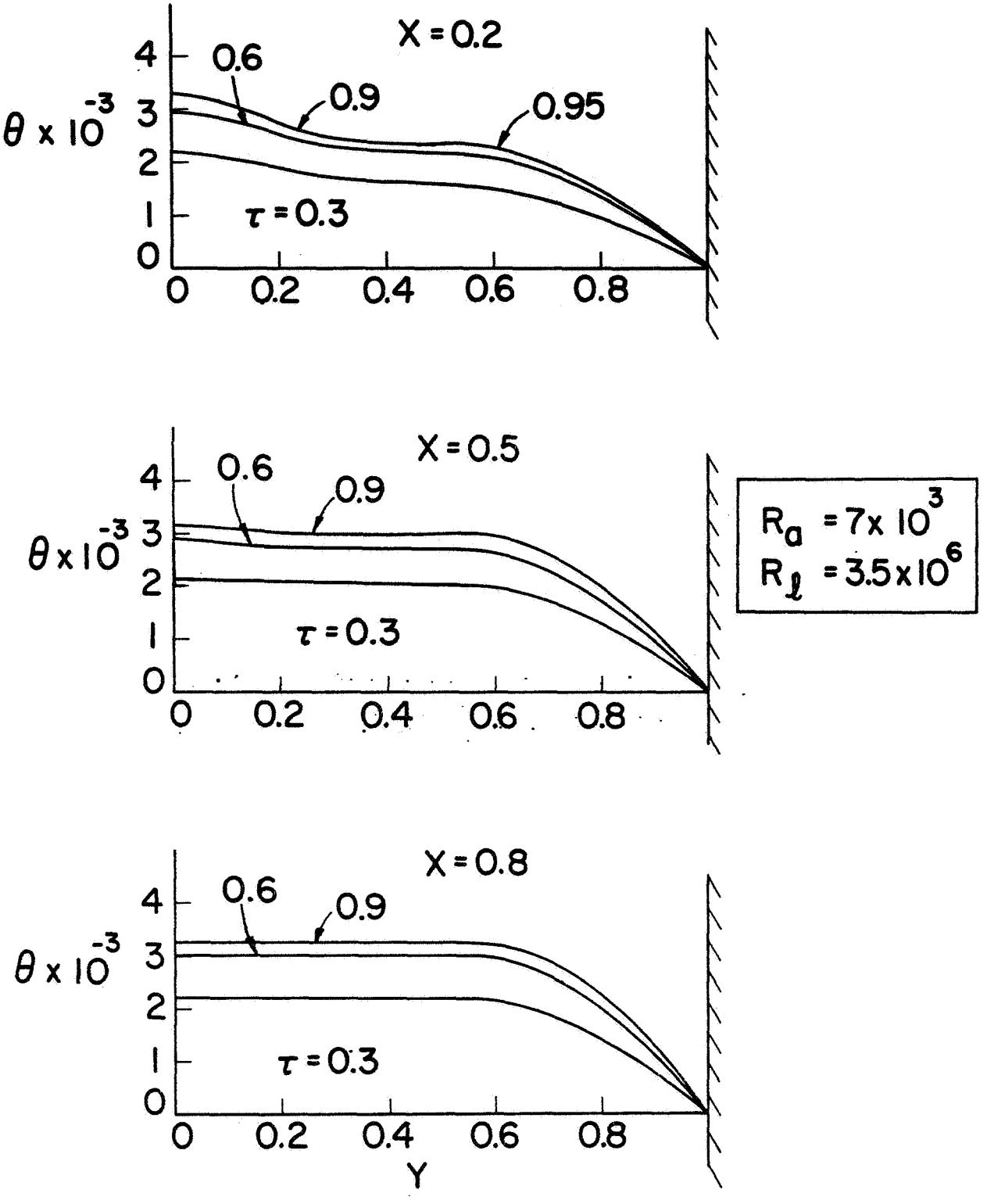


Figure 2

TEMPERATURE DISTRIBUTION ACROSS CONTAINER FOR LOW RAYLEIGH'S NUMBER

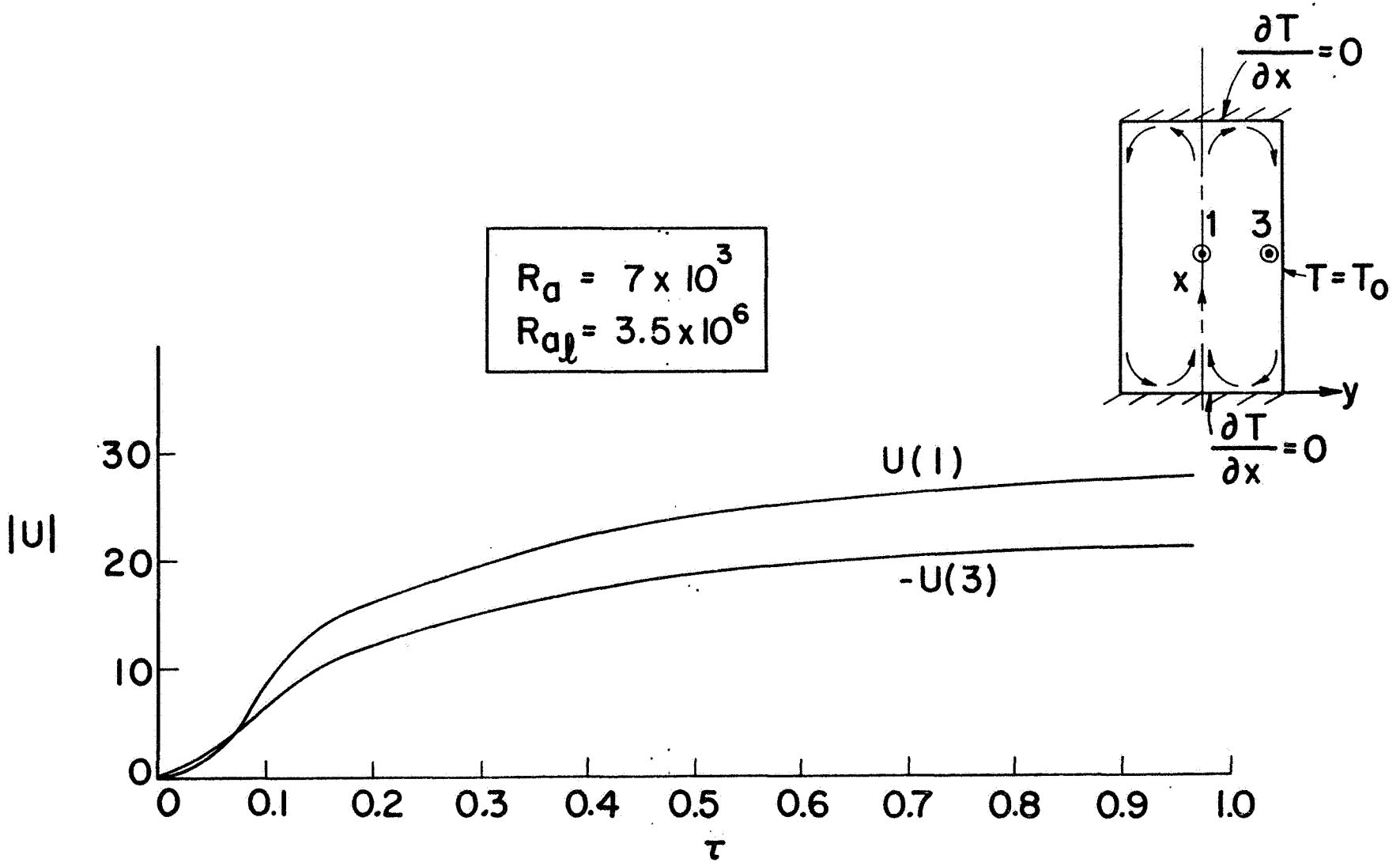


Figure 3
VELOCITY TRANSIENTS FOR THE LOW RAYLEIGH'S NUMBER

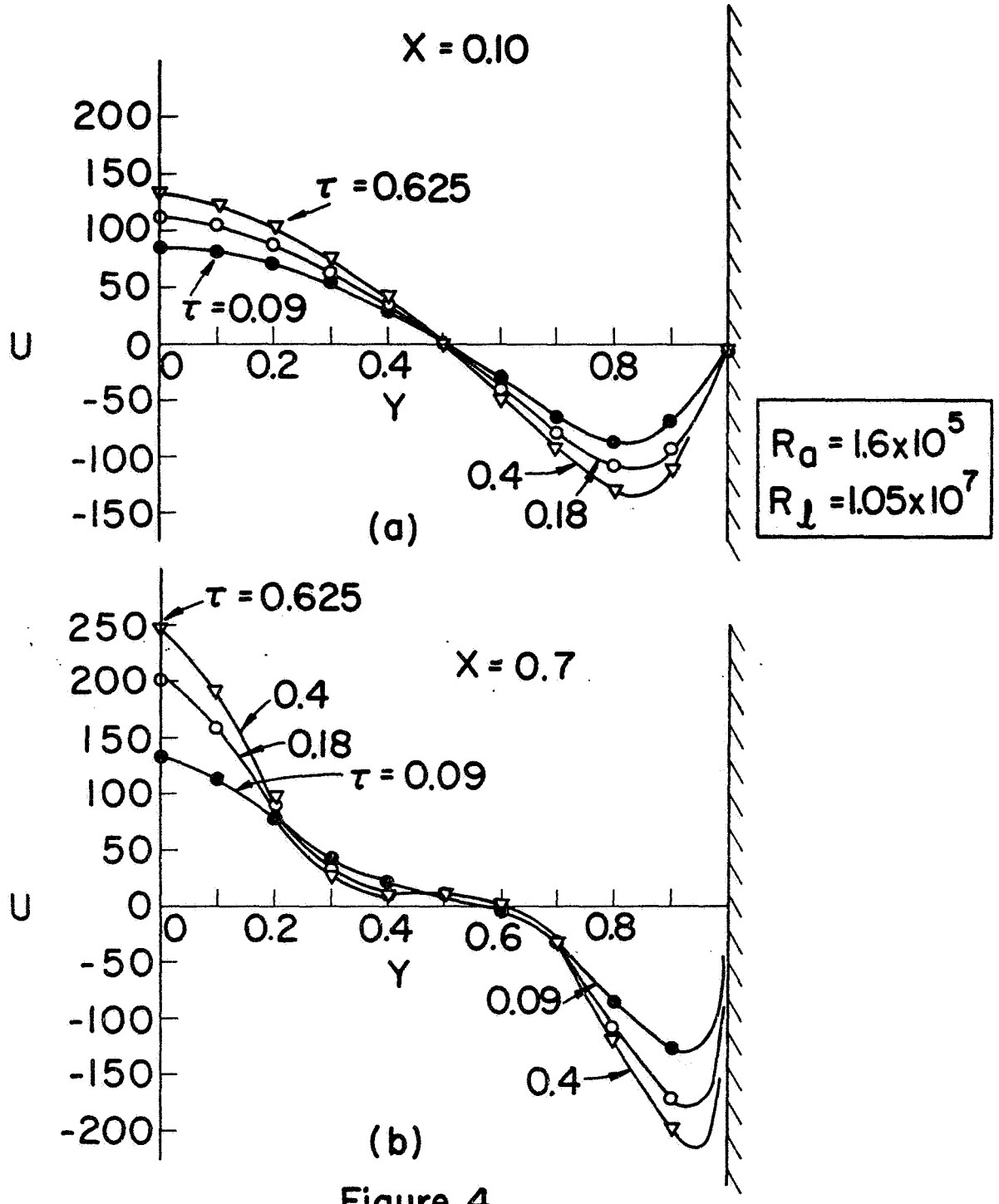


Figure 4

VELOCITY DISTRIBUTION ACROSS CONTAINER FOR THE HIGHER RAYLEIGH'S NUMBER

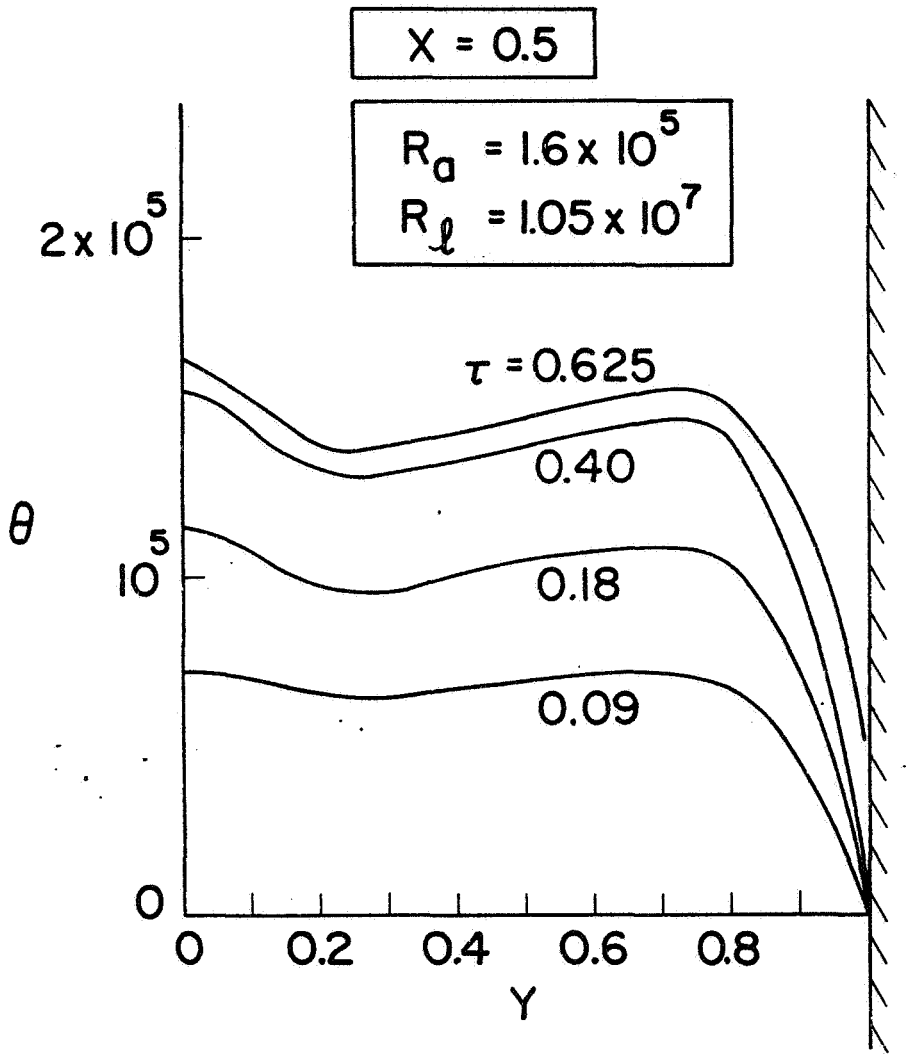


Figure 5

TEMPERATURE DISTRIBUTION ACROSS CONTAINER FOR THE HIGHER RAYLEIGH'S NUMBER

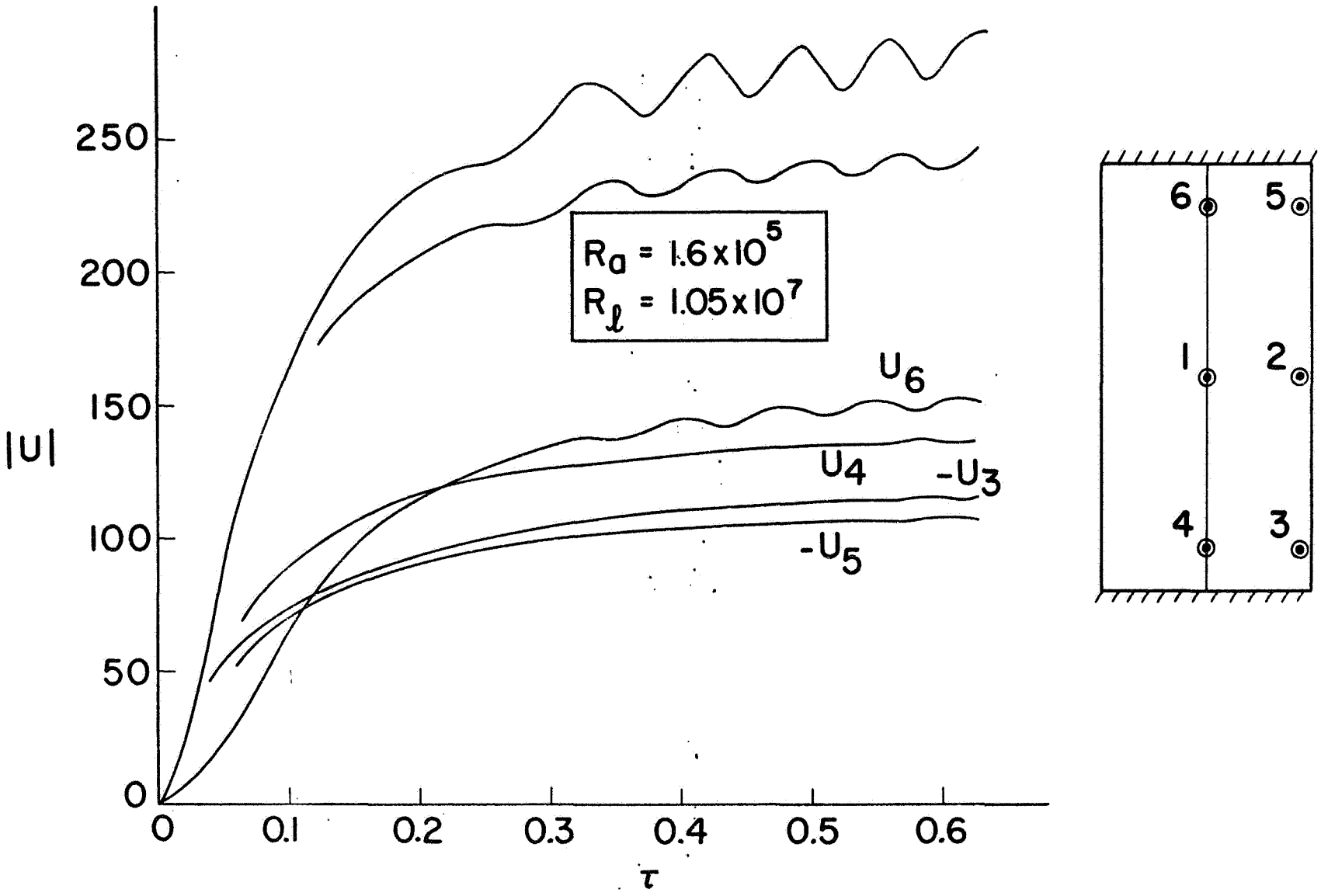


Figure 6

VELOCITY TRANSIENTS FOR THE HIGHER RAYLEIGH'S NUMBER

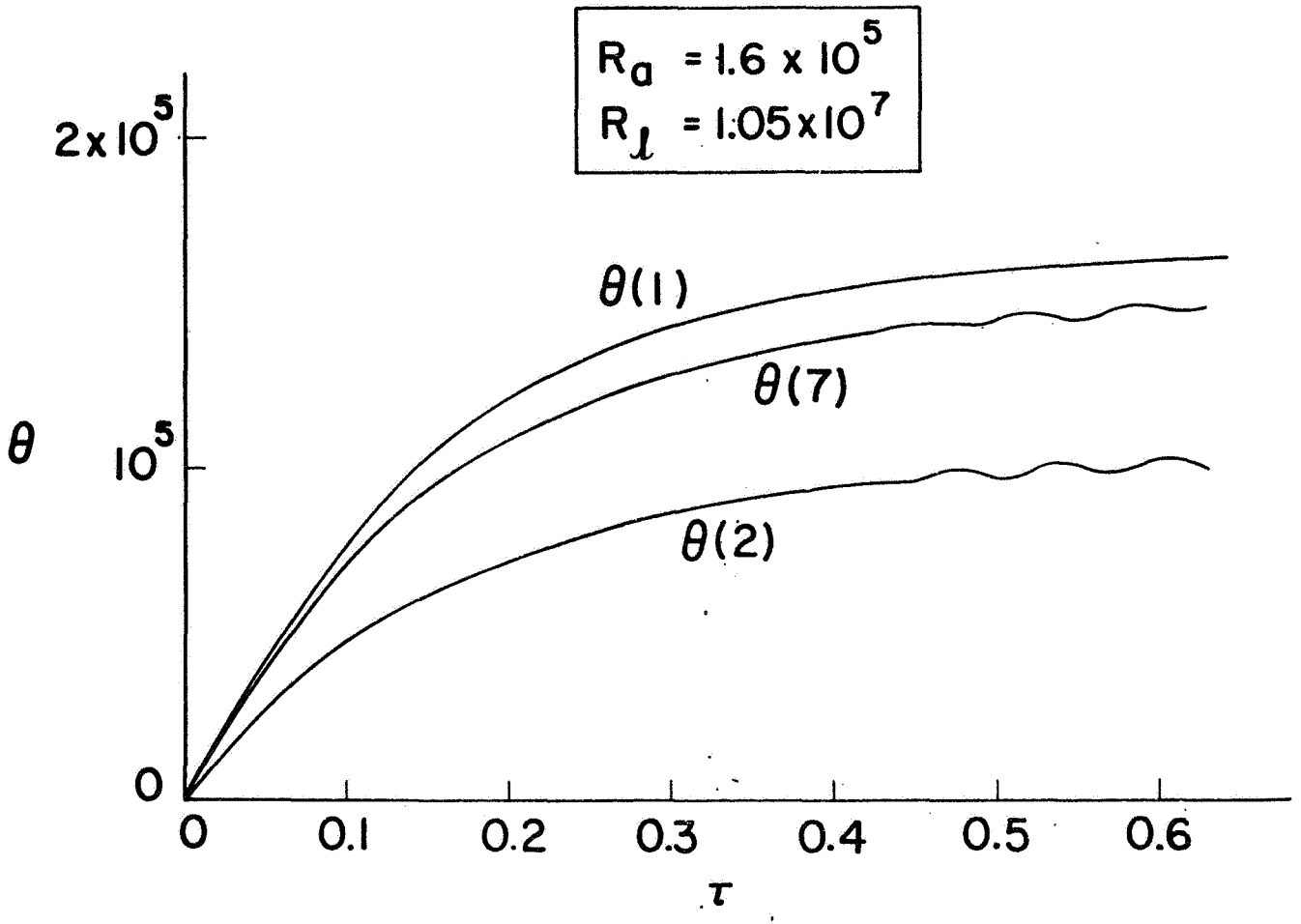


Figure 7

TEMPERATURE TRANSIENTS FOR THE HIGHER RAYLEIGH'S NUMBER

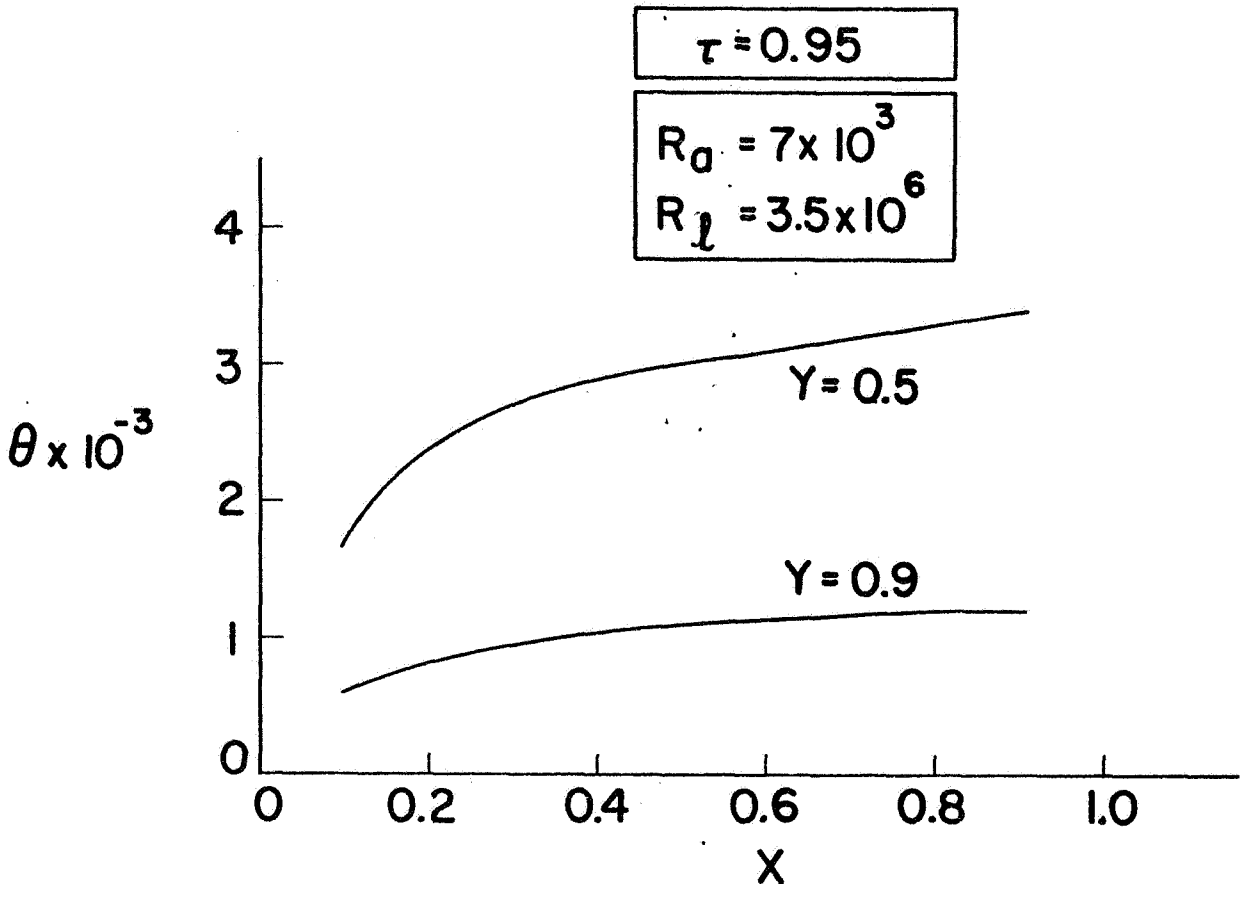


Figure 8

AXIAL TEMPERATURE GRADIENTS

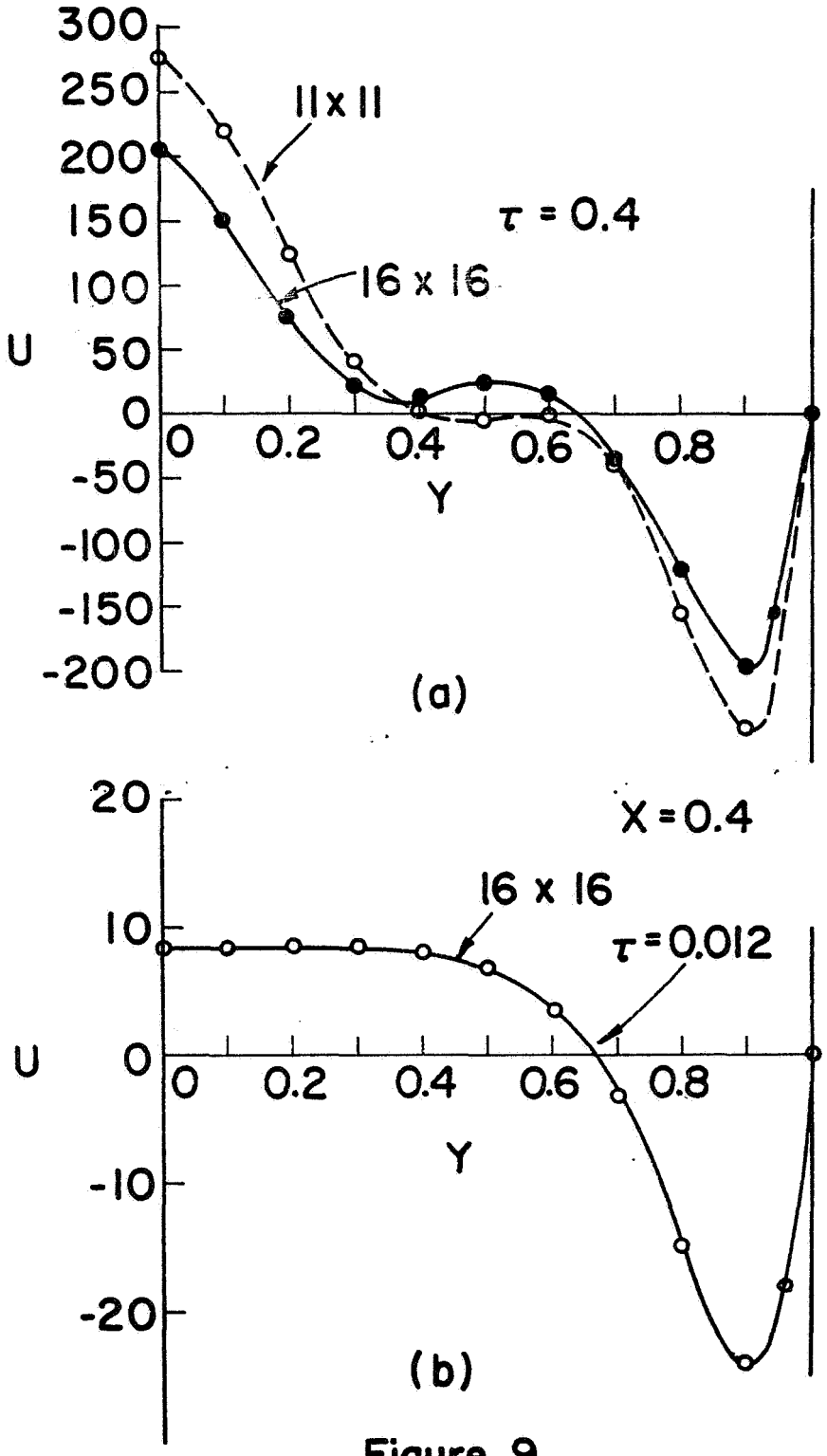


Figure 9

EFFECT OF GRID SIZE ON VELOCITY DISTRIBUTION

TRANSIENT, LAMINAR, FREE-CONVECTION HEAT AND MASS TRANSFER IN CLOSED, PARTIALLY FILLED, LIQUID CONTAINERS

by
John A. Clark, Hussein Z. Barakat
University of Michigan
Ann Arbor, Michigan

Preceding page blank

THE UNIVERSITY OF MICHIGAN
COLLEGE OF ENGINEERING
Department of Mechanical Engineering
Heat Transfer and Thermodynamics Laboratory

TRANSIENT, LAMINAR, FREE-CONVECTION HEAT AND MASS TRANSFER IN CLOSED, PARTIALLY FILLED, LIQUID CONTAINERS

John A. Clark
Hussein Z. Barakat

ORA Project 04263

under contract with:

NATIONAL AERONAUTICS AND SPACE ADMINISTRATION
GEORGE C. MARSHALL SPACE FLIGHT CENTER
CONTRACT NO. NAS-8-825
HUNTSVILLE, ALABAMA

administered through:

OFFICE OF RESEARCH ADMINISTRATION ANN ARBOR

Preceding page blank

TABLE OF CONTENTS

	Page
NOMENCLATURE	v
ABSTRACT	vii
I. INTRODUCTION	
II. REVIEW OF THE LITERATURE	1
A. Analytical Studies	3
B. Experimental Studies	8
III. THEORETICAL ANALYSIS	13
A. Formulation	13
1. Statement and physics of the problem	13
2. General model	14
3. Simplified model	18
B. The Solution	22
C. Finite-Difference Approximations	23
D. Stability and Convergence	27
IV. RESULTS	34
A. The Effect of Gride Size	37
B. Comparison with Experiment	38
V. CONCLUSIONS	40
ACKNOWLEDGMENT	41
REFERENCES	42
APPENDIX COMPUTER PROGRAM	45

NOMENCLATURE

a	half the width of the container
b	the initial height of the liquid
C_p	constant pressure specific heat, Btu/lbm°F
Gr	*Grashof number* = $g\beta(T_s-T_o)a^3/\nu^2$
g	the acceleration of gravity, ft/sec^2
h_{fg}	latent heat of evaporation or condensation Btu/lbm
k	thermal conductivity, Btu/hr ft °F
p	pressure
Pr	Prandtl number = γ/α
Ra	Rayleigh number (GrPr)
$(q/A)_w$	heat flux at the walls of the tank per unit area, Btu/hr/ft^2
T	temp R
t	time, sec
u	x-component of the velocity, ft/sec
v	y-component of the velocity, ft/sec
U	dimensionless x-component of the velocity
V	dimensionless y-component of the velocity
x	axial distance, ft
X	dimensionless x
y	transverse, or normal distance measured from center line, ft
Y	dimensionless y

$$w = \frac{a^2}{b^2}\frac{\partial^2\psi}{\partial X^2} + \frac{\partial^2\psi}{\partial Y^2}$$

α thermal diffusivity, ft^2/sec

β coefficient of thermal expansion

ρ density, lbm/ft^3

μ viscosity, lbm/ft/sec

ν kinematic viscosity, ft^2/sec

ϕ dissipation function for two-dimensional incompressible flow is given by

$$\phi = 4\left(\frac{\partial u}{\partial x}\right)^2 + \left(\frac{\partial v}{\partial x} + \frac{\partial u}{\partial y}\right)^2$$

τ dimensionless time

Θ dimensionless temperature

ψ stream function

λ an eigenvalue

Subscripts

c cold wall

g vapor

h hot wall

s saturation or liquid surface

i,j denotes position in the space grid

o denotes initial conditions

w wall

Superscript

n denotes the time level

ABSTRACT

13028

The two-dimensional, laminar, transient, natural convection heat and mass transfer in a closed rectangular container with a free surface is studied. The x-momentum, the y-momentum, and the continuity equations are coupled to obtain the vorticity transport equation, which is integrated numerically using the finite-difference approximation. The problem of stability, which is associated with the difference equations, is studied. The convergence of the solution of the difference equations so that of the differential equation is examined. Results of the calculations for different boundary conditions are given. Comparison of the theoretical results with two experimental measurements from the literature indicate qualitative agreement.

Author

I. INTRODUCTION

This report presents the initial results of a program of research dealing with transient, free convection inside closed containers. The problem reported is the first phase of a program directed at an understanding and prediction of fluid behavior in closed containers subject to various disturbances, including those of ambient heat flux, change in wall temperature, pressurization, change in gravitational field, and liquid discharge. The objectives of the general program are the prediction of transient velocity profiles, temperature stratification, and pressure histories in such containers.

The present report treats laminar transient free convection in a two-dimensional container having a liquid-vapor interface. Transient processes are introduced by a sudden increase in the temperature of the container wall and by a sudden application of heat flux to the external surfaces of the container. For a system at constant pressure and at normal gravity the resulting transient flow patterns and temperature stratification are computed.

The problem is formulated from the complete Navier-Stokes equations coupled with those from the First Law of Thermodynamics and the Conservation of Mass. Boundary-layer approximations are not made since the geometry and boundary conditions invalidate complete boundary-layer flow and require additional momentum considerations not usually found in boundary-layer calculations. Reduction of the governing equations is done by numerical procedures using

Preceding page blank

an IBM 7090 digital computer. Special attention is given to the problem of convergence and stability of the numerical solution.

Combined with the experimental program presently under way, these results will aid in the establishment of criteria for the onset of transition flow in the container, the start of surface boiling, and will be useful in formulating the solution for the case of turbulent convection.

II. REVIEW OF THE LITERATURE

In the past, considerable effort has been given to the study of natural convection heat and mass transfer. Many problems have been solved under different conditions of geometry and arrangements. These studies have been of an analytical as well as an experimental nature. An extensive survey of literature showed that the problem of natural convection in closed-end tubes with a free surface has not been considered analytically, however, some problems with related geometries have been considered. The extrapolation of the results of these studies to other geometry can give misleading results owing to the complicated nature of transient free-convection phenomena.

A. ANALYTICAL STUDIES

The case of a vertical element immersed in an infinite fluid initially at rest has received the most attention of many investigators. The time-steady laminar flow equations were first solved by Pohlhausen[25] for air. The experimental results of Schmidt and Beckman[2] are in good agreement with Pohlhausen's solution. Later, Ostrach[20] solved the same problem using numerical methods with high-speed digital computer for different values of Prandtl number ranging from 0.01 to 1000.

The transient free convection from vertical flat plates, with and without appreciable thermal capacity and variable fluid properties, has been studied by different investigators for different boundary conditions.[8,29,30,33,34]

Leitzke[16] considered the steady-state natural convection between two

parallel, infinite flat plates oriented in the direction of body force in which one plate is heated and the other is cooled uniformly. The measured temperature distribution across the fluid is in good agreement with the theory. A generalization of the same problem was carried on by Ostrach,[20,21] in which the plates are maintained at constant temperatures not necessarily equal, and the effect of heat sources and frictional heating was included. As anticipated, the effect of heat sources and viscous heating increases the temperatures and the velocities between the plates. The transient free convection in a duct formed by two infinite parallel plates with arbitrary time variations in the wall temperature and the heat generation was studied by Zeiberg and Mueller.[37]

The two-dimensional steady-state convection in a long rectangle, of which the two long sides are vertical boundaries held at different temperature and the two horizontal boundaries either insulated or have linear temperature distribution, was considered by Batchelor.[1] He did not solve for the velocity or temperature distribution, but he considered the determination of the rate of heat transfer between the two vertical boundaries and the type of different flow regimes that occur for a given value of Rayleigh's number and aspect ratio. For Rayleigh's numbers less than 10^3, Batchelor uses a power series expansion in terms of Rayleigh's number Ra for the dimensionless temperature Θ and the stream function. On substitution of the power series in the governing differential equations and equating coefficients of the like powers of Ra, the problem is reduced to the solution of a series of linear partial differential equations. The Nusselt number, defined as

$$NU = (q/A)_w/K(T_h-T_c) \quad ,$$

is estimated to be of the order

$$NU = \ell/d + 10^{-8}\ Ra^2 \quad ,$$

where d is the distance between the plates and ℓ the height of the duct. For the case of $\ell/d \to \infty$, he argues that for the regions not near the ends the temperature and the stream function take their asymptotic values, which are given by the solution of two infinite parallel plates, one heated and the other cooled. For infinite values of Ra, he postulates that there is an isothermal core having constant vorticity. He found that the governing equations for the general case could not be represented by a polynomial of small degree nor could they be handled by the Oseen type of linearization.

Poots[26] solved the same problem handled by Batchelor. He obtained a numerical solution based on the use of orthogonal polynomials for the solution of the governing differential equations. Following Batchelor, the stream function and the nondimensional temperature were assumed to be represented by the complete double series of orthogonal functions

$$\Theta = \sum_{n=1}^{\infty}\sum_{m=1}^{\infty} A_{nm} \sin n\pi x \sin m\pi y$$

and

$$\psi = \sum_{n=1}^{\infty}\sum_{m=1}^{\infty} B_{nm}X_n(x)Y_m(y) \quad ,$$

where the A and B are constants which were evaluated numerically. The governing differential equations were reduced to two coupled algebraic equations to be solved simultaneously. The functions $X_n(x)$ were chosen to satisfy the fourth order Sturm-Liouville system and the orthogonality property. The method of solution is tedious, and the calculations are practically impossible for Rayleigh's numbers greater than 10^4 and aspect ratios greater than 4. The results for Rayleigh's number 10^4 and aspect ratio unity are shown in Fig. 14. There is an isothermal core having uniform temperature; there is also a constant vorticity in the core. In the region between the core and the cavity walls, the temperature and the stream function oscillate once near the core and then tend smoothly to their appropriate values at the cavity wall. The boundary layer is continuous between the wall and the core.

Lighthill[18] examined natural convection flows generated by large centrifugal forces in a tube closed at one end and open at the other end to an infinite reservoir, where the tube walls are maintained at a constant temperature. Such a situation exists in cooling gas-turbine blades. He predicted that one of the following three regimes may exist, depending upon the product of Grashof number and the radius-to-length ratio of the tube. The assumed flow regimes are:

1. Similarity flow. For small values of this product, i.e., for large values of length-to-radius ratio for a given Grashof number, the boundary layer fills the tube. The velocity and temperature profiles are fully developed. He predicted that for this type of flow, the velocity and temperature distribution are similar at each section of the tube, only their scale is

ncreasing as the orifice is approached. Assuming that the velocity and temperature vary linearly along the tube, he concluded that there is an aspect ratio for which the temperature changes from its value at the orifice to the value at the bottom. Extending the tube beyond the length determined by the above ratio, the additional length is filled with fluid at rest at the wall's temperature.

2. Boundary-layer type of flow. For high values of the product of Grashof number and radius-to-length ratio, i.e., for short tubes, the flow is of boundary-layer type. In the extreme case, when the boundary layer fills a negligible portion of the tube area, the flow approximates the free-convection flow up a flat plate.

3. Non-similarity regime. This is the type of flow predicted to exist for values of length-to-radius ratio which lie between the values corresponding to the first and the third case. The boundary layer fills a large portion of the tube section. He used the Squire technique to solve the first and the third cases.

Hammitt[9] considered the case of a closed vertical cylinder with internal heat generation. He used the Lighthill technique, modified to account for the heat sources. The agreement between the calculated and measured values of Nusselt's number is not good. This is probably due to some of the inevitable assumptions which are made: (1) small inertia forces compared to buoyancy and shear, (2) radial extend of the temperature and velocity boundary layers is the same, (3) the boundary-layer approximations apply. The first assumption is valid for large Prandtl numbers; the second is valid for

Prandtl numbers near unity. The disadvantage of this method of solution is that it is in capable of detailed examination of the end conditions.

Following Lighthill, Ostrach and Thornton[22] considered a geometrically similar case with a linear wall temperature. In Ostrach's paper, as well as in Lighthill's paper, attention was given to the stagnation of natural convection flows at the closed end. The same problem considered by Lighthill was solved by Levy,[17] using integral methods. He assume that the upward flow consists of a layer of thickness δ near the wall, the remainder of the tube being filled with cold fluid flowing downward. He assumes three regimes of flow similar to those postulated by Lighthill. If the tube length is less than or equal to a length ℓ, the stagnation region does not exist and the upflow convective layer increases with x. For axial distance $x > \ell_1$, δ reaches a constant value d, and such a flow occurs for $\ell_1 < x < \ell_2$. For $x > \ell_2$, there is a stagnation region at the closed section of the tube.

Romonov,[28] also using integral techniques, solved the same problem considered by Lighthill and Levy. His calculations agree with those of Lighthill for infinite Prandtl number, but they differ considerably for Prandtl numbers near unity. The measured and the calculated temperatures are in a good agreement for different wall temperatures.

B. EXPERIMENTAL STUDIES

A large number of experimental studies have involved flat plates immersed in an infinite fluid at rest and either heated or cooled. In general, there has been good agreement between theory and experiment. Considerable exper-

imental work has been done in the field of natural convection in tubes and enclosures. This work has concerned specialized applications and particular configurations. Most of the experiments were in connection with cooling gas-turbine blades and nuclear reactor applications. Although most, if not all, of these experiments are not applicable to this study, they will be helpful in indicating the general trend and the type of experimental equipment required.

Probably the most comprehensive experimental studies of natural convection in thermosyphons are those conducted by Martin[19] in an attempt to check the theoretical work of Lighthill. His results agree qualitatively, although the measured heat-transfer coefficients are nearly twice as large as those predicted by Lighthill. The three regimes predicted by Lighthill were identified from measurements of heat transfer rates. The heat transfer rate was greatest for large values of theproduct of Grashof number and the radius-to-length ratio. The rate was highest at the bottom of the tube, which indicates that there is boundary-layer type of flow. At small values of the product, theheat transfer varied linearly from the orifice to zero at the bottom of the tube, from which Martin concluded that there is a similarity regime. A region of instabilities, characterized by nonsinusoidal oscillatory flow, occurred between the above two steady regimes.

Siegel and Norris[31] shed some light on the oscillatory flow mentioned by Martin by exploring the air flow patterns in the space between two heated wide plates, closed at the bottom, open at the top, and insulated at the sides. For spacing of 0.28 of the plate height, the flow pattern was symmetric, with

upward flowing boundary layers near each plate surface and downflow in between. When the spacing was reduced to 0.21 of the height, the flow pattern became asymmetric, with half the cross section occupied by upward (near one plate) and the half near the other plate occupied by downward flow. For smaller spacings, the asymmetric pattern presisted with periodic non-sinusoidal reversal in flow direction and temperature fluctuations.

Curren and Zalabak[4] conducted an experimental investigation to determine the effect of length-to-diameter ratio of closed end coolant passages on natural-convection water cooling of gas turbines. They reported no significant difference in the heat transfer for the different length-to-diameter ratios investigated ranging from 5:1 to 25.5:1. For the largest length-to-diameter ratio, 25.5:1, the boundary layer fills 87% of the tube cross section.

The visual studies of Sparrow and Kauffman[36] of free convection of water in a narrow vertical enclosure, cooled at the top through a copper surface and open at the bottom to a heated reservoir, revealed that the flow pattern is not steady. No region of the enclosure is permanently a region of upflow or of downflow. The size of the various upflow and downflow regions varied along the length of the enclosure at a given time. The number and size of upflow and downflow regions also varied with time. However, end effects were observed, and a continuous downflow took place in a 3/4-inch band adjacent to both walls. Generally, the dominating character of the flow was instability.

Hartnett, et al.,[10,11,15] studied the free-convection heat transfer for

the geometry postulated by Lighthill, but with a constant heat flux at the tube wall and water and mercury as working fluids. The effect of inclining the tube was also investigated. Temperature oscillations of the same nature as those reported by Martin and Siegel and Norris were observed. Contrary to the results reported by Curren and Zalabak, the heat transfer was considerably influenced by length-to-radius ratio. A decrease in length-to-radius ratio from 22.5 to 15 results in approximately 100 percent increase in the Nusselts numbers.

Skipper, et al.,[32] studies the natural-convection flow pattern in viscous oil in rectangular tanks heated at the center by vertical coil heater. The flow pattern consisted of a narrow chimney of hot oil rising vertically around and above the heater surface, and a horizontal layer of hot oil at the free surface separated by a sharp vertical gradient from the remaining cold oil below. The hot oil layer had a small vertical temperature gradient, with maximum temperature at the top. The hot oil layer at the surface became increasingly thick with continued heating. The hot oil was found to flow downward at the walls of the tank, while there were suggestions of circulating currents at the side of the rising chimney. The flow pattern shown suggests that a vortex was formed at the free surface near the center line where the hot rising chimney is bifurcated and spread horizontally along the surface. Eichhorn[6] observed similar vortices. These vorticies were formed at the free surface of water near the walls of a cylindrical tube 2 inches diameter and 5-inches long, uniformly heated at the walls and open at the top.

Some of the literature pertaining to the problem at hand will be mentioned later in this study where its application is more important.

III. THEORETICAL ANALYSIS

A. FORMULATION

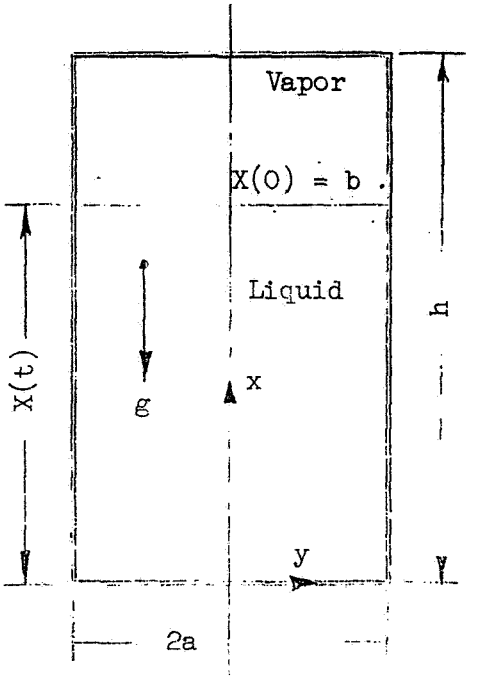
1. Statement and Physics of the Problem

A closed container is partially filled with a cryogenic liquid. Initially the liquid and the vapor which fills the ullage volume are assumed to be in equilibrium at the temperature T_o, the stauration temperature corresponding to the initial pressure P_o. Previous tests indicate that boiling due to heat leaks from the ambient is a surface phenomenon only; vapor bubble formation is confined to very near the surface; the rest of the liquid does not contain vapor bubbles, and a small change in the ullage pressure is sufficient to cause boiling to cease.[13] From this initial condition, the wall of the vessel is assumed to undergo a step change in temperature or is assumed to be subjected to a uniform heat flux. Simultaneously, the pressure in the ullage volume is changed to P_s, which may be equal to or greater than P_o. The measurements reported in Refs. 3 and 7 indicate that the interface temperature rises very rapidly to T_s, the saturation temperature corresponding to the pressure P_s in the ullage space for these conditions. Buoyant forces, caused by density variations in the liquid, set up natural convection currents. The liquid-vapor system tends to adjust to the new non-equilibrium condition by transferring mass and energy across the interface. The controlling factor is the interface temperature, and each region transfers heat independently of the bulk temperature of the other region. An imbalance of the

heat transfer at the liquid-vapor interface is counterbalanced by a phase change, i.e., either transient evaporation or condensation occurs at the interface. In this analysis, the problem is formulated in its general form, taking into consideration the interaction between the liquid and the vapor phase. Later the problem is simplified, making it tractable for analysis without seriously impairing its utility.

2. General Model

Consider a rectangular two-dimensional tank of width 2a and height h. The initial height of the liquid is b, and the depth of the vapor is c. The origin of the coordinate system is taken at the middle of the tank bottom with x positive in the direction of the liquid. The g-level is sufficiently high so that the effect of surface tension can be neglected. The location of the liquid-vapor interface at any one time is given by $x = X(t)$. The two-dimensional transient conditions will be considered.



The differential equations governing the velocity and temperature distribution in the liquid and vapor regions are:

The momentum equations:

The x-momentum equation:

$$\rho\left(\frac{\partial u}{\partial t} + u\frac{\partial u}{\partial x} + v\frac{\partial u}{\partial y}\right) = -\rho g - \frac{\partial p}{\partial x}$$

$$+ \frac{\partial}{\partial x}\left[\mu\left\{2\frac{\partial u}{\partial x} - \frac{2}{3}\left(\frac{\partial u}{\partial x} + \frac{\partial v}{\partial y}\right)\right\}\right] + \frac{\partial}{\partial y}\left[\mu\left(\frac{\partial u}{\partial y} + \frac{\partial v}{\partial x}\right)\right] \qquad (1)$$

The y-momentum equation:

$$\rho\left(\frac{\partial v}{\partial t} + u\frac{\partial v}{\partial x} + v\frac{\partial v}{\partial y}\right) = -\frac{\partial P}{\partial y} + \frac{\partial}{\partial x}\left[\mu\left(\frac{\partial u}{\partial y} + \frac{\partial v}{\partial x}\right)\right]$$

$$+ \frac{\partial}{\partial y}\left[\mu\left\{2\frac{\partial v}{\partial y} - \frac{2}{3}\left(\frac{\partial u}{\partial x} + \frac{\partial v}{\partial y}\right)\right\}\right] \qquad (2)$$

The energy equation:

$$\rho\, C_p\left(\frac{\partial T}{\partial t} + u\frac{\partial T}{\partial x} + v\frac{\partial T}{\partial y}\right) = \frac{\partial P}{\partial t} + u\frac{\partial P}{\partial x} + v\frac{\partial P}{\partial y}$$

$$+ \frac{\partial}{\partial x}\left(\kappa\frac{\partial T}{\partial x}\right) + \frac{\partial}{\partial y}\left(\kappa\frac{\partial T}{\partial y}\right) + \mu\,\phi \qquad (3)$$

where, ϕ = dissipation function (see Nomenclature)

The continuity equation:

$$\frac{\partial \rho}{\partial t} + \frac{\partial(\rho u)}{\partial x} + \frac{\partial(\rho v)}{\partial y} = 0 \qquad (4)$$

Initial conditions:

$$T(x,y,o) = T_g(x,y,o) = T_o \tag{5}$$

$$u(x,y,o) = v(x,y,o) = u_g(x,y,o) = v_g(x,y,o) = 0 \tag{6}$$

Boundary conditions:

(a) Velocity boundary conditions.

Assuming the no-slip condition to prevail at the tank walls, the following boundary conditions are obtained:

$$u(o,y,t) = u(x, \pm a,t) = 0 \tag{7}$$

$$v(o,y,t) = v(x, \pm a,t) = 0 \tag{8}$$

$$u_g(h,y,t) = \dot{m}_g/(P_g \cdot A) \tag{9}$$

$$u_g(x, \pm a,t) = v_g(x, \pm a,t) = v_g(h,y,t) = 0 \tag{10}$$

Assuming zero shear stress at the liquid-vapor interface, the interfacial boundary conditions could be stated as:

$$u(X,y,t) = u_g(X,y,t) = \frac{dX}{dt} \tag{11}$$

$$\frac{\partial v}{\partial x}(X,y,t) = \frac{\partial v_g}{\partial x}(X,y,t) = 0 \tag{12}$$

From the geometric symmetry of the configuration with respect to the y-

axis, it is assumed that the y-component of the velocity vector is zero at the axis of the tank and that the x-component of the velocity is an even function of y, i.e.,

$$v(x,o,t) = 0 \tag{13}$$

$$\frac{\partial u}{\partial y}(x,o,t) = 0 \tag{14}$$

(b) Thermal boundary conditions.

The bottom and the upper surface of the tank are either insulated, subjected to a uniform heat flux, or kept at a constant temperature. The walls are either subjected to a uniform heat flux or kept at a constant temperature. Owing to symmetry, the temperature will be an even function of Y.

(1)
$$\frac{\partial T}{\partial y}(x,o,t) = \frac{\partial T_g}{\partial y}(x,o,t) = 0 \tag{15}$$

(2) - a. $\frac{\partial T}{\partial x}(o,y,t) = \frac{\partial T_g}{\partial x}(h,y,t) = 0$

b. $k\frac{\partial T}{\partial x}(o,y,t) = k_g\frac{\partial T_g}{\partial x}(h,y,t) = (q/A)_w$

c. $T(o,y,t) = T_g(h,y,t) = T_w$ (16)

(3) - a. $k\frac{\partial T}{\partial y}(x, \pm a,t) = k_g\frac{\partial T_g}{\partial y}(x, \pm a,t) = (q/A)_w$

b. $T(x, \pm a,t) = T_g(x, \pm a,t) = T_w$ (17)

(4) - a. $T(X,y,t) = T_g(X,y,t) = T_s$

b. $\frac{\partial T}{\partial x}(b,y,t) = \frac{\partial T_g}{\partial x}(b,y,t) = 0$ (18)

Any case considered in this work is a combination of the thermal boundary condition, given by Eq. (15), and one of each of the other three boundary conditions given by Eqs. (16), (17), and (18).

Applying the conservation of energy across the interface

$$\rho h_{fg}\left(\frac{dX}{dt}\right) = k\left(\frac{\partial T}{\partial x}(X,y,t)\right) - k_g\left(\frac{\partial T_g}{\partial x}(X,y,t)\right) \qquad (19)$$

In addition to the boundary conditions stated above, we have the equation of state $P = f(\rho,T)$ for the vapor region. Also, an overall energy and mass balance, considering the system composed of the vapor and liquid regions, is automatically satisfied by any exact solution; it provides a means of checking assumptions or simplifications introduced later in this analysis. As another check on the solution, the net rate of fluid flow across any section of the liquid tank is equal to zero, i.e., $\int_{-a}^{a} u\,dy = 0$

3. Simplified Model

Due to the complexity of the problem, only the liquid region is considered, for which a simplified model is adapted. In reality, the amount of evaporation or condensation is small; therefore, the interfacial displacement is neglected, and the interface is assumed to be always at $x = b$. The pressure of the vapor is considered to be constant; consequently the interface temperature is constant. Constant fluid properties μ, C_p, k and ρ are assumed. Density varia-

tions are allowed in the x-momentum equation only. The pressure terms and the dissipation function in the energy equation are neglected.

Initially the pressure throughout the tank is the hydrostatic pressure. The variations in pressure and density caused by the fluid motion and temperature gradients from initial values are expected to be small. Therefore the following assumptions are introduced:

$$P = P_o + P'$$

and

$$\rho = \rho_o + \rho'$$

where P_o is the initial hydrostatic pressure, P' the change in pressure from the initial value, ρ_o initial density, and ρ' the change in density.

Since the pressure variations are small, the density changes due to pressure are negligible, and density variations are caused mainly by temperature changes. Then ρ' can be closely approximated by

$$\rho' = \rho - \rho_o \approx \rho_o \beta(T_o - T) \tag{22}$$

where β is the coefficient of thermal expansion.

Similarly,

$$\frac{\partial P}{\partial x} = -\rho_o g + \frac{\partial P'}{\partial x} \tag{23}$$

$$\frac{\partial P}{\partial y} = \frac{\rho P'}{\partial y} \tag{24}$$

Substituting the above expressions in the momentum equations:

The x-momentum:

$$\rho\left(\frac{\partial u}{\partial t} + u\frac{\partial u}{\partial x} + v\frac{\partial u}{\partial y}\right) = \rho_o \beta g(T-T_o) - \frac{\partial P'}{\partial x} + \mu\left(\frac{\partial^2 u}{\partial x^2} + \frac{\partial^2 u}{\partial y^2}\right) \qquad (25)$$

The y-momentum:

$$\rho\left(\frac{\partial v}{\partial t} + u\frac{\partial v}{\partial x} + v\frac{\partial v}{\partial y}\right) = -\frac{\partial P'}{\partial y} + \mu\left(\frac{\partial^2 v}{\partial x^2} + \frac{\partial^2 v}{\partial y^2}\right) \qquad (26)$$

The continuity equation:

$$\frac{\partial u}{\partial x} + \frac{\partial v}{\partial y} = 0 \qquad (27)$$

The energy equation:

$$\frac{\partial T}{\partial t} + u\frac{\partial T}{\partial x} + v\frac{\partial T}{\partial y} = \alpha\left(\frac{\partial^2 T}{\partial x^2} + \frac{\partial^2 T}{\partial y^2}\right) \qquad (28)$$

The substitutions necessary to reduce the above differential equations to nondimensionalized forms are:

$$u = \frac{\alpha b}{a^2} U \quad , \quad v = \frac{\alpha}{a} V$$

$$T-T_o = \frac{\nu\alpha b}{\beta g a^4} \theta \quad , \quad t = \frac{a^2}{\alpha} \tau$$

$$x = bX \quad , \quad y = aY \qquad (29)$$

S : Substituting Eq. (29) in the differential equations, differentiating the x-momentum equation with respect to y and the y-momentum equation with respect to x, combining the two equations, and introducing the stream function, the following equations are obtained:

$$\frac{\partial}{\partial\tau}\left(\frac{a^2}{b^2}\frac{\partial^2\psi}{\partial X^2}+\frac{\partial^2\psi}{\partial Y^2}\right)+\frac{\partial\psi}{\partial Y}\frac{\partial}{\partial X}\left(\frac{a^2}{b^2}\frac{\partial^2\psi}{\partial X^2}+\frac{\partial^2\psi}{\partial Y^2}\right)-\frac{\partial\psi}{\partial X}\frac{\partial}{\partial Y}\left(\frac{a^2}{b^2}\frac{\partial^2\psi}{\partial X^2}+\frac{\partial^2\psi}{\partial Y^2}\right)$$

$$=\mathrm{Pr}\frac{\partial\theta}{\partial Y}+\mathrm{Pr}\left[\frac{a^2}{b^2}\frac{\partial^2}{\partial X^2}\left(\frac{a^2}{b^2}\frac{\partial^2\psi}{\partial X^2}+\frac{\partial^2\psi}{\partial Y^2}\right)+\frac{\partial^2}{\partial Y^2}\left(\frac{a^2}{b^2}\frac{\partial^2\psi}{\partial X^2}+\frac{\partial^2\psi}{\partial Y^2}\right)\right] \tag{29a}$$

and

$$\frac{\partial\theta}{\partial\tau}+\frac{\partial\psi}{\partial Y}\frac{\partial\theta}{\partial X}-\frac{\partial\psi}{\partial X}\frac{\partial\theta}{\partial Y}=\frac{a^2}{b^2}\frac{\partial^2\theta}{\partial X^2}+\frac{\partial^2\theta}{\partial Y^2} \tag{30}$$

where the stream function ψ is defined by

$$U=\frac{\partial\psi}{\partial Y}$$

$$V=-\frac{\partial\psi}{\partial X}$$

The initial conditions

$$\theta(X,Y,0)=0 \tag{31}$$

$$\psi(X,Y,0)=0 \tag{32}$$

and the boundary conditions are:

$$\psi(X,1,\tau) = \frac{\partial\psi}{\partial X}(X,1,\tau) = \frac{\partial\psi}{\partial Y}(X,1,\tau) = 0 \tag{33}$$

$$\psi(0,Y,\tau) = \frac{\partial\psi}{\partial X}(0,Y,\tau) = \frac{\partial\psi}{\partial Y}(0,Y,\tau) = 0 \tag{34}$$

$$\psi(1,Y,\tau) = \frac{\partial^2\psi}{\partial X^2}(1,Y,\tau) = \frac{\partial^2\psi}{\partial Y^2}(1,Y,\tau) = 0 \tag{35}$$

$$\psi(X,0,\tau) = \frac{\partial^2\psi}{\partial X^2}(X,0,\tau) = \frac{\partial^2\psi}{\partial X^2}(X,0,\tau) = 0 \tag{36}$$

$$\frac{\partial\theta}{\partial X}(0,Y,\tau) = \frac{\partial\theta}{\partial Y}(X,0,\tau) = 0 \tag{37}$$

$$\frac{\partial\theta}{\partial Y}(X,1,\tau) = Gr^* \quad , \text{ or}$$

$$\theta(X,1,\tau) = \theta_w \tag{38}$$

$$\theta(1,Y,\tau) = \theta_s \quad , \text{ or } \frac{\partial\theta}{\partial X}(1,Y,\tau) = 0 \tag{39}$$

where:

$$Gr^* = (a/b)Pr\ g\beta a^4(q/A)_w/(k\nu^2) \tag{40}$$

$$\theta_s = \frac{a}{b}(T_s-T_o)Pr\ g\beta a^3/\nu^2 = (a/b).Pr.Gr \tag{41}$$

From the above system of equations and boundary conditions, clearly U, V, and θ are functions of x,y,τ, a/b, Pr, Gr, and Gr*.

B. THE SOLUTION

The nonlinear, fourth order system of Eq. (29a) and (30) is not amenable to mathematical treatment using classical methods. Furthermore, Ostromov[24] and Batchelor[1] found that neither the successive approximation method nor the series expansion is suitable for handling such a system of equations for any

arbitrary Pr and Gr. Therefore it was decided to employ a numerical method for the solution; the finite-difference approximation was chosen for the work in this report. The advantage of this method over other numerical methods is that the boundary-layer assumption is no longer necessary. Instead, the full Navier-Stokes equations can be solved. The results obtained by this method can be used to check the validity of the simplifying assumptions made by others.

C. FINITE-DIFFERENCE APPROXIMATIONS

The fourth order, nonlinear system of Eq. (29a) and (30) is transformed to a second order, nonlinear system as follows:

Let

$$w = \frac{a}{b}\frac{\partial^2\psi}{\partial X^2} + \frac{\partial^2\psi}{\partial Y^2} \tag{42}$$

Upon substitution in Eq. (29a), the following equation is obtained:

$$\frac{\partial w}{\partial \tau} + U\frac{\partial w}{\partial X} + V\frac{\partial w}{\partial Y} = Pr\frac{\partial \theta}{\partial Y} - Pr\left[\frac{a^2}{b^2}\frac{\partial^2 w}{\partial X^2} + \frac{\partial^2 w}{\partial Y^2}\right] \tag{43}$$

$$\frac{\partial \theta}{\partial \tau} + U\frac{\partial \theta}{\partial X} + V\frac{\partial \theta}{\partial Y} = \frac{a^2}{b^2}\frac{\partial^2 \theta}{\partial X^2} + \frac{\partial^2 \theta}{\partial Y^2} \tag{44}$$

By definition, w is twice the negative of the vorticity, and Eq. (43) is known as the vorticity transport equation. For convenience U and V are substituted for $\partial\psi/\partial Y$ and $-\partial\psi/\partial X$. By this transformation, the system of Eq. (30) and (31) is reduced to three second-order, nonlinear equations which are

easier to handle by difference methods compared to the two nonlinear, fourth order Eqs. (29a) and (30).

The differential Eqs. (42) (43), and (44) are approximated by a system of difference equations. Each first order term in Eqs. (43) and (44) can be expressed in forward, backward, or central differences. The choice of the type of difference approximation is determined by whether implicit or explicit difference method is desired and by the stability requirements, to be discussed later. From the beginning of this analysis, explicit methods were felt to be more suitable for handling Eqs. (43) and (44), because the principal interest is in transient phenomena for small physical time. This implies that, for better accuracy, small time steps should be used from the beginning of computation. Desinberre[5] showed that explicit methods are superior to implicit methods as far as accuracy is concerned; he also found that the accuracy requirement restricts the size of the time increment, in the case of implicit methods, to values smaller than required by stability considerations. When explicit methods are used, the nonlinear terms $U(\partial w/\partial X)$, $V(\partial w/\partial Y)$, $U(\partial \Theta/\partial X)$, and $V(\partial \Theta/\partial Y)$ have to be approximated by forward difference when the sign of the velocity is negative, and by backward difference when the velocity is positive.[35] Central differences are used if implicit schemes are desired. Since the velocity components change sign in the domain ofinterest, four different sets of finite-difference equations are required, and the appropriate set of equations at each location or nodal point is determined accordingly. The four sets of difference equations corresponding to differential Eqs. (43) and (44) are:

(i) $U \geq 0,\ V \geq 0$

$$\frac{w'_{i,j}-w_{i,j}}{\Delta\tau} + U_{i,j}\frac{w_{i,j}-w_{i-1,j}}{\Delta X} + V_{i,j}\frac{w_{i,j}-w_{i,j-1}}{\Delta Y}$$

$$= Pr\frac{\theta'_{i,j}-\theta'_{i,j-1}}{\Delta Y} + Pr\left[\frac{a^2}{b^2}\frac{w_{i+1,j}-2w_{i,j}+w_{i-1,j}}{(\Delta X)^2} + \frac{w_{i,j+1}-2w_{i,j}+w_{i,j-1}}{(\Delta Y)^2}\right] \quad (45a)$$

$$\frac{\theta'_{i,j}-\theta_{i,j}}{\Delta\tau} + U_{i,j}\frac{\theta_{i,j}-\theta_{i-1,j}}{\Delta X} + V_{i,j}\frac{\theta_{i,j}-\theta_{i,j-1}}{\Delta Y}$$

$$= \frac{a^2\,\theta_{i+1,j}-2\theta_{i,j}+\theta_{i-1,j}}{(\Delta X)^2} + \frac{\theta_{i,j+1}-2\theta_{i,j}+\theta_{i,j-1}}{(\Delta Y)^2} \quad (46a)$$

(ii) $U \geq 0,\ V \leq 0$

$$\frac{w'_{i,j}-w_{i,j}}{\Delta\tau} + U_{i,j}\frac{w_{i,j}-w_{i-1,j}}{\Delta X} + V_{i,j}\frac{w_{i,j+1}-w_{i,j}}{\Delta Y}$$

$$= Pr\frac{\theta'_{i,j}-\theta'_{i,j-1}}{\Delta Y} + Pr\left[\frac{a^2}{b^2}\frac{w_{i+1,j}-2w_{i,j}+w_{i-1,j}}{(\Delta X)^2} + \frac{w_{i,j+1}-2w_{i,j}+w_{i,j-1}}{(\Delta Y)^2}\right] \quad (45b)$$

$$\frac{\theta'_{i,j}-\theta_{i,j}}{\Delta\tau} + U_{i,j}\frac{\theta_{i,j}-\theta_{i-1,j}}{\Delta X} + V_{i,j}\frac{\theta_{i,j+1}-\theta_{i,j}}{\Delta Y}$$

$$= \frac{a^2}{b^2}\frac{\theta_{i+1,j}-2\theta_{i,j}+\theta_{i-1,j}}{(\Delta X)^2} + \frac{\theta_{i,j+1}-2\theta_{i,j}+\theta_{i,j-1}}{(\Delta Y)^2} \quad (46b)$$

(iii) $U \leq 0,\ V \geq 0$

$$\frac{w'_{i,j}-w_{i,j}}{\Delta\tau} + U_{i,j}\frac{w_{i+1,j}-w_{i,j}}{\Delta X} + V_{i,j}\frac{w_{i,j}-w_{i,j-1}}{\Delta Y}$$

$$= \Pr\frac{\theta'_{i,j}-\theta'_{i,j-1}}{\Delta Y} + \Pr\left[\frac{a^2}{b^2}\frac{w_{i+1,j}-2w_{i,j}+w_{i-1,j}}{(\Delta X)^2} + \frac{w_{i,j+1}-2w_{i,j}+w_{i,j-1}}{(\Delta Y)^2}\right] \quad (45c)$$

$$\frac{\theta'_{i,j}-\theta_{i,j}}{\Delta\tau} + U_{i,j}\frac{\theta_{i+1,j}-\theta_{i,j}}{\Delta X} + V_{i,j}\frac{\theta_{i,j}-\theta_{i,j-1}}{\Delta Y} =$$

$$= \frac{a^2}{b^2}\frac{\theta_{i+1,j}-2\theta_{i,j}+\theta_{i-1,j}}{(\Delta X)^2} + \frac{\theta_{i,j+1}-2\theta_{i,j}+\theta_{i,j-1}}{(\Delta Y)^2} \quad (46c)$$

(iv) $U \leq 0,\ V \leq 0$

$$\frac{w'_{i,j}-w_{i,j}}{\Delta\tau} + U_{i,j}\frac{w_{i+1,j}-w_{i,j}}{\Delta X} + V_{i,j}\frac{w_{i,j+1}-w_{i,j}}{\Delta Y}$$

$$= \Pr\frac{\theta'_{i,j}-\theta'_{i,j-1}}{\Delta Y} + \Pr\left[\frac{a^2}{b^2}\frac{w_{i+1,j}-2w_{i,j}+w_{i-1,j}}{(\Delta X)^2} + \frac{w_{i,j+1}-2w_{i,j}+w_{i,j-1}}{(\Delta Y)^2}\right] \quad (45d)$$

$$\frac{\theta'_{i,j}-\theta_{i,j}}{\Delta\tau} + U_{i,j}\frac{\theta_{i+1,j}-\theta_{i,j}}{\Delta X} + V_{i,j}\frac{\theta_{i,j+1}-\theta_{i,j}}{\Delta Y}$$

$$= \frac{a^2}{b^2}\frac{\theta_{i+1,j}-2\theta_{i,j}+\theta_{i-1,j}}{(\Delta X)^2} + \frac{\theta_{i,j+1}-2\theta_{i,j}+\theta_{i,j-1}}{(\Delta Y)^2} \quad (46d)$$

The prime refers to the value of the variables at the present time step, and the unprimed variables correspond to those at the previous time step.

The two-dimensional space domain of interest is bounded by $0 \leqq X \leqq 1$, $-1 \leqq Y \leqq 1$. Only the region to the right of the x-axis is considered because of geometrical symmetry with respect to this axis. The integers i and j denote the x and y position respectively, with $i = 2$, $j = 2$ as the origin, $X = (i-2)$, Δx and $Y = (j-2)$.

D. STABILITY AND CONVERGENCE

The method used in this section follows that of Refs. 27 and 12. The theoretical background for the method may be found in Ref. 27, which presents an excellent discussion of the subject.

Stability is a necessary condition for the solution of the difference equations to converge to the solution of the differential equations as the size of the increments Δx, Δy, and Δt tend to zero. In other words, it is important to identify the behavior of the approximation error as the size of the increments goes to zero and to establish the restrictions to be imposed on the difference equations in order that the error will tend to zero as the increments Δx, Δy, and Δt go to zero. This requires that there be no unlimited amplification of the error as the computing cycles become infinite in the limit.

The Von Neumann method of stability analysis is used in this problem. This method is strictly valid for constant-coefficient difference equations while the equations involved have variable coefficients U and V; however,

very good approximation for the stability criterion is obtained by treating the variable coefficients as constants throughout the analysis and then letting the variable coefficients take on their most adverse values in determining the restriction on the time increment size. The fundamentals of the application of this method of stability analysis are best illustrated by the problem in hand. The method will be applied for the case $U \geq 0$, $V \geq 0$. The stability criterion holds irrespective of the sign of U or V. The absolute value of U and V must be used in the equations or inequalities describing the stability criterion, and the appropriate difference equations must be used according to the sign of U and V, as described earlier.

The solution of the difference equations can be written as a Fourier series, the form of which is:[27]

$$w_{i,j}^{(n)} = \sum_{K_1} \sum_{K_2} \xi^{(n)} e^{i(K_1 X + K_2 Y)} \tag{47}$$

$$\varrho_{i,j}^{(n)} = \sum_{K_1} \sum_{K_2} \mu^{(n)} e^{i(K_1 X + K_2 Y)} \tag{48}$$

where K_1 and K_2 are integers, n is a superscript denoting the nth time period, and ξ and μ are functions of K_1 and K_2. Substituting the system of Eqs. (47) and (48) into Eqs. (45a) and (46a), the following equations are obtained after some algebraic manipulations:

$$\sum_{K_1}\sum_{K_2}\left\{\xi^{(n+1)} - \xi^{(n)}\left(a_1+a_2\, e^{-iK_1\Delta X} + a_3\, e^{-iK_2\Delta Y} + a_4\, e^{iK_1\Delta X} + a_5\, e^{iK_2\Delta Y}\right)\right.$$

$$\left. + a_6\,\mu^{(n+1)}\right\} e^{i(K_1X+K_2Y)} = 0$$

$$\sum_{K_1}\sum_{K_2}\left\{\mu^{(n+1)} - \mu^{(n)}\left(c_1+c_2\, e^{-iK_1\Delta X} + c_3\, e^{-iK_2\Delta Y} + c_4\, e^{iK_1\Delta X} + c_5\, e^{iK_2\Delta Y}\right)\right\}$$

$$\times\, e^{i(K_1X+K_2Y)} = 0$$

From the above equations, it is concluded that the difference equations are satisfied if

$$\xi^{(n+1)} = \xi^{(n)}\left(a_1+a_2\, e^{-iK_1\Delta X} + a_3\, e^{-iK_2\Delta Y} + a_4\, e^{iK_2\Delta Y} + a_5\, e^{iK_2\Delta Y}\right) + a_6\,\mu \qquad (49)$$

and

$$\mu^{(n+1)} = \mu^{(n)}\left(c_1+c_2\, e^{-iK_1\Delta X} + c_3\, e^{-iK_2\Delta Y} + c_4\, e^{iK_1\Delta X} + c_5\, e^{iK_2\Delta Y}\right),$$

where:

$$a_1 = 1 - \left(2\,\frac{a^2}{b^2}\,\frac{Pr}{(\Delta X)^2} + 2\,\frac{Pr}{(\Delta Y)^2} + \frac{|U_{i,j}|}{\Delta X} + \frac{|V_{i,j}|}{\Delta Y}\right)\Delta\tau$$

$$a_2 = \left(\frac{a^2}{b^2}\,\frac{Pr}{(\Delta X)^2} + \frac{|U_{i,j}|}{\Delta X}\right)\Delta\tau$$

$$a_3 = \left(\frac{Pr}{(\Delta Y)^2} + \frac{|V_{i,j}|}{\Delta Y}\right)\Delta\tau$$

$$a_4 = \frac{a^2}{b^2}\frac{Pr}{(\Delta X)^2}\Delta\tau$$

$$a_5 = Pr\frac{\Delta\tau}{(\Delta Y)^2}$$

$$c_1 = 1 - \left(2\frac{a}{b}\frac{1}{(\Delta X)} + \frac{2}{(\Delta Y)} + \frac{|U_{i,j}|}{\Delta X} + \frac{|V_{i,j}|}{\Delta Y}\right)\Delta\tau$$

$$c_2 = \left(\frac{a^2}{(b\ \Delta X)^2} + \frac{|U_{i,j}|}{\Delta X}\right)\Delta\tau$$

$$c_3 = \left(\frac{1}{(\Delta Y)^2} + \frac{|V_{i,j}|}{\Delta Y}\right)\Delta\tau$$

$$c_4 = \left(\frac{a}{(b\ \Delta X)}\right)^2 \cdot \Delta\tau$$

$$c_5 = \frac{\Delta\tau}{(\Delta Y)^2}$$

No definition has been given to a_6 since it has no effect on this analysis.

The system of Eqs. (49) and (50) are of the form:

$$\xi^{(n+1)} = a_{11}\,\xi^{(n)}(K_1,K_2) + a_{12}\,\mu^{(n)}(K_1,K_2) \tag{51}$$

$$\mu^{(n+1)} = a_{21}\,\xi^{(n)}(K_1,K_2) + a_{22}\,\mu^{(n)}(K_1,K_2) \tag{52}$$

In the matrix notation, the above equalities can be written as

$$\begin{pmatrix} \xi^{(n+1)} \\ \mu^{(n+1)} \end{pmatrix} = \begin{pmatrix} a_{11} & a_{12} \\ a_{21} & a_{22} \end{pmatrix}\begin{pmatrix} \xi^{(n)} \\ \mu^{(n)} \end{pmatrix} \tag{53}$$

The quantity between the first parentheses on the right-hand side of Eq. (53) is called the amplification matrix. The Von Neumann condition necessary for stability is: $|\lambda_{max}| \leq 1$, where λ_{max} is the largest eigenvalue of the amplification matrix. The eigenvalues are given by

$$\begin{vmatrix} a_{11}-\lambda & a_{12} \\ a_{21} & a_{22}-\lambda \end{vmatrix} = 0$$

Substituting the values of a_{11}, a_{12},...etc. in the above determinant and solving for λ, we get

$$\lambda_1 = a_1 + a_2 e^{-iK_1\Delta Y} + a_3 e^{-iK_2\Delta Y} + a_4 e^{iK_1\Delta X} + a_5 e^{iK_2\Delta Y} \qquad (54)$$

$$\lambda_2 = c_1 + c_2 e^{-iK_1\Delta X} + c_3 e^{-iK_2\Delta Y} + c_4 e^{iK_1\Delta X} + c_5 e^{iK_2\Delta Y} \qquad (55)$$

The coefficients a_1, a_2,...,c_1,c_2...etc. all are positive except a_1 and c_1, which may be positive or negative. The largest absolute values of λ_1 and λ_2 occur when all the terms in Eqs. (54) and (55) are real, i.e., when $K_1\Delta X$ $K_1\Delta X = K_2\Delta Y = 2\pi$ then,

$$\lambda_{1\,max} = a_1 + a_2 + a_3 + a_4 + a_5 \qquad (56)$$

$$\lambda_{2\,max} = c_1 + c_2 + c_3 + c_4 + c_5 \qquad (57)$$

Substituting the values of a_1, a_2,..., c_1,...,c_5 in λ_{max}

$$\lambda_{1\,max} = \lambda_{2\,max} = 1 \qquad (58)$$

Therefore, we can conclude that λ_{max} will not exceed unity and will not impose any stability restrictions. If there be any restrictions, they are to prevent the minimum value of λ from becoming less than -1.

The minimum of the eigenvalues occurs when $K_1\Delta X = K_2\Delta Y = \pi$ and is given by

$$\lambda_{r\,min} = a_1 - a_2 - a_3 - a_4 - a_5$$

$$\lambda_{2\,min} = c_1 - c_2 - c_3 - c_4 - c_5$$

or

$$\lambda_{1\,min} = 1 - 2\,\Delta\tau\left(2\,Pr\left(\frac{a}{b\,\Delta X}\right)^2 + 2\,\frac{Pr}{(\Delta Y)^2} + \frac{|U_{i,j}|}{\Delta X} + \frac{|V_{i,j}|}{\Delta Y}\right) \qquad (59)$$

$$\lambda_{2\,min} = 1 - 2\,\Delta\tau\left(2\left(\frac{a}{b\,\Delta X}\right)^2 + \frac{2}{(\Delta Y)^2} + \frac{|U_{i,j}|}{\Delta X} + \frac{|V_{i,j}|}{\Delta Y}\right) \qquad (60)$$

Therefore, for $|\lambda| \leq 1$, the following inequalities should be satisfied:

$$\Delta\tau\left(\frac{2a^2}{b^2(\Delta X)^2} + \frac{2}{(\Delta Y)^2} + \frac{|U_{i,j}|}{\Delta X} + \frac{|V_{i,j}|}{\Delta Y}\right) \leq 1 \qquad (61a)$$

$$\Delta\tau\left(2\,Pr\left(\frac{a}{b\,\Delta X}\right)^2 + 2\,\frac{Pr}{(\Delta Y)} + \frac{|U_{i,j}|}{\Delta X} + \frac{|V_{i,j}|}{\Delta Y}\right) \leq 1 \qquad (61b)$$

Equations (61a,b) are requisite for stability. For values of Prandtl number less than unity, inequality Eq. (61a) is more restrictive and, therefore, should be used. For higher values of Prandtl number, inequality Eq.(61b) must be used.

The numerical solution is carried as follows:

1. The temperature distribution is first calculated using Eq. (45);

2. The advanced values of temperature θ' are used in Eq. (46) to calculate w';

3. The stream function is calculated at each time step, using Eq. (42). The solution of Eq. (42) is done numerically, using successive row relaxation followed by successive column relaxation.[36]

IV. RESULTS

Calculations have been carried out for the case of a container with an insulated bottom whose walls are subjected to a uniform heat flux, and the liquid surface is maintained either at the initial temperature T_o, at a temperature, T_s, higher than T_o, or is adiabatic. The last case is expected to approximate the transient convection in the liquid when exposed to a non-pressurized gas. Different levels of heat flux were considered, including 10 and 1000 Btu/hr/ft^2.

For these calculations, the fluid properties chosen were those of liquid nitrogen initially at atmospheric pressure, the initial saturation temperature was 140°R. The fluid properties were evaluated at a temperature equal to the average of the initial temperature and the liquid surface temperature. The values of the liquid properties were taken from Ref. 38 and are summarized in Table I. The height of the liquid b, is 1 ft, and the width of the con-

TABLE I

FLUID PROPERTIES

Thermal diffusivity α, ft^2/sec	8.62×10^{-7}
Thermal conductivity K, Btu/hr/ft^2-°R	0.0775
Kinematic viscosity ν, ft^2/sec	1.68×10^{-6}
Coefficient of thermal expansion, β, °R^{-1}	1.33×10^{-3}
Prandtl number	1.91

tainer is 1/2 ft.

The flow pattern for the case of a constant wall heat flux of 10 Btu/hr/ft^2 and liquid surface maintained at initial temperature T_o is shown in Figs. 1, 2 and 3, using a 21 x 21 grid corresponding to $\Delta X = \Delta Y = 0.05$. These results show the streamline pattern at different time levels—50 sec, 2 min, and 3.6 min respectively. An interesting streamline pattern is observed at the free surface. For a short time after the beginning of heating, the boundary layer rising along the container walls turns smoothly changing its direction from upward to downward flow (Fig. 1). The downward-moving particles near the rising boundary layer reverse direction and join the upward flow, thus giving rise to the vortex near the free surface. The fluid away from the edge of the boundary layer flows nearly to the bottom of the container, where it joins the upward-moving fluid. For greater times following the introduction of the transient, the streamlines near the free surface show the presence of fluid oscillations (Figs. 2 and 3). These oscillations first form near the wall, their amplitude grows with time, and they move towards the centerline of the container. The calculations show that this oscillatory phenomenon is repeated with time in the sequence described (Figs. 2,3,4, and 5).

The effect of increasing the level of heat flux on the flow pattern is clearly shown in Fig. 4, which shows the flow pattern obtained after heating for 51 sec with a wall flux of 1000 Btu/hr/ft^2 and the surface temperature maintained at the initial temperature T_o. The comparison between Figs. 1 and 4, which correspond essentially to the same time, shows that the oscillatory

streamline pattern develops earlier for high heating rates than the low heating rates. Except for the latter effect, the flow pattern at the higher heating rates has the same characteristics as that for the low heating rate. The magnitude of the velocities, of course, is higher for the higher heat flux.

The streamlines for the case of a constant wall heat flux of 1000 $Btu/hr/ft^2$ and adiabatic interface are shown in Fig. 7.

Figures 8 and 9 show the streamlines and the isothermals, respectively, obtained at 1000 $Btu/hr/ft^2$ wall heat flux and the interface temperature maintained at 160°R, which corresponds to the saturation temperature for a pressure of 45 psia. The axial temperature gradient in the boundary layer is negligible for about 70 percent of the container height at a time of 48 sec. At the upper portion of the container, near the free surface, the axial temperature gradients are considerably greater. On the other hand, the transversal temperature gradient is greater at the lower portion of the tank and becomes smaller near the free surface. The temperature distribution exhibits the same character in all the cases analyzed. These phenomena can be explained as follows: for small times, the fluid near the container walls flows upward in a thin boundary layer. In its upward movement, the hot fluid entrains some of the cold fluid at the edge of the boundary layer. This heated boundary layer is discharged at and just below the free surface, where its transverse velocity is highest. To satisfy continuity, the heated fluid which is discharged at the free surface causes the colder fluid to move downward, thus producing a series of horizontal isotherms. With time these

isotherms penetrate further below the free surface. At the lower portion of the container, the transversal temperature gradient is very high near the wall and negligible in the remainder of the container. It is smaller near the free surface, where the boundary-layer flow is discharged. The thermal boundary layer fills the entire cross section in this region.

A. THE EFFECT OF GRID SIZE

Calculations were made for the case of constant wall heat flux of 10 $Btu/hr/ft^2$ with the fluid surface at its initial temperature, using 21 x 21, 16 x 16 and 11 x 11 grids. The streamline patterns are shown in Figs. 1-4, 6. The oscillatory pattern is obtained in each case, but it is on a smaller scale for the 11 x 11 grid. The axial velocity distribution obtained at a given time is plotted for various axial positions in Fig. 10. The values obtained using 16 x 16 and 21 x 21 are in close agreement. Figure 10 shows that the difference between the values obtained using different grids is greater near the wall and at the center line; otherwise they are in substantial agreement.

Figure 11 shows the dimensionless wall temperature at a location x = .6 plotted against dimensionless time. The deviation is greatest for small times. The difference decreases with time and is practically negligible for dimensionless time of 0.003, which corresponds to about 3.6 min.

Figure 12 presents the velocity at different locations as a function of the grid size. Examination of this figure reveals that the velocities change monotonously with the grid size. Their values are expected to converge

to the true solution for a number of divisions of the order of 30 x 30. This is seen from the extrapolation shown as dotted lines in the figures. The rate of convergence is slower near the boundary and at the center than at intermediate positions.

The computations were done on the IBM 7090 digital computer at the Computing Center of The University of Michigan. The machine time required to complete the calculations and to print the results for U,V,T,w, and ψ every 20 steps is 1.7 sec per time step for the 11 x 11 grid. The corresponding times for the 16 x 16 and the 21 x 21 grids are 8 and 11 sec, respectively, for printing the results every five steps.

B. COMPARISON WITH EXPERIMENT

An investigation of the literature on natural convection showed that few present results are applicable to those reported here. These include the work of Eichhorn[6] and S. K. Fenster, et al.,[7] there is other literature concerning flow phenomena in free convection, but, except those cited, none included systems with a free surface.

Eichhorn conducted visual studies of the natural convection laminar flow of water using an electrically heated cylinder 2-inches diameter and 5-inches long. His results are shown in Fig. 13. The magnitude of the heat flux was not given. From the discussion it is concluded that the results represent the unsteady state. Figures 13a and 13b show the flow pattern observed at high heating rate; Fig. 13c shows that obtained at low heating rates. At low heating rates, the streamlines assume a damped-wave shape. At high heating

rates, annular vortices repeatedly form near the free surface, roll up until a certain size is reached, whereupon they move away from the cylinder, and another vortex vegins to form. The comparison of Figs. 1-8 with the results of Fig. 13 shows that the shape of streamlines observed agrees with that obtained from the theoretical solutions presented here.

Fenster, et al., studied experimentally the transient phenomena associated with the pressurization of liquid nitrogen initially boiling at constant heat flux. Although the initial temperature distribution agrees with that assumed in this analysis, the initial velocity distribution does not. At any instant after pressurization, there was no difference between the temperature at the tank centerline and midway between the centerline and the wall at an axial location below 0.6 of the liquid height. These results indicate that the isotherms are horizontal in the core of the tank, which agrees with the calculated isotherms shown in Fig. 9.

Temperature oscillations of the type shown in Fig. 9 were also obtained by Poots[26] for the steady state solution of the temperature distribution in a two-dimensional closed cavity. In this case, the walls are kept at a constant temperature, one wall hotter than the other, and the upper and lower surfaces assume a linear temperature distribution. These results are shown in Fig. 14.

V. CONCLUSIONS

The equations describing the transient, two-dimensional, laminar, natural convection in a rectangular closed container having a vapor-liquid interface have been solved using explicit finite-difference approximations. The velocity and temperature distributions indicate that, for small time periods, the flow is of a boundary-layer type, except near the bottom and the liquid-vapor interface. No indications of numerical instability were encountered. The size of the time increment was restricted to small values by stability considerations based on the method of Von Neumann. However, a small time increment is desirable in order to obtain accurate transient results at small time. On the other hand, if steady state results are desired, the number of computations using the explicit method will be large for fine grids and for systems having a high heat flux. The machine time may be of the order of 2 hours in this case,[12] and the use of implicit methods would be superior. However, the application of implicit-difference methods to this problem and to problems with other geometry is being continued.

The results obtained using the present method agree qualitatively with related cases reported in the literature.

ACKNOWLEDGMENT

The authors wish to thank Profs. V. S. Arpaci and W. J. Yang for their valuable suggestions and assistance. The assistance of Professor R.C.F. Bartels, Director of the Computing Center, The University of Michigan, during the initial stages of this work is gratefully acknowledged.

REFERENCES

1. Batchelor, Quart. Applied Math. 12, pp. 209-203, 1954.

2. E. Schmidt and W. Beckmann, Forsch Ing-Wes. 1, 391 (1930).

3. J. A. Clark, G. J. Van Wylen and S. K. Fenster, "Transient Phenomena Associated with the Pressurized Discharge of a Cryogenic Liquid from a Closed Container." Advances in Cryogenic Engineering, 5, pp. 467-480.

4. A. N. Curren and C. F. Zalabak, "Effect of Closed End Coolant Passages on Natural Convection Water Cooling of Gas Turbine Blades." NACA RM R55J 18-a.

5. Dusinberre, "A Note on the "Implicit" Method for Finite-Difference Heat Transfer Calculations." ASME Trans, J. Heat Transfer, Series C, pp. 94-95, Feb. 1961.

6. R. Eichhorn, "Flow Visualization and Velocity Measurement in Natural Convection with Tellurium Die Method." ASME Trans, J. Heat Transfer, 83, Series C, pp. 379-381.

7. S. K. Fenster, G. J. Van Wylen and J. A. Clark, "Transient Phenomena Assoicated with the Pressurization of Liquid Nitrogen Boiling at Constant Heat Flux." Advances in Cryogenic Engineering, 5, pp. 226-234.

8. B. Gebhart, "Natural Convection Transients." ASME Trans., J. Heat Transfer, Series C, 85, pp. 184-185. See also J. Heat Transfer, 85, p. 10 and 83, p. 61.

9. F. G. Hammitt, "Heat and Mass Transfer in Closed, Vertical, Cylindrical Vessels with Internal Heat Sources for Homogeneous Reactors." Ph.D. Thesis, Univ. of Mich., Dec. 1957.

10. J. P. Hartnett, W. E. Welch and F. W. Larsen, "Free Convection Heat Transfer to Water and Mercuty in an Enclosed Cylindrical Tube." Nuclear Engineering and Science Conference, preprint 27, Session XX, Chicago, March 17-21, 1958.

11. J. P. Hartnett and W. E. Welch, "Experimental Studies of Free Convection Heat Transfer in a Vertical Tube with Uniform Heat Flux." Trans, ASME, 79, p. 1651, 1957.

12. J. D. Hellums, "Finite-Difference Computation of Natural Convection Flow." Ph.D. Thesis, Univ. of Mich, Sept. 1960.

13. F. Herzbert, "Effective Density of Boiling Liquid Oxygen." Advances in Cryogenic Engineering, 5.

14. Landau and Lifshitz, "Fluid Mechanics." Adison-Wesly, 1959.

15. F. W. Larsen and J. P. Hartnett, "Effect of Aspect Ratio and Tube Orientation on Free Convection Heat Transfer to Water and Mercuty in Enclosed Circular Tubes." ASME, Trans., J. Heat Transfer, 83, Series C, pp. 87-93.

16. A. F. Leitzke, "Theoretical and Experimental Investigation of Heat Transfer by Natural Convection Between Parallel Plates." NACA Report 1223, 1955.

17. S. Levy, "Integral Methods in Natural Convection Flow." ASME paper No. 55, APM-22.

18. M. J. Lighthill, "Theoretical Consideration on Free Convection in Tubes." Quart. J. Mech. and Appl. Math., 6, pp. 398-439, 1953.

19. B. W. Martin, "Free Convection in an Open Thermosyphen with Special Reference to Turbulent Flow." Proc. Roy. Soc., Series A, 230, pp. 502-530, 1955.

20. S. Ostrach, "An Analysis of Laminar Free Convection Flow and Heat Transfer About a Flat Plate Parallel to the Direction of the Generating Body Force." NACA Report 111, 1953.

21. S. Ostrach, "Laminar Natural Convection Flow and Heat Transfer to Fluids With andWithout Heat Sources With Constant Wall Temperature." NACA Tn-2863, Dec. 1952.

22. S. Ostrach, "Combined Natural and Forced Convection Laminar Flow and Heat Transfer to Fluids With and Without Heat Sources in Channels With Linearly Varying Wall Temperature." NACA Tn-3141, April 1954.

23. S. Ostrach and P. R. Thronton, "On the Stagnation of Natural Convection Flows in Closed End Tubes." ASME paper No. 57-SA-2.

24. G. A. Ostromov, "Free Convection Under the Conditions of the Internal Problem." NACA TM-1407.

25. E. Pohlhausen, ZAMM1, 115 (1921).

26. G. Poots,"Heat Transfer by Laminar Free Convection in Enclosed Plane Gas Layers." Quart. J. Mech. and Appl. Math., XX, Pt. 3, pp. 257-273, 1958.

27. R. D. Richtmyer, "Difference Methods for Initial Value Problem." Interscience Publication, 1957.

28. A. G. Romonov, "Study of Heat Exchange in a Deal End Channel Under Free Convection Conditions." Izvestiya Akademii Nau, USSR. Otdeleni Tekhnisheskikh, No. 6, pp. 63-76, 1956.

29. R. S. Schechter, "Natural Convection Heat Transfer in Regions of Maximum Fluid Density." AIChE paper No. 57-HT-25.

30. R. Seigel, "Transient Free Convection from a Vertical Flat Plate." ASME paper No. 57-Sa-8.

31. R. Seigel and R. H. Norris, "Test of Free Convection in a Partially Enclosed Spaces Between Two Heated Vertical Plates." ASME paper No. 56-SA-5.

32. R.G.S. Skipper, I.S.C. Holt and O. A. Saunders, "Natural Convection in Viscous Oil." International Development in Heat Transfer, Pt.5, pp. 1003-1009.

33. E. M. Sparrow and J. L. Gregg, "The Variable Fluid Property." ASME paper No. 57-A-46.

34. E. M. Sparrow, J. L. Gree, "Similar Solutions for Free Convection from a Nonisothermal Vertical Plate." ASME paper No. 57-SA-3.

35. E. M. Sparrow and S. J. Kaufmann, "Visual Study of Free Convection in a Narrow Vertical Enclosure." NACA RM E55 L 14-a, Feb. 1956.

36. J. Todd, "Survey of Numerical Analysis." McGraw-Hill, Chap. 11, 1962.

37. S. L. Zeiberg and W. K. Mueller, "Transient Laminar Combined Free and Forced Convection in a Duct." ASME Trans., J. Heat Transfer, 84, Series C, pp. 141-148.

38. "A Compendium of the Properties of Materials at Low Temperature Phase I and II." R. B. Stewart and V. J. Johnson, Editors.

APPENDIX

COMPUTER PROGRAM

The computer program used for the cases of constant wall flux or constant step change in wall temperature and the interfacial temperature specified is given on the following pages. The program is written in MAD language. The symbols U,V,T,W,T_O,T_S,k,A, and B are the same as in the text. The meaning of the principal symbols which are not defined in the program are given below:

Dx = Δx

Dy = Δy

DT = ΔT

M = No. of divisions in the x-direction

N = No. of divisions in the y-direction

GA = Acceleration due to gravity

SF = Stream function

ST = The value of the stream function at the previous time step

W = The value of W at the previous time step

WL = The value of W at the advanced time step

TL = The value of temperature at the previous time step

NT = Total number of time steps

NE = Number of interations

TJI = Dimensionless wall temperature T_w for the case of step change in wall temperature

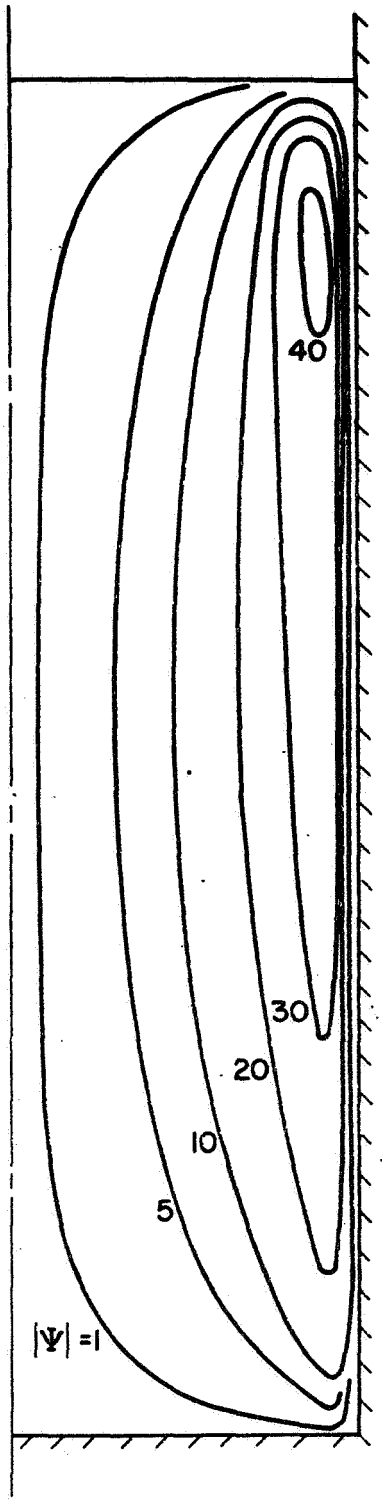
TI = Dimensionless interfacial temperature.

```
  HUSSEIN Z. BARAKAT              S265F                    020   300
  HUSSEIN Z. BARAKAT              S265F                    020   300
$COMPILE MAD,EXECUTE,DUMP,PRINT OBJECT,PUNCH OBJECT
        DIMENSION U(2000,DIM),V(2000,DIM),TL(2000,DIM),T(2000,DIM),
       1ST(2000,DIM),SF(2000,DIM),WL(2000,DIM),W(2000,DIM),DI(100),
       2 EI(100),EJ(100), F(100)
         VECTOR VALUES DIM=2,1,0
        INTEGER I,J,M,N,NT,NE,N1,N2,N3,I1,I3,I4,N4,NTC,J2 ,H,N5,N6,
       1 N7,N8
        EXECUTE FTRAP.
START   READ AND PRINT DATA
        DIM(2)=N+2
        EXECUTE ZERO.(U(2,2)...U(M+2,N+2),V(2,2)...V(M+2,N+2),T(1,1).
       1..T(M+2,N+2),TL(1,1)...TL(M+2,N+2),ST(2,2)...ST(M+2,N+2),
       2SF(2,2)...SF(M+2,N+2),W(2,2)...W(M+2,N+2),WL(2,2)...WL(M+2,
       3N+2),EI(1)...EI(N+2),DI(1)...DI(N+2),F(1)...F(N+2) ,EJ(1)...
       4  EJ(M+2))
         TC=TC
         TS=TS
        QSURF=QSURF
           A=A
         K=K
        TIME=0
        NT=0
        DX=1./M
        DY=1./N
        I1=M/2
        J2=N/2
          R=AOVERB
        DX2=DX*DX
        DX3=DX2*DX
        DY2=DY*DY
        DY3=DY2*DY
        DXY=DX2/DY2
         DYX=DY2/DX2
         BI=2.*(1+DXY)
         BJ=2.*(1.+DYX)
        C1=GA*PR*BETTA*QSURF*(A.P.4)*R/K/NEW/NEW
          THROUGH ZZ,FOR J=3,1,J.G.N+1
         EI(2)=0
ZZ       EI(J)=1./(BJ-EI(J-1))
          THROUGH VV,FOR I=3,1,I.G.M+1
         EJ(2)=0
VV       EJ(I)=1./(BI-EJ(I-1))
        THROUGH THETAA,FOR I=2,1,I.G.M+2
THETA    TL(I,N+2)=TJ1
        NTC=0
BBACK    NTC=NTC+1
        THROUGH BEHH,FOR J=2,1,J.G.N+3
        TL(M+2,J)=T1
BEHH    T(M+2,J)=T1
        THROUGH ALEFF,FOR I=2,1 ,I.G.M+1
ALEFF    T(I,N+2)=TL(I,N+2)+2.*C1*DT3/DY+TC*DT3*2.*(TL(I,N+1)-
       1TL(I,N+2))/DY2+TC*2T3*R*R*(TL(I+1,N+2)-2.*TL(I, N+2)+TL(I-1,
       2N+2))/DX2
            T(1,N+2)=T(3,N+2)
        THROUGH AALEF,FOR I=2,1,I.G.M+1
         THROUGH AALEF,FOR J=2,1,J.G.N+1
        T(I,J)=TL(I,J)+DT3*R*R*(TL(I+1,J)-2.*TL(I,J)+TL(I-1,J))/DX2
```

```
                1+DT3*(TL(I,J+1)-2.*TL(I,J)+TL(I,J-1))/DY2
                T(1,J)=T(3,J)
                 T(1,1)=T(3,1)
   AALEF        T(I,1)=T(I,3)
                THROUGH XX,FOR I=1,1,I.G.M+1
                THROUGH XX,FOR J=1,1,J.G.N+2
   XX            TL(I,J)=T(I,J)
                WHENEVER NTC.L.N4,TRANSFER TO BBACK
   BACK          NT=NT+1
                THROUGH SIGMA,FOR I=1,1,I.G.(M+2)
                THROUGH SIGMA,FOR J=1,1,J.G.N+2
   SIGMA         TL(I,J)=T(I,J)
                WHENEVER NT.G.N1,DT=DT1
                 SMAX=0
                THROUGH GAMMA,FOR I=3,1,I.G.(M+1)
                THROUGH GAMMA,FOR J=3,1,J.G.(N+1)
                 WHENEVER PR.L.1
                S=R*R*2./DX2/PR+2./PR/DY2+.ABS.U(I,J)/DX+.ABS.V(I,J)/DY
                OTHERWISE
                S=R*R*2./DX2+2./DY2+.ABS.U(I,J)/DX+.ABS.V(I,J)/DY
                 END OF CONDITIONAL
                WHENEVER SMAX.L.S
                SMAX=S
   GAMMA         END OF CONDITIONAL
                SN=DT*SMAX
                WHENEVER SN.G.1.,DT=1./SMAX
                TIME=TIME+DT
                THROUGH BEH,FOR J=1,1,J.G.N+2
                T(M+2,J)=T1
   BEH          TL(M+2,J)=T1
                THROUGH ALEF,FOR I=2,1,I.G.(M+1)
   ALEF          T(I,N+2)=TL(I,N+2)+2.*C1*DT/DY+TC*DT*2.*(TL(I,N+1)-
               1TL(I,N+2))/DY2+TC*DT*R*R*(TL(I+1,N+2)-2.*TL(I,N+2)+TL(I-1,
               2N+2))/DX2
                THROUGH DELTA,FOR I=2,1,I.G.(M+1)
                THROUGH DELTA,FOR J=2,1,J.G.N+1
                WHENEVER U(I,J).GE.0
                BT=TL(I,J)-TL(I-1,J)
                OTHERWISE
                BT=TL(I+1,J)-TL(I,J)
                END OF CONDITIONAL
                WHENEVER V(I,J).GE.0
                CT=TL(I,J)-TL(I,J-1)
                OTHERWISE
                CT=TL(I,J+1)-TL(I,J)
                END OF CONDITIONAL
                T(I,J)=TL(I,J)+DT*(T(I+1,J)-2.*T(I,J)+T(I-1,J))*R*R/DX2+DT*(
               1T(I,J+1)-2.*T(I,J)+T(I,J-1))/DY2-U(I,J)*DT*BT/DX-V(I,J)*DT*C
               2T/DY
                T(1,J)=T(3,J)
   DELTA         T(I,1)=T(I,3)
                T(1,N+2)=T(3,N+2)
                 T(1,1)=T(3,1)
                  WHENEVER NT.G.N5,EPSLN3=EPSLN4
                THROUGH YY,FOR I=3,1,I.G.M+1
                THROUGH YY,FOR J=3,1,J.G.N+1
                W(I,N+2)= -TM*U(I,N+1)/DY
                W(2,J)=-TM*V(3,J)/DX
                WHENEVER U(I,J).GE.0
```

```
                B=(W(I,J)-W(I-1,J))/DX
                OTHERWISE
               B=(W(I+1,J)-W(I,J))/DX
                END OF CONDITIONAL
                WHENEVER V(I,J).GE.0
                C=(W(I,J)-W(I,J-1))/DY
                OTHERWISE
                C=(W(I,J+1)-W(I,J))/DY
               END OF CONDITIONAL
                D=(W(I+1,J)-2.* W(I,J)+W(I-1,J))/DX2
                E=(W(I,J+1)-2.*W(I,J)+W(I,J-1))/DY2
              WL(I,J)=W(I,J)+DT*(R*R*D+E)*PR+PR*DI*(T(I,J)-T(I,J-1))/DY
             1-U(I,J)*DT*B-V(I,J)*DT*C
              WL(I,N+2)= W(I,N+2)
YY            WL(2,J)=W(2,J)
              NE=0
JJ            NE=NE+1
              WHENEVER NE.G.N6
              PRINT RESULTS NE,NE, NT,TIME,SF(2,2)...SF(M+2,N+2),ST(2,2)
             1 ...ST(M+2,N+2),RMAX
              TRANSFER TO EE
               END OF CONDITIONAL
              I=2
II            I=I+1
              I4=I
               THROUGH LM,FOR J=3,1,J.G.N+1
               DI(J)=(ST(I-1,J)+ST(I+1,J))*DYX-DY2*WL(I,J)
              F(2)=0
LM            F(J)=(DI(J)+F(J-1))*EI(J)
             THROUGH LN,FOR J=1,1,J.G.N-1
              I=I4
               H=N+2-J
              SF(I,H)=EI(H)*SF(I,H+1)+F(H)
LN            ST(I,H)=SF(I,H)
             WHENEVER I.L.M+1,TRANSFER TO II
              J=2
HH           J=J+1
              I4=J
                THROUGH MM,FOR I=3,1,I.G.M+1
              DI(I)=(ST(I,J-1)+ST(I,J+1))*DXY-DX2*WL(I,J)
              F(2)=0
MM            F(I)=(DI(I)+F(I-1))*EJ(I)
              THROUGH NN,FOR I=1,1,I.G.M-1
              J=I4
              H=M+2-I
NN           SF(H,J)=EI(H)*SF(H+1,J)+F(H)
              WHENEVER J.L.N+1,TRANSFER TO HH
               RMAX =0
              THROUGH AAA,FOR I=3,1,I.G.M+1
              THROUGH AAA,FOR J=3,1,J.G.N+1
             WHENEVER((I-4.)/N8-(I-4)/N8).E.0 .AND. ((J-4.)/N8-(J-4)/N8)
            1.E.0
             R3=.ABS.((SF(I,J)+1.0E-30)/(ST(I,J)+1.0E-30))
              WHENEVER RMAX .L.R3,RMAX=R3
AAA           END OF CONDITIONAL
               WHENEVER RMAX .G.EPSLN3
              THROUGH LL,FOR I=3,1,I.G.M+1
              THROUGH LL,FOR J=3,1,J.G.N+1
LL            ST(I,J)=SF(I,J)
```

```
                TRANSFER TO JJ
                OTHERWISE
                 CONTINUE
               END OF CONDITIONAL
               THROUGH ALPHA,FOR I=1,1,I.G.(M+2)
               THROUGH ALPHA,FOR J=1,1,J.G.(N+2)
ALPHA           ST(I,J)=SF(I,J)
               THROUGH BETA,FOR I=3,1,I.G.(M+2)
                THROUGH BETA,FOR J=2,1,J.G.N+1
                 SF(M+3,J)=-SF(M+1,J)
               U(I,J)=(SF(I,J+1)-SF(I,J))/DY
BETA            V(I,J)=(SF(I,J)-SF(I+1,J))/DX
               WHENEVER NT.L.N2,PRINT RESULTS NT,DT,TIME,U(2,2)...
              1U(M+2,N+2),V(2,2)...V(M+2,N+2),T(1,1)...T(M+2,N+2) ,NE  ,
              2SF(2,2)...SF(M+2,N+2),WL(2,2)...WL(M+2,N+2)  ,RMAX
               NTO=(NT+0.)/N3-NT/N3
               WHENEVER NTO.E.0
               UR=-U(I1,2)/2.
               THROUGH DAL,FOR J=3,1,J.G.(N+2)
DAL             UR= UR+U(I1,J)
               PRINT RESULTS NT,DT,TIME,UR,U(2,2)...U(M+2,N+2),
              1V(2,2)...V(M+2,N+2),T(1,1)...T(M+2,N+2),SF(2,2)...SF(M+2,N+2)
              2 ,NE  ,WL(2,2)...WL(M+2,N+2)  ,RMAX
               OTHERWISE
                CONTINUE
               END OF CONDITIONAL
               WHENEVER T2.G.2,TRANSFER TO GEEM
               WHENEVER T(I1,N+2).G.T3,TRANSFER TO LAMDA
               TRANSFER TO BACK
GEEM            WHENEVER NT.L.N7,TRANSFER TO BACK
                THROUGH AA,FOR I=3,1,I.G.M+1
               THROUGH AA ,FOR J=3,1,J.G.N+1
               WHENEVER ((I-3.)/N8-(I-3)/N8).E.0 .AND. ((J-3.)/N8-(J-3)/N8)
              1.E.0
               R1=.ABS.((SF(I,J)-ST(I,J))/ST(I,J))
               R2=.ABS.((T(I,J)-TL(I,J))/TL(I,J))
                WHENEVER R1.G.EPSLON .OR.R2.G.EPSLN2,TRANSFER TO BACK
AA               END OF CONDITIONAL
LAMDA             I3=M/2
                UR3=-U(I3,2)/2.
               THROUGH LAM,FOR J=3,1,J.G.(N+2)
LAM              UR3=UR3+U(I3,J)
               PRINT RESULTS NT,DT,TIME,UR3,U(2,2)...U(M+2,N+2),
              1V(2,2)...V(M+2,N+2),T(1,1)...T(M+2,N+2),SF(2,2)...SF(M+2,N+2)
              2 ,NE ,RMAX
               TRANSFER TO START
EE              CONTINUE
              END OF PROGRAM
$ DATA
```



Flow Pattern

wall flux = 10, Btu/hr/ft^2

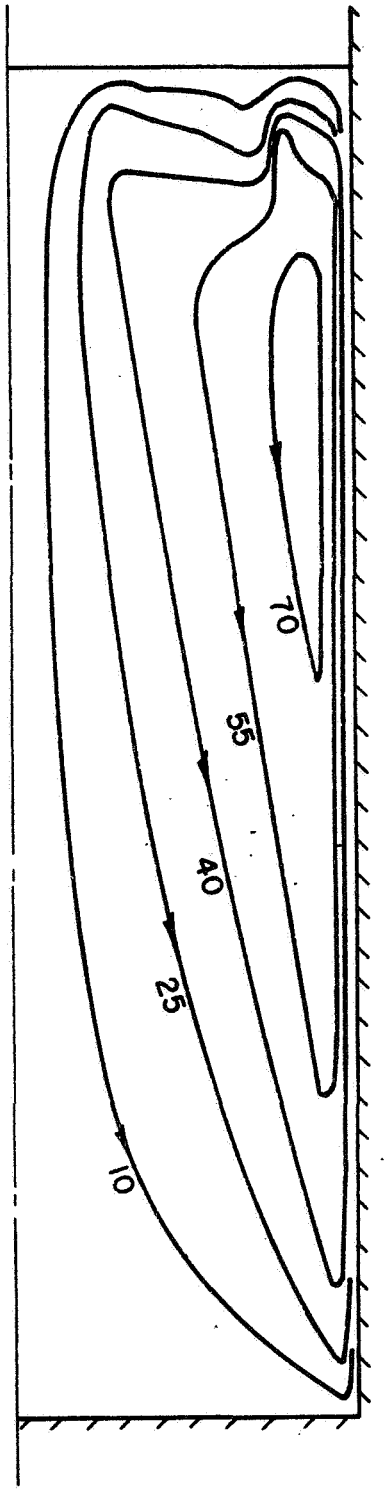
surface temp. = T_o

$\tau = 6.785 \times 10^{-4}$

$\approx$ 50 sec

21 x 21 grid

Fig. 1



Flow Pattern

wall flux = 10, Btu/hr/ft^2

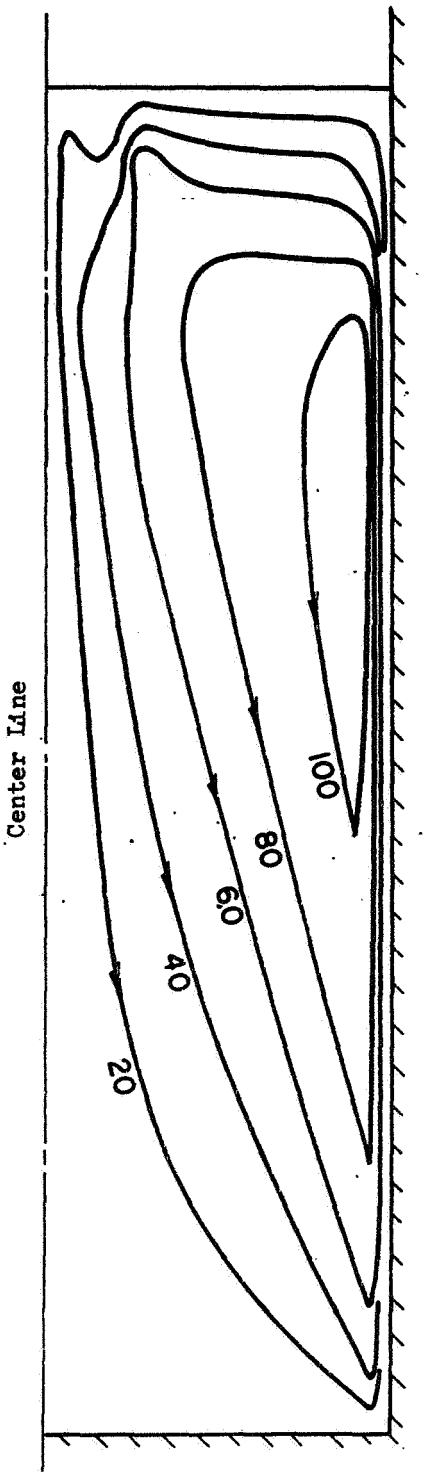
surface temp. = T_o

$\tau = 1.67 \times 10^{-3}$

$\approx$ 2 min

21 x 21 grid

Fig. 2



Flow Pattern

wall flux = 10, Btu/hr/ft^2

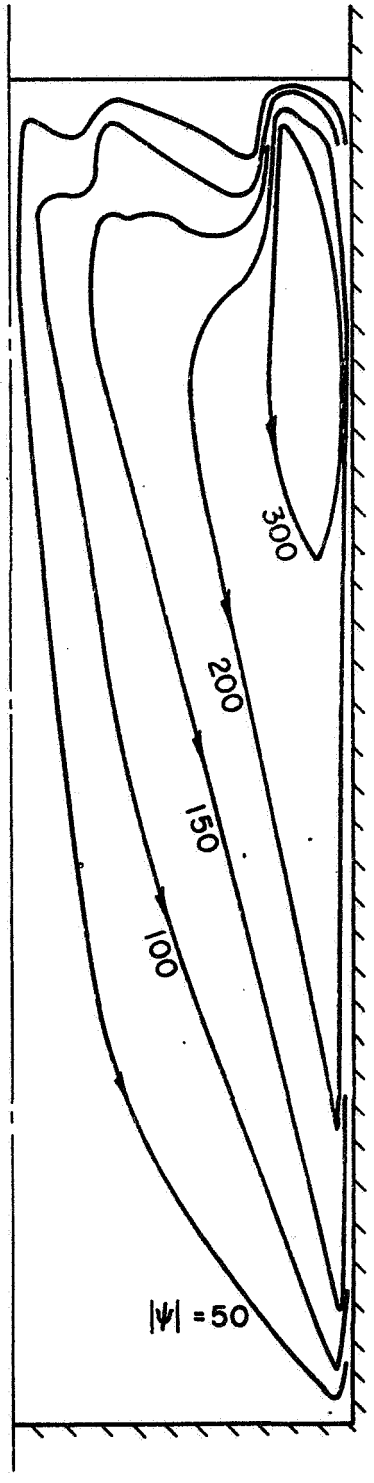
surface temp. = T_o

τ = .003

$\approx$ 3.6 min

21 x 21 grid

Fig. 3



Flow Pattern

wall flux = 1000, Btu/hr/ft^2

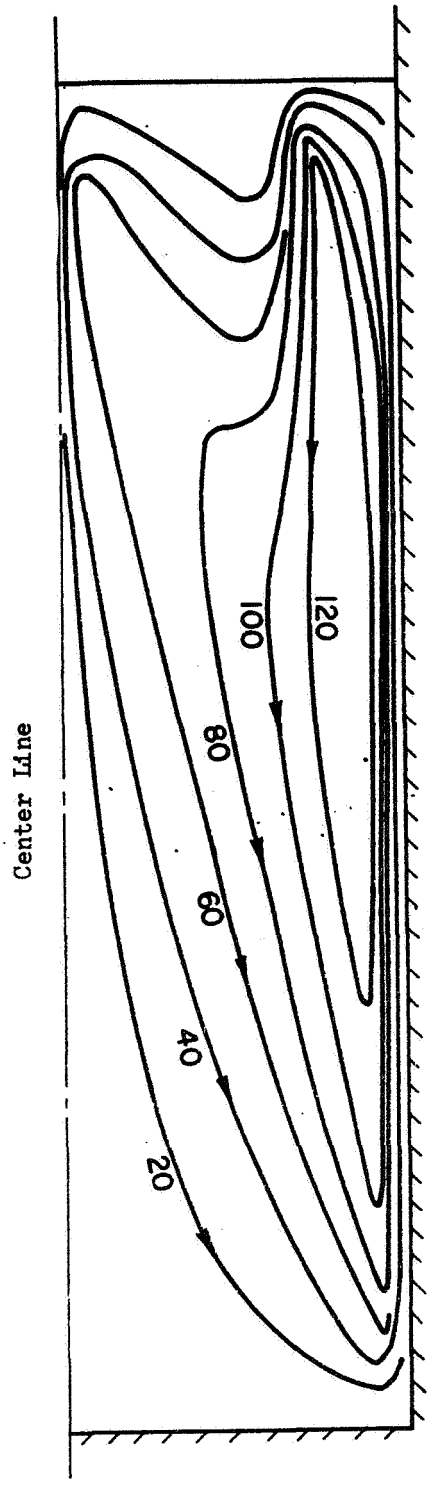
surface temp. = T_o

$\tau = 7.07 \times 10^{-4}$

$\approx$ 51 sec

21 x 21 grid

Fig. 4



Flow Pattern

wall flux = 10

surface temp. = T_o

τ = .003785

≈ 4.540 min

16 x 16 grid

Fig. 5

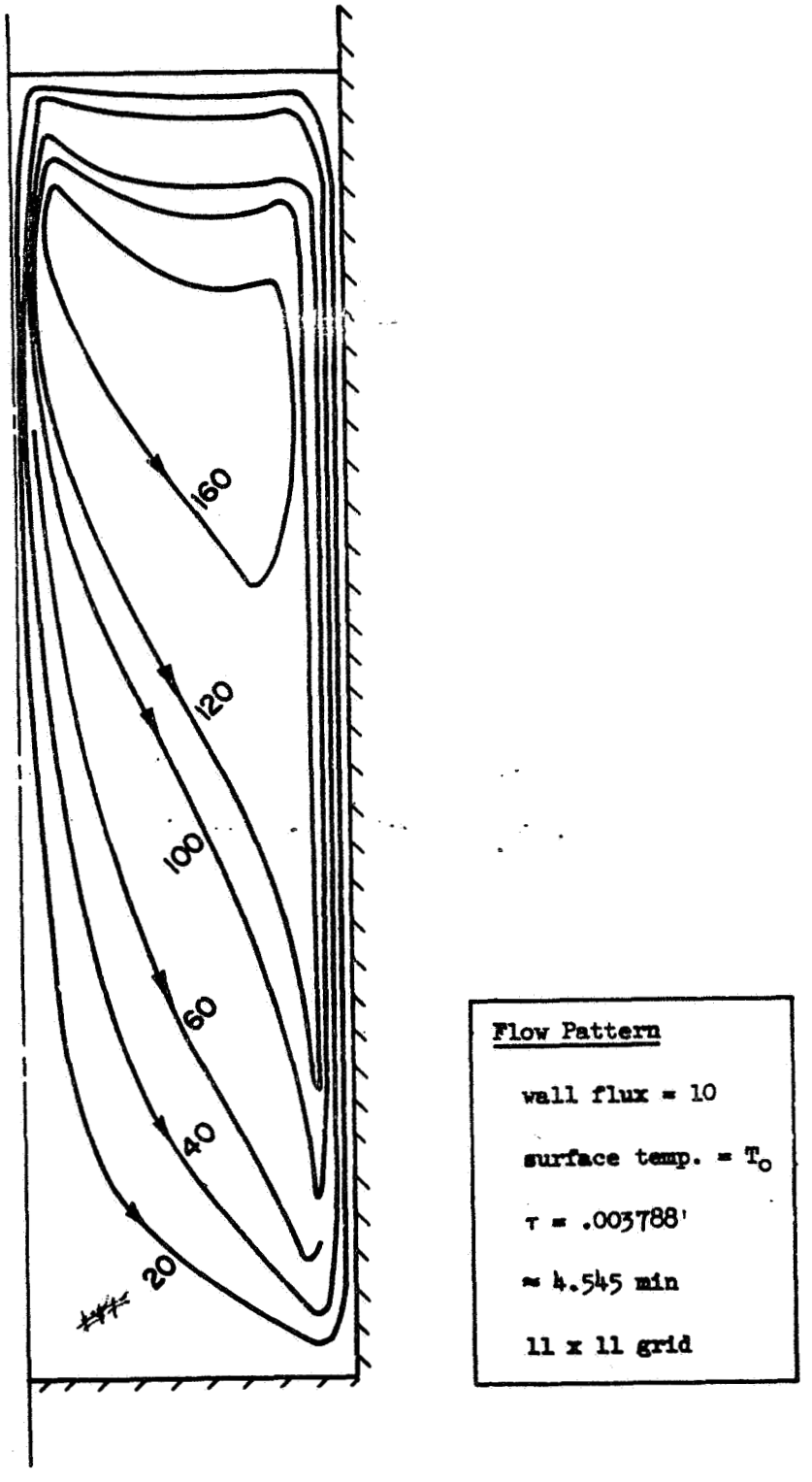
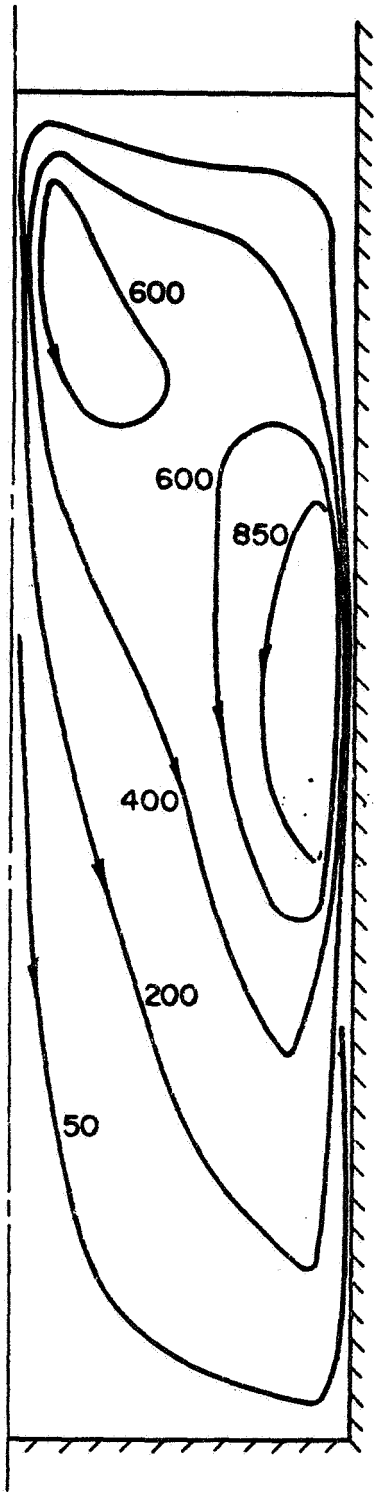

160
120
100
60
40
20
Flow Pattern
wall flux = 10
surface temp. = T_o
τ = .003788'
≈ 4.545 min
11 x 11 grid

Fig. 6



Streamline Pattern

wall flux = 1000 Btu/hr/ft^2

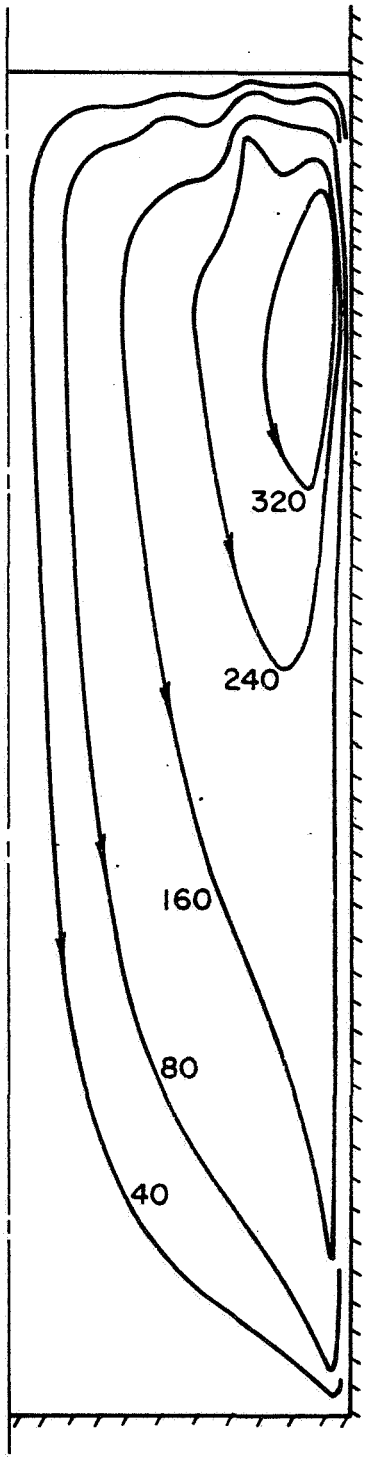
adiabatic upper surface

$\tau = 0.00114$

≈ 3.42 min

11 x 11 grid

Fig. 7



Streamline Pattern

wall flux = 1000, Btu/hr/ft^2

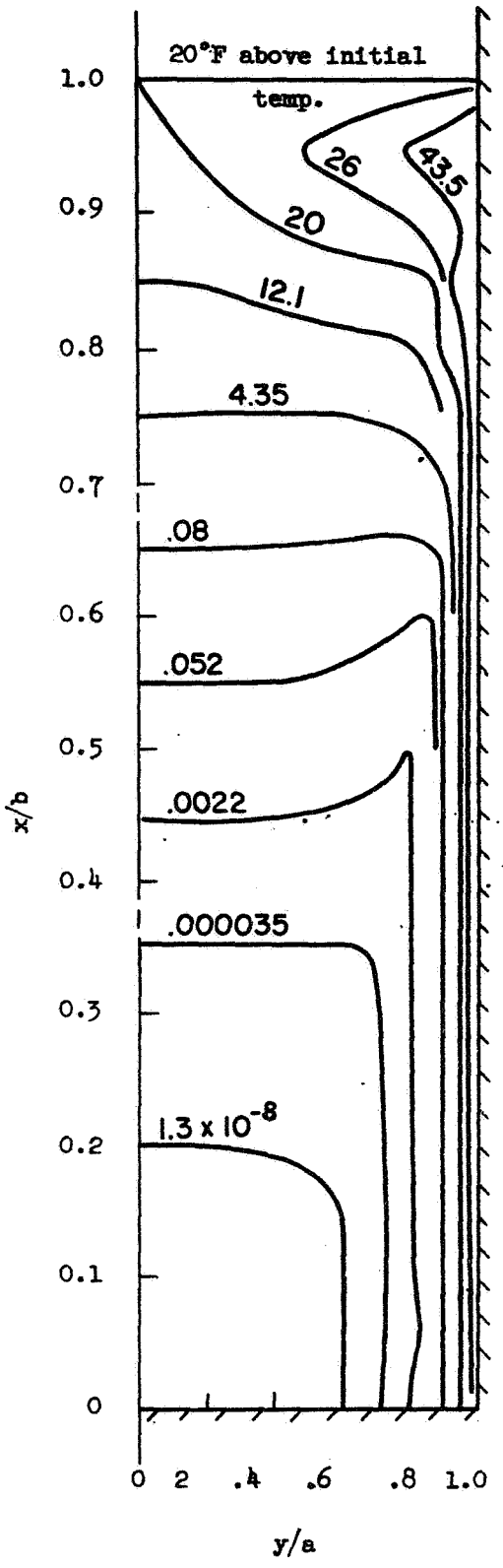
surface temp. = T sat.

$\tau = 6.6 \times 10^{-4}$

$\approx$ 48 sec

21 x 21 grid

Fig. 8



Isothermals

wall flux = 1000, Btu/hr/ft^2

free surface temp. = T_s

$\tau = 6.6 \times 10^{-4}$

$\approx$ 48 sec

21 x 21 grid

Fig. 9

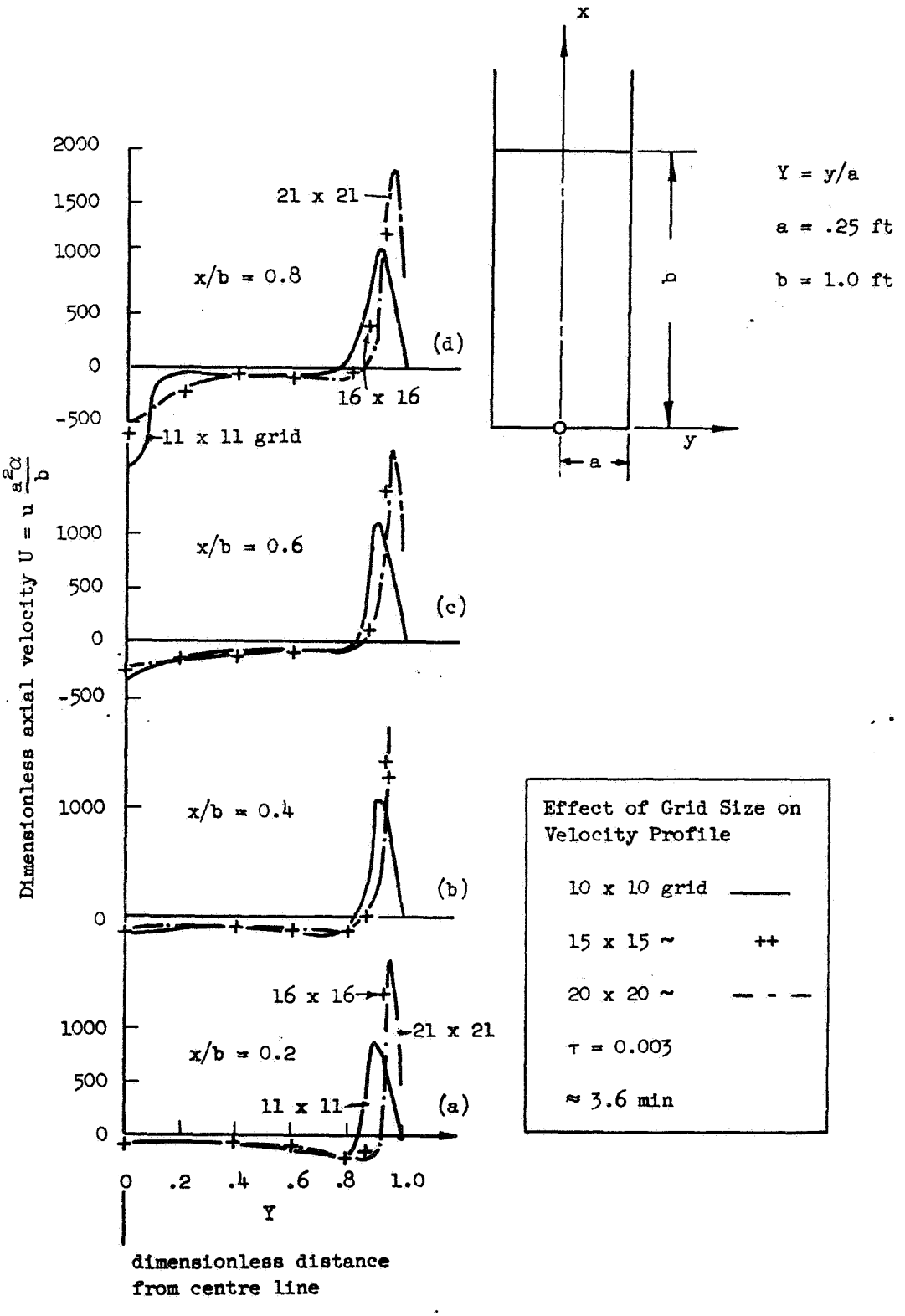

x
Y = y/a
a = .25 ft
b = 1.0 ft
y
a
2000
1500
1000
500
0
-500
21 x 21
x/b = 0.8
(d)
16 x 16
11 x 11 grid
x/b = 0.6
(c)
x/b = 0.4
(b)
16 x 16
21 x 21
x/b = 0.2
11 x 11
(a)
Dimensionless axial velocity U = u a²α/b
0 .2 .4 .6 .8 1.0
Y
dimensionless distance from centre line
Effect of Grid Size on Velocity Profile
10 x 10 grid
15 x 15 ~
20 x 20 ~
τ = 0.003
≈ 3.6 min

Fig. 10

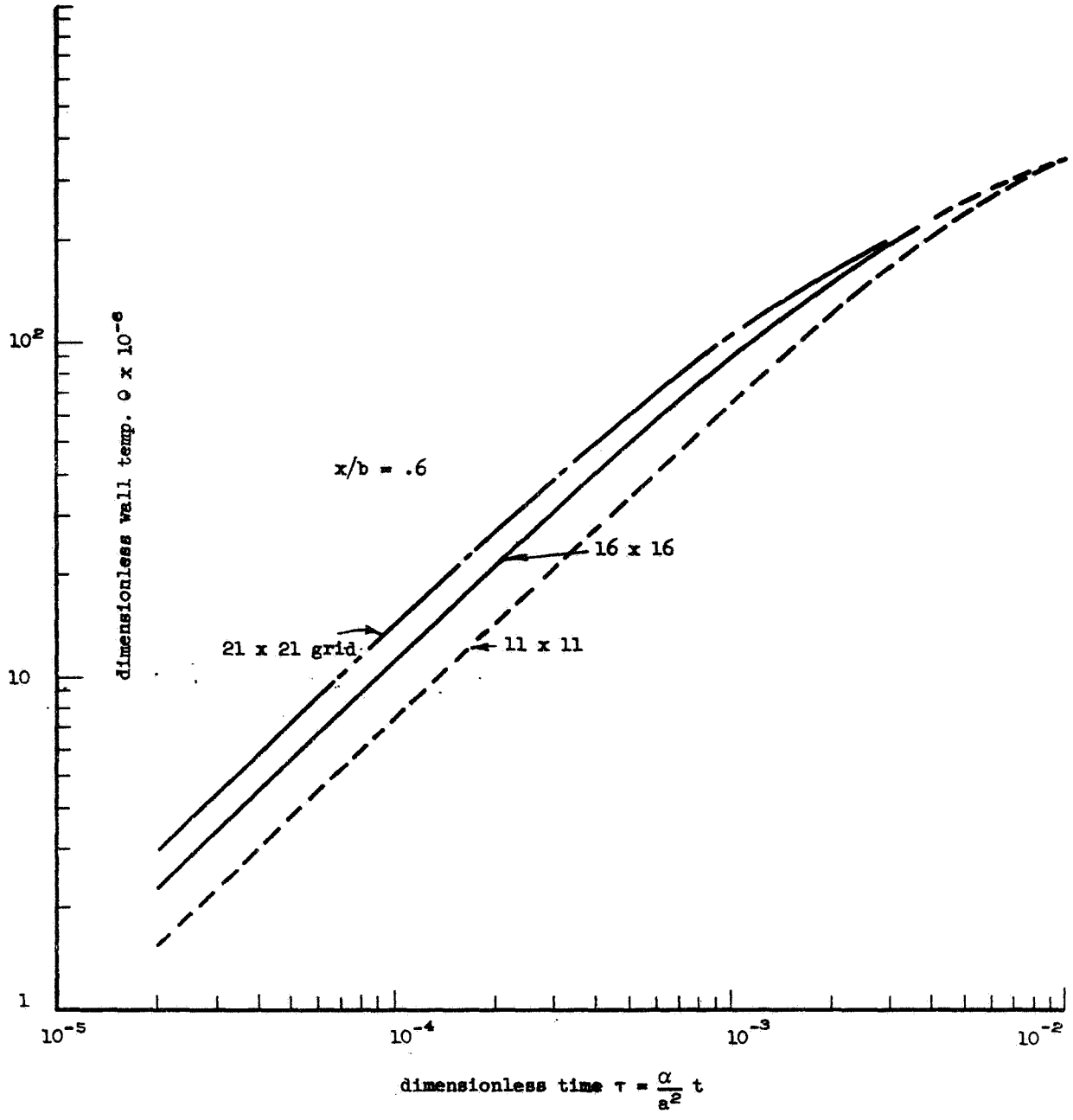

10^2
10
1
dimensionless wall temp. $\theta \times 10^{-6}$
x/b = .6
16 x 16
21 x 21 grid
11 x 11
10^{-5}
10^{-4}
10^{-3}
10^{-2}
dimensionless time $\tau = \frac{\alpha}{a^2} t$

Fig. 11

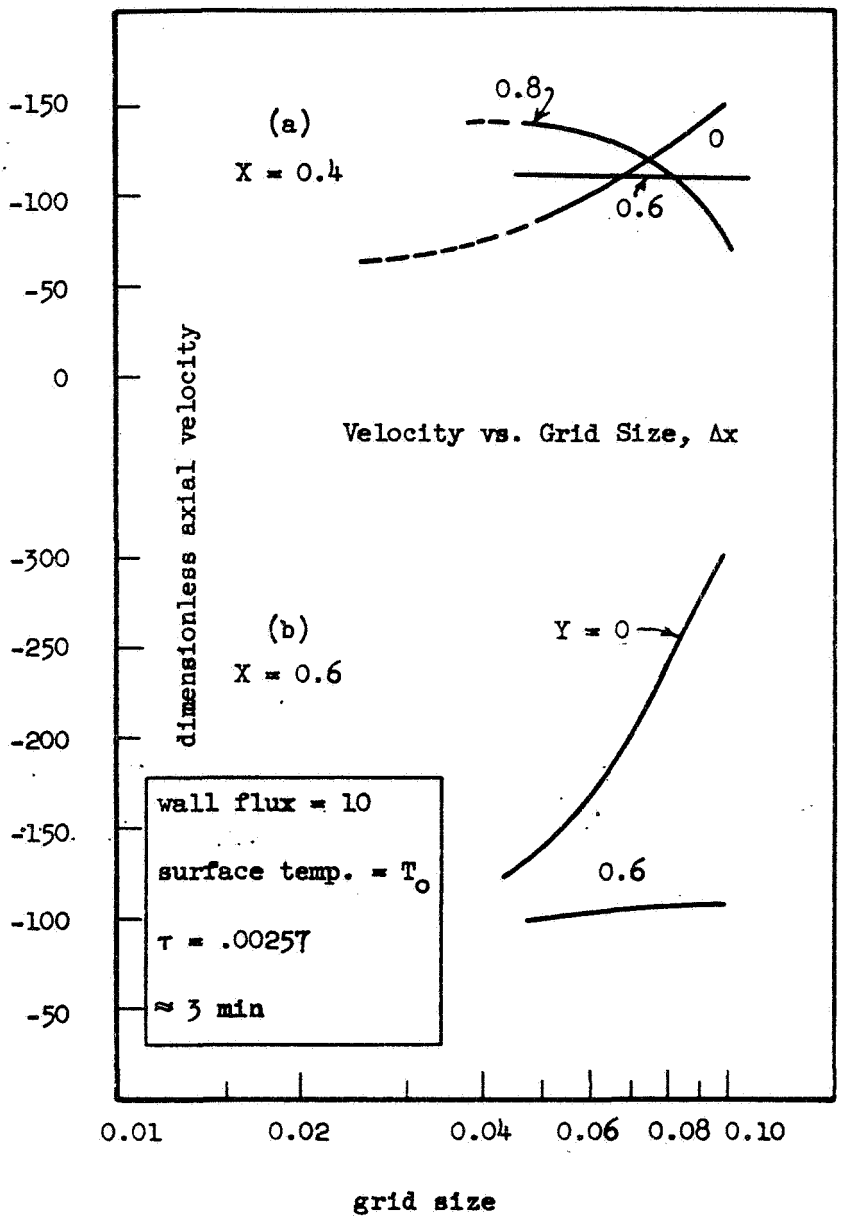

-150
-100
-50
0
-300
-250
-200
-150
-100
-50
(a)
X = 0.4
0.8
0
0.6
Velocity vs. Grid Size, Δx
dimensionless axial velocity
(b)
X = 0.6
Y = 0
0.6
wall flux = 10
surface temp. = T_o
τ = .00257
≈ 3 min
0.01
0.02
0.04
0.06
0.08
0.10
grid size

Fig. 12

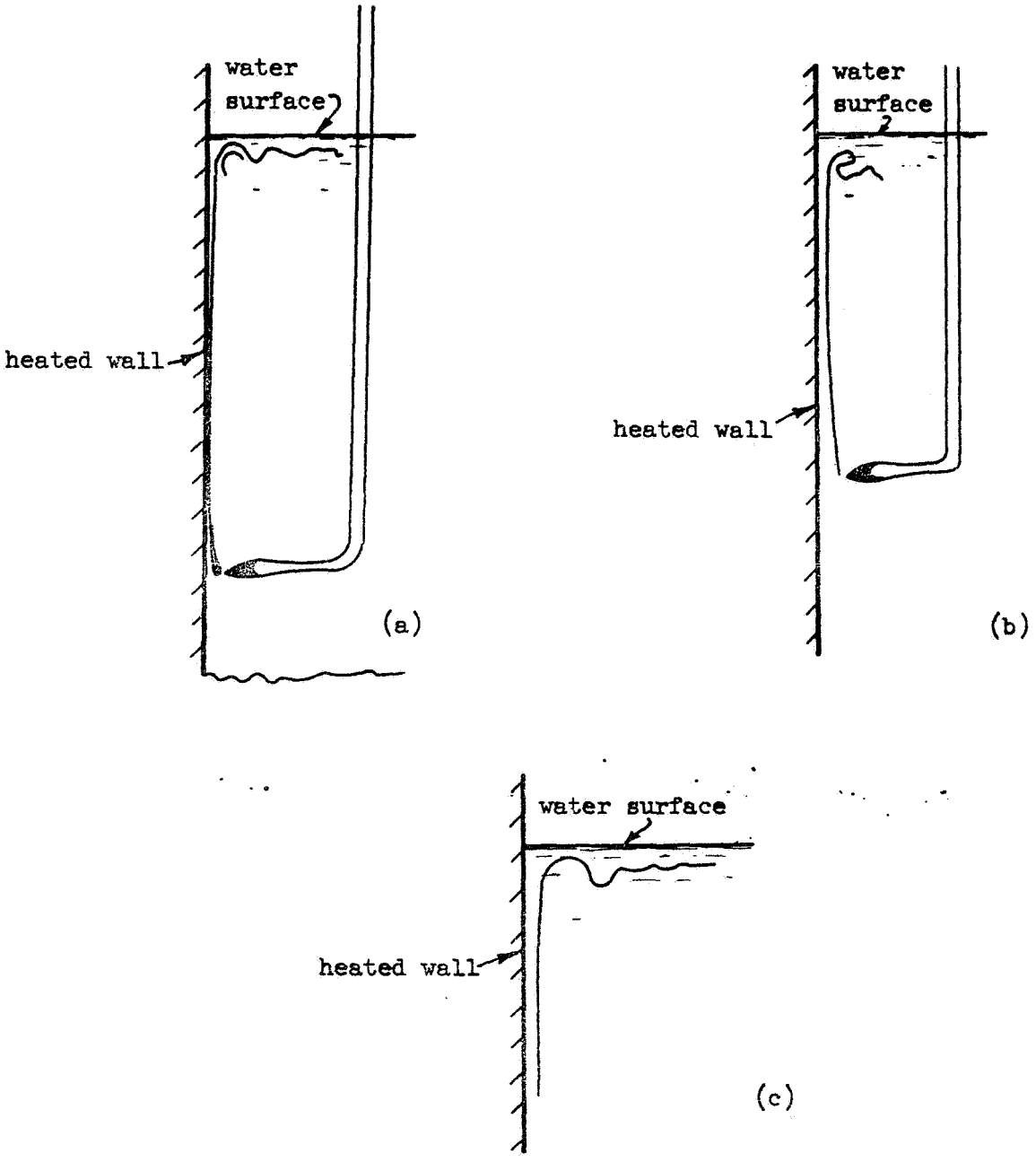
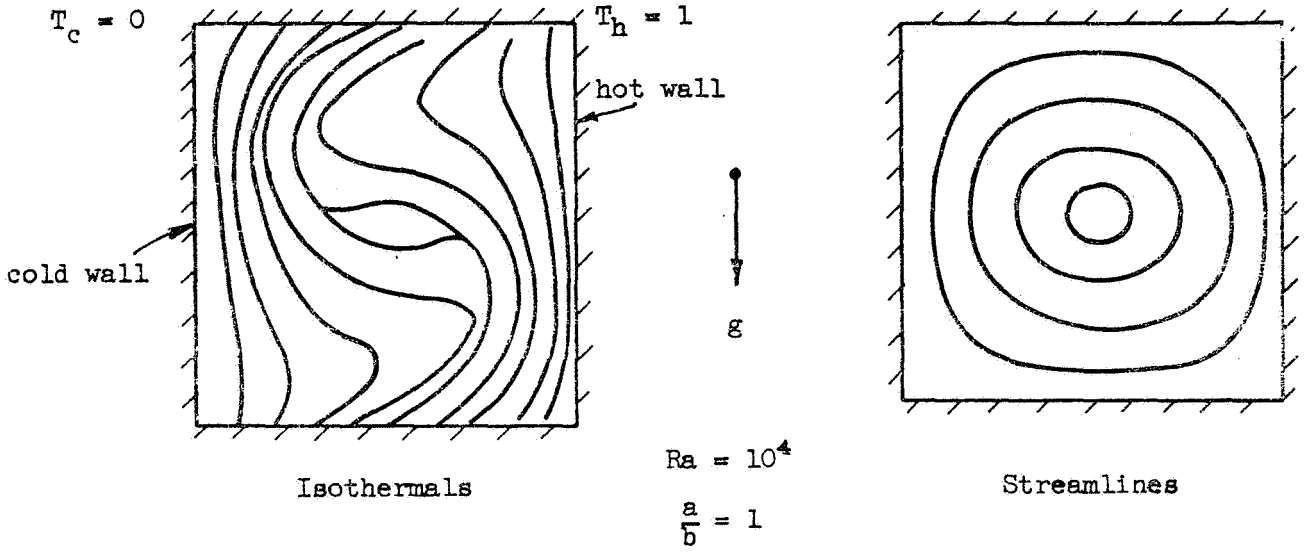

water surface
heated wall
(a)
water surface
heated wall
(b)
water surface
heated wall
(c)

Fig. 13



$Ra = 10^4$

$\frac{a}{b} = 1$

Fig. 14

X65-12[illegible]

A HYPOTHESIS FOR HELIUM ADSORPTION/DESORPTION IN SLUSH HYDROGEN

by
Clarence A. Schalla
Lockheed Missiles and Space Company
Sunnyvale, California

Preceding page blank

INTRODUCTION

Helium solubility in liquid hydrogen at subcooled temperatures and at normal pressures is extremely low, being proportional to liquid temperature. Helium dilution in slush (liquid-solid) hydrogen, on the other hand, can be expected to be appreciable. There is no information available on the adsorption of helium by gas-solid interfaces of the solids in slush hydrogen. This paper introduces an initial hypothesis concerning it. Also introduced is the hypothesis of helium desorption cooling of slush hydrogen. The latter, if observed, would be the antithesis to the hydrogen stratification phenomena. Accordingly, slush germination via desorption cooling under supercooled conditions of storage is here postulated to anticipate triple-point anomalies in future exploratory investigations with slush hydrogen. That is, such data may very well show variances with the normally singular triple-point of hydrogen.

The concern over the solubility of helium in liquid hydrogen has been not unlike that of nitrogen solubility in liquid oxygen. Both of these gaseous absorbates are commonly used as purgants and pressurants. Any solubility carryover and evolution would somewhat handicap propellant utilization (because of early onset of cavitation). Accordingly, propellant dilution with these inert gases does precipitate apprehensions over nozzle flow control and metering systems sensitivity.

Helium solubility in saturated and in subcooled liquid hydrogen is considered to be low for the normal range of pressures concerned. Refer to Table I.

When considering mixtures of liquid-solid (slush) hydrogen, however, a new concern arises over the slush dilution counterpart of liquid solubility, namely slush adsorption. Appreciable adsorptivity conceivably exists at the surface of the hydrogen solids. In storing and transferring slush the necessary high partial pressure ratio of helium to slush hydrogen could create a pronounced dilution of hydrogen. From Figure 1, it may be noted that slush exists only at the triple point temperature of 24.9°R and pressure of 1.0209 psia. No solubility/adsorption data whatsoever exists in this regime. This adsorption hypothesis is intended as a research approach leading to acquisition of such data.

BRIEF GENERAL THEORY OF ADSORPTION

The adsorption of gases by solids is a surface property. Adsorption is basically an exothermic process because the molecules of the helium must have less freedom in the adsorbed state than they do in the gaseous state. In ordinary practice the phenomenon would seem to be the special property of a few porous solids, such as charcoal, silica gel, or activated alumina; but more careful investigation shows that the surface of every solid can adsorb a thin layer of gas, often no more than one molecule in thickness.

HYDROGEN ADSORPTION HYPOTHESIS

Hydrogen solids appear to be crystalline and they are considered to have a sharp melting point rather than a softening range. Therefore, such solids have many interfaces, and physical adsorption is to be expected.

The basis for such postulation is derived from Figure 2, where a singular anomaly of data plotted appears to be significant. Specifically, it is to be noted that in the subcooled liquid range of 24.9 to 36.5°R, only the low pressure (15 psia) parameter deviates with an opposite slope.

This indicates an increase in the solubility rate with decreasing temperatures until the slush hydrogen (triple point) temperature of 24.9°R is reached. At this point the pseudo curve in Figure 2 is shown to express a radical increase in adsorptivity. Its terminal magnitude will depend on the quality (solids content) of slush, the dispersion of the solids, and their crystalline characteristics. Upon solidification, the activity of the helium molecules decreases with temperature and adsorption accordingly will diminish. In Figure 2 the decreasing helium solubility with increasing temperatures in the subcooled state for the anomalous 15 psia parameter occurs possibly because of an exothermic mechanism.

The relationship between the solubility and adsorption capabilities for the various states of hydrogen are presented qualitatively in Figure 3. The slush quality (solids content) effect on the variation of adsorption is particularly notable. Again one must be reminded that this is a pseudo mechanism that here is being introduced in lieu of data that might even prove otherwise.

DESORPTION HYPOTHESIS

Desorption or helium evolution is the converse to the solubility and adsorption processes. In an isentropic expansion, such as may occur during depressurization of hydrogen storage in space, the adsorbed helium is presumed to desorb as shown in Figure 4. During such desorption conditions in hydrogen venting, the evolved helium gas is likely to induce Joule-Thomson cooling of the hydrogen involved. Figure 5 presents this mechanism, which can occur in a temperature regime well below the helium inversion temperature.

It is here postulated that when Joule-Thomson cooling of helium does develop during a desorption process, a supercooled slush hydrogen condition would occur wherever subcooled hydrogen conditions exist. Accordingly, slush hydrogen would germinate at these supercooled points, to be detected at variance with the characteristic thermodynamic conditions of the triple point state. Such could be considered the antithesis to the hydrogen stratification phenomenon.

Any such hydrogen slush anomalies and thermodynamic variations from helium adsorption could handicap slush production and propellant utilization control.

CONCLUSIONS

With these adsorption/desorption hypotheses it is implied that exploratory work will reveal anomalies and phenomena somewhat detrimental to the space use of slush hydrogen. However, this may be construed, it is apparent that research effort and implemental instrumentation development is overdue in work at and around the triple point of hydrogen. Because helium is a prominent adjunct to the handling and storage of slush hydrogen, it also appears that such concerted research and development be directed to flight-type sensing instrumentation and controls.

In formulating the hypotheses of this paper, various thermodynamic processes were probed with pseudo data and quasi conditions. This was principally for the purpose of presenting a realistic approach in applying research logic in what can be used in a plan to define exploratory tests and instrumentation requirements.

BIBLIOGRAPHY

1. "The Surface Chemistry of Solids," by S. J. Gregg, Reinhold Publishing Corporation, New York, 1961.

2. "Physical Chemistry of Surfaces," by Arthur W. Adamson, Interscience Publishers, Inc., New York, 1960.

3. "Solid Surfaces and the Gas-Solid Interface," Advances in Chemistry Series No. 33, American Chemical Society, Washington, D.C., 1961.

4. "A Compendium of the Properties of Materials at Low Temperature (Phase II)," WADD Technical Report 60-56, Part IV, December, 1961.

TABLE I

HELIUM ADSORPTION DATA DEFICIENCIES

ADSORBENT FLUID	HELIUM DILUENT	
	SOLUBILITY	ADSORPTIVITY
	(Below 100 psia)	
LIQUID NITROGEN (SATURATED)	NIL (0.2% MAX.)	——
SUBCOOLED NITROGEN (65% SUBCOOLED)	NIL (0.1% MAX.)	——
SLUSH NITROGEN	——	UNKNOWN
LIQUID HYDROGEN (SATURATED)	NIL (0.9% MAX.)	——
SUBCOOLED HYDROGEN (45% SUBCOOLED)	NIL (0.35% MAX.)	——
SLUSH HYDROGEN	——	UNKNOWN

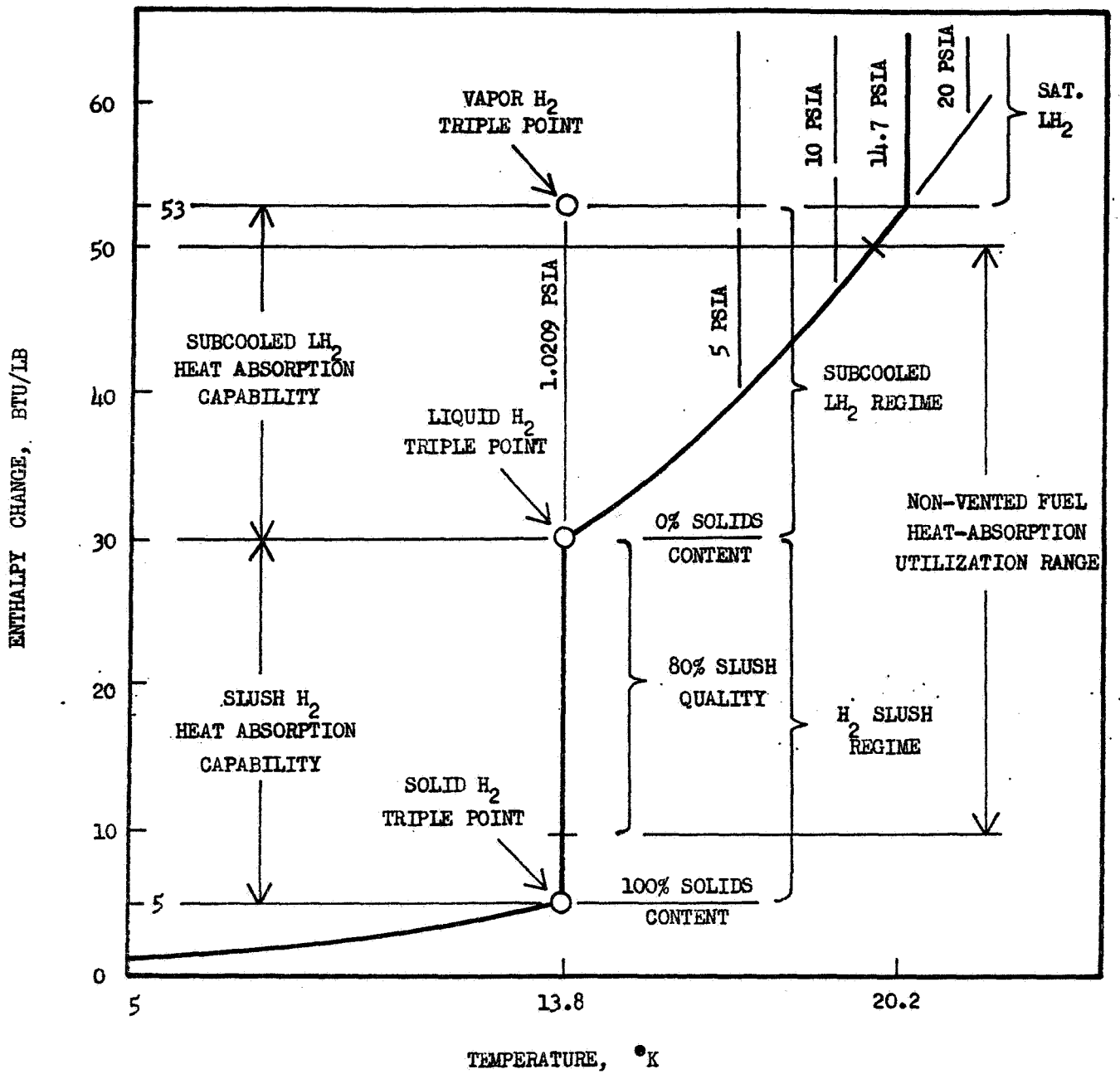


Figure 1 Slush/Subcooled Hydrogen Thermodynamic Characteristics

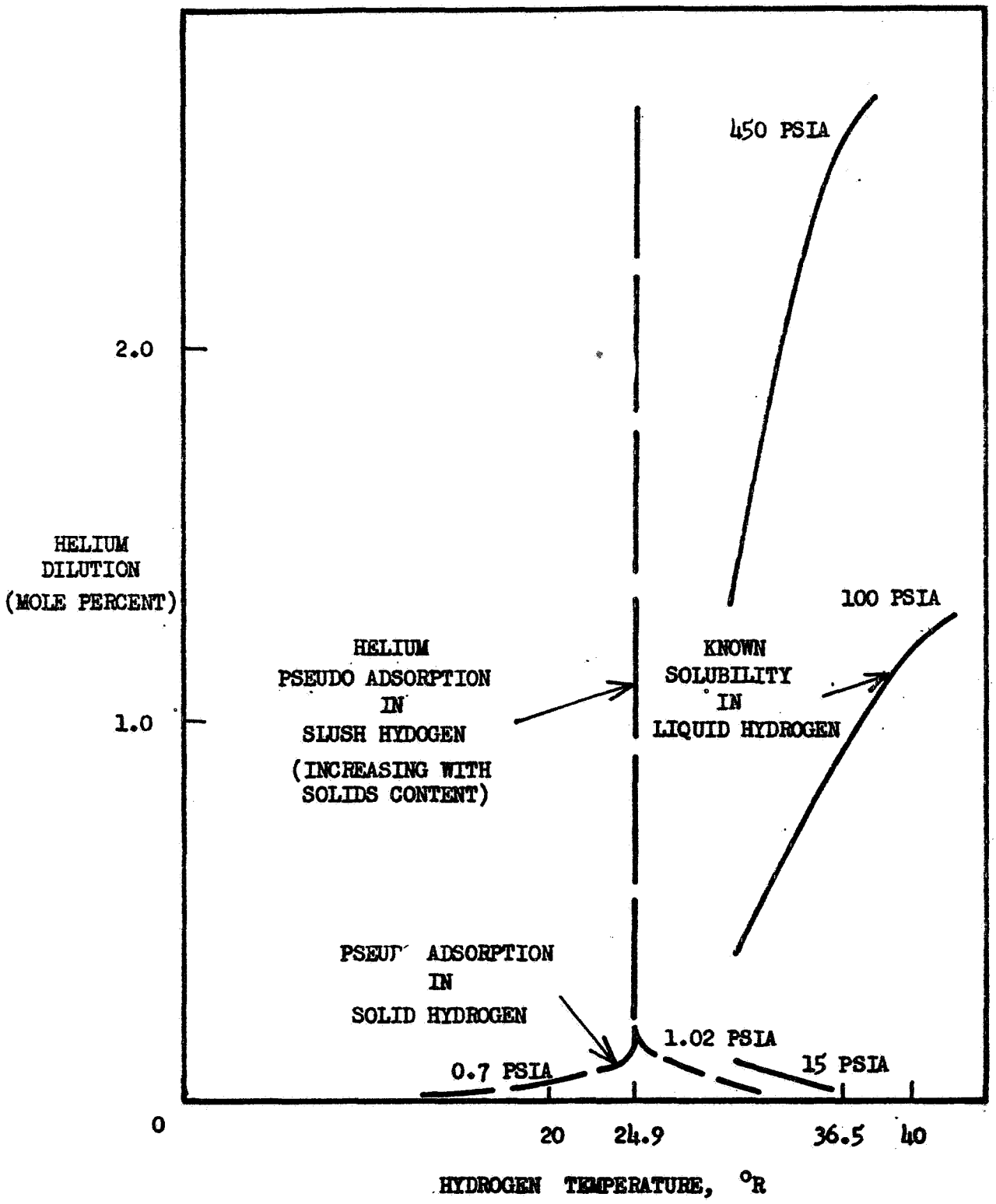


Figure 2 Helium Solubility and Pseudo Adsorption for Hydrogen

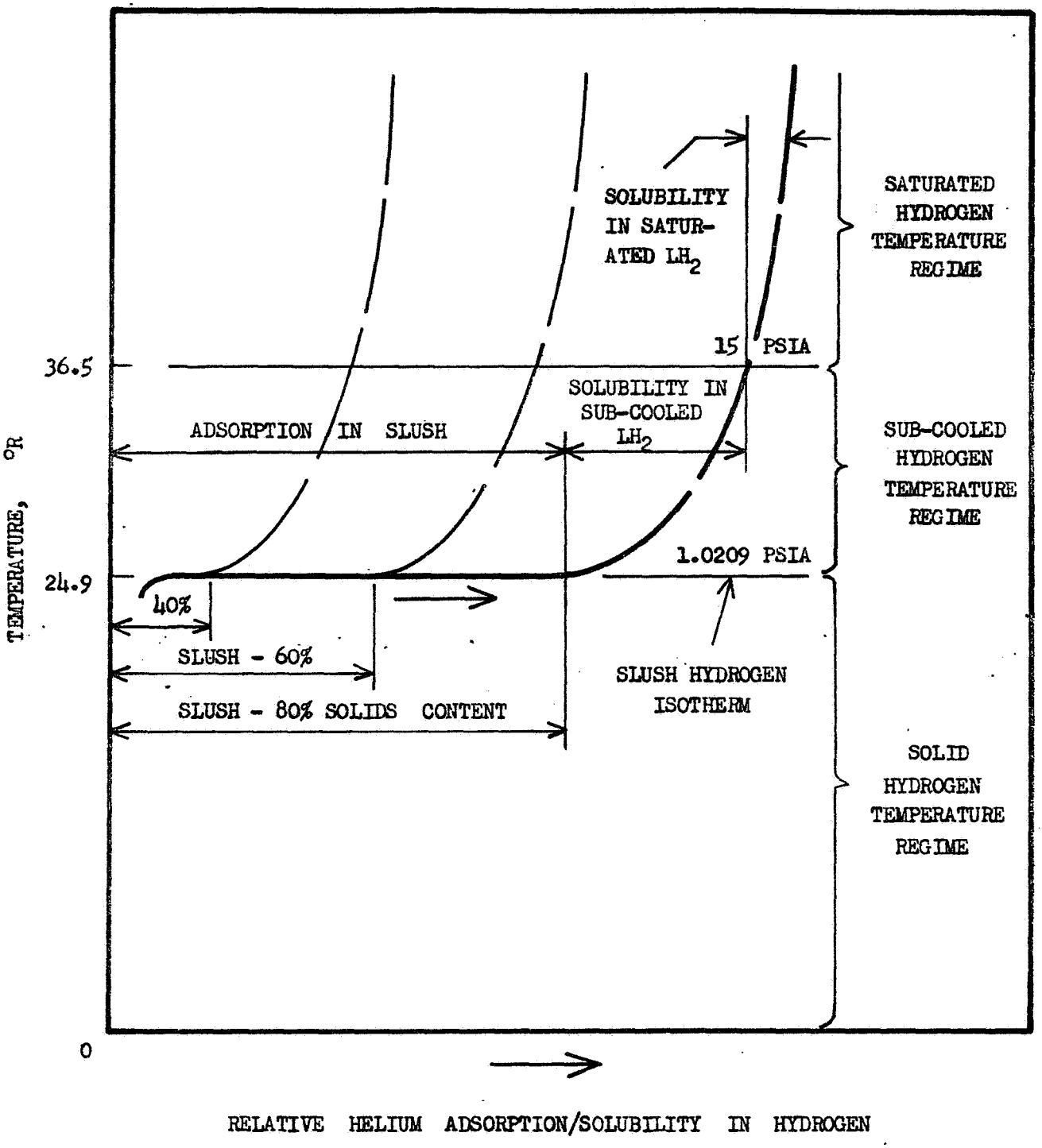


Figure 3 Variation of Helium Pseudo Adsorption with Slush Hydrogen

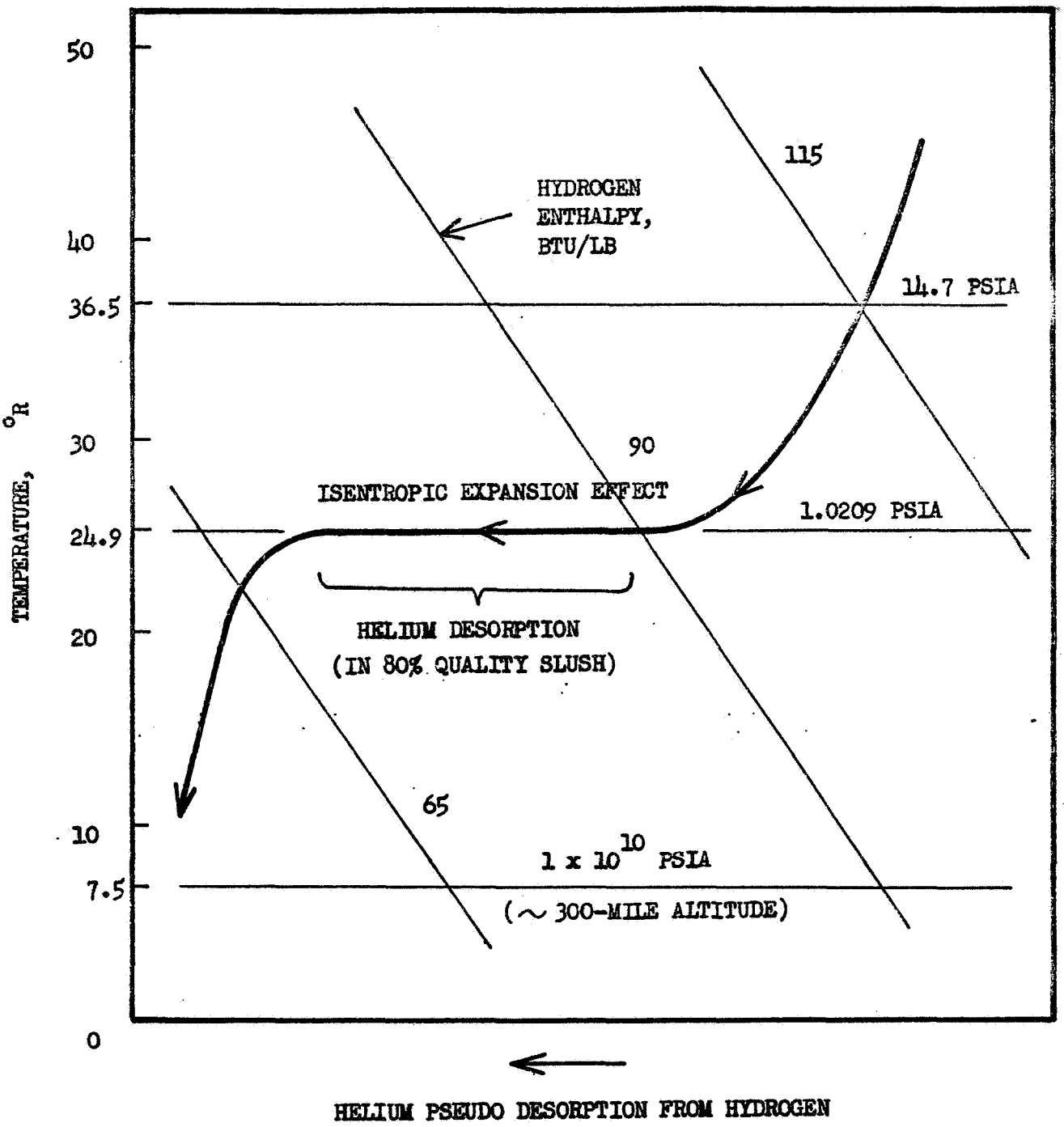


Figure 4 Helium Pseudo Desorption (evolution) for Isentropic Expansion (Simulating Space Vehicle Tank Depressurization)

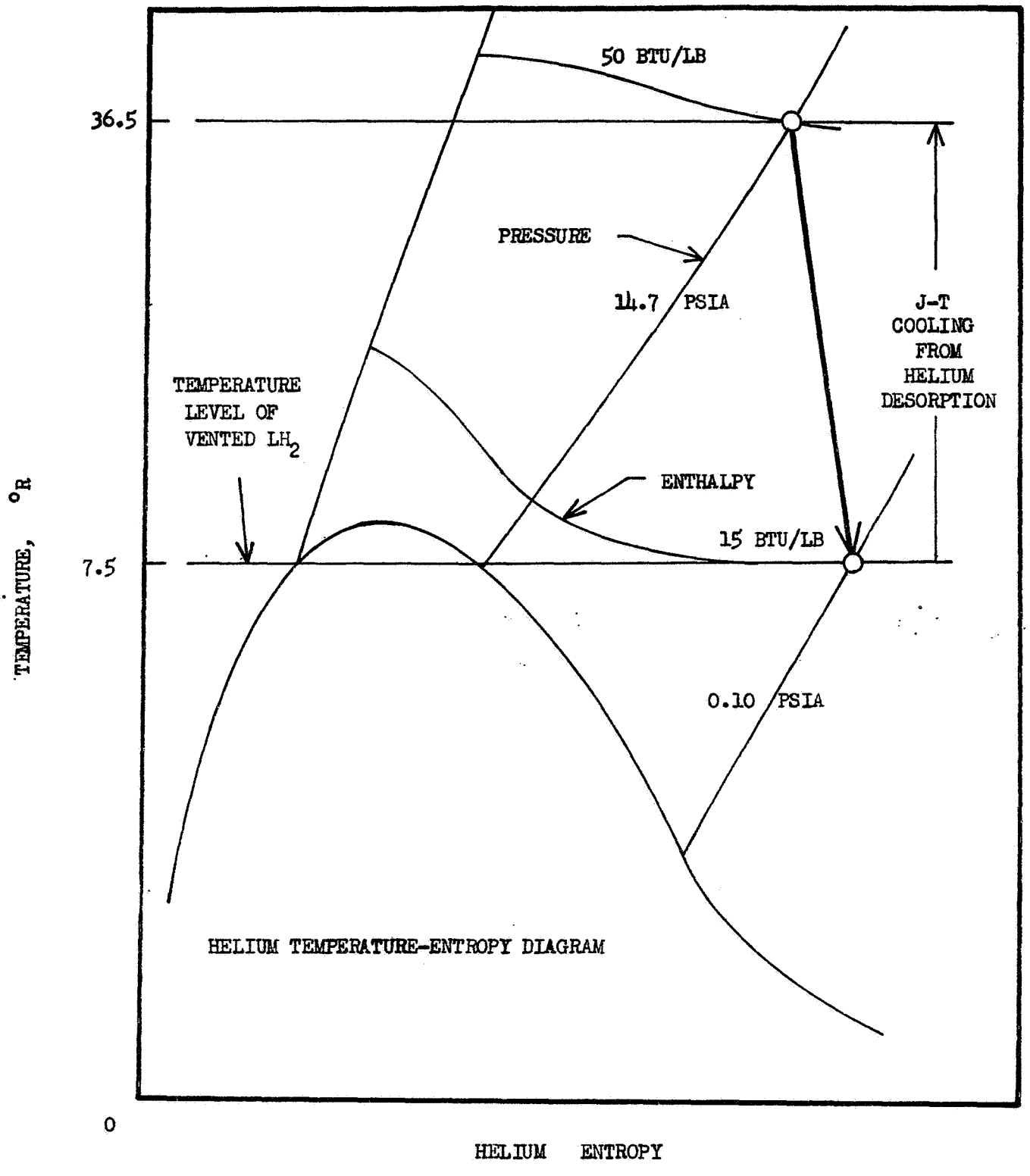


Figure 5 Cooling Effect from Helium Pseudo Desorption During Hydrogen Isentropic Expansion (Tank Depressurization)

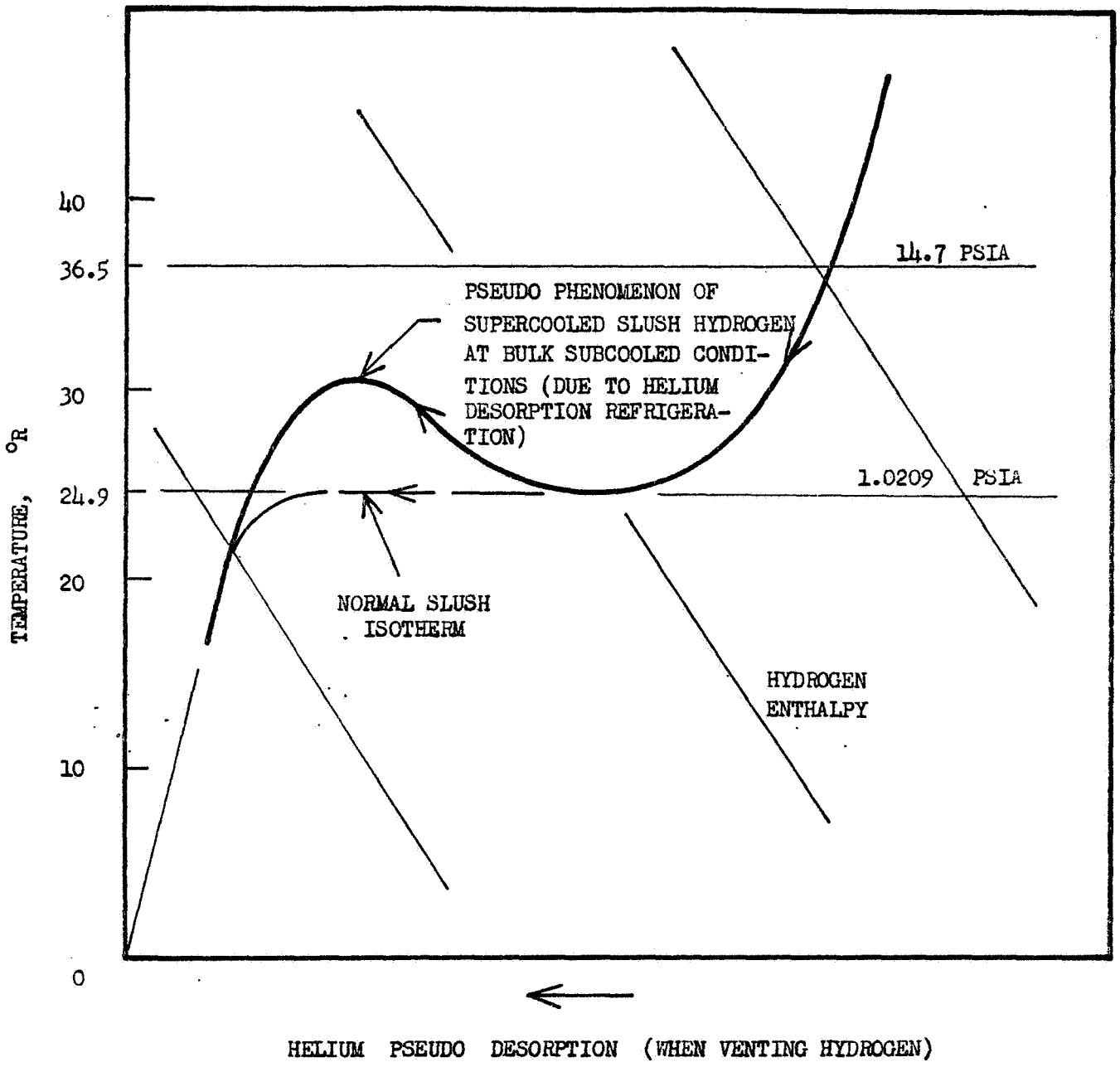


Figure 6 Helium Pseudo Desorption as a Theory for the Pseudo Phenomenon of Hydrogen Triple Point Anomalies

SELECTING LIQUID LEVEL TRANSDUCERS FOR CRYOGENIC SERVICE

by
D. A. Burgeson
National Bureau of Standards
Boulder, Colorado

Preceding page blank

SELECTING LIQUID LEVEL TRANSDUCERS FOR CRYOGENIC SERVICE

ABSTRACT

Point level transducers locate the vapor/liquid interface by detecting a difference in magnitude of the property between the vapor and liquid phases. The transducer respectively converts the presence of vapor or liquid into an output signal which is binary (i. e. either on or off). Knowledge of the transducer position and its mode of indication (vapor or liquid) can permit accurate location of the cryogenic fluid interface.

Several commercial transducers operate by using different properties of the vapor and liquid phase of a cryogen. Several have shown a resolution of the liquid interface of 0. 020 inch or less in liquids nitrogen and hydrogen.

Selecting the most suitable transducer for an application from those available requires knowledge of the use environment. The accuracy desired, the mechanical and electrical needs of transducer system and system measured, all require proper matching. The user of a liquid level transducer should know if the transducer is pressure or vapor velocity (temperature) sensitive. We present guidelines to help the user select a suitable checklist for transducer evaluation.

This work is continuing, and further unpublished details may be obtained from the author .

X66-11137

ANALYTICAL AND EXPERIMENTAL STUDY OF STRATIFICATION IN STANDARD AND REDUCED GRAVITY FIELDS

by

E. Y. Harper, S. E. Hurd, A. M. Levy, and D. M. Tellep
Lockheed Missiles and Space Company
Sunnyvale, California

ANALYTICAL AND EXPERIMENTAL STUDY OF STRATIFICATION IN STANDARD AND REDUCED GRAVITY FIELDS

E. Y. Harper, S. E. Hurd, A. M. Levy, D. M. Tellep

ABSTRACT

13030

Temperature stratification of a subcooled fluid in a cylindrical tank subjected to a uniform sidewall flux is studied both analytically and experimentally. Using an integral technique, a closed form solution for the stratified layer growth and liquid temperature rise is obtained for both the laminar and turbulent boundary layer flow regimes. The solution is based on the assumption of time-invariant dimensionless temperature profiles in the stratified layer before the layer reaches the tank bottom. The solution identifies the significant dimensionless parameters which govern stratification.

Stratification experiments were carried out in three different vessels with six different fluids. The experiments demonstrated the utility of noncryogenic experiments in the study of propellant stratification. The tests covered a modified Grashof number range of 10^8 to 10^{14} and thereby simulated conditions in large cryogenic tanks over a wide range of gravity levels and heat flux conditions. The experiments demonstrated that the dimensionless temperature profiles in the stratified layers were time-invariant over the complete range of Grashof numbers tested. The shape of the dimensionless temperature profile determines a parameter defined as the energy integral which is an empirical term in the analysis. The energy integral was determined over a wide range of modified Grashof numbers covering six orders of magnitude (10^8 to 10^{14}) and was found to be independent of the Prandtl Number.

Author

A correlation has also been developed which extends the stratification predictions to times after the stratified layer reaches the tank bottom.

ACKNOWLEDGMENT

This study was supported under Contract NAS 8-11525 by the National Aeronautics and Space Administration George C. Marshall Space Flight Center. The contract was under the technical supervision of Gordon K. Platt and Frank E. Swalley, Fluid Mechanics and Thermodynamics Branch, Propulsion Division, Propulsion and Vehicle Engineering Laboratory. The Independent Research Program of Lockheed Missiles & Space Company also provided some support.

NOMENCLATURE

c_p	specific heat, $Btu/lb_m\ ^\circ F$
Gr^*_H	$g \beta\ qH^4/k\ \nu^2$, modified Grashof number based on H
Gr^*_x	$g \beta\ qx^4/k\ \nu^2$, modified Grashof number based on x
Gr_x	$g \beta\ (T_b - T_w)\ x^3/\nu^2$, Grashof number based on x
g	local acceleration, ft/sec^2
g_o	standard acceleration, ft/sec^2
H	height of liquid surface, ft
h	$q/(T_b - T_w)$, heat transfer coefficient, $Btu/ft^2 - sec - ^\circ F$
I	$\int_0^1 \theta\, d\eta$, energy integral
k	thermal conductivity, Btu/ft - sec - °F
Nu_x	hx/k , Nusselt number
Pr	$\mu c_p/k$, Prandtl number
q	wall heat flux, Btu/ft^2 - sec
R	tank radius, ft
Ra	Gr_x Pr , Rayleigh number
Ra*	Gr^*_x Pr , modified Rayleigh number
T	temperature, °F, °R
t	time, sec
u	x-component of the boundary layer velocity, ft/sec
v	fluid velocity, ft/sec
x	coordinate parallel to tank wall, measured from tank bottom, ft
y	coordinate perpendicular to tank wall, measured from tank wall, ft

NOMENCLATURE (Cont'd.)

z	coordinate parallel to tank wall, measured from liquid surface, ft
β	coefficient of volumetric expansion, $1/°R$
Δ	stratified layer thickness, ft
δ	boundary layer thickness, ft
η	z/Δ , dimensionless distance from liquid surface
θ	$(T - T_b)/(T_s - T_b)$, dimensionless temperature rise
μ	dynamic viscosity, $lb_m/ft\text{-}sec$
ν	kinematic viscosity, ft^2/sec
ρ	density, lb_m/ft^3
ϕ_H	$\nu t/H^2$, dimensionless time
ϕ_{H_o}	$\nu t_o/H_2$, dimensionless time at which $\Delta/T = 1$

SUBSCRIPTS

b	liquid bulk
0	time when $\Delta/H = 1$
s	liquid surface
w	heated wall

INTRODUCTION

Stratification is defined as the development of temperature gradients in a contained fluid as a result of external heating. Stratification is assumed to occur because a free-convection boundary layer carries the heated fluid at the wall to the top of the tank, forming a growing layer of stratified liquid which is at a higher temperature than the bulk.

This phenomenon is of particular importance in cryogenic propellant tanks, and it may have a significant effect on vehicle design and operation. In particular, the design of venting devices, pressurization systems, insulation systems, propellant feed pumps, and tank structures may be substantially influenced by propellant stratification. In order to ensure reliable designs, and to avoid excessive penalties due to conservatism in prediction methods, a sound analytical model and experimental data applicable to the conditions of interest are required.

In the present study, stratification of a subcooled fluid in a cylindrical tank subjected to a uniform sidewall heat flux is considered. Since the wall boundary layer is assumed to be the primary mechanism for propellant stratification, a review of the flow regimes for free-convection boundary layers will be given, and results will be presented to indicate the range of boundary layer parameters characteristic of cryogenic propellants in standard and reduced gravity fields. An analysis will then be outlined which utilizes an integral technique to obtain a solution for the development of the stratified layer and

for the associated liquid temperature rise. Finally, the results of stratification experiments conducted in noncryogenic fluids will be presented and compared to the analytical model developed.

FLOW REGIMES FOR FREE-CONVECTION BOUNDARY LAYERS

ONSET OF CONVECTIVE MOTION

The problem of the onset of convective motion for horizontal layers of fluid has been studied extensively by Rayleigh[1] and others [2,3,4]. These studies indicated that the significant dimensionless parameter is the Rayleigh number given by

$$Ra = Gr_x Pr = \left[\frac{g\beta(T_b - T_w)x^3}{\nu^2}\right]\left(\frac{\mu c_p}{k}\right) \qquad (1)$$

and that convective motion is established for values of the Rayleigh number greater than 1100 to 1700. The x appearing in the Rayleigh number is here the layer thickness.

For situations in which the fluid is bounded by vertical surfaces, there has been no detailed analytic or experimental work to determine the onset of convective motion. Grober, et al.[5], suggest that a critical value of the Rayleigh number of 1700 may be assumed to mark the beginning of convective motion in a fluid bounded by vertical surfaces. In this case, the x appearing in the Rayleigh number is again the layer thickness.

For a vertical flat plate, it is possible to use the data obtained by Schmidt and Beckmann[6] to compute an approximate value of Rayleigh number when a laminar boundary-layer structure can be discerned. The Rayleigh number is between 430 and 16,000. The x appearing in the Rayleigh number is the distance from the leading edge of the plate.

BOUNDARY LAYER TRANSITION

A laminar free-convection boundary layer is established on vertical surfaces at a relatively low Rayleigh number. This laminar boundary layer persists as the Rayleigh number increases, until at some critical value the flow becomes unstable and the boundary layer becomes turbulent. As with forced convection, transition from laminar to turbulent flows does not occur at a discrete condition but probably takes place over a range of Rayleigh numbers. The literature on free convection[5,7,8] suggests Rayleigh numbers at transition for free-convection boundary layers with a uniform wall temperature ranging from 0.7×10^9 to as high as 2×10^9. A transition Rayleigh number of 10^9 is most often quoted.

The Rayleigh number as given above incorporates the conventional Grashof number that is defined on the basis of the temperature difference between the wall and the bulk fluid. In most applications of interest, the heat flux to the propellant is the known quantity rather than the temperature difference. When the heat flux is known, the analyses of Refs. 9, 10, and 11 indicate that the modified Grashof number Gr^* is the proper dimensionless parameter. The modified Grashof number is given by

$$Gr_x^* = \frac{g\beta q x^4}{k \nu^2} \tag{2}$$

The two Grashof numbers are related in the following manner:

$$Gr_x^* = Gr_x Nu_x \tag{3}$$

Sparrow and Gregg[9] have pointed out that the modified Grashof number plays the same role for the case of a uniform wall heat flux as the conventional Grashof number does for the case of a uniform wall temperature.

For laminar free-convection boundary layers on vertical surfaces, the local Nusselt number as obtained from Saunders[12] is

$$Nu_x = 0.43(Gr_x P_r)^{1/4} \tag{4}$$

Combining Eqs. (3) and (4) and using a transition Rayleigh number of 10^9, a modified Rayleigh number at transition of 10^{11} is obtained.

The fact that transition occurs at $Ra \approx 10^9$ and $Ra^* \approx 10^{11}$ is in part confirmed by the data of Dotson[13]. Dotson's data for air follow the laminar prediction by Sparrow and Gregg[9] at values of Ra^* up to 0.7×10^{11}. In addition, the discussion of Sparrow and Gregg's paper by D. P. Timo[9] confirms the transition value of 10^{11}.

MODIFIED RAYLEIGH NUMBERS FOR CRYOGENIC PROPELLANTS

The magnitude of the modified Rayleigh number was evaluated for liquid hydrogen and oxygen for a wide range of accelerations, for characteristic lenghts of 1 and 10 ft, and for heat fluxes of 1, 10, and 100 Btu/ft^2-hr. The results of the calculations are shown in Fig. 1.

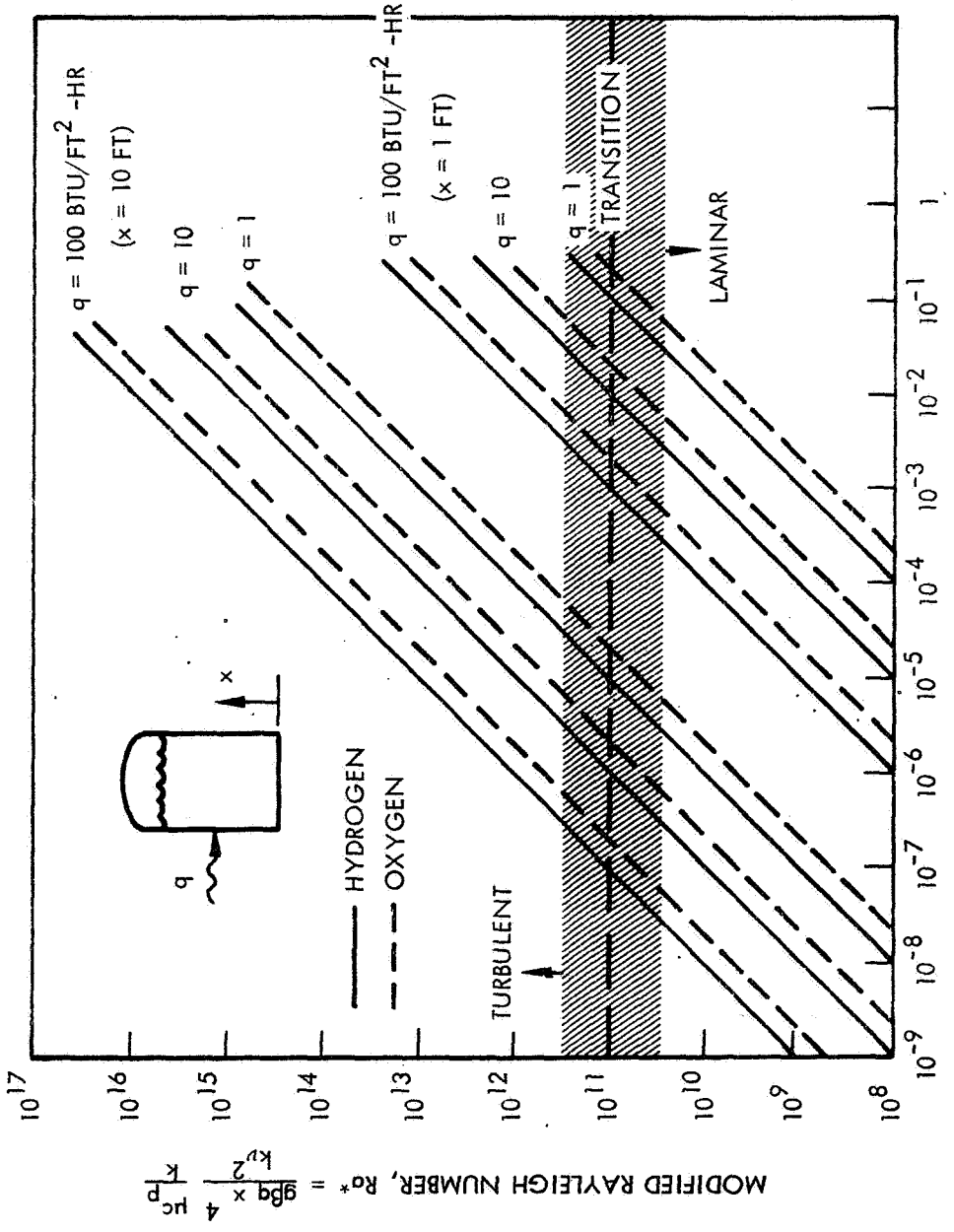


Fig. 1 Variation of Modified Rayleigh Number With Gravity Field for Liquid Hydrogen and Oxygen

Since the values of Ra^* for liquid hydrogen and oxygen are comparable, the discussion applies to both liquids. For boost-phase conditions, g/g_o is of the order of one and the modified Rayleigh number ranges from 10^{13} to 10^{18} for the conditions examined; therefore, the wall boundary layers will be entirely turbulent. Under reduced gravity conditions, the modified Rayleigh number is decreased but is still sufficiently large for free-convection boundary layers to persist; the boundary layer may be laminar, rather than turbulent, particularly at the bottom of the tank. For example, at an acceleration of 10^{-6} g/g_o, the bottom foot or two of the tank will be well into the laminar boundary layer regime, while at the top of the tank Ra^* is large enough to ensure turbulent flow.

In order to develop a model for predicting stratification under a wide range of accelerations, it is necessary then to consider a range of modified Rayleigh numbers extending into both laminar and turbulent flow regimes for the free-convection wall boundary layers.

INTEGRAL ANALYSIS

The model used for the analysis of stratification is shown in Fig. 2. A cylindrical tank is assumed to accelerate along its longitudinal axis, with a uniform and time-independent sidewall heat flux to the liquid. For a subcooled liquid, the energy transfer at the free surface is negligible. In the stratified layer, the temperatures are independent of radial and azimuthal location. Below the stratified layer and outside the boundary layer, the temperature is constant and equal to the initial bulk temperature of the liquid. The tank radius is considered to be large compared with the boundary layer thickness. The most significant assumption made in the analysis is that the stratified layer is characterized by a dimensionless temperature profile which is invariant with time The analysis is

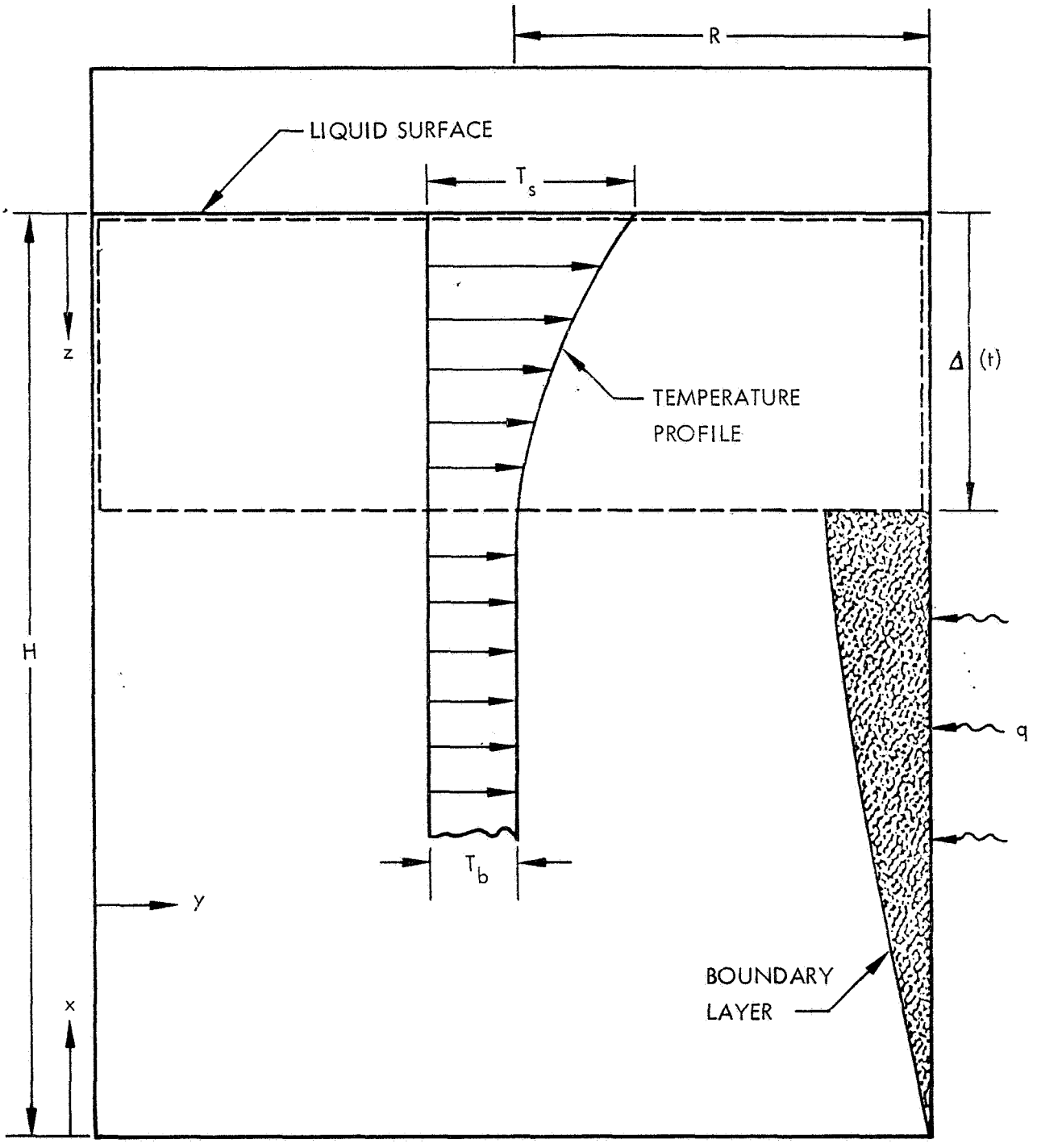


Fig. 2 Geometry Used for Stratification Analysis

restricted to times when the thickness of the stratified layer is less than the height of the liquid.

With these assumptions as energy balance yields

$$2\pi RH \int_0^t q\, dt = \pi R^2 \rho c_p \int_0^{\Delta(t)} (T - T_b)\, dz \tag{5}$$

An energy integral which represents the average temperature rise in the stratified layer, normalized with respect to the surface temperature rise, is now introduced:

$$I = \int_0^1 \theta\, d\eta \tag{6}$$

where θ is a dimensionless temperature rise and η is a dimensionless distance from the liquid surface given by

$$\theta = \frac{T - T_b}{T_s - T_b}, \quad \eta = \frac{z}{\Delta(t)} \tag{7}$$

Since it is assumed that the energy integral is invariant with time and the sidewall heat flux is constant, an expression in dimensionless form for the surface temperature rise is obtained from Eqs. (5) and (6),

$$\frac{T_s - T_b}{q\, H/k} = \frac{2(H/R)\, \phi_H}{I\, Pr\, \Delta(t)/H} \tag{8}$$

where $\phi_H = \nu t/H^2$ is a dimensionless time. The assumption that the energy integral is time invariant must be justified experimentally and the value of the energy integral must be empirically determined.

Since the surface temperature rise depends on the fraction of the liquid stratified, $\Delta(t)/H$, the next step in the integral analysis is to obtain an expression for the stratified layer growth from a mass balance. For a liquid of constant density the continuity equation may be written as

$$\int_{A(t)} \vec{v} \cdot \vec{n}\, dA = 0 \tag{9}$$

where $\vec{v}$ is the fluid velocity measured with respect to a fixed reference frame, and $\vec{n}$ is the outward normal to the control volume enclosed by $A(t)$. $A(t)$ represents the area which encloses the stratified layer as shown in Fig. 2 by a dashed line. When expanded, Eq. (9) becomes

$$2\pi R \left[\int_0^{\hat{\delta}} u\, dy\right]_{x = H - \Delta(t)} - (\pi R^2 - 2\pi R \hat{\delta})_{x = H - \Delta(t)} \frac{d\Delta(t)}{dt} = 0 \tag{10}$$

where u is the x-component of the boundary layer velocity.

If, as before, it is assumed that $\hat{\delta}$ is much less than R,

$$\frac{2}{R}\left[\int_0^{\hat{\delta}} u\, dy\right]_{x = H - \Delta(t)} = \frac{d\Delta(t)}{dt} \tag{11}$$

The problem of evaluating $\Delta(t)$ is then reduced to that of obtaining an expression for the volumetric flow in the boundary layer. Solutions to the boundary layer equations for both laminar and turbulent free-convection were used to obtain expressions for the volumetric flow for the case of a uniform wall heat flux.

For laminar flow, Sparrow and Gregg[9] have obtained an exact similarity solution to the boundary layer equations. The following equation expresses the volumetric flow in a boundary layer of unit width:

$$\int_0^\infty u\,dy = 3.62\,\nu(Gr_x^*)^{1/5}\,F(\infty) \tag{12}$$

The value of $F(\infty)$ may be obtained as a function of Prandtl number from Sparrow and Gregg's numerical solution. For Prandtl numbers between 1 and 30, the following approximation of their results is used:

$$F(\infty) = \frac{0.436}{(Pr)^{0.388}} \tag{13}$$

From Eqs. (11), (12), and (13), an expression for the growth of the stratified layer is obtained corresponding to the exact laminar boundary layer solution:

$$\frac{\Delta(t)}{H} = 1 - \left[1 - 0.630\left(\frac{H}{R}\right)\phi_H\frac{(Gr_H^*)^{1/5}}{(Pr)^{0.388}}\right]^5 \tag{14}$$

A solution for a turbulent free convection boundary layer with a uniform wall heat flux was obtained by Morse[10] using the velocity and temperature profiles employed by Eckert and Jackson[14] in their solution for a uniform wall temperature. Morse's solution is not strictly applicable for Prandtl numbers different from one. A modification of his solution has been made to extend it to higher Prandtl numbers[15]. The modified analysis, which employes the extended Reynolds analogy used by Eckert and Jackson[14], yields

$$\int_0^\infty u\,dy = 0.326\,\frac{\nu}{Pr^{2/3}}\left(\frac{Gr_x^*}{1 + 0.443\,Pr^{2/3}}\right)^{2/7} \tag{15}$$

Then, the expression for the stratified layer growth becomes

$$\frac{\Delta(t)}{H} = 1 - \left[1 + 0.0924\left(\frac{H}{R}\right)\frac{\phi_H}{Pr^{2/3}}\left(\frac{Gr_H^*}{1 + 0.443\,Pr^{2/3}}\right)^{2/7}\right]^{-7} \tag{16}$$

The liquid surface temperature rise may now be computed using Eq. (8) and the appropriate expression for the stratified layer growth, Eq. (14) or (16).

It should be noted that the turbulent prediction requires infinite time for the stratified layer to reach the tank bottom, while the laminar expression predicts this occurrence in finite time, as one would expect. The turbulent prediction, however, becomes less valid as the stratified layer approaches the tank bottom, since as $\Delta/H \rightarrow 1$, the boundary layer becomes laminar.

EXPERIMENTAL STUDIES

A series of stratification experiments were conducted with several fluids in cylindrical containers to obtain basic data and evaluate the analytical prediction method. Although interest in the problem of stratification arises mainly in connection with cryogenic propellant tanks, the phenomenon of stratification is not unique to cryogenic liquids and its study can profitably be pursued with other liquids once theoretical considerations are available to establish the simulation laws.

The use of noncryogenic liquids for stratification experiments greatly reduces test costs, makes possible greater flexibility in control of test conditions, and considerably simplifies instrumentation. It also makes possible the achievement of laminar free-convection boundary layers, thus simulating stratification under reduced gravity conditions.

OBJECTIVES AND PLAN OF EXPERIMENTS

A primary objective of the present experiments was to determine the validity of the assumption of time-invariant dimensionless temperature profiles in the stratified layer, and to establish the magnitude and functional dependence of the energy integral on the modified Grashof and Prandtl numbers.

In order to obtain stratification data corresponding to low gravity conditions in cryogenic tanks, tests were conducted with modified Grashof numbers in the range from 10^8 to 10^{10}. Since the modified Grashof number is proportional to the tank height to the fourth power, these relatively small Grashof numbers were most easily obtained by using a small tank. For this purpose, a tank was constructed from a block of wood with a 3-inch diameter hole in the center. A strip of 0.001-inch thick stainless steel shim stock was fastened to the inside wall of the tank and was used as a resistance heater to supply a uniform heat flux to the stratifying liquid.

An intermediate range of modified Grashof numbers, from 2.3×10^{10} to 1.5×10^{14}, as well as a Prandtl number range from 4.5 to 32, were covered using six different fluids in a 9.75-inch diameter tank. This tank was made from a thin-walled (0.025 in.) cylinder and was placed in a radiant heating facility and uniformly heated with a concentric array of tungsten filament quartz lamps.

A third facility used to obtain stratification data was a 10.75-inch inside diameter pressure tank which utilized a resistance heater like that in the 3-inch diameter tank. In this tank, data have been obtained for modified Grashof numbers ranging in excess of 10^{14} by actively pressurizing the liquid, thereby subcooling it. Large heat fluxes, with correspondingly high wall temperatures, were then imposed without the occurrence of nucleate boiling. Another objective was to conduct tests with a fluid which has a Prandtl number close to one (that of liquid hydrogen). This was accomplished by subcooling water at temperatures ranging to 370° F in the pressure tank. Also, in the pressure tank it was possible to run stratification tests which were immediately preceded by a period wherein the fluid was simultaneously heated and vented near its saturation state. This initial venting procedure allowed the boundary layer and bulk flow fields to develop prior to active pressurization and the initiation of stratification. Data obtained from these tests were used to evaluate the effect of transient flow field development upon the results obtained from the 3-inch and 9.75-inch diameter tanks.

The three test tanks described above had flat insulated bottoms. Thermocouples, mounted on nonconducting probes, were used to measure fluid temperatures along the cylindrical axis of each tank. The 9.75-inch diameter tank was also instrumented with wall thermocouples in order to determine whether or not boiling occurred and to check the method used for calculating the wall temperature. More details on the facilities are given in Ref. 16.

All tests were conducted with aspect ratios (H/R) of 2.3.

EXPERIMENTAL RESULTS

All fluid properties used in the graphical presentation of results were evaluated using the mean mixed temperature of the fluid in the stratified layer. To be consistent with the model used for analysis, time was measured from the instant the surface thermocouple first sensed a temperature rise. Heat fluxes were determined by graphically integrating the temperature profiles. Figure 3 shows some temperature profiles which are typical of the data obtained in all three tanks. In parts (a) and (b) of the figure, two sets of profiles obtained in the pressure tank with water are shown. These two runs indicate the significant change in temperature profile shape apparently caused by a change in the modified Grashof and Prandtl numbers. Two sets of temperature profiles obtained with trichloroethylene in the 3-inch and 9.75-inch tanks are given in parts (c) and (d) of the figure. A significant dependence of profile shape on Grashof number alone is evident. The Prandtl number was the same in both tests. These general relationships appear to be independent of the fluid or tank used.

Before a comparison of the data with one of the predictions can be made, a suitable boundary layer transition criterion must be indicated. The previous discussion of boundary layer transition established a value of 10^{11} as characteristic for the modified Rayleigh number at transition. When transition occurs halfway up the tank wall, at $x = H/2$, then $Gr_H^* Pr = 1.6 \times 10^{12}$. Data for which $Gr_H^* Pr$ is greater than 1.6×10^{12} have been compared with predictions for turbulent boundary layers, and data for which $Gr_H^* Pr$ is less than 1.6×10^{12} have been compared with laminar boundary layer predictions.

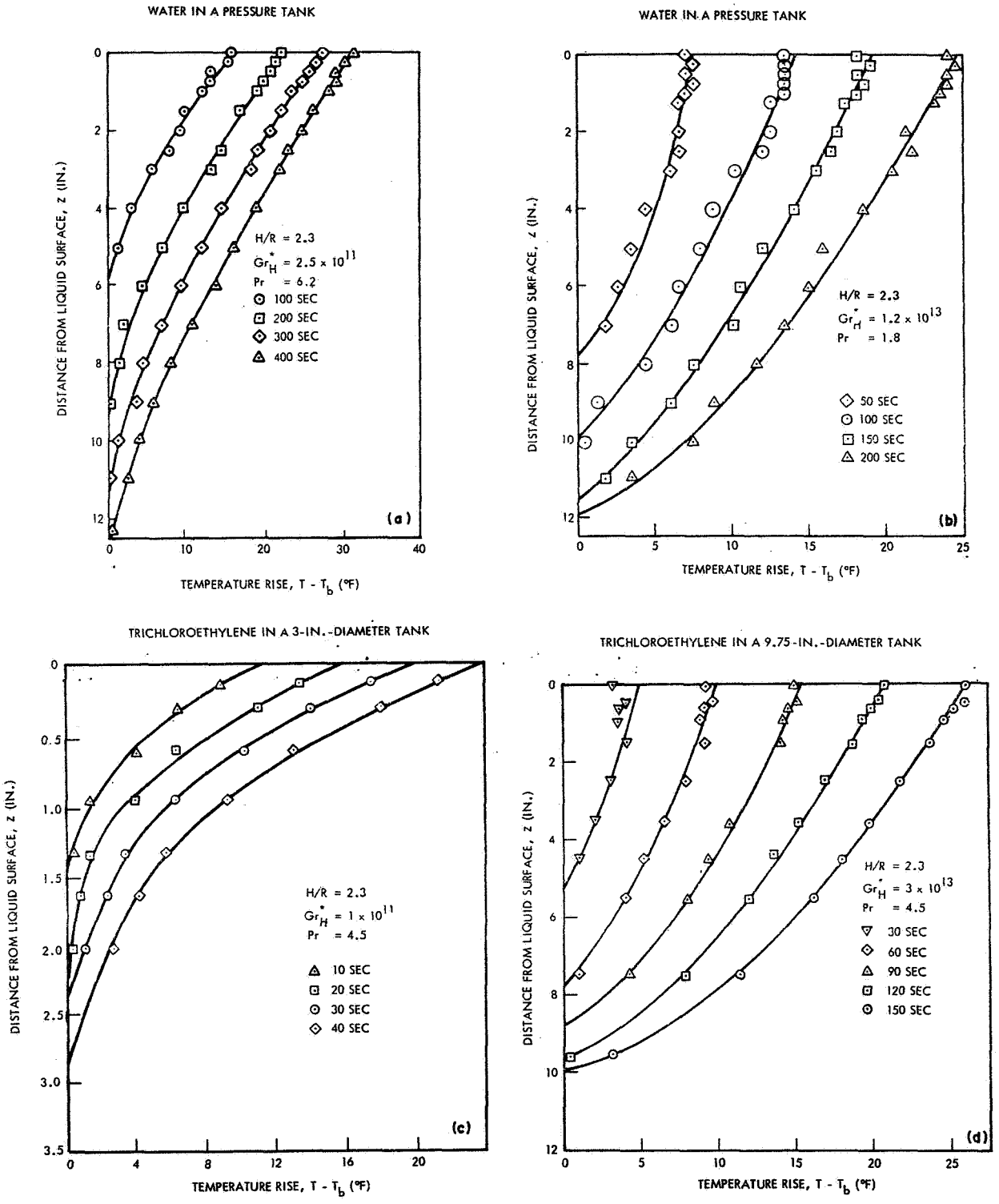


Fig. 3 Stratification Temperature Profiles

It was necessary to calculate wall temperatures for the 3-inch diameter tank and the pressure vessel in order to determine whether or not boiling occurred. The boundary layer analyses of Refs. 9 and 10 were used to calculate the temperature difference across the boundary layer at vertical locations corresponding to the axial thermocouples. The wall temperature profile was then determined by adding the boundary layer temperature difference to the corresponding measured bulk temperature. The accuracy of this method was confirmed by wall temperature measurements obtained in the 9.75-inch diameter tank. All the results presented in this paper correspond to times before any point on the tank wall reached the liquid saturation temperature.

The stratified layer depth, $\Delta(t)$, as a function of time can be obtained from the temperature profile plots by noting the intersection of the curves with the z-axis. In Fig. 4 the dimensionless form of the stratified layer depth, $\Delta(t)/H$, is compared with the prediction based on the exact laminar boundary layer solution (Eq. 14). In some of the 3-inch tank tests the bottom of the tank was at a higher temperature than the initial liquid temperature because of heat stored in the tank bottom from a previous test. As a result, some of the profiles obtained from tests in the 3-inch tank were greatly distorted by heat conducted from the tank bottom into the bulk fluid. This distortion made a determination of the experimental value for $\Delta(t)/H$ almost impossible. Although all of the data obtained in the laminar region are shown in Ref. 16, only data which were considered to be well defined are shown in Fig. 4. In order to extend the Prandtl number range of stratification data, tests were run using a calcium chloride-water solution (Pr = 10) and a glycerol-water solution (Pr = 30). The measured stratified layer growth for these runs was much less than that predicted by the exact laminar boundary layer solution[16]. Furthermore, the divergence from the prediction appeared to become greater

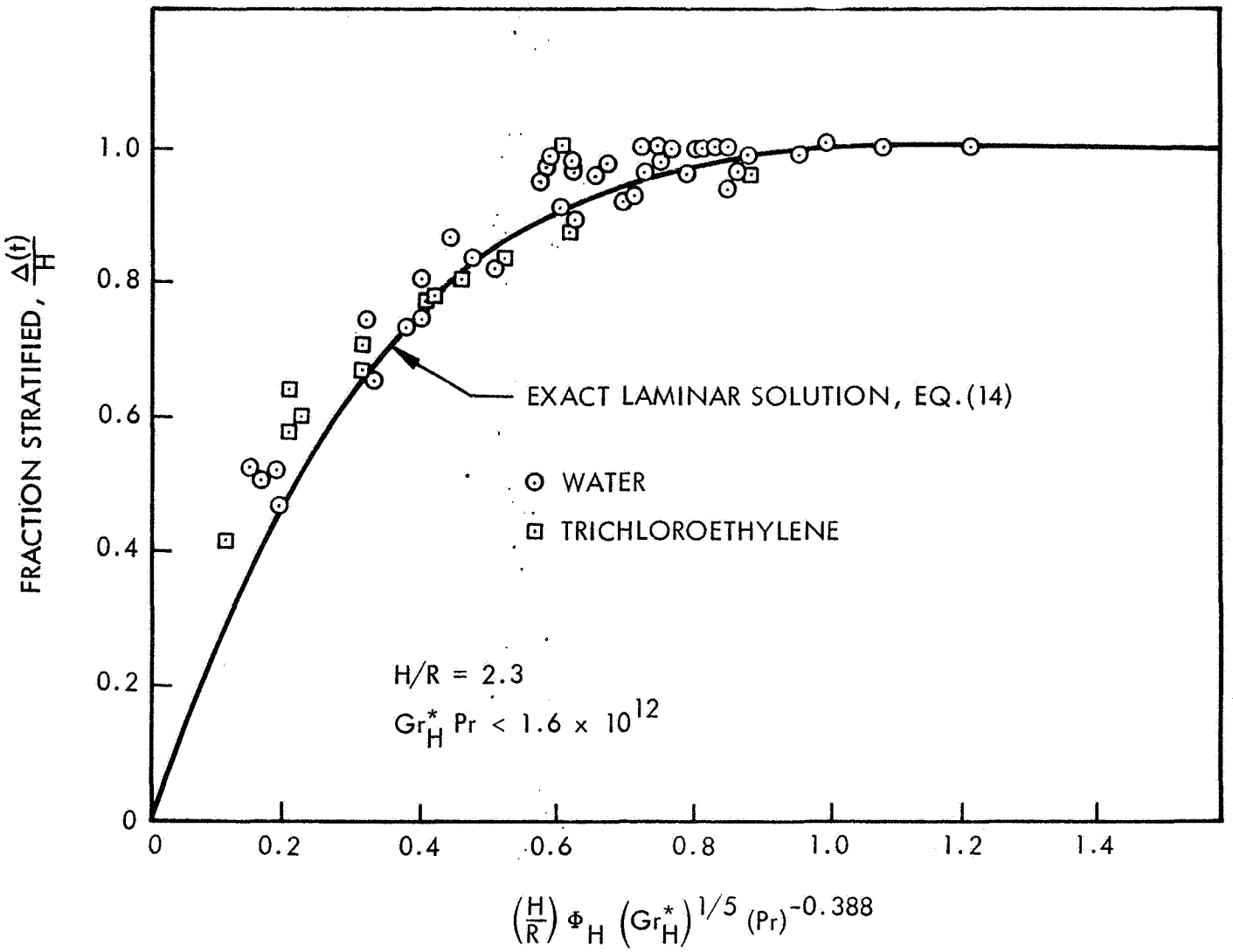


Fig. 4 Comparison of Observed and Predicted Stratified Layer Growth

as the Prandtl number was increased. Since the reason for this deviation is not entirely understood at this time, it must be concluded that the exact laminar stratified layer growth analysis is valid only for fluids with Prandtl numbers between 1 and 8.

In Fig. 5, experimental values for the stratified layer depth for which $Gr^*_H Pr$ is greater than 1.6×10^{12} are compared with the modified turbulent prediction (Eq. 16). The prediction curve bounds the lower side of the data. An attempt was made to correlate the data on the basis of a transitional analysis[17], since transition from laminar to turbulent flow in the boundary layer occurs in most of the tests. This attempt did not succeed in reducing the scatter exhibited by the data.

Figure 6 gives the dimensionless form of the stratification temperature profiles which were presented in Fig. 3. This figure shows that the temperature profiles are, in fact, similar (time-invariant in dimensionless form) as assumed in the analysis. In other words, it has been confirmed that the energy integral is a function only of Gr^*_H, Pr, and H/R. The value of the energy integral, which is indicative of the temperature profile shape or of the energy distribution within the stratified layer, was obtained for each run by graphical integration of the dimensionless profile. Examination of these data revealed no apparent dependence of I upon Prandtl number, leaving the modified Grashof number and aspect ratio as the correlation variables.

The energy integral is plotted as a function of modified Grashof number in Fig. 7. Data have been obtained for a range of modified Grashof numbers which covers more than six orders of magnitude, extending from 10^8 to over 10^{14}. The filled symbols in Fig. 7 represent runs in which the venting procedure, described previously, allowed the boundary layer and bulk flow fields to develop prior to the initiation of stratification.

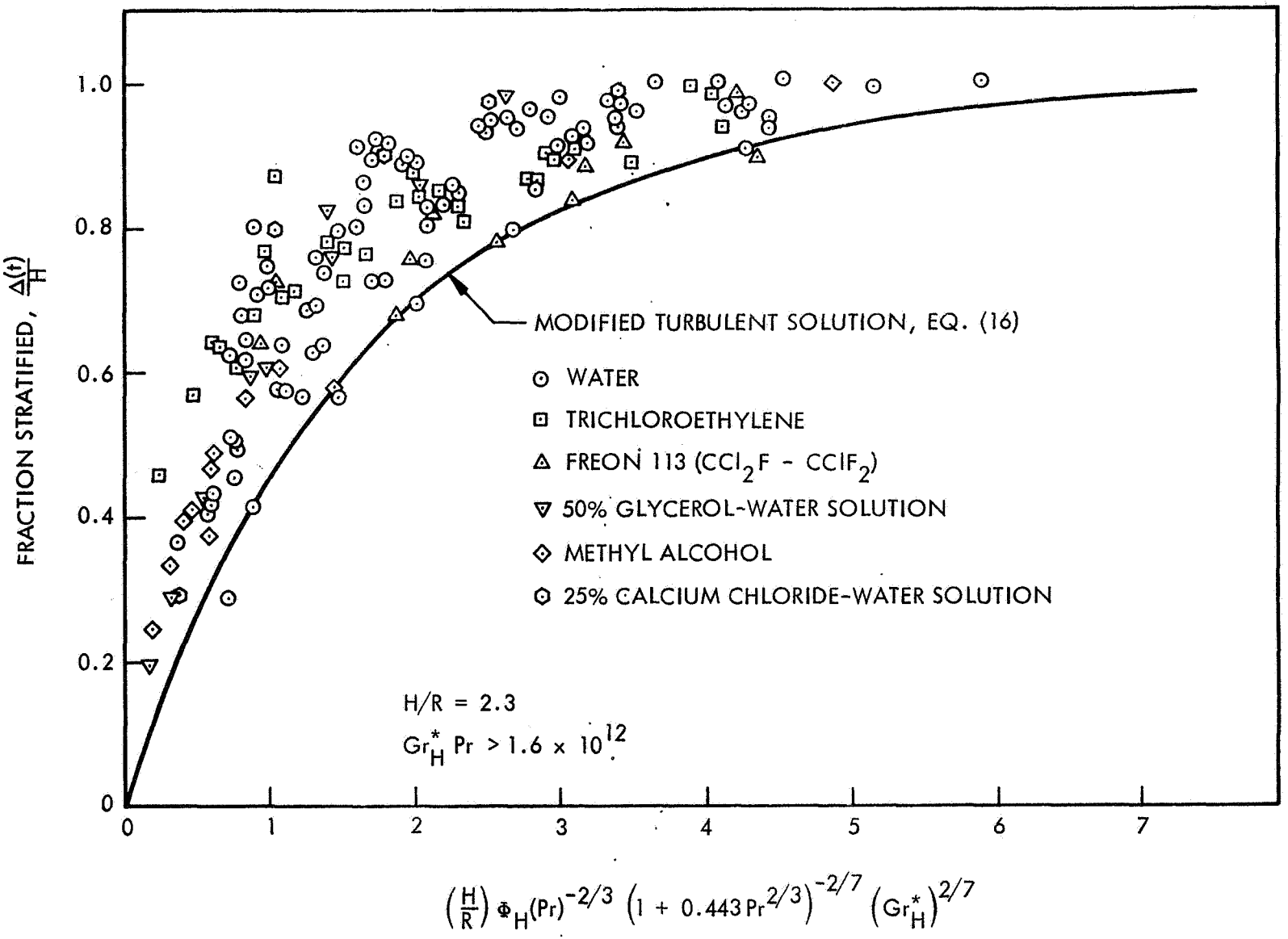


Fig. 5 Comparison of Observed and Predicted Stratified Layer Growth

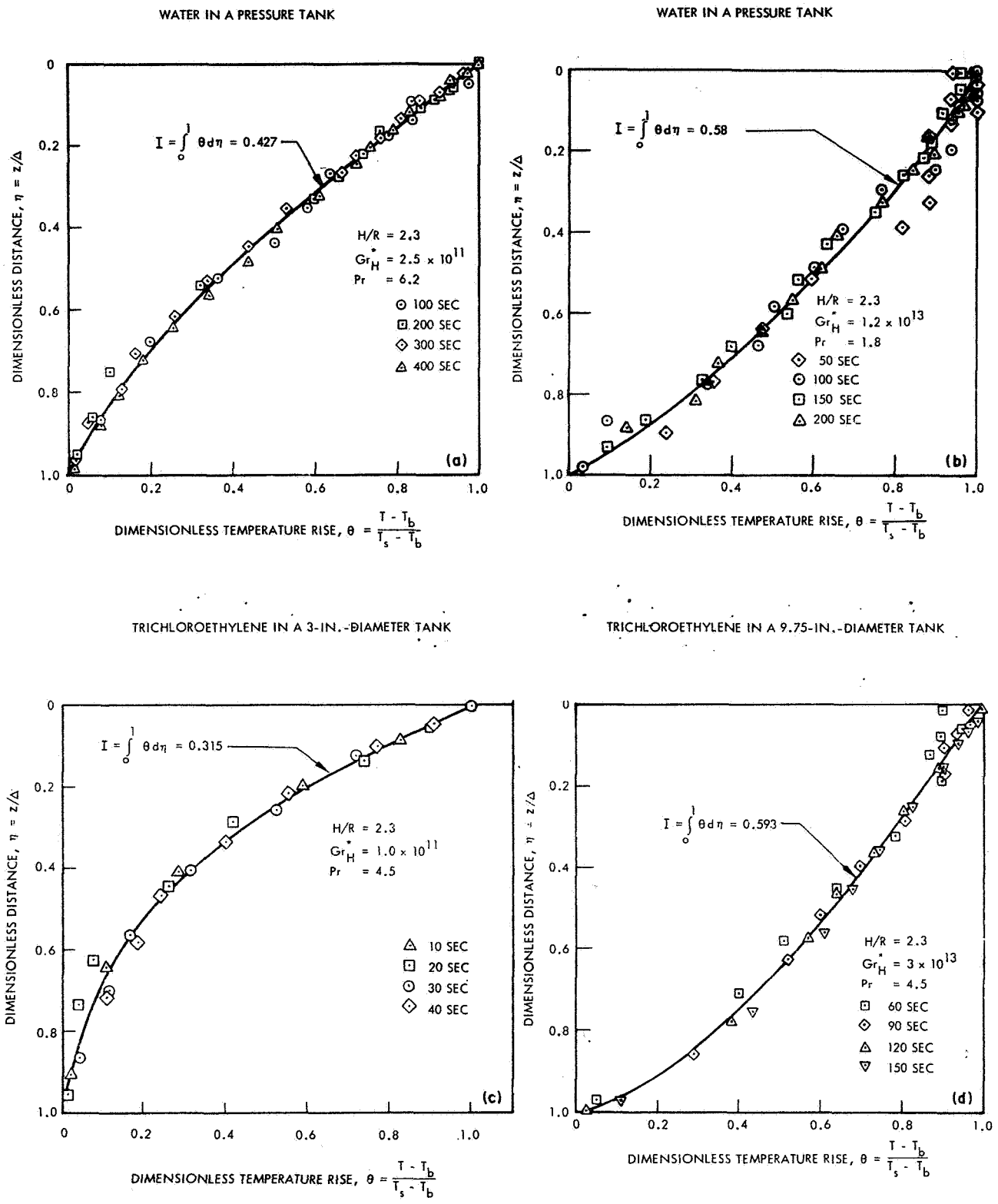


Fig. 6 Dimensionless Stratification Temperature Profiles

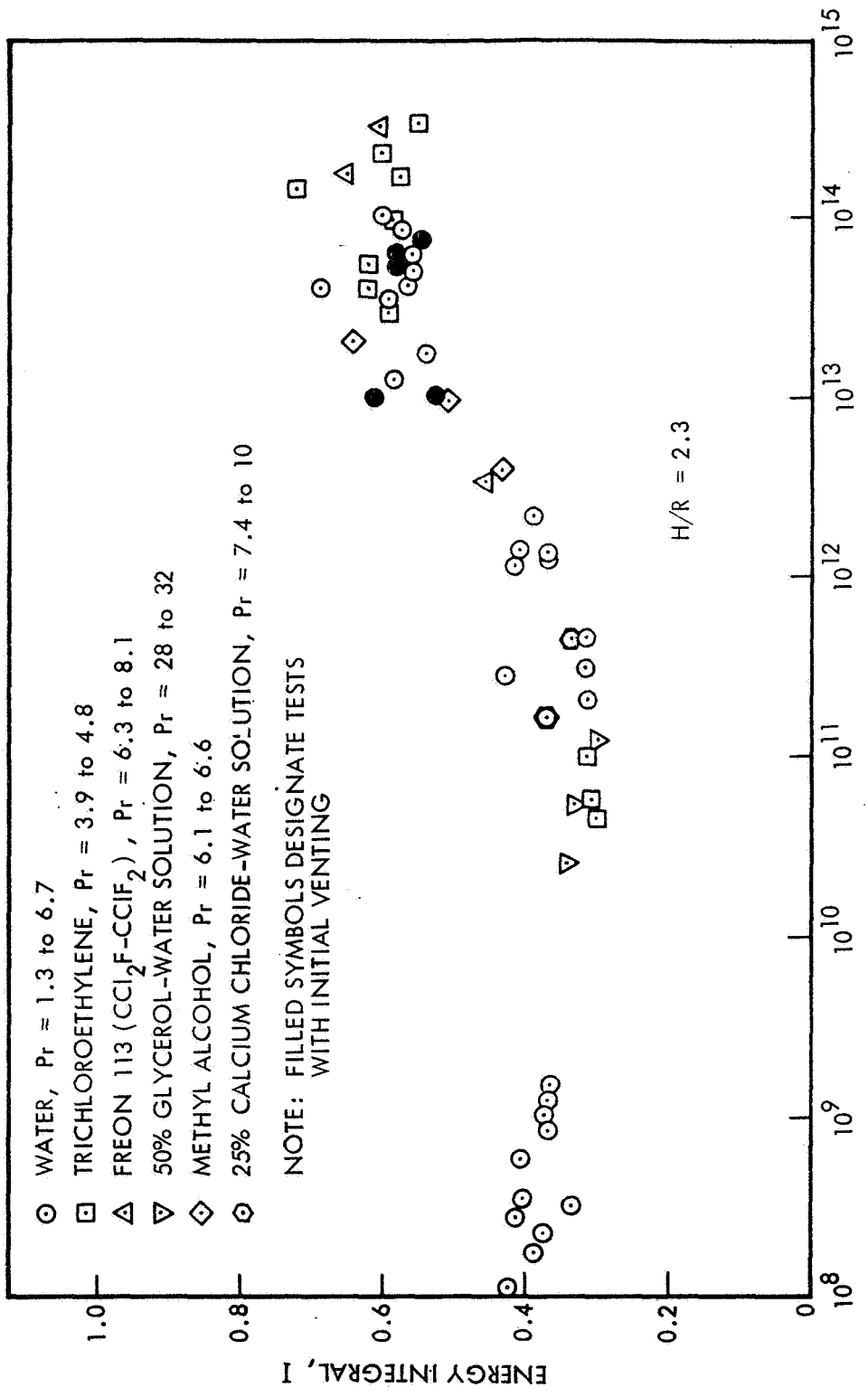


Fig. 7 Energy Integral Correlation

The data obtained from these runs indicated that the initial boundar layer and surface spreading transients did not have a significant effect upon the results obtained in the pressure tank. It has been assumed that this evaluation of transient effects is valid for results obtained from the 3-inch and 9.75-inch diameter tanks.

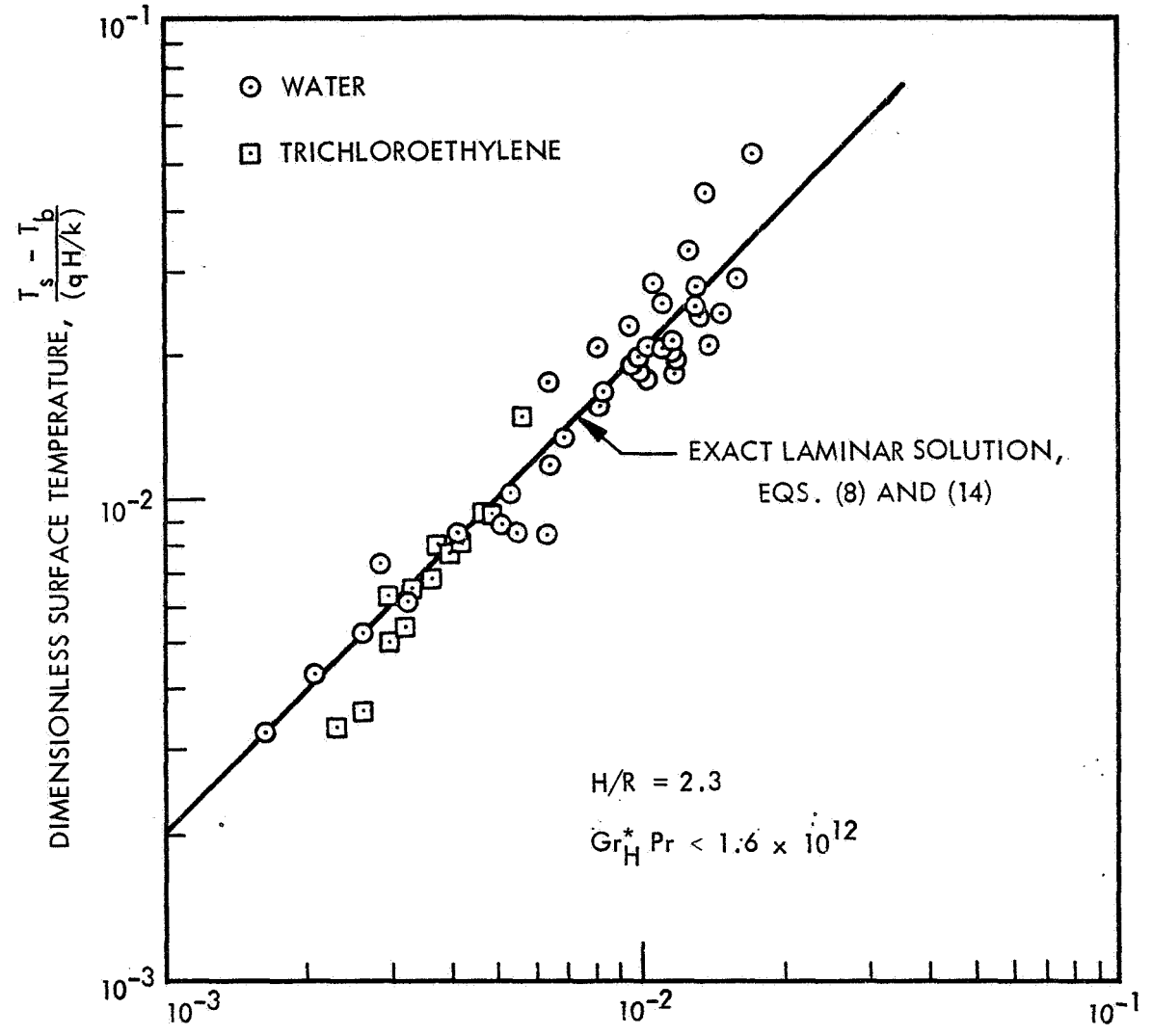
Experimental values for the liquid surface temperature rise are compared with the predictions in Figs. 8 and 9. Almost all of the deviation between data and prediction in these figures can be attributed to the difficulty encountered in accurately predicting the stratified layer growth.

CORRELATION OF STRATIFICATION DATA FOR TIMES AFTER STRATIFIED LAYER REACHES TANK BOTTOM

The integral analysis cannot be used to predict the results of stratification for times after the stratified layer has reached the tank bottom. Since this represents an important time of interest, an attempt to correlate the available data has been made. To obtain such a correlation, two assumptions, suggested by the data, were made.

It was assumed that the dimensionless form of the surface temperature rise, $(T_s - T_b)/(q\,H/k)$, is a linear function of the dimensionless time divided by the Prandtl number, ϕ_H/Pr. The second assumption suggested by the data was that the surface temperature rise can be approximated by the mean mixed temperature rise for very large values of ϕ_H/Pr. These assumptions result in the following expression for the surface temperature rise after the stratified layer reaches the tank bottom:

$$\frac{(T_s - T_b)}{(q\,H/k)} = 2\left(\frac{H}{R}\right)\frac{\phi_H}{Pr} + 2\left(\frac{H}{R}\right)\frac{\phi_{H_o}}{Pr}\frac{(1 - I)}{I} \qquad (17)$$



$$\frac{(H/R)\,\Phi_H}{IPr\left\{1 - \left[1 - 0.630\,(H/R)\,\Phi_H \dfrac{(Gr_H^*)^{1/5}}{(Pr)^{0.388}}\right]^5\right\}}$$

Fig. 8 Comparison of Observed and Predicted Liquid Surface Temperature Rise

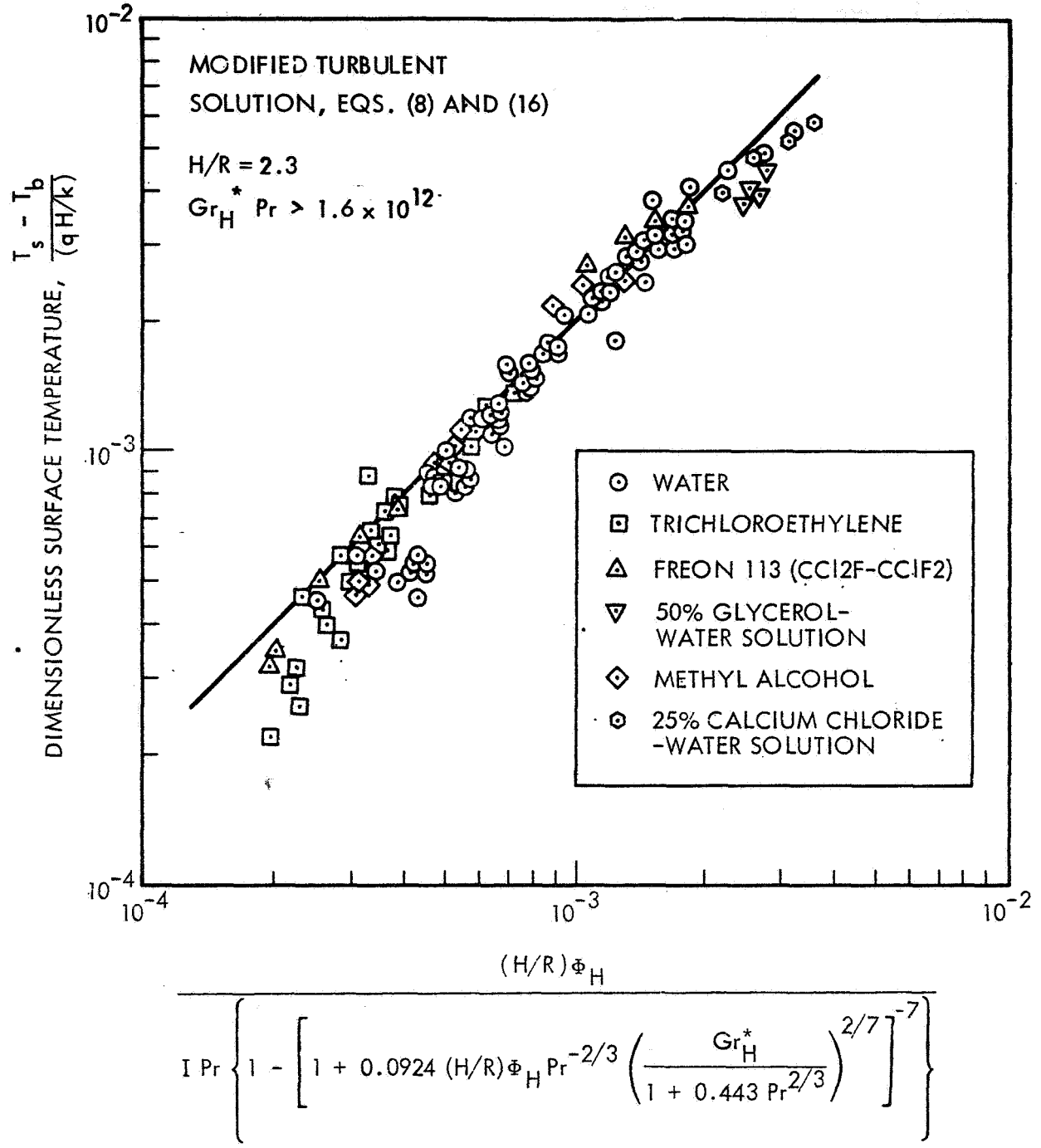


Fig. 9 Comparison of Observed and Predicted Liquid Surface Temperature Rise

where ϕ_{H_o} is the dimensionless time at which the stratified layer reaches the tank bottom. The value of ϕ_{H_o} may be obtained from available boundary layer analyses for both the laminar and turbulent flow regimes. From the exact laminar boundary layer solution,

$$\phi_{H_o}\Big|_{\text{Laminar}} = 1.59 \frac{(\text{Pr})^{0.388}}{(\text{H/R})(\text{Gr}_H^*)^{1/5}} \tag{18}$$

Since the stratified layer never reaches the tank bottom in the modified turbulent analysis, an arbitrary value for $\Delta(t)/H$ of 0.95 is taken for the evaluation of ϕ_{H_o}. Thus

$$\phi_{H_o}\Big|_{\text{Turbulent}} = \frac{5.75(\text{Pr})^{2/3}}{(\text{H/R})} \left(\frac{1 + 0.443\ \text{Pr}^{2/3}}{\text{Gr}_H^*} \right)^{2/7} \tag{19}$$

In the above expressions for ϕ_{H_o}, all fluid properties should be evaluated at the reference temperature corresponding to the time ϕ_{H_o}. The data available for times after $\Delta(t)/H = 1$ are presented in Figs. 10 and 11. Most of the deviation between the data and correlation can be traced to an inaccurate prediction of ϕ_{H_o}. As time becomes large, the terms containing ϕ_{H_o} become relatively small, and errors in these terms become less significant.

CONCLUSIONS

The closed-form solution, based on an integral analysis, for predicting stratification of subcooled fluids in cylindrical containers with uniform sidewall heating identified the basic dimensionless parameters as: the modified Grashof number, the Prandtl number, the tank aspect ratio, and a dimensionless time. It thus was extremely useful in planning the experiments.

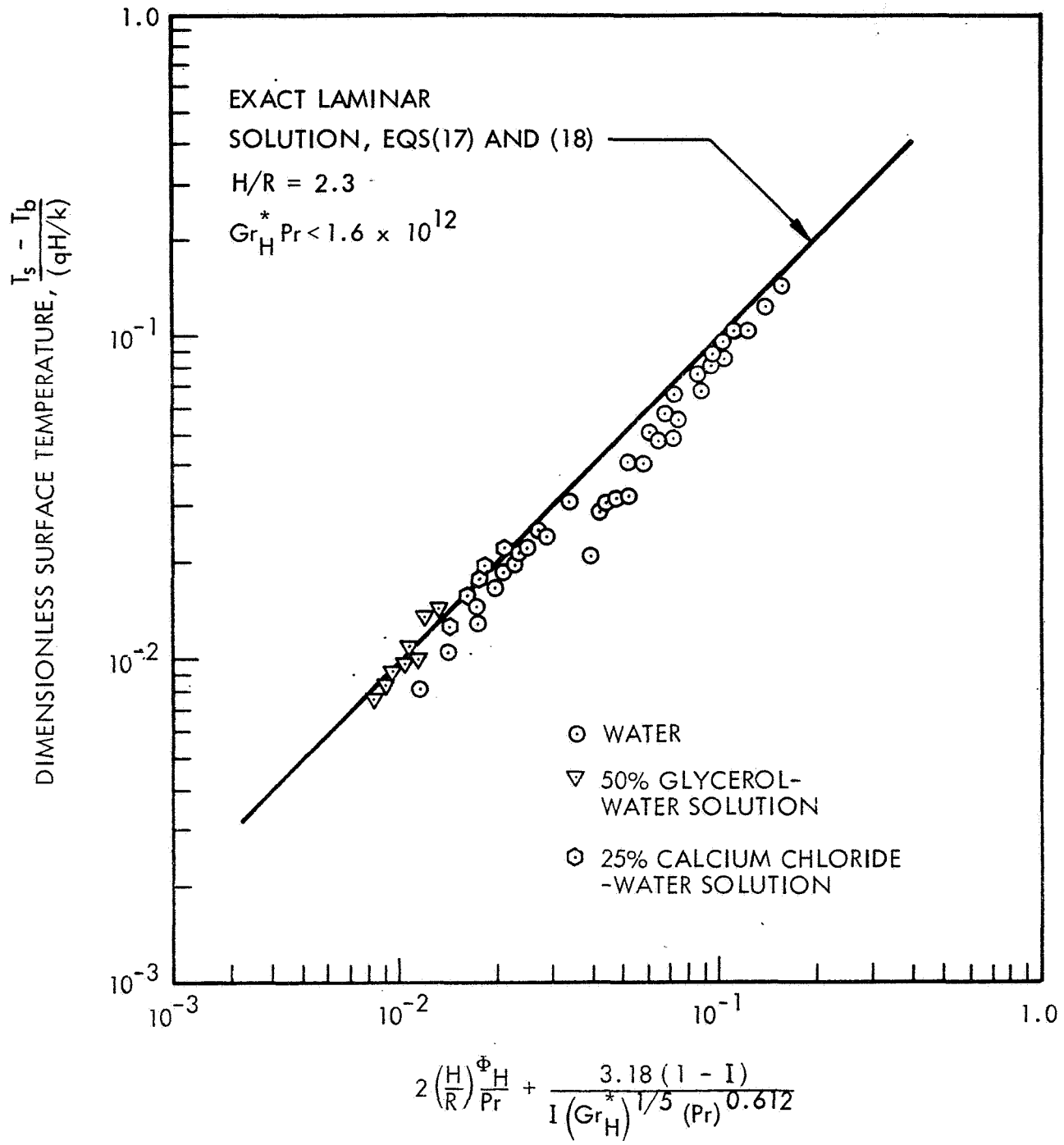


Fig. 10 Correlation of Liquid Surface Temperature Rise for Times After $\Delta/H = 1$

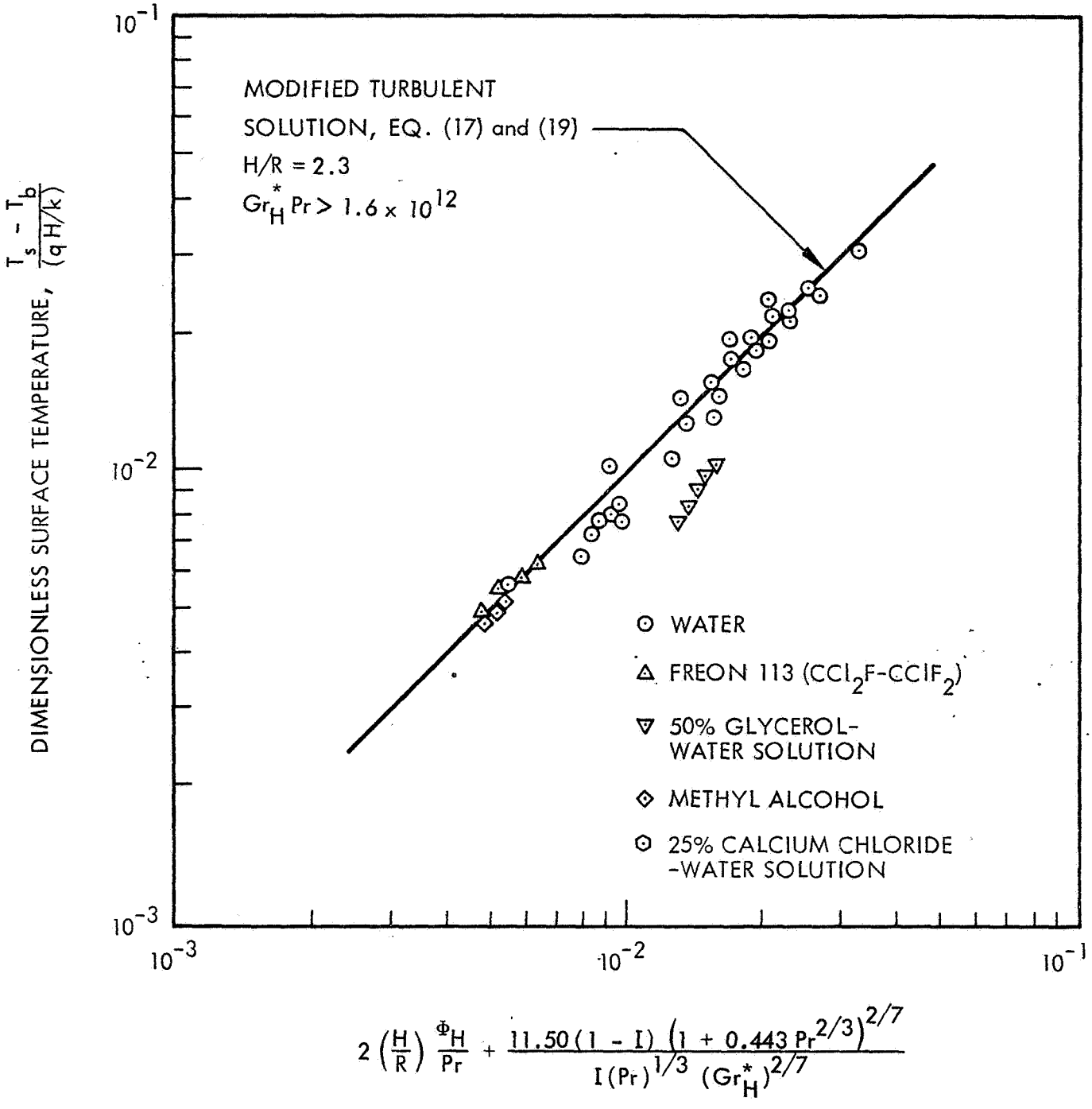


Fig. 11 Correlation of Liquid Surface Temperature Rise for Times After $\Delta/H = 1$

The experimental results verified a principal assumption made in the analysis that the nondimensional temperature profiles in the growing stratified layer are time-invariant. The nondimensional profile shape appears to be a weak function of Prandtl number and a strong function of Grashof number for a given tank aspect ratio. Correlation of this functional dependence allows explicit prediction of the liquid temperature rise. The correlation has been made over a range of modified Grashof numbers from 10^8 to 10^{14} for an aspect ratio $H/R = 2.3$.

The experimental results generally confirmed the stratification analysis in terms of the stratified layer growth and the liquid surface temperature rise.

The initial conditions that exist in a vented cryogenic tank were simulated by conducting stratification tests in a pressure vessel with initially saturated water at Prandtl numbers near one. The results indicate that boundary layer and surface spreading transients do not affect the shape of the temperature profiles.

For times after the stratified layer reaches the tank bottom, when the integral analysis is no longer valid, the experimental data has been successfully correlated by an empirical extension of the analysis.

The fact that theoretical and experimental results are given in terms of dimensionless parameters permits application to a wide variety of conditions. It is significant to note the difference between stratification of subcooled fluids under standard-gravity and reduced-gravity conditions. It was pointed out that, for cryogenic propellants, the tank wall free-convection boundary layer will persist under reduced gravity conditions but that it may be laminar rather than turbulent. For the same heat flux to the propellant, the surface temperature rise will be faster under reduced gravity conditions than

under standard gravity conditions. The reason is that the mass flux in the wall boundary layer is reduced with a reduction in acceleration; hence, the incoming energy is contained in a thinner, and therefore hotter, stratified layer. This result indicates that stratification data obtained at standard gravity do not in general apply to reduced gravity conditions unless attention has been devoted to proper scaling of the test.

The present study of subcooled stratification in a cylindrical tank with sidewall heating is being continued to determine the effect of tank aspect ratio and to consider combined sidewall and bottom heating.

REFERENCES

1. Lord Rayleigh, "On Convection Currents for a Horizontal Layer of Fluid When the Higher Temperature is on the Under Side," Philos. Mag., Vol. 32, 1916, pp. 529-545
2. H. Jeffreys, "Some Cases of Instability in Fluid Motion," Proc. Roy. Soc. (London), Series A., Vol. 118, 1928, p. 195
3. A. R. Low, "On the Criterion for Stability of a Layer of Viscous Fluid Heated From Below," Proc. Roy. Soc. (London), Series A., Vol. 125, 1929, p. 180
4. R. J. Schmidt and O. A. Saunders, "On the Motion of a Fluid Heated from Below," Proc. Roy. Soc. (London), Series A, Vol. 165, 1938, p. 216
5. H. Grober, S. Erk, and U. Grigull, Fundamentals of Heat Transfer, McGraw-Hill, New York, 1961, p. 314
6. E. Schmidt and W. Beckmann, "Das Temperatur und Geschwindigkeitsfeld von einer Wärme abgebenden senkrechten Platte bei natürlicher Konvektion," Tech. Mech. u. Thermodynam., Vol. 1, 1930, pp. 341, 391
7. W. H. Giedt, Principles of Engineering Heat Transfer, D. Van Nostrand, Princeton, N. J., 1957, p. 217
8. E. R. G. Eckert and R. M. Drake, Jr., Heat and Mass Transfer, McGraw-Hill, New York, 1959
9. E. M. Sparrow and J. L. Gregg, "Laminar Free Convection From a Vertical Plate with Uniform Surface Heat Flux," Trans. of the ASME, Feb 1956, pp. 435-440

10. Lockheed Missiles & Space Company, Informal Nates Concerning the Natural Convection Boundary Layer in the RIFT Tank, by F. H. Morse, FM 42, Aug 1962

11. Lockheed Missiles & Space Company, Dimensional Analysis for Non-Draining Cylindrical Propellant Tank, by J. H. Chin, LMSC-802337, TSN/10, Sep 1962

12. O. A. Saunders, "Natural Convection in Liquids," Proc. Roy. Soc. (London), Series A, Vol. 172, 1939, p. 55

13. J. P. Dotson, "Heat Transfer from a Vertical Plate by Free Convection," M. S. Thesis, Purdue University, May 1954

14. E. R. G. Eckert and T. W. Jackson, Analysis of Turbulent Free Convection Boundary Layer on Flat Plate, NACA Report 1015, 1950

15. Lockheed Missiles & Space Company, Theoretical and Experimental Studies of Zero-G Heat Transfer Modes, Contract NAS 8-11525, Monthly Progress Report for the period 1 Sep 1963 to 29 Sep 1963

16. Lockheed Missiles & Space Company, Analytical and Experimental Study of Liquid Orientation and Stratification in Standard and Reduced Gravity Fields, Report No. 2-05-64-1, Contract NAS 8-11525, July 1964

17. T. Fujii, "An Analysis of Turbulent Free Convection Heat Transfer from a Vertical Surface," Bull. of the JSME, Vol. 2, No. 8, 1959, pp. 559–563

ORBITAL TESTS TO INVESTIGATE THERMAL BEHAVIOR OF CRYOGENS UNDER WEIGHTLESSNESS

by
Juan C. Elizalde
TRW Space Technology Laboratories
Redondo Beach, California

Preceding page blank

ORBITAL TESTS TO INVESTIGATE THERMAL BEHAVIOR OF CRYOGENS UNDER WEIGHTLESSNESS

by Juan C. Elizalde

ABSTRACT

13031

This document presents the results of a study of orbital tests to investigate pressure rise, boil-off losses and related thermal problems of cryogenic propulsion systems near weightlessness. The problems whose solution is sought are defined, which leads to a concrete list of test objectives, applicable to a wide spectrum of missions. Significant aspects of tests are discussed, such as acceleration levels, similarity, container size and shape, test duration, thermal environment, etc., as well as details of a possible test package, in an effort to clarify the nature, scope, feasibility and implementation of this type of test. Finally, guidelines for the preparation of a meaningful program of orbital tests are given.

Author

I. INTRODUCTION

A large number of space missions of immediate interest require storage of cryogenic propellants for fairly long periods. High-energy upper stages, lunar and planetary missions require that cryogens be conserved for periods of hours to months prior to engine firings. However, the thermal processes in a two-phase fluid system in zero or low gravity are not well understood, and pose problems which seriously affect the feasibility of those missions.

The radical changes in gravity-dependent heat transfer mechanisms (convection, boiling and condensation) under weightlessness coupled with the "zero-g" configuration of the liquid and vapor phases, give origin to temperature gradients in the fluid which cannot be predicted with normal-gravity analytical and experimental data. These gradients affect in turn the pressure in tanks and, therefore, the design and operation of open and closed systems.

Every study of cryogenic storage in space that the author has had the opportunity to read assumes isothermal fluids. The "optimized" results thus obtained, including comparisons of active versus passive systems and calculations of insulation and tankage weight, are likely to be grossly in error. It is hoped that the following discussion will sufficiently emphasize the inadequacy of "equilibrium thermodynamics" to design cryogenic systems.

As in most engineering problems, both analytical and experimental work is needed to understand the thermal processes in a cryogenic tank during coast. A realistic analytical model of fluid thermal behavior, unavailable at present, must be developed. In addition, the simplifications inherent to such model require experimental evidence to achieve reliable

design of cryogenic systems. In well insulated cryogenic tanks, temperature changes are very slow, with the consequence that the usual zero-g test methods (drops, aircraft parabolas, sounding rocket trajectories) provide periods of weightlessness that are too short to investigate those phenomena. Long-duration orbital tests are probably the best, possibly the only means of obtaining the required information. This document presents the results of a study on the nature, scope, feasibility and implementation of such tests.

II. STATEMENT OF PROBLEM

A. Forms of Storage

The problem that concerns us here is the storage of cryogenic propellants in a space vehicle. We want to conserve propellants safely and with small losses during the coast periods preceding engine firings, and do it with acceptable weight penalties in insulation and tank structure. To help see the problem in its proper perspective, let us briefly review the possible forms of propellant storage.

Single-phase storage (subcritical liquid or supercritical fluid) would avoid the uncertainties of liquid/vapor configurations in zero-g and provide ease of operation. However, weight penalties are very high; with subcritical liquid, a small increase in temperature results in a very large increase in pressure, requiring thick-walled tanks; with supercritical fluid, the storage pressure is very high (about 200 psia for LH_2, 800 psia for LO_2), and the unusable gaseous residuals are very large. Supercritical storage is advantageous where fairly small amounts of fluid are involved, but for large propellant tanks structural weight may be prohibitive.

Three-phase storage ("slush") is, like initially subcooled two-phase storage, a means of increasing the thermal capacity of the system by displacing its reference point to lower temperature levels. Aside from the reduction in tank and/or insulation weight that can be thus obtained, it does not appear that the thermal problems for these systems are different from those found in saturated two-phase systems, a condition that, given sufficient time, is reached by three-phase systems anyway.

Two-phase storage has the advantage of relatively small and light tankage, while it presents the usual "zero-g" problems found in liquid/vapor systems. Justifiably or not, two-phase storage of cryogenic propellants has been the choice throughout the industry for every space mission, present and planned. Therefore, the thermal problems involved merit a closer look. Vented or unvented systems are considered, depending on amount of fluid and mission duration. The thermal problems associated with both schemes are discussed in the following section.

B. Closed (Unvented) System

The main uncertainty in the non-venting scheme is the rate of pressure rise in the tanks. Usually it is assumed that the liquid is at uniform temperature, with all the mass acting as a heat sink, and with the tank pressure being simply the vapor pressure corresponding to that average temperature. Temperature (and pressure) rise is then determined by heat input and thermal mass, and the insulation is sized so that the equilibrium vapor pressure does not exceed a prescribed value, compatible with tank strength. Results

obtained in this fashion are probably unduly optimistic, since the real conditions in the tank are likely to be quite different. We know from analytical and experimental studies that a cryogen in a closed tank under normal gravity may be heavily "stratified," particularly if heating through the lateral walls is greater than through the bottom (Refs. 1, 2, 3). This is due to the formation of a warm boundary layer which deposits strata of warm liquid next to the ullage space. Under low gravity, as we will see later, it appears that this behavior still exists and the fluid would be "stratified." Even if the fluid were perfectly weightless, with no buoyancy forces to sustain convection, it would present the temperature profile of a solid heated at one of its boundaries. Large temperature differences within the fluid could be expected in this case (Ref. 4). Temperature gradients will then be found in the liquid during coast, with some regions warmer and some colder than in the uniform temperature case. Since the pressure in the tank corresponds to the temperature of the liquid/vapor interface (Ref. 5), the pressure could be lower or higher than for uniform conditions, depending on whether the ullage is located in "cold" or "warm" regions of the liquid.

A serious situation, however, arises if the ullage is in contact with the wall. In this case, the low heat capacity of the vapor results in a rapid increase of pressure in the tank. Although condensation would tend to decrease the pressure, a warm layer of liquid forms adjacent to the liquid/vapor interface, so that for all practical purposes the ullage behaves as an isolated system. The

warm liquid interface and low conductivity of the liquid result in an effective "insulation" between the warm vapor and the bulk of the liquid.

Figure 1 is an example of the importance of these problems. It shows the increase in tankage weight as a function of maximum interface temperature in a cryogenic tank, taking saturated conditions at 14.7 psia as a reference. It can be seen that very small gradients in the liquid result in very large weight penalties.

It should be mentioned that low-g tests with liquid hydrogen in Aerobee sounding rockets indicate that a pressure rise quite different from that predicted for uniform conditions does indeed take place.

C. Open (Vented) System

A number of devices have been designed or proposed for venting of cryogenic tanks under weightlessness. Some of them are intended to position the ullage in a predictable location so that the vent can be located there. To this category belong screens, cylinders or similar surfaces making use of "capillary" (surface tension) effects, and dielectrophoretic devices. Centrifugal separators and expansion valve-heat exchanger combinations, on the other hand, could operate without ullage control. Although most of these devices appear to work well when the ullage is large (30% or more of tank volume), it is not clear that they will do so with the smaller ullages which are desirable to reduce tank size and weight. It would then be necessary to settle the propellant by thrust application to permit venting without liquid losses. The question then arises of

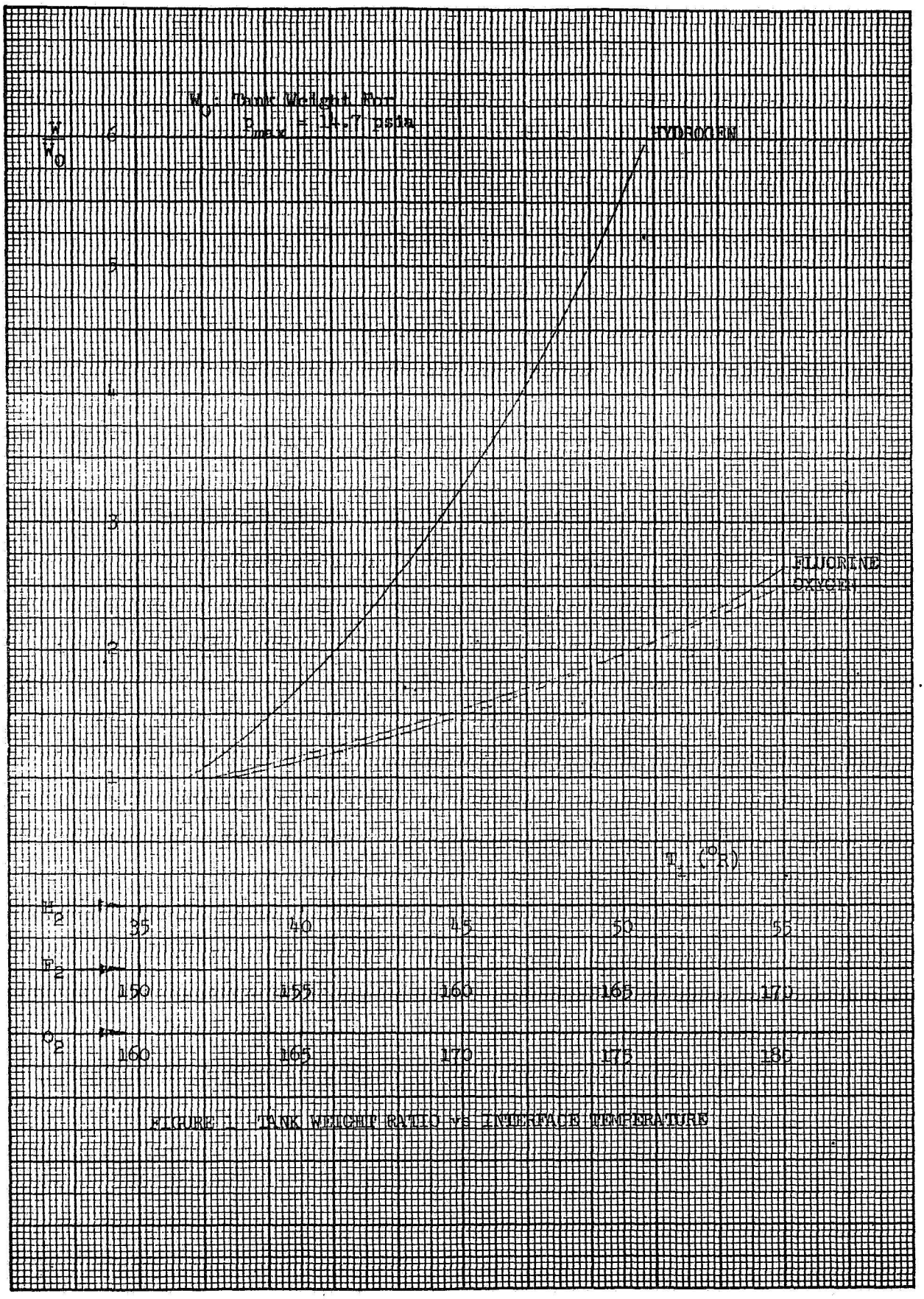


FIGURE - TANK WEIGHT RATIO vs INTERFACE TEMPERATURE

how much propellant is required for this thrusting. Continuous venting to maintain a constant pressure in the tank requires, of course, continuous thrusting. This may be provided by an auxiliary rocket or propellant boil-off, but in either case the propellant requirements are excessive except for missions with a few hours' coast.

Intermittent venting appears less costly, and is frequently proposed for longer missions. The vent valve would have "open" and "close" settings, separated by a few psia. When the "open" level is reached, the valve opens and venting of the vapor occurs until the pressure decreases to the "close" level. The pressure rise taking place between venting periods will be essentially the same process as that described for the non-venting case, with the result that the frequency of the venting cycles will be affected by the fluid temperature profiles and ullage location. In addition, upon opening the venting valve, the pressure in the tank decreases and the liquid becomes locally superheated. The heat absorbed between venting periods and stored as sensible heat will probably be liberated in a mass boiling process, which, unless properly regulated, may result in flashing or boil-over. The intensity of boiling will depend on the pressure drop rate allowed by the valve and the temperature gradients in the liquid.

An exception to the above consideration may be a vent valve consisting of an expansion valve and heat exchanger, which relies on cooling of the propellant mass by the expanded venting fluid, either liquid or gas. The successful operation of this device

depends on liquid stirring or some form of energy transfer so that heat extraction can be felt in the whole tank and not only locally.

The preceding discussion, although just a bare outline of the uncertainties faced by the designer, should make it evident that many important problems must be solved before cryogen-propelled vehicles for lunar and planetary missions can be launched. Long duration orbital tests should provide many of the answers.

III. ASPECTS OF ORBITAL TESTS

A. General Considerations

The scope of a program of orbital tests with cryogens strongly depends on the available experiment carrier. To be sure, the test package imposes some requirements on the carrier, mainly on orbit altitude to assure low aerodynamic drag, and on tumbling or spinning rates to maintain low acceleration levels. If the carrier is able to meet the latter, the package may remain with it; otherwise, it will have to be ejected and provide its own attitude control during the test period. Conversely, the capacity and number of carriers affect the size and weight of the package, variables to be investigated, and possibly such aspects as telemetry and test fluid. The following sections are intended to supply the criteria for selection of a carrier and of test objectives towards a rational program.

The complexity of thermal phenomena in very low gravity coupled with the difficulty of obtaining experimental data in such environment results in very limited knowledge in the field. Basic investigations are certainly in order to gain insight into these problems. However, the urgent need for design criteria strongly suggests the

conduct of engineering experiments to provide it. The type of test discussed in this document is conceived to supply data useful to the designer, even though it may not always give us a full understanding of the thermal processes involved.

B. Missions of Interest

The tests should attempt to reproduce, with due consideration to scaling effects, the conditions of cryogenic vehicles to be designed in the near future. They include:

1. High-energy chemical upper stages

   7-10,000 lbs. class

   30-40,000 lbs. class

2. Lunar vehicles

   Logistic vehicles (one-way transit)

   High-energy Apollo (lunar rendezvous)

   Direct manned vehicle (landing and return stages)

3. Satellite inspectors

4. Planetary vehicles

   Main deboost stages

   Descent and landing stages

   Return stages

5. Radioisotope powered vehicles

These missions are representative of most applications of cryogenic propellant storage, and should help to decide on test conditions.

C. Test Objectives

Detailed consideration of the problems discussed in Part II

leads to a clear identification of program objectives. Basically, tests should be aimed at providing data for reliable two-phase storage of cryogenic propellants. Primary objectives of the tests should be to determine:

1. Pressure history in a closed cryogenic tank near weightlessness. Actual pressure rise rather than isothermal fluid values must be known to design tankage and insulation.
2. Boil-off losses and frequency of venting cycles in a vented tank. This information is needed to establish total propellant needed for a mission, accounting for boil-off, as well as additional impulse if settling of the liquid were required prior to venting.

Depending on carrier capacity, schedule and number of flights, secondary objectives would be selected from the following list.

3. Effect of acceleration on pressure and boil-off.
4. Effect of ullage size on pressure and boil-off.
5. Effectiveness of ullage-positioning devices, particularly for small ullage. Screens, conical or cylindrical structures and dielectrophoretic devices may be included.
6. Practical means of eliminating or reducing temperature gradients in the fluid, such as stirring or spinning a tank equipped with mixing baffles.
7. If propellant settling is required to assure venting without liquid losses, required thrusting level and duration

should be established, as determined by size and distribution of bubble population.

8. Allowable venting rate to avoid boil-over.

9. Effect of sloshing such as may be caused by re-orientation maneuvers or residual oscillations due to engine shut-off perturbations.

10. Checking of scaling laws to permit extrapolation of test results to larger tanks.

11. Performance of expansion valve-heat exchanger vent system.

12. Evaluation of cryogenic insulation techniques.

D. Acceleration

To decide on the acceleration level for a test, we must first review the accelerations experienced by the fluid in a space vehicle. Table I is a summary of typical external forces acting on a space vehicle during coast and the resulting accelerations. Actual values will vary for each vehicle, of course. To compare orders of magnitude, we have taken as an example a typical vehicle for a manned or logistic lunar mission, of the 100,000 lbs. class and about 20 ft. in diameter. On the basis of the table, we can categorize missions from the standpoint of acceleration during coast, as follows:

a) Continuous low thrust, $a/g_o \simeq 10^{-4}$. (Examples: stages in which boil-off is used for attitude or ullage control, and radioisotope powered stages).

b) Low-altitude orbit, $a/g_o \simeq 10^{-6}$. Probably limited to short parking orbit phase of missions.

c) High-altitude orbit and transfer orbit with oriented vehicle,

TABLE I. Typical Accelerations in a Space Vehicle

SOURCE	CONDITIONS	a/g_o
1. Solar Pressure	At 1 AU; low absorptance surface	10^{-10}
2. Centrifugal (vehicle rotation)		
a) to maintain vehicle	Low earth orbit; r = 10 ft.	10^{-6}
parallel to earth surface	High earth orbit; r = 10 ft.	10^{-8}
b) limit cycle to maintain	Typical angular velocity due	
vehicle oriented towards	to limit cycle: 0.05 deg/sec;	10^{-8}
sun or star	r = 10 ft.	
3. Thrust for ullage control or from radioisotope propulsion	Typical thrust: 10 lbs.	10^{-4}
4. Aerodynamic drag	C_D = 2; H = 100 N mi.	10^{-6}
	250 N mi.	10^{-8}
	400 N mi.	10^{-9}

$a/g_o \simeq 10^{-8}$. To this category belong most cryogenic missions now being planned.

d) Interplanetary missions with advanced orientation systems, $a/g_o \simeq 10^{-10}$ and lower.

To these we could add the case of tumbling vehicles, which is, however, unlikely due to thermal control and guidance considerations.

It must be noted that thrusting, drag and radiation pressure generate uniform acceleration fields, while rotation due to attitude control results in variable, divergent fields.

We should now see what is the effect of these acceleration levels on gravity-dependent processes.

First, let us examine the effect of acceleration on the distribution of liquid and vapor in a tank. Normally, hydrostatic regimes are defined in terms of the Bond number, which is the non-dimensional ratio of gravitational to surface forces:

$$Bo = \frac{\rho_L L^2 a}{\sigma_{LV}}$$

If Bo is greater than unity, the gravitational forces (liquid "weight" for a given g level) dominate and the liquid is settled, with an interface more or less curved depending on the acceleration. This is what we may term "low gravity" behavior. If Bo is less than unity, surface tension dominates and we have the typical "zero g" behavior, with the ullage possibly no longer "above" the liquid. Experimental work by Massica et. al. shows that this criterion works quite well (Ref. 6). The change of regime at Bo = 1 is only approximate, of

course. Only for Bo $\gg$ 1 or Bo $\ll$ 1 we can be sure that we have either gravity-dominated or surface tension-dominated type of behavior.

A somewhat different criterion of hydrostatic behavior can be adopted. If, instead of Bo, we take the ratio of actual forces, $\rho_L V_L a/\sigma_{LV}\pi D$, which can be called Bo^*, we avoid the use of the rather arbitrary characteristic length L. This is advantageous if the liquid height is very different from the tank diameter, as, for instance, in a tank where little liquid is left. Figure 2 shows the boundary between gravity- and surface tension-dominated regimes ($Bo^* = 1$) for LH_2 and LN_2 in cylindrical tanks for two different percentages of liquid volume. The figure helps to visualize the fact that "zero-g" hydrostatic behavior is reached at widely different accelerations for different tank sizes.

Regarding natural convection, the character of the process is described by the Rayleigh number

$$Ra = Gr\ Pr = \left(\frac{a\beta\Delta T L^3}{\nu^2}\right)\left(\frac{c_p \mu}{k}\right)$$

Vliet et. al. (Refs. 7 and 8) use a modified Rayleigh number Ra^* when it is more convenient to correlate similar cases in terms of the heat flux through the wall rather than wall temperature:

$$Ra^* = \left(\frac{a\beta q''_w L^4}{k\nu^2}\right)\left(\frac{c_p \mu}{k}\right)$$

The regimes are given as:

$Ra^* < 1$: conduction-dominated transfer

$1 < Ra^* < 10^5$: viscous flow throughout vessel

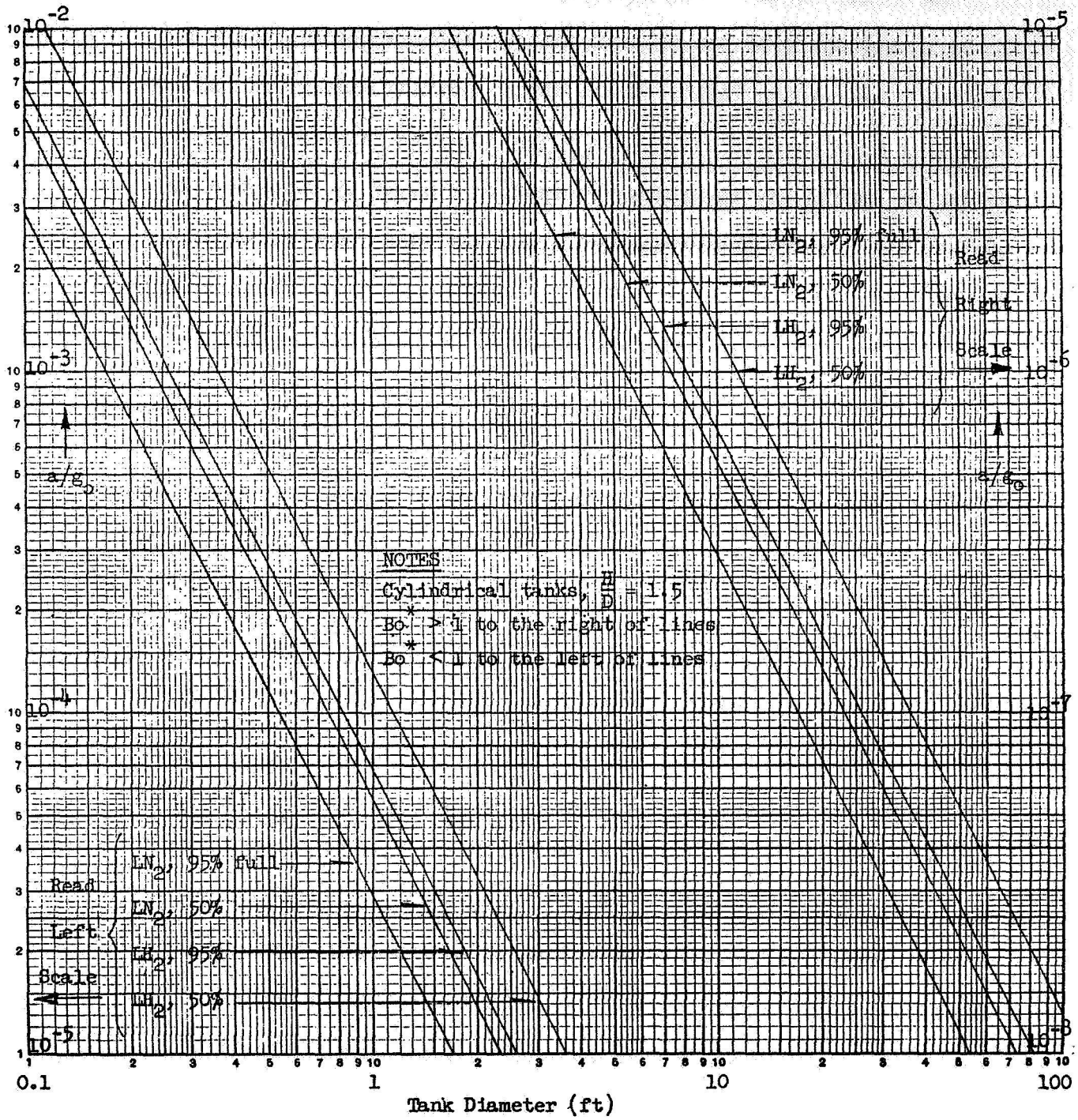


FIGURE 2 BOUNDARY BETWEEN GRAVITY-DOMINATED AND SURFACE TENSION-DOMINATED HYDROSTATIC REGIMES ($Bo^* = 1$)

$10^5 < Ra^* < 10^{11}$: laminar boundary layer

$Ra^* > 10^{11}$: turbulent boundary layer.

These limits apply to the case of heating through lateral walls and uniform acceleration field. Where bottom heating and/or non-uniform, divergent acceleration exist, the regimes may be different. In any event, we should try to achieve convection similarity between actual vehicle and test by having approximately the same order of magnitude for Ra^*.

Finally, let us consider boiling. There is no evidence that boiling will occur for the very low heat flux found in well insulated cryogenic tanks. Aircraft tests with liquid hydrogen reported by Sherley (Ref. 9) showed that, for the duration of the "zero-g" maneuver (about 10 sec.), the lowest heat flux at which nucleate boiling was observed was 250 BTU/hr-ft^2, while a typical value for a foil-insulated tank is 1 BTU/hr-ft^2. Of course, boiling may occur for lower heat fluxes but, due to residual convection, require for its inception longer periods than were available in those tests.

When there is nucleate boiling, data from Reference 9 indicates that there is practically no difference in the boiling curves for LH_2 in very low and normal gravity. It has been suggested that this is so because the dynamic forces associated with bubble formation are larger than gravity-induced buoyancy forces. More rigorously, one should consider all the forces relevant to the pool boiling process: bubble dynamic, surface tension, and buoyancy forces. If either the buoyancy or the dynamic force is greater than the surface tension force as the bubble grows, one may conclude that the bubble

will detach from the wall. Further, if the dynamic force is much greater than the buoyancy force, the process should be relatively insensitive to gravity. Adelberg (Ref. 10) presents a bubble Froude number, ratio of dynamic to buoyancy forces, and gives the approximate expression

$$Fr_B \sim \frac{3\,R_{max}}{a\,t_{max}^{\,2}}$$

where R_{max} : maximum bubble radius (break-away size)

t_{max} : time required for the bubble to grow to the size R_{max}.

In this expression, R_{max} and t_{max} should be known from experimental data (probably inexistent) or computed with some of the theoretical relations proposed by various authors* (Ref. 11).

Unlike hydrostatic behavior and convection, boiling phenomena are not directly affected by container size**. So, in a test, we should try to have the same acceleration and heating levels as in the actual vehicle. If this is not possible, we should evaluate the bubble Froude number; if $Fr_B \gg 1$ for both vehicle and test, acceleration is probably not critical and we can use the same heat flux;

---

*For instance, for bubble growth:

$$D = \frac{4k\Delta T}{H_V\,\rho_V\sqrt{\pi\alpha}}\;t^{\frac{1}{2}}$$

$$D_{max} = \left[\frac{6\sigma_{LV}}{a(\rho_L - \rho_V)}\;\;\frac{k\Delta T}{q''}\right]^{1/3}$$

**A small container may result in greater curvature of the heating surface, more rapid pressure rise or restrictions in convective currents, which might affect boiling.

if $Fr_B \gg 1$ is not met, and the same acceleration cannot be provided, boiling correlation does not appear possible. Of course, the above considerations assume that boiling does occur, but it may well be that, for the low heat flux found in most applications, this will not be the case.

In sum, we have seen that, in selecting the acceleration for a scaled test, we have to consider the Bond number, Rayleigh number, and possibly bubble Froude number. An inspection of their expressions shows that it is not possible to satisfy the equality of the two (or three) numbers simultaneously. For instance (if we assume the same fluid), for a 1/10 scale test container, we could match the Bond number with an acceleration in the test 10^2 times greater than in the actual vehicle. But then, to match the Rayleigh number, we would require an acceleration 10^4 times greater. The situation would be even more complicated if we were to test with a different fluid. However, it may be sufficient to select the test conditions so that we have the same <u>regimes</u> as those of the actual vehicle. The following procedure is proposed:

a) Use as a test fluid the propellant of interest. Then we can write

$$\frac{(Bo^*)\ \text{vehicle}}{(Bo^*)\ \text{test}} = \frac{(aL^2)\ \text{vehicle}}{(aL^2)\ \text{test}}$$

$$\frac{(Ra^*)\ \text{vehicle}}{(Ra^*)\ \text{test}} = \frac{(aL^4)\ \text{vehicle}}{(aL^4)\ \text{test}}$$

b) Select a and L so that we have the same convective and hydrostatic regime.

c) Use the same heat flux as in the actual vehicle.

d) In case there is boiling, and if for the vehicle $Fr_B \gg 1$, try to select a so that this is also the case in the test.

E. Test Fluid

We have seen in the preceding section that similarity considerations favor the use of the propellants of interest for testing. Hydrogen, oxygen and fluorine, proposed for many cryogenic vehicles, should be preferred. Of these, hydrogen is of the greatest interest because:

a) For unvented tanks, structural weight penalties due to higher-than-predicted pressure increase would be severe for large hydrogen tanks.

b) For vented tanks, each pound of unpredicted hydrogen boil-off would render useless several pounds of oxygen or fluorine.

Safety considerations might prevent use of these fluids for tests on certain carriers. If so, tests with liquid nitrogen, although less desirable, may still yield useful information, mainly for two purposes:

a) to show if pressure rise and/or boil-off are substantially different from those predicted for isothermal fluids.

b) to check results obtained with analytical models, so that these can be refined and used with more confidence to predict behavior of other propellants.

Use of a non-cryogenic fluid is also justifiable on the same grounds, with the restriction that the liquid be at saturation temperature. However, testing with the real propellants remains as the most attractive possibility.

F. Container Size

In Section D we have discussed already the similarity considerations that affect the size of the container. In addition, there is the hard fact of carrier capacity, which will place an upper limit on package size. Aside from these factors, a relatively large container has several advantages:

a) it avoids the distortion of thermal processes due to "crowded" conditions in the tank. For example, bubbles growing and not yet detached from the walls may touch the main ullage and be "absorbed" by it due to a proximity not found in a real tank; and the convective currents or boundary layer may not have enough space to develop as they would in larger vessels.

b) for a given temperature gradient, temperature differences in the fluid will be larger and more easily detected by instrumentation.

c) larger amounts of liquid permit a test of longer duration.

Cryogenic propellant tanks may range from 2 to 20 ft. in diameter, but the 5 to 10 ft. sizes are more frequently proposed. Models of 1 to 3 ft. diameter would be of reasonable size and weight, provide fairly long tests, and possibly avoid serious distortion of thermal processes. Models much smaller than 1 ft. are, we feel, of questionable value for the type of test discussed here, although probably quite adequate for basic research.

If the carrier capacity or number of flights permit it, two or more containers of different size should be tested under the same conditions, to establish the validity of the similarity reasoning

of Section D and permit more confident extrapolation of results to full-size tanks.

G. Container Shape

Container shape should affect the thermal processes in very low gravity. For one thing, the ullage location and shape, as determined by minimum energy considerations, is different for containers of different shape. This results in different temperature profiles in the fluid, as well as in a different apportionment of heating between the liquid and vapor phases. Also, boundary layer development, if we have such a regime, will be affected by the curvature of the walls. Ideally, then, we would like to investigate the shapes usually proposed for cryogenic tankage: cylinder with hemispherical or spheroidal caps, sphere, spheroid and perhaps toroid. In practice, and for the sake of economy, it may be preferable to investigate thoroughly one shape, probably a cylinder, and run one test under the same conditions of acceleration, heating and propellant mass for other shapes of interest, to assess the magnitude of the difference in pressure rise and boil-off.

H. Thermal Environment

In Section C we have seen that it is desirable to have for the test the same heat flux as in the vehicle. Most missions of interest require storage of cryogens for several days and have propellant tanks well isolated from the environment with foil insulation. Each mission has a different heat flux profile depending on orientation, vicinity to the earth or planet, maneuvers for mid-course corrections or navigation, etc. However, the thermal lag of the insulation and

surrounding structure results in relatively small and slow variations of heat input to the fluid. A possible special case is a vehicle so oriented that the sun shines almost permanently on one side, so that there is a pronounced difference in heat flux between the "hot" and "cold" sides of the tanks.

For a meaningful simulation of actual conditions, the following methods are proposed for the tests:

a) If the test carrier or ejected test package have an attitude control system with sun-seeking capability, the test container may be exposed to the same environment as the actual vehicles. Conditions in the tank may be measured with the package aligned with the sun vector. Then a programmed change of attitude may orient the package with one side facing the sun, to establish the influence of uneven heating. This approach has the disadvantage of requiring a rather complex attitude control system and logic, as well as restricting the possible test carriers.

b) A more attractive method is to have a very well insulated package, so that external heating is lower than in the actual vehicle, and provide the desired heat flux with heaters applied to the tank or to an intermediate radiating wall. This method has several advantages: it imposes no restrictions on package or carrier attitude; it permits varying the heat flux to investigate its effect on fluid conditions; and, by proper wiring, it permits checking the effect of uneven heating with no change in package attitude.

Although an external power source would be necessary, the very low heat flux values and small container size would require reasonably low power.

I. Ullage Space

We have seen that the location of the ullage space may have a major influence in tank pressure, depending on its location with respect to the walls. This location is in turn determined, among other factors, by the ratio of ullage volume to tank volume. For very small accelerations, the equilibrium configuration of the ullage is a sphere submerged in the liquid.* However, as the ullage volume grows, its diameter may become larger than the tank's smallest dimension (the diameter in an elongated cylindrical tank, for instance) and the sphere becomes two hemispheres bounding a central section in contact with the walls. The vapor can then be heated directly and tank pressure should increase rapidly. On the other hand, if the acceleration confines the ullage against the wall, a small ullage is likely to result in higher pressure, due to its low heat capacity and, more important, to the small liquid/vapor interface area on which condensation takes place. It may well be that an appreciable reduction in the rate of pressure rise could be obtained with a moderate increase in ullage volume.

It is of interest, therefore, to investigate the effect of ullage size on the conditions in the tank. In a test, this can be accomplished by filling the vessel so that we start, for instance,

*Reynolds (Ref. 12) predicts that a wall-bound ullage will be found even for very small accelerations.

with 5% ullage. As the test progresses, successive venting cycles increase the ullage size, so that we cover the range from an almost full to an almost empty tank. Between venting cycles, we reproduce the case of pressure rise in a closed system for the various values of ullage volume, and we can also see its influence on venting frequency and boil-off losses.

J. Test Duration

Usually, "zero-g" tests end with the "zero-g" period, whether a free fall, aircraft trajectory or sounding rocket flight. For an orbital test, the period of weightlessness is practically indefinite, so the test ends instead when all the cryogenic fluid has been boiled off. Figure 3 shows test duration for spherical vessels of various diameters, originally 95% full with liquid hydrogen or liquid oxygen, and for typical heat fluxes. It has been assumed that all the heat input to the fluid results eventually in boiling losses.

A long duration test permits changing the test conditions to investigate the effect of some variables on thermal processes, such as heat flux, acceleration and venting rate. The end of venting periods is a convenient time to change the variables. The maximum boil-off losses in each venting period (if no liquid is lost during venting), are approximately given by

$$\frac{M_V}{M_T} = \frac{C_V (T_2 - T_1)}{H_V}$$

where T_2 and T_1 are the saturation temperatures corresponding to the "open" and "close" pressure settings of the vent valve. Since T_2-T_1 is only a few degrees for low pressures, the fraction of fluid lost

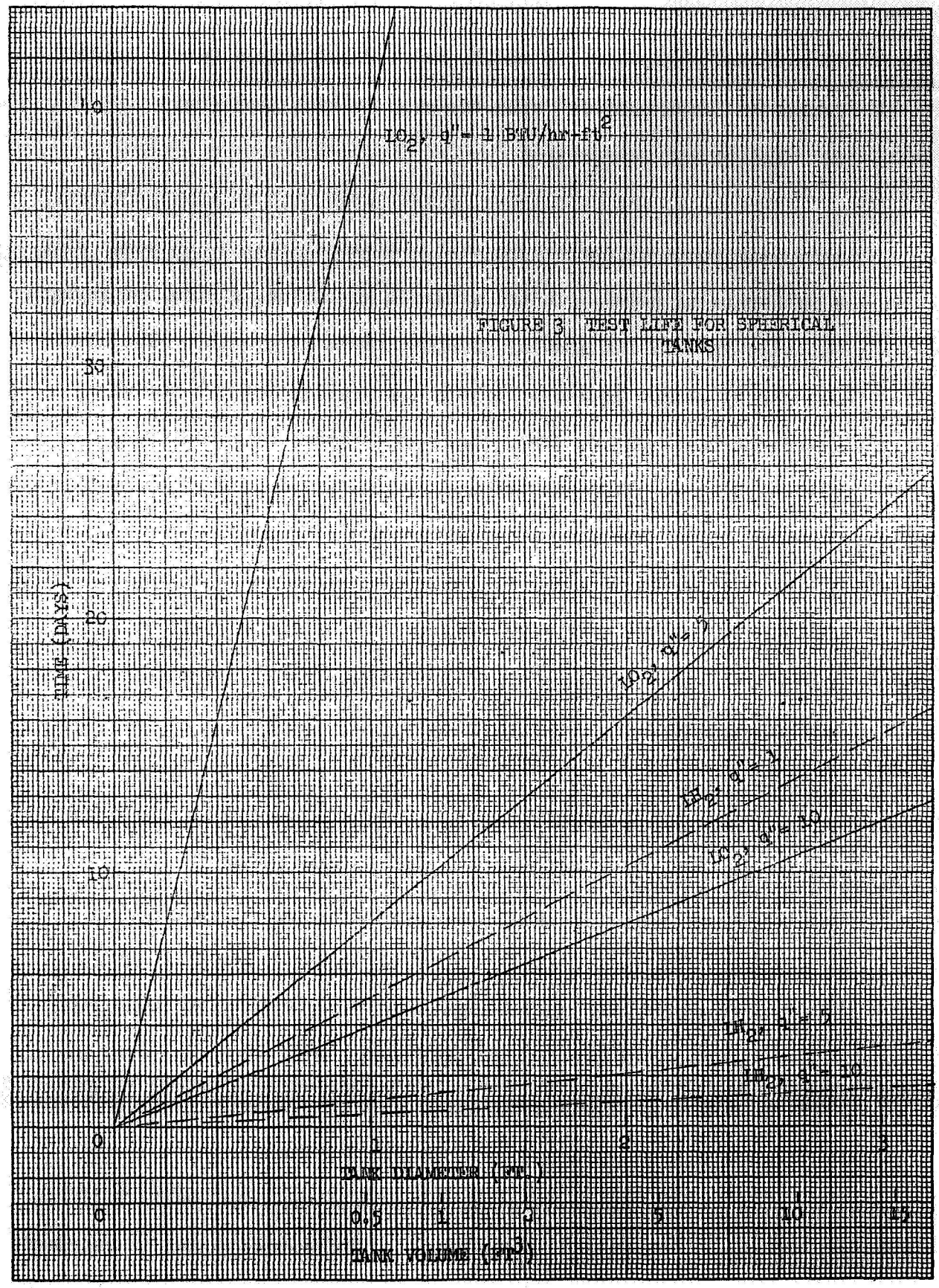


FIGURE 3 TEST LIFE FOR SPHERICAL TANKS

in each venting period is small, so we would have a fairly large number of "test periods" with the same initial pressure.

K. Analytical Correlation

Obviously, the usefulness of the tests will be much greater if test data could be correlated with analytical results obtained with a mathematical model. To the writer's knowledge, a model of cryogen behavior in very low gravity is unavailable at present. The complications of ullage location in very low gravity and the variable, divergent acceleration field found in rotating or oscillating vehicles makes questionable the application of available models to the "zero-g" case. The very thorough review of stratification phenomena by Clark (Ref. 7) does not mention any such model. This writer is engaged at present with some associates in a study of a suitable analytical model which, with some fortune, would enable correlation of future test data.

IV. TEST PACKAGE

In this section we describe in some detail a possible test package to implement the type of orbital test under consideration.

The container is a triple-wall vacuum vessel of cylindrical or spherical shape. The inner wall is stainless steel, compatible with LH_2, and a relatively poor conductor, to decrease the influence of conduction along the walls on fluid temperature gradients. The middle wall is copper, to provide fairly uniform radiation heating of the inner vessel, but made in two halves with a thermal barrier interposed between them to enable uneven heating of the fluid. Between the middle and outer walls foil insulation is placed, about 1.5 inches thick. The vacuum vessel is required

for control in the atmosphere, where the insulation would be otherwise ineffective, and to permit installation of the experiment on the carrier well before launch with little or no fluid loss.

Heaters capable of dissipating up to 5 watts/ft^2 are applied to the copper wall and permit accurate knowledge of heat input to the vessel. Inaccuracy in the prediction of heat leaks from the environment is of no consequence because they are small compared to heater power. The heaters are wired so that it is possible during the test to heat only half of the container.

A vent valve with "open" and "close" settings of 40 and 30 psia, respectively, is used. This range should permit fairly long "test periods" between venting cycles. The valve allows a very slow decrease in pressure to avoid boil-over. Valves with different pressure settings and vent rates may be installed in other packages. The vapor is vented through a T to avoid imparting spurious accelerations to the package. For one of the tests, the heat exchanger type of valve may be installed to evaluate its performance.

The vessel is mounted on a spin table driven by pressurized gas which is activated on command to ascertain the effect of spinning the vessel and resulting fluid mixing on vessel pressure. This may be replaced by a stirring mechanism in the fluid for the same purpose.

The instrumentation consists of:

a) Three accelerometers to measure accelerations along three perpendicular axes.*

*Units of the pendular type are available which can measure 10^{-3} to 10^{-5} g's with $\pm$ 2% accuracy. Another type, using an electrostatically floated mass is being developed which can measure down to the 10^{-7} g's level and possibly lower.

b) Pressure transducers (two, for redundancy).

c) Platinum resistance temperature transducers (number dependent on container size), mounted on the outer surface of the inner container.

d) Open/closed signals for valve operation.

e) Current meter for heater power dissipation.

f) Calibrated orifice or turbine flowmeter.

V. TEST GUIDELINES

The preceding discussion suggests guidelines which should be of help in planning a program of orbital tests. Clearly, a number of reasons ranging from new technical findings to available funds may dictate changes to these guidelines. Yet, they may prove useful, if nothing else, as a starting point for further discussion.

1. Basic objectives of the tests are:
   a) Pressure history in a closed container
   b) Boil-off losses and frequency of venting in an intermittently vented container.
2. Identify the missions for whose support the tests are intended, and determine the expected range of important variables, such as acceleration and heat flux. "Cryogens in zero g" is much too vague an objective for the tests.
3. Determine test acceleration levels (in conjunction with container size) on the basis of similarity considerations, to have, as far as possible, the same regime of heat transfer mechanisms as in the actual vehicle.
4. Orbit altitude must be chosen so that acceleration due to air

drag is compatible with test objectives. In most cases, orbits no lower than 300 N mi. will be necessary.

5. Use the propellants of interest as test fluids whenever possible.
6. Within the limits imposed by similarity, use test containers as large as carrier payload capacity permit, if possible not much smaller than 1 ft. diameter.
7. Select test carrier on the basis of requirements 3 through 6 above. An alternative is to have a test bed, ejected or boosted into the desired orbit, with its own attitude control, telemetry and power supply systems.
8. If weight allowance permits it, test simultaneously two or more containers of different size.
9. Reproduce in the test as closely as possible the heat flux into the actual tanks. This can probably be more conveniently accomplished with internal heaters in a heavily insulated container.
10. Start the test with a small ullage space, so that in the successive periods between venting cycles the range from almost full to almost empty tanks can be investigated.
11. Plan the number of tests and test procedures to investigate the effect on pressure and boil-off of as many as possible of the following variables:
    a) Acceleration
    b) Heat flux
    c) Ullage space
    d) Container size
    e) Container shape

f) Fluid

g) Venting rate

12. In addition to the basic test objectives under 1, consider investigation of:

a) Stirring or spinning to "homogenize" fluid.

b) Expansion valve-heat exchanger vent system.

c) Ullage control devices.

d) Sloshing

e) Thrust for propellant settling.

f) Insulation techniques

13. Generate a suitable analytical model for correlation of test data.

VI. CONCLUSIONS

Orbital tests are the best and perhaps the only method of obtaining urgently needed experimental data for the design of cryogenic propulsion systems in very low gravity. Such tests appear feasible and should provide meaningful engineering data. A small number of tests with a package of reasonable size and weight would cover a wide spectrum of missions and variables. It is hoped that this paper will stimulate the planning and conduct of such tests.

NOMENCLATURE

a = acceleration

Bo = Bond number

C_D = drag coefficient

C_p = specific heat at constant pressure

C_V = specific heat at constant volume

D = diameter

Fr_B = bubble Froude number

g_o = acceleration of gravity on earth

Gr = Grashof number

H = orbit altitude

H_V = heat of vaporization

k = thermal conductivity

L = characteristic length

M = mass

p = pressure

Pr = Prandtl number

q'' = heat flux

r = radius of curvature in circular motion

R = bubble radius

Ra = Rayleigh number

Ra^* = modified Rayleigh number

t = time

T = absolute temperature

W = weight

α = thermal diffusivity

β = coefficient of thermal expansion

ΔT = temperature difference between heater and bulk fluid

μ = dynamic viscosity

ν = kinematic viscosity

ρ = density

σ = surface free energy (surface tension)

SUBSCRIPTS

L = of the liquid

T = total

V = of the vapor

w = at the wall

REFERENCES

1. T. E. Bailey and R. F. Fearn, "Analytical and Experimental Determination of Liquid Hydrogen Temperature Stratification," Advances in Cryogenic Engineering, Vol. 9, Plenum Press, 1964.

2. J. W. Tatom, et. al., "Analysis of Thermal Stratification of Liquid Hydrogen in Rocket Propellant Tanks," op. cit.

3. J. H. Robbins and A. C. Rogers, Jr., "An Analysis on Predicting Thermal Stratification in Liquid Hydrogen," AIAA Annual Meeting, June 1964.

4. J. R. Olivier and W. E. Dempster, "Orbital Storage of Liquid Hydrogen," NASA TN D-559, August 1961.

5. J. A. Clark, "A Review of Pressurization, Stratification and Interfacial Phenomena," 1964 Cryogenic Engineering Conference, Philadelphia, Pennsylvania.

6. W. J. Massica, et. al., "Hydrostatic Stability of the Liquid-Vapor Interface in a Low-Acceleration Field," NASA TN D-2444, August 1964.

7. G. C. Vliet, et. al., "Stratified Layer Flow Model - A Numerical Approach to Temperature Stratification in Liquids Contained in Heated Vessels," AIAA Aerospace Sciences Meeting, New York, January 1964.

8. R. G. Schwind and G. C. Vliet, "Observations and Interpretations of Natural Convection and Stratification in Vessels," Proceedings, 1964 Heat Transfer and Fluid Mechanical Institute, Stanford University Press, 1964.

9. J. A. Sherley, "Nucleate Boiling Heat-Transfer Data for Liquid Hydrogen at Standard and Zero Gravity," Cryogenics Conference, Los Angeles, August 1962.

10. M. Adelberg, "Zero Gravity Heat Transfer," Annual Meeting of the Institute of Environmental Sciences, Los Angeles, April 1963.

11. R. Siegel and E. G. Keshock, "Effects of Reduced Gravity on Nucleate Boiling Bubble Dynamics in Saturated Water," A.I.Ch.E. Journal, July 1964.

12. W. C. Reynolds, "Hydrodynamic Considerations for the Design of Systems for Very Low Gravity Environments," Technical Report Number LG-1, Dept. of Mechanical Engineering, Stanford University, September 1961.

STATIC AND DYNAMIC BEHAVIOR OF THE LIQUID-VAPOR INTERFACE DURING WEIGHTLESSNESS

by
E. W. Otto
Lewis Research Center
Cleveland, Ohio

Preceding page blank

STATIC AND DYNAMIC BEHAVIOR OF THE LIQUID-VAPOR INTERFACE DURING WEIGHTLESSNESS

by E. W. Otto

Lewis Research Center

ABSTRACT

13032

The problems encountered in attempting to operate systems containing a free liquid-vapor interface in a weightless environment are summarized. The literature reporting the research applicable to or directed toward solutions for these problems is reviewed. Results of the research defining the configuration of the interface as a function of liquid properties and system geometry are discussed. The results of experimental studies of the dynamic behavior of the interface in response to changes in gravity level, to outflow disturbances, and to acceleration disturbances are presented. This study places particular emphasis on determination of the scaling laws that permit prediction of the interface behavior as a function of model size.

Author

STATIC AND DYNAMIC BEHAVIOR OF THE LIQUID-VAPOR INTERFACE DURING WEIGHTLESSNESS

by E. W. Otto

Lewis Research Center

1. INTRODUCTION

The increasing sophistication of space vehicles and their missions has subjected an increasing variety of liquid-vapor systems containing a free interface to a new environment--that of zero gravity. On the Earth these systems rely almost invariably on the body force created by the Earth's gravitational field to separate and locate the liquid and vapor in a consistent predictable manner. Thus, liquids settle to the bottom of tanks, vapors separate from liquids and can be vented off if necessary at the high points in systems, and free convection and buoyancy effects assist in the transfer of heat. In a zero-gravity or weightless environment, however, the gravitational or acceleration body forces are absent, which introduces a number of questions concerning the behavior of the liquid, both static and dynamic, and the effect on heat-transfer phenomena. This paper presents a survey of the various problem areas in the liquid-vapor systems to be used aboard spacecraft and a review of the literature reporting the research applicable to or directed toward the solutions for these problems. The results of experimental studies of the behavior of the interface in response to changes in gravity level, to outflow disturbances, and to acceleration disturbances with particular emphasis on the scaling laws governing the phenomena are also presented.

2. PROBLEM AREAS

2.1 Propellant Tank Systems

A schematic diagram of a typical space vehicle propellant tank system is shown in Fig. 1(a). Main propellant tanks contain a large, free liquid-vapor interface that is subject to a number of disturbances, such as heat gain and acceleration perturbations, as shown.

The primary function of a propellant tank system is to store the liquid in readiness for use by the engine. Thus the behavior of the interface and the propellant in response to the various disturbances will be important to the engine restart operation. If these perturbations are sufficiently severe, they may move liquid completely away from the area of the pump inlet, thus making it necessary to collect the liquid by acceleration of the vehicle along the thrust axis before attempting to restart the engine. Even if the liquid is over the inlet there is the problem of a limited quantity of liquid being available to the pump due to the possible pull-through of the liquid immediately above the tank outlet and the consequent ingestion of excessive vapor.

The heat gained by the tank may necessitate venting during long storage conditions. The required frequency of venting will depend on the effect of the zero-gravity environment on the heat-transfer mechanism. The success of the venting operation will depend on the behavior of the liquid in response to the disturbances. It may be necessary to collect the liquid and vapor before each vent cycle in the same manner as for the engine starting operation.

The perturbations of the attitude control system, if sufficiently

severe or if in resonance with the natural frequency of the surface, may cause liquid to move over the top of the tank and down the other side. Aside from causing trouble with venting procedures and possibly pumping operations, this liquid circulation constitutes a shifting center of gravity of the vehicle and may cause severe stability problems in the attitude control system.

2.2 Space Power Systems

A schematic diagram of a typical space power system is shown in Fig. 1(b). Two free liquid-vapor interfaces normally occur in these systems, one in the evaporator and one in the condenser. The behavior of these interfaces is complicated by the addition of heat in the evaporator, the removal of heat in the condenser, and the probable impact of droplets at high velocity on the interface in the condenser.

The principal fluid dynamic problems in these systems are the avoidance of liquid carryover from the evaporator to the turbine and of vapor carryover from the condenser to the pump inlet. In a normal gravity or equivalent acceleration environment these problems are avoided by proper elevation and orientation of the various components. In a weightless environment where the stabilizing effects of buoyancy are absent, however, liquid and vapor carryover may become difficult to avoid. The situation may be aggrevated by random acceleration from attitude thrustors, drag, crew movements, etc. Further complications will come from the loss of obvious positional stability between tubes of evaporators and condensers employing multiple tubes and from possible changes in heat-transfer mechanisms in the tubes.

2.3 Life Support Systems

A schematic diagram of a typical configuration of a life support system employing a subcritical or liquified storage system for the oxygen is shown in Fig. 1(c). Two large, free liquid-vapor interfaces occur in these systems, one in the oxygen supply tank and one in the water receiver tank. A third liquid-vapor interface is found in the water separator.

The problems in the tank systems are similar to those encountered in the main propellant tank except that here the principal problem is to produce or vent vapor from the tank without loss of liquid. In the case of the oxygen supply tank this vapor is generated by the addition of heat, and any changes in heat-transfer mechanisms will become important as in the propellant tank system and in the evaporator of the space power system. In addition, because the heat must be added to the liquid in order to generate vapor, the configuration, location, and dynamic behavior of the liquid will be important in designing the heating system. The acceleration perturbations imposed by attitude thrusters, drag, crew movements, etc. will cause movements of the liquid in each tank similar to that in the main propellant tank.

The separation of water or water vapor from a moving gas stream is usually accomplished by impingement of the air stream against a cooled surface, which condenses the water vapor. The water then drains by gravity to the receiver. In a weightless environment the draining action is lost and other means must be found to remove the water from the condensing surface.

2.4 Fuel Cell Systems

Figure 1(d) shows a typical fuel cell system using oxygen and hydrogen, both stored in a liquid state. The problems encountered in this system are the same as those of life support systems.

2.5 Miscellaneous Systems

The principal fluid dynamic problems in weightlessness have been illustrated in the previous discussions of the various systems. These problems occur to a greater or lesser extent in all space vehicle systems containing liquid and vapor. There are certain zero-gravity problems, however, that are not fully covered by the previous examples and that have been receiving and will continue to receive a great deal of attention--namely the biomedical problems. Those aspects of the biomedical problem that involve a liquid-vapor interface are subject to the same fluid behavior description as for mechanical systems, although they are probably not subject to the same solutions. Many of the biomedical problems appear, however, to be related to the effect on individual cell behavior of the loss of molecular body forces, which is beyond the scope of this paper.

2.6 Summary of Problems

Despite the great variety of systems, the fluid behavior problems can be resolved into a few basic categories as follows:

1. Interface Configuration
    a. Shape and location of the interface
    b. Separation of liquid and vapor
2. Interface Dynamics
3. Pool Boiling Heat-Transfer Mechanisms
4. Evaporation and Condensation Phenomena

It will be found convenient to discuss the fluid behavior phenomena in terms of these broad categories. In the following section a review of the analytical and experimental research studying these phenomena will be made. This is not intended to be an exhaustive review but a broad treatment to aquaint the reader with the general state of the art. Many of the references cited contain extensive bibliographies with which the subject may be pursued in more detail.

3. RESEARCH EFFORTS

3.1 Discussion of Analytical Concepts

In studying the change in fluid behavior or basic mechanisms between 1-g and 0-g, one is led to examine the change in forces or force levels in going from one gravity field to the other. In general, the forces acting on a liquid are the inertial forces and the intermolecular forces, which are exhibited in the form of the surface-tension forces. Under 1-g or earthbound conditions a liquid in a container is restrained from accelerating freely in the gravity field. Under these conditions the inertial forces predominate, and only small effects of the surface-tension forces are noticeable. Typically, the effects of dominant inertial forces are the shaping of liquids in tanks, the weight of the liquid, the hydrostatic pressure of liquid columns, the rise of vapor bubbles in liquids due to buoyancy, and the convection currents in liquids as a result of heat inputs. Although the surface-tension forces are small in comparison with inertia forces at 1-g, their effects are still observable in the meniscus of liquids in contact with solid bodies and in the capillary rise or depression in small diameter tubes.

When a liquid or a system containing liquid and vapor is allowed to accelerate freely in the local gravity field, the inertia forces disappear and the surface-tension forces remain. These forces are dominant in determining the equilibrium configuration and the liquid configuration dynamics, and they play a larger role in the heat-transfer mechanics. Research concerning the behavior of fluids in a weightless environment has therefore involved study of surface-tension or surface-energy phenomena and of

their effect on fluid behavior.

3.1.1 Early History of Surface-Energy Studies

The history of the study of surface-tension phenomena can be traced as far back as Leonardo da Vinci and Sir Isaac Newton. It was Young, however, who first established the theory by demonstrating how the principles of surface tension and contact angle can be used to explain a great many capillary phenomena. The theory was put on a firm mathematical foundation by Laplace and later Poisson. Further developments were made by Gauss, who applied the principle of conservation of energy to the system and obtained not only the equation of the free surface but also the conditions of the contact angle. Other earlier investigators include Dupre, Rayleigh, Gibbs, and Plateau, who utilized soap bubbles and other devices to determine the equilibrium configuration of liquids. Later investigations were carried out by Langmuir and Harkins in the United States and by Adam and Burdon in England

3.1.2 Liquid Contact Angle

Consider a liquid in contact with a solid surface as shown in Fig. 2. The free surface energies at the solid liquid-vapor interfaces may be represented by the surface-tension forces acting in the direction of the surfaces. The angle at which the liquid meets the solid surface, measured in the liquid, is the contact angle.

For the liquid to be in equilibrium with the solid surface, the surface-tension forces at the solid liquid-vapor interfaces must be in balance parallel to the solid surface. Therefore,

$$\sigma_{vs} = \sigma_{ls} + \sigma_{vl} \cos \theta \tag{1}$$

and

$$\theta = \cos^{-1} \frac{\sigma_{vs} - \sigma_{ls}}{\sigma_{vl}} \tag{2}$$

where σ_{vs}, σ_{ls}, and σ_{vl} are the surface tensions, or surface energies, of the vapor-solid, liquid-solid, and vapor-liquid interfaces, respectively, and θ is the contact angle. (Equation (1) is known as the Young-Dupre equation.) It is observed that the contact angle depends on the magnitudes of the three surface-tension forces. When $(\sigma_{vs} - \sigma_{ls})/\sigma_{vl}$ is between 0 and 1, the contact angle lies between 0° and 90°, and the common convention is to call the liquid a wetting liquid. If, however, $(\sigma_{vs} - \sigma_{ls})/\sigma_{vl}$ lies between 0 and -1, the contact angle will lie between 90° and 180°, and the liquid is said to be nonwetting liquid. The contact angle should remain constant in any gravity field, including a weightless environment, because the intermolecular forces that are exhibited in the surface-tension forces are independent of the level of the gravity field.

3.1.3 Pressure Difference Across the Liquid-Vapor Interface

Although the property commonly referred to as surface tension is an energy, it behaves in every way like a tension and tries to make the surface as small as possible. Thus a drop of liquid tends to become spherical, and the tendency of the surface to contract increases the pressure inside the drop. Because the pressure everywhere inside the drop is the same, this pressure difference between the inside and outside of the drop is the

pressure drop across the interface and is given by the following expression:

$$\Delta P = \frac{2\sigma}{R} \tag{3}$$

where R is the radius of the drop or more generally the radius of curvature of the interface for a spherical interface. This expression is found everywhere in the literature and is simply derived by equating the surface-tension force acting along a meridian circumference to a pressure difference times the circular area enclosed by this meridian circumference. If the interface is not spherical, the pressure drop is given by the more general equation

$$\Delta P = \sigma \left(\frac{1}{R_1} + \frac{1}{R_2} \right) \tag{4}$$

3.1.4 Dimensionless Parameters

Dimensionless parameters have been employed in the field of fluid mechanics to describe behavior similarities between systems of different size and to define different behavior regions. For instance, Reynolds number and Rayleigh number define the conditions required to obtain similar flow and convection current characteristics, respectively, in different sized systems, and they also define regimes of different behavior. Other dimensionless parameters that have been found useful in the field of fluid mechanics are Grashof number, Prandtl number, Froude number, Nusselt number, Mach number, etc. These parameters are useful to the theorist in providing an insight into the basic behavior mechanism and useful to the engineer when studying the behavior of full-sized systems through the use of models.

Two dimensionless parameters that are useful in the field of capillarity are Bond number, the ratio of gravitational or acceleration forces to capillary or surface-tension forces, and Weber number, the ratio of pressure or inertia forces to surface-tension forces. These parameters are defined in terms of the physical constants of the system as follows:

$$Bo = \frac{F_a}{F_c} = \frac{Ma}{\sigma L} = \frac{\rho L^3 a}{\sigma L} = \frac{\rho}{\sigma} L^2 a \tag{5}$$

$$We = \frac{F_i}{F_c} = \frac{(\text{Pressure drop})(\text{Area})}{\sigma L} = \frac{1/2\ \rho V^2 L^2}{\sigma L} = \frac{\rho}{\sigma} V^2 L \tag{6}$$

where ρ is the liquid density, L is a dimension characteristic of the system, a is the acceleration imposed on the system (equals 1-g when at rest on Earth), and V is the local flow velocity.

Bond number (Eq. (5)) defines the acceleration or gravity regimes in which either acceleration or capillary forces dominate. For instance, when the Bond number is larger (greater than one) acceleration forces dominate, whereas when the Bond number is small (less than one) the surface-tension forces will be dominant in determining the fluid mechanisms. Bond number should also be useful in predicting the critical acceleration of the liquid gas interface.

Weber number (Eq. (6)) defines the behavior of the interface in the presence of flow forces. When the Weber number is large the flow forces predominate and the capillary forces are insignificant, whereas when the Weber number is small the capillary forces will shape the interface. By rearranging the expression for Weber number an indication of the transition time for zero-gravity phenomena, such as interface formation or wave

period, may be obtained:

$$We = \frac{\rho}{\sigma} V^2 L = \frac{\rho}{\sigma} \left(\frac{L}{T}\right)^2 L = \frac{\rho}{\sigma} \frac{L^3}{T^2} \tag{7}$$

$$T = \left(\frac{\rho}{We\sigma}\right)^{1/2} L^{3/2} \tag{8}$$

The value of Weber number will be empirical depending on the specific configuration.

Reynolds [1] has portrayed the various hydrodynamic regimes as a function of Bond and Weber numbers as shown in Fig. 3, which is taken from his work. A new dimensionless parameter is introduced in this diagram--namely, the Froude number, which is the square root of the ratio of Weber number to Bond number. It defines the boundary between the inertia dominated regime and the acceleration dominated regime. This diagram provides a useful means of visualizing the several hydrodynamic regimes as defined by the several dimensionless parameters.

3.1.5 Effect on Facility Requirements

Several types of zero-gravity facilities have been proposed such as drop towers, airplanes, ballistic rockets, orbiting vehicles, and drops from balloons, helicopters, and canyon bridges. Each of these involves the technique of free fall, or equilibrium with the local gravity field, to obtain a zero-gravity environment. Of these, the drop tower employing a drag shield around a freely-floating experiment, the airplane flown on a ballistic trajectory, and the ballistic rocket have been the most used.

The study of the various aspects of fluid mechanics in zero gravity requires zero-gravity facilities with different characteristics. For

instance, the bubble behavior produced by heat transfer is a high speed phenomenon, and only a short-time facility such as a drop tower is required. On the other hand, if the heat-transfer characteristics in a system are being studied, as in a closed propellant tank, a facility offering several minutes of zero-gravity time is required, such as a ballistic rocket. The study of forced convection mechanics, or the behavior of evaporators or condensers, requires relatively short times such as are available in drop facilities or airplanes. In these studies, the interface is generally so small that small perturbations of the order of a few milli-g's are not important as indicated by the Bond number criterion. In studying the behavior of large liquid vapor interfaces as in models of propellant tanks, however, the acceleration level provided by the facility becomes important as does the initial disturbance. If the zero-gravity time is long enough for the initial disturbance to damp out or be negated by a collection and release maneuver, however, it becomes less of a consideration.

The expressions for Bond and Weber numbers (Eqs. (5) and (6)) can be used to provide an estimate of the zero-gravity time and maximum gravity level allowable in a facility to perform interface studies. A plot of the predicted interface formation time and allowable acceleration or g level as a function of model size is shown in Fig. 4. The allowable acceleration level results from the expression for Bond number using an experimentally determined Bond number near one with L corresponding to the radius. The interface formation time is obtained from the expression for time developed from the Weber number relation using a Weber number of

one and an experimentally determined characteristic length (L). The most significant aspect of Fig. 4 is the low acceleration or g level required for interface experiments in the 2- to 20-inch range (the most desirable model range). This requirement also implies that the initial disturbance shall be low. It is this acceleration and disturbance requirement that has prevented the successful use of airplane facilities for interface experiments even though their 15-second time has been very attractive.

3.2 Interface Configuration

3.2.1 Shape and Location of the Interface

The configuration of the liquid-vapor interface under weightless conditions has been studied analytically by several investigators. Benedikt [2] and Reynolds [1]* have calculated exact solutions for the configuration of the interface between parallel plates as a function of the gravity level or Bond number and, from these calculations and the principles involved, have inferred the configuration of the interface in other geometries. Li [3] has used the principle of the minimization of the free surface energies to predict the interface configuration in many geometries. All these analyses indicate that the interface configuration is primarily dependent on the contact angle and that during weightlessness the liquid vapor interface tends to assume a constant curvature surface that intersects the tank wall at the contact angle.

The results of the calculations for the configuration of the interface between two parallel plates as obtained by Reynolds are presented in Fig. 5. The calculations present the interface configurations for a relatively wetting liquid (contact angle, 10^{o}) and a relatively nonwetting liquid (contact angle, 140^{o}) each at a series of Bond numbers from zero (true weightlessness) to infinity (essentially representative of 1 g). At a Bond number of zero the interface is a surface of constant curvature intersecting the wall at the contact angle. The contact angle determines whether the surface is concave or convex. The increased

*Reynolds indicated that he also found the calculations in the works of Rayleigh.

distortion of the surface from its constant curvature configuration as Bond number increases is apparent.

The results of the calculations for the two-dimensional case may be used to infer the configuration in three-dimensional geometries. Figure 6 shows the predicted configuration for cylinders and for spheres as a function of the contact angle and for the volume fraction of liquid in spheres. These predicted configurations are for a Bond number of zero. Five general configurations are shown for spheres ranging from an imbedded vapor bubble for all fillings at zero-degree contact angle to an imbedded liquid mass for all fillings at the hypothetical contact angle of 180°. The curved line indicates the combination of contact angles and fillings at which the interface is flat as depicted by the center diagram. The diagrams on either side of center are generally representative of the configurations obtained for the combination of contact angles and fillings in the surrounding area. The configurations predicted for cylinders do not show the end effects that would be encountered in tanks with normal ends. For tanks with hemispherical ends, the configurations may be inferred from the configuration for spheres.

Experimental verification of the predicted interface configurations has depended heavily on a suitable zero-gravity facility. The author and his colleagues conducted a series of experiments [4 and 5] in the NASA Lewis Research Center 2.3-second drop-tower facility that verified the predicted configurations. These experiments were conducted using liquids with three different contact angles in spheres, cylinders, and cones at several different fillings. The results for the range of conditions can be represented by Fig. 6; however, photographs of several

interface configurations are shown in Fig. 7. Clodfelter [6] has recently used the 1.85-second drop facility at Wright Field to confirm some of these results and has extended the work to show some interesting end effects in flat-bottomed cylinders.

3.2.2 Separation of Liquid and Vapor

Although the analytical and experimental results indicate that the interface configuration can be predicted for simple containers given the contact angle and ullage volume, the location of the liquid and vapor is often undesirable from the standpoint of reliable pumping and venting. This is especially true for a wetting liquid (typical of most propellants currently being considered) in spherical or nearly spherical tanks, because the location of the vapor bubble is random. Under these conditions reliable pumping and venting cannot be assured, and a substantial portion of the zero-gravity research effort is concentrated on methods of obtaining reliable separation of the liquid and vapor.

3.2.2.1 Acceleration Fields

The method that is in use at the present time is the creation of an acceleration field by the use of ullage rockets. Although this method appears to work well, it becomes heavy if more than a few engine starts or venting cycles are required. Spinning the propellant tank has been proposed as a means of separating liquid and vapor but has not received much serious consideration. The use of an acceleration field to separate liquid and vapor, however, appears practical in the case of liquid separators, in evaporator tubes, and possibly in condenser tubes. In the case of liquid separators, energy from the gas and liquid stream would be used to create a centrifuge action to separate the liquid. In the

evaporator and the condenser tubes, a spiral tape inserted in the tube has been proposed. Evans [7] studied such a geometry by using bubbles in water and found the separation good.

3.2.2.2 Capillary Baffles

The analyses for defining the configuration of the interface indicated a reduction of system energy as the interface changed from its normal gravity configuration to the zero-gravity configuration. It therefore appeared promising to study the ability of tank geometries providing appreciable changes in surface energy to position the liquid and vapor in acceptable configurations. A simple configuration that probably has occurred to most investigators in the field and has been suggested and analyzed by Reynolds [1] is a tube mounted over the pump inlet concentric with the vertical centerline with holes around the bottom to allow fluid transfer between the tank and the tube as shown in Fig. 8(a). An analysis using either surface energy or capillary pressure drop can be made, which shows that a wetting liquid should rise in the tube when the tube diameter is less than one-half of the tank diameter and fall if it is greater than one-half of the tank diameter. This behavior is a positive demonstration of the tendency of the surface energy to minimize [8]. Because of this minimization of the surface energy, the liquid then takes the configuration in weightlessness shown in Fig. 8(b). The liquid is maintained over the area of the pump inlet, while the vapor is maintained in the area of the vent.

The author and his colleagues have studied the performance of this geometry in a series of experiments in the drop tower [8 and 9] and in the MA-7 spacecraft [10]. A desirable characteristic of this geometry

in spheres and to some extent in cylinders is its ability to recapture the liquid following an excessive acceleration disturbance. This effect, which is shown in Fig. 9, shows the results of drop-tower tests in which the standpipe baffle was at various initial angles to the gravity vector. For the 90° test the time available was insufficient to allow complete filling of the baffle. The tendency of the baffle to fill with liquid was also noted at 180°, but again the time was insufficient to allow complete filling of the baffle. The most serious shortcoming of this baffle configuration is its inability to provide reliable positioning of the vapor bubble over the vent if the standpipe is more than 50 percent of the height of the sphere. If the tank is filled to more than 83 percent the resulting ullage bubble will float free [9].

In an effort to overcome the shortcomings of the standpipe design, the geometry shown in Fig. 10 was proposed [9]. This design utilizes a sphere within the spherical tank somewhat offset in the direction of the pump inlet. The action is such that the vapor bubble tends to return to the location (over the vent) where it can become most nearly spherical (which represents the condition of minimum energy) after an excessive acceleration. For a geometry in which the inner sphere is 50 percent of the tank diameter and the offset is 10 percent of the tank diameter, the tank can be filled to 95 percent without the ullage bubble floating feee. The tapering sections provide a stable interface position around the tank as it empties, and the geometry provides an excellent resistance to vapor pull-through during pumping in addition to the capability of complete volume pump-out. By mounting the inner sphere on webs between it and the lower half of the tank, an even stronger pumping geometry is created.

3.2.2.3 Screens

The use of screens has been proposed as a means of trapping a sufficient quantity of propellant over the pump inlet to start the engine. The staff of the Bell Aerosystems Company [11] has made an extensive study of the ability of screens to retain propellants over the pump inlet. In all cases, small mesh screens were employed that were capable of retaining liquids in model tanks in a normal-gravity field. A screen configuration that was studied intensively is shown in Fig. 11 (taken from [11]). When the acceleration is directed normal to the screen as in Fig. 11(a), the screen lies in an equipotential surface of the acceleration field, and the volume trapped behind the screen is equivalent to a closed tube with a screen across the open end. The small mesh screens stabilize the surface while the actual holding force is provided by the ullage gas pressure as shown in the enlarged section. In this configuration a screen with a mesh of approximately 0.1 inch should be capable of retaining liquid against an acceleration equivalent to normal gravity. The ability of screens to retain propellant against transverse vehicle accelerations as shown in Fig. 11(b) is much less than for normal accelerations. This configuration is more analogous to an open tube with a stabilizing screen across one end. In this case, there is a head difference subject to the acceleration that, in turn, sets up a pressure difference that then must be retained by the pressure difference developed across the interface in the screen openings as shown in the enlarged section. The mesh of screens to resist transverse accelerations must be much finer than for normal accelerations because of this differential head.

Two configurations using screens that appear promising are shown in Fig. 12 (taken from the Bell study [11]). Of these the spiral hose design appears more promising because of its ability to achieve complete bubble-free expulsion for any filling of the tank. It is interesting to note that in this configuration the ability to retain propellant against adverse vehicle accelerations is equal for the transverse and axial directions.

Screens do not provide positioning of the vapor bubble over the vent except for very complicated geometries involving multiple screens, which appear to have shortcomings in obtaining complete expulsion. Their main advantage appears to be the ability to resist a higher acceleration disturbance than baffle systems for a given weight.

3.2.2.4 Dielectrophoresis

The principle of dielectrophoresis has been proposed as a means of orienting or positioning the liquid and vapor in the propellant tank. When a dielectric liquid and vapor are placed in a nonuniform electric field the liquid will tend to move into the region of highest field strength. This principle has been well known for some time and can be found in texts on classical electromagnetics. Blackmon [12] has studied the application of the principle to the positioning of liquid in a propellant tank both analytically and experimentally and has demonstrated collection into predicted configurations. The staff of the Bell Aerosystems Company [11] has also made a study of systems employing dielectrophoresis to position liquid in the tank. Their experiments included the measurement of the pressure induced by the electric field, which they found to be variable and not completely predictable. Thus,

while they agreed that liquid could be collected in an electrode system in zero gravity, they could not predict the ability of the system to retain the liquid against a random acceleration. It appeared that the induced pressure inconsistencies may have been due to practical geometry problems causing unwanted field concentrations and to time and temperature variation of the electrical properties of liquids. The conclusions from both investigations were that dielectrophoresis may be a useful effect, but that more knowledge concerning the electrical properties of the liquids and more development is necessary.

3.2.2.5 Temperature Gradient

A physical effect that may be useful in the separation of liquid and vapor during weightlessness makes use of the dependence of surface tension on temperature. The surface tension decreases with temperature until it reaches zero at the critical temperature where the fluid phases and, therefore, the interface are not separately definable. If a vapor bubble is located in a liquid in which there is a temperature gradient, the temperature of the liquid vapor interface will be higher at one pole of the bubble than at the other. Under this situation the liquid in the warmer interface where the surface tension is lower will flow to the region of colder temperature and higher surface tension. This effect constitutes a movement of the vapor bubble from cold to warm regions.

The phenomenon has been studied in experiments by Young, Goldstein, and Block [13] in which bubbles were restrained from rising in a normal-gravity field by a sufficiently high temperature gradient. Their results indicate that although the effect is not normally noticeable at normal gravity because of strong buoyancy effects, it may be useful in or near

zero-gravity conditions. Because the bubbles tend to stay at a warm surface, it may be an unwanted effect in heat-transfer systems.

3.3 Interface Dynamics

The previous discussion has been concerned mainly with the configuration of the interface, the location of the liquid and vapor, and the means of influencing the configuration or location under the condition of no external disturbances to the system. When disturbances such as attitude control accelerations or outflow disturbances are imposed, however, the established interface or fluid configuration will be distorted or disturbed. If the disturbance is sufficiently large, the established interface may break, and the liquid, therefore, will move to a new position. The dynamic behavior of the interface in response to these disturbances is of importance because of its affect on various propellant management problems, such as pumping and venting operations, and on the stability of the attitude control system. It is expected that Bond and Weber numbers will be of significance in describing dynamic behavior because they incorporate the effects of acceleration, inertia, and surface energy.

3.3.1 Interface Formation Time Following a Change in Acceleration Level

One phase of interface dynamic behavior that has been under study is the time required for the interface to form its zero-gravity configuration after release from a normal-gravity or high-acceleration field. Benedikt [14] derived an expression for the oscillation time of an initially deformed freely falling mass of liquid. Functionally his expression is equivalent to the expression for Weber number, and it indicates that the transition time is a function of the ratio of density to surface tension

to the one-half power and of a characteristic dimension of the interface to the three-halves power. It is similar to an expression for the oscillation frequency of a liquid jet issuing from a noncircular hole derived by Rayleigh [15].

The author and his colleagues have conducted drop-tower experiments [16] in which the time required for the interface to form in spheres and cylinders after entering zero gravity was measured, which confirmed the functional relationship suggested by Benedikt. The results of these experiments are presented in Figs. 13 and 14. The formation time given in these experiments is that required for a point on the interface and on the vertical axis of the container to move from the 1-g to the 0-g position as depicted by the small diagrams.

The general expression for formation time as a function of fluid properties and dimensions of the system derived from the Weber number by substituting a length divided by time is rearranged as follows:

$$T = \left(\frac{1}{We}\right)^{1/2}\left(\frac{\rho}{\sigma}\right)^{1/2}(CD)^{3/2} \tag{9}$$

where D is the diameter of the container, C is an empirical constant, and the other symbols are as defined previously. Equation (9) indicates that formation time should vary with $D^{3/2}$ and with $(\rho/\sigma)^{1/2}$. The solid lines on Figs. 13(a) and 14(a) are drawn at a three-halves-power slope. The solid lines on Figs. 13(b) and 14(b) are drawn at a one-half-power slope. In each case the data fit the lines closely, which indicates a good correlation with theory. If a Weber number of one is assumed, then the term CD may be considered the characteristic dimension of the system. For spheres, the value of C was determined at 0.292 and for cy-

inders at 0.277. Although the size range is small as limited by the drop-tower time, good correlation with theory inspires confidence in the use of the Weber number expression to predict the time response in large vehicle tanks.

As part of this program studying the interface formation time, experiments were conducted [8] in which the velocity in capillary tubes was measured. Such information is useful for determining the interface formation time in tanks employing capillary tube baffles such as in Fig. 8. A part of the results of this study is presented in Fig. 15(a) where the variation of height of the liquid in the capillary tube with time in zero gravity is given for several tube diameters. The tank diameter for these experiments was 7 centimeters. The solid lines are analog computer solutions of the equation

$$\ddot{Z} = \frac{\frac{2\sigma \cos\theta}{\rho}\left(\frac{1}{R_c} - \frac{1}{R_t - R_c}\right) - \frac{1}{2} K\dot{Z}^2 - \frac{8\nu(l_t + Z)}{R_c^2}\dot{Z}}{\left(1 - \frac{A_t^2}{A_a^2}\right)Z + l_t + \frac{A_t}{A_c} l_c + \frac{A_t}{A_a} l_a} \qquad (10)$$

for liquid rise as a function of time. A schematic drawing showing the system geometry from which Eq. (10) was derived is shown in Fig. 15(b). This equation was derived from Newton's fundamental force-mass relation and accounts for forces due to surface tension, entrance losses, and friction drag. This equation involves no empirical constants and can be evaluated from the physical constants of the system with the exception of the constant K applied to the entrance loss term, which is calculated by approximate means. In the solutions shown in Fig. 15(a) this

constant was taken as 2.28, as calculated by Langhaar [17] for the entrance loss to viscosimeter tubes.

The correlation of the data with the analysis was found to be satisfactory for variations in tube diameter and initial height of liquid in the tube. The degree of correlation indicates that Eq. (10) incorporates the principal physical phenomena and is useful for calculating the velocities and displacements in capillary systems in zero gravity.

3.3.2 Interface Behavior During Outflow Disturbance

A large portion of the zero-gravity research work has been given to the determination of means of assuring that liquid is located over the pump inlet prior to engine starting. Comparatively little work has been devoted, however, to a study of the effect of the outflow disturbance on the interface nearest to the outlet. There is an almost complete absence of literature reporting either analytical or experimental studies of the phenomena. A recent paper by Povitskii and Lyubin [18] has analyzed the velocity along the free surface of the interface as affected by outflow velocity. The results of their analysis indicates that for liquid depths greater than the diameter of the outlet tube, the free surface is not appreciably disturbed beyond a diameter corresponding to four times the depth.

Because the outflow velocity creates a velocity gradient in the liquid above the outlet that appears to carry through to the interface, it is expected that the Weber number may be the scaling relation useful in relating the distortion of the interface between various system sizes. For more severe velocity gradients and greater distortions, however, the

viscosity may have an effect so that the Reynolds number may also be required to properly scale the phenomena.

Nussle [19] has conducted outflow experiments under zero-gravity conditions in the drop tower to study the behavior of the interface under this disturbance and to attempt to determine a scaling parameter. At the present time experiments have been conducted only with flat-bottom cylinders and with initial liquid depths greater than one tank diameter. However, three ratios of outlet diameter to tank diameter, a size range from two centimeters to 16 centimeters diameter, and the effect of baffles at the liquid outlet and gas inlet have been studied.

Photographs of the behavior of the interface during outflow under zero-gravity are presented in Fig. 16(a) for the condition of a high outlet velocity and no baffles. It will be noted that although the outlet velocity is relatively high, the interface does not distort sufficiently to permit vapor blow-through until it is relatively close (one or two diameters of the outlet tube) to the bottom. The interface does distort considerably from the hemispherical equilibrium zero-gravity configuration with the result that considerable liquid is left on the walls at blowthrough. Also the interface shows considerable wave distortion apparently from the impingement of the inlet gas.

Schematic diagrams of the configuration of the interface at the moment of vapor blow-through are presented in Fig. 16(b) for a range of outflow velocities and for several inlet and outlet baffle combinations. These diagrams show that as the outflow velocity is increased, more liquid is left on the walls of the tank. The addition of the outlet baffle to direct the flow streamlines along the tank wall provides some

improvement but not as much as might be expected. The use of a crude baffle over the gas inlet provides more improvement than might be expected indicating that the impingement of the inlet gas is a primary cause of interface distortion. The combination of inlet and outlet baffles results in reducing the amount of liquid remaining on the wall almost to the amount left at low outflow velocities.

One of the objectives of these studies was to determine the effect of such parameters as outlet velocity, ratio of outlet diameter to tank diameter, and absolute tank size on the interface distortion to enable prediction of allowable outlet velocities for a nominal interface distortion in full size vehicles. The results of these efforts are presented in Fig. 17 where interface velocity on the tank centerline (which when compared with the average interface velocity is a measure of the distortion) is plotted as a function of outflow velocity for several ratios of outlet to tank diameter and a range of tank sizes from 2 to 16 centimeters diameter. These experiments were run with a gas inlet baffle but no outlet baffle. Although the distortion of the interface does increase with average interface velocity, it is not severe even at very high average interface velocities. The average interface velocities in full size vehicles are in general less than 10 cm/sec. The effect on interface distortion of the ratio of outlet to tank diameter appears only in its effect on average interface velocity. The most surprising result is that although the tank size was varied over an 8:1 range no effect of size can be discerned. The results of these studies indicate therefore that no particular difficulties with

interface distortion should be encountered in full-sized tanks for liquid depths equal to a tank diameter or greater. Data at low liquid depths are not yet available although it appears from Fig. 16(b) that simple baffles will satisfactorily solve any problems of vapor blow-through.

3.3.3 Interface Behavior During Acceleration Disturbance

There are a number of acceleration disturbances that will occur in connection with the operation of space vehicles such as those resulting from attitude control system operation, crew movements, docking jolts, and atmospheric drag. The acceleration perturbation may be intermittent as in the case of attitude control operation or steady as in the case of drag or of liquid collection by thrust preparatory to engine starting. These disturbances will occur at all angles to the vehicle thrust axis and will tend to move the liquid opposite (relative to the tank) to the direction of the acceleration. The surface-tension forces give the interface the ability to resist or be stable to a certain amount of acceleration, which is expected to be defined by the Bond number criterion (the ratio of acceleration to surface-tension forces). The study of interface behavior in response to acceleration disturbances may be divided for convenience into two phases, one for acceleration disturbances less than, and one for disturbances greater than a critical value at which the stability limit of the interface is exceeded.

There is a great deal of literature starting with Maxwell in 1890 and continuing with the contributions to hydrodynamics by Lamb and the contributions to surface stability by Taylor that can be applied to the definition of the behavior in response to acceleration perturbations. A great amount of it deals with the situation in which the acceleration is directed perpendicular to the interface from the less-dense to the more-dense fluid. The classical approach to the problem of hydrostatic stability has consisted in examining the character of the solution of the equations of disturbances applied to the interface. If the exponents of the series solution are pure imaginary, the disturbed interface will oscillate in time, and the undisturbed state of the interface is considered stable. If the exponents are real, the disturbance is unbounded in time, and the undisturbed state is considered unstable. The required boundary condition is a fixed contact angle at the wall. In the case of disturbed equilibrium, this leads algebraically to the usual criterion of minimum potential energy as a necessary condition for stability. Variational techniques have been used in minimizing the sum of the gravitational and free-surface potentials subject to the constraint of constant liquid volume. The resultant Euler differential equation is solved con-

Preceding page blank

sistent with the required boundary conditions. The solutions are necessarily approximate, largely because of the nonlinearity of the differential equations and the difficulty encountered with a rigorous mathematical formulation for a 0° contact-angle boundary condition.

These analyses have been primarily interested in studying the dynamics of the interface and have, in the course of these studies, determined the stability limit of the interface--that is, the value of the acceleration at which the interface will break. As noted, this point is expected to be defined by Bond number, and the value obtained is called the critical Bond number. The various analyses in the literature quote values of critical Bond numbers from 0.15 to the value of 14.68 obtained by Maxwell. Recently, Masica [20] measured the critical Bond number in cylindrical tubes using the normal gravitational field as the acceleration disturbance. Part of his results are shown in Figs. 18 to 20 for different orientations of the acceleration field and position of the interface relative to the edge of the tube. The critical diameter is shown as a function of the specific surface tension σ/ρ. The left axis intercept of the solid line approximating the data is proportional to the critical Bond number and is computed as follows using Fig. 18 as an example. The equation of the solid line that is drawn at a slope of one-half is, after converting the critical diameter to centimeters,

$$D = 0.184 \left[\frac{\sigma}{\rho a(0.01)}\right]^{1/2} \tag{11}$$

When arranged in the form of the Bond number expression (Eq. (5)) and substituting the radius for the diameter, Eq. (11) becomes

$$\left[\frac{0.184}{(2)(0.1)}\right]^2 = \frac{\rho}{\sigma} aR^2 = 0.84 = Bo_{critical} \qquad (12)$$

The Bond number (based on a radius) of 0.84 agrees with the value obtained analytically by Bretherton [21] and that obtained experimentally by Hattori [22] for this configuration and acceleration direction. A variation in Bond number depending on the specific surface tension was observed for the situation in which the acceleration was directed normal to the axis of the cylinder as shown in Fig. 19. The value was 1.12 for specific surface tensions less than 43 cm^3/sec^2 and 2.53 for specific surface tensions greater than 43 cm^3/sec^2. For the configuration in which the liquid was at the edge of the tube as shown in Fig. 20, a strong edge effect was noted in that the Bond number was 3.37.

In these experiments the specific surface tension was varied over a 6:1 range, thus establishing its functional relationship in the Bond number expression. The experiments were performed, however, with only one acceleration disturbance--that of the normal gravitational field. Masica [23] has recently extended these studies in the drop tower to include acceleration fields equivalent to one-tenth and one one-hundredth that of normal gravity for the configuration of Fig. 18. Acceleration forces on the container and gravitational body forces on the liquid were treated as equivalent. The results of these experiments are presented in Fig. 21. These data fit an extension at the same slope of the solid line in Fig. 18 and establish the functional relationship of acceleration in the Bond number expression.

The results of these experiments can be used to predict the critical acceleration for the interface in large vehicle propellant tanks. Fig-

ure 22 presents the critical acceleration in g's as a function of tank diameter in inches for a specific surface tension of 28.28 cm^3/sec^2, which is representative of many propellants. The data obtained at one, one-tenth, and one one-hundredth g are shown. The critical acceleration for vehicles of 100 to 400 inches in diameter is indicated as 10^{-6} to 10^{-7} g's.

Accelerations less than the critical value may be encountered in situations of low residual atmospheric drag or solar pressure or from attitude control disturbances or crew movements. Residual drag or solar pressure will result in a continuous acceleration which will distort the interface in a generally predictable manner. The operation of attitude controls or crew movements however cause intermittent acceleration perturbations which may set up an oscillation of the interface. In high gravitational or acceleration fields (high Bond numbers) the frequency of oscillation is determined by the gravitational or acceleration forces. In a zero-gravity environment (zero Bond number) the surface tension forces are the only remaining restoring forces and determine the frequency. The damping of these oscillations is dependent on the viscosity for both high and low Bond number situations. It will be important to avoid these frequencies in attitude control systems.

There is an extensive literature concerning the dynamics of free surfaces but only for the condition of an unbounded surface or where contact angle effects can be ignored. Satterlee and Reynolds [24] have calculated the natural frequency of the surface at low Bond numbers for several contact angles and have obtained some experimental verification (best at low contact angles) of their analysis. Their results are

presented in terms of a dimensionless frequency parameter which is a linear function of the Bond number and has a finite value at zero Bond number.

For the situation in which an acceleration greater than the critical value is applied along the axis of the tank from the vapor to the liquid, as when the drag exceeds the critical value of the interface, or during collection maneuvers, the work of Taylor [25], Bretherton [21], Hattori [22], and Goldsmith and Mason [26], which are studies of the motion of a bubble which fills the tube, can be applied. The results of some of these studies defining the velocity of the interface as a function of Bond number are given in Fig. 23 together with some data by Masica for high Bond numbers at 1-g and for low gravitational values. The data shown tend to establish the functional relationship of the acceleration, the specific surface tension, and the size in the relation of the interface velocity parameter and Bond number. The results of these experiments can be used to predict the velocity, on the tank axis, of the penetration of the ullage vapor into the liquid during a collection thrust and thus allow a rough prediction of the time for vapor to reach the "top" of the tank for a situation in which the tank is partly full. No work is apparent as yet on the behavior of the liquid as it gathers in the "bottom" of the tank.

3.4 Heat Transfer

There has been a great deal of interest in the change in the heat-transfer mechanism in a weightless environment. The mechanism of heat input to a tank under space conditions corresponds to that of a classical pool-boiling situation, the various regions of which are shown in Fig. 24 for a 1-g field. The coordinates are heat flux plotted as a function of temperature difference.

Reproduced from best available copy.

The heat-transfer regions start with conduction at very low flux, and, as flux is increased, progress through convection and nucleation, and finally, at very high flux, progress to the mechanism of film boiling. The regions of convection and nucleation may be substantially affected by the loss of gravity. Convection currents should certainly be absent in a zero-gravity environment, although residual currents may persist for some time. The nucleation regime may be markedly affected by changes in the gravity field because of the dependence of bubble velocity on buoyancy. If the velocity becomes zero because of loss of buoyancy, the nucleation region may be replaced by a film mechanism of boiling. This situation would be predicted by the Rohsenow [27] nucleation concept, which is gravity dependent. A nucleation model has been proposed by Forster and Zuber [28] that may be independent of gravity in that bubbles are removed from the surface by a flow field set up around the bubble because of its rate of expansion. If this model is correct, the nucleation region should be relatively unaffected by a zero-gravity environment and would probably extend down to cover the convection region. Siegel [29] performed the first low-gravity experiments studying the pool boiling mechanism under several gravity fields from essentially zero to one. He was primarily interested in studying photographically the change in ebullition and vapor removal. During a discussion of his paper [30] presented to the ASME, he stated that in the nucleation regime he noted no change in the temperature difference obtained at a given heat flux, which tends to support the nucleation concept that is independent of gravity.

A series of experiments using liquid hydrogen has been performed by General Dynamics/Astronautics [31] in which the heat transfer in the

Preceding page blank

nucleate range as a function of temperature difference was measured at 1-g and 0-g conditions. Results of this study are shown in Fig. 25. These results indicate that zero gravity has little effect on heat transfer in the nucleate region, which supports the nucleation model that is independent of gravity. The experiments by Merte and Clark [32] using liquid nitrogen and by Clodfelter [33] have also tended to support the nucleation concept that is independent of gravity.

The primary effect of the heat-transfer mechanism that is of interest in space vehicle propellant tank systems is the pressure rise within the container. This pressure rise is difficult to calculate because of the uncertainty in the liquid configuration, the variation in the direction of the radiant heat source, and the uncertainty about the heat-transfer mechanisms that may apply to the liquid and vapor portions of the tank even though the mechanism in the liquid seems reasonably well established. In comparing pressure rise data at 1-g and 0-g, it has been found convenient to compare the actual pressure rise with that which can be calculated by making several different assumptions about the heat distribution within the tank. The position that experimental data assumes in relation to the theoretical models on a pressure against heat added plot is then an indication of how the energy is being distributed within the tank. Figure 26 is a plot of pressure against heat added for three theoretical models. The first model assumes homogeneous conditions thoughout the tank and is a common calculation that is performed to compare data of this type. The second model assumes that all of the energy absorbed by the dewar goes into the evaporation of liquid with the vapor phase temperature always being equal to the saturation temperature corresponding to sphere pressure

and the liquid phase temperature remaining constant at the saturation temperature corresponding to seal-off pressure. The third model is a practical upper limit on the pressure against heat added plot much as the homogeneous model is the lower limit. The third model assumes that all the energy is delivered to the vapor phase with no energy transfer at the liquid-vapor interface so that the vapor becomes superheated.

There are two important factors that would be expected to cause a different rate of pressure rise in a storage tank when normal gravity quiescent and zero-gravity tests are compared. The first factor is the change in configuration, or position of the liquid and vapor within the storage tank. As shown in Fig. 6, for a half-filled spherical tank the normal-gravity configuration has the interface bisecting the tank, while the zero-gravity configuration has a spherical interface with the tank walls totally wetted and the vapor bubble randomly located in the interior of the tank. The second factor affecting the rate of pressure rise in a storage tank is the reduction in buoyancy and convection due to the reduction in the gravity field.

For a normal-gravity test only part of the storage tank is covered with liquid so that a large amount of the heat that is added goes directly into the vapor phase. This heating of the vapor causes it to become superheated. Some of the hot vapor will come in contact with the liquid-vapor interface causing evaporation from the surface. The energy that enters the storage tank through the liquid wetted walls goes into forming bubbles and superheating the liquid in a thin layer directly adjacent to the wall. Convection currents will carry the hot liquid to the surface where evaporation takes place, and buoyancy will cause the bubbles to

rise rapidly to the liquid-vapor interface and join the vapor space. Because the bubbles rise rapidly through the liquid there is little condensation and consequently little heating of the liquid. The surface evaporation model is based on the assumption that all of the added heat goes into evaporating liquid with no heating of the remaining liquid. Consequently, depending on the heat-transfer rate and distribution, it would be expected that experimental normal-gravity quiescent pressure rise data would be clustered around the surface evaporation model theoretical line. It would also be expected that high heat-transfer rates or heating only from the top of the tank would cause faster pressure rises than the model predicts, and that low heat-transfer rates or heating only from the bottom of the tank would cause lower pressure rises than the model predicts.

Initially during a zero-gravity test the walls of a spherical storage tank would be liquid wetted. Consequently, in contrast to the normal-gravity quiescent test, there will be no direct heating of the vapor phase, and the bubbles that form on the wall of the tank will be faced with some depth of liquid to penetrate in order to reach the vapor space. The bubbles will pinch off the wall due to dynamic forces that, for most cryogenic liquids, are much greater than buoyant forces even under normal-gravity conditions. Because of the absence of gravitational forces, it is expected that the bubbles will tend to drift rather slowly in the subcooled liquid and condense, thus giving their energy to the liquid. A nearly homogeneous condition should be the result.

There are many zero-gravity configurations that will not have totally wetted tank walls due to tank geometry, internal baffles, and the use of ullage control rockets. Also, in spheres and other normally totally

wetted configurations, the possibility exists that the vapor bubble may drift to one side of the tank. If the evaporation rate is higher than the rate at which the surface can be rewetted, a dry spot will appear and grow until the evaporation balances the inflow of liquid. Under these conditions there will again be direct heating of the vapor and higher rates of pressure rise must be expected.

The majority of the experimental work, being performed at Lewis Research Center in support of the prediction of the thermodynamic history of storage tanks containing liquid propellants, is being carried out using 9-inch-diameter dewars containing liquid hydrogen. The affect on the rate of pressure rise of several experimental variables, including the use of internal baffles, the heat flux rate and distribution, and the initial percent filling, is being explored. Rocket vehicles are being used to obtain several minutes of low-gravity environment. The experimental results of the ground tests and flights are classified confidential and are reported in references 34 to 40.

3.5 Evaporation and Condensation

The free liquid-vapor interfaces in evaporators and condensers have not contributed to operational and performance problems as they have in the tanks of other systems. This is due to the small diameter of tubes used in evaporators and condensers (usually less than 1/2 in.), which according to the Bond number criterion makes them stable to accelerations of 0.03 g or more for the smaller tubes (0.1 g for 5/16-in. tube). Acceleration perturbations of this magnitude will not ordinarily be in the operating spectrum of the vehicle except when under boost thrust, which will permit normal operation of the system.

Because forced convection will exist in evaporators and condensers designed for minimum weight, it is unlikely that there will be any appreciable change in the heat-transfer mechanism. The possibility of generation of bubbles within the liquid in the evaporator or the inclusion of vapor in the liquid in the condenser was originally of some concern; however, the reasonably large stability of the interface and the use of counterflow heat exchangers to provide subcooling below the interface and a temperature gradient to move bubbles toward the interface has virtually eliminated these problems. Also Evans [7] has shown that either a spiral wire or a twisted tape in a tube will centrifuge liquid to the outside and increase the separation stability margin. These configurations are permissible in evaporator tubes where the pressure drop they impose has only a small effect on cycle efficiency.

Although it appears that the interface in an individual tube will have, or can be provided with, a reasonable degree of stability, there is still the problem of stability of the interface level between individual tubes in the face of acceleration perturbations from directions other than on the tube axis and directed from the liquid to the vapor. The forces available to counteract this change in level are the changes in pressure drop within the tube with change in level (condensing length) and the change in surface-tension force if the tubes are tapered and if the liquid wets the wall. However, the magnitude of the surface-tension forces are very small for practical tube sizes and tapers, which leaves the pressure drop as the main stabilizing parameter. In the evaporator where the working pressure is high, it is practical to design with a reasonable pressure drop thus providing a satisfactory ability to resist

adverse accelerations. Even so, the dimensions of the evaporator normal to the tube bundle axis should be kept as small as possible to minimize the head that must be resisted by change in pressure drop for accelerations normal to the tube axis. The situation is similar to that described for screens in propellant tanks.

The position of the condenser in the cycle does not allow as much generosity with design pressure drop as in the evaporator without serious effect on the efficiency. Thus, a substantial portion of the zero-gravity research concerned with condensers has been concentrated on the pressure-drop characteristics. The correlation that has been used for two-phase pressure drop at normal gravity is the Lockhart-Martinelli correlation [41], which involves the Reynolds number and thus the viscosity. Reynolds [1] has proposed that the effects of surface-tension be introduced into two-phase pressure-drop correlations for use at zero gravity. In his analysis, surface tension effects are introduced by assuming that the friction drag is proportional to the size of condensed droplets adhering to the wall, which increases the tube roughness. The assumption of wall bound droplets is in keeping with the tendency for the surface energy to minimize.

Most of the actual zero-gravity data obtained to date has been concerned with observation of droplet and interface behavior and only qualitative measurement of the pressure drop. No effort is apparent in the literature as yet to systematically study the pressure drop in zero gravity as a function of the various parameters and to attempt a correlation with theory. The Lewis Research Center is conducting an experimental

study (using an airplane as a zero-gravity facility) of the pressure drop in condensers with mercury as the working fluid in which several parameters are varied. This study is incomplete, but preliminary results indicate that the pressure drop in zero gravity is slightly but consistently higher than the pressure drop under normal gravity. The pressure drop in these experiments is somewhat higher than predicted by the Lockhart-Martinelli correlation at low velocities but corresponds well at high velocities.

4. CONCLUDING REMARKS

This paper has reviewed the analytical and experimental research directed toward the solution of the problems encountered with liquid-vapor systems in weightlessness and has presented the results of some recent experimental work studying the correlation of certain aspects of the dynamic behavior of the interface with the applicable dimensionless scaling parameters. The various problems encountered in the liquid-vapor systems were grouped into the categories of interface configuration, interface dynamics, pool boiling heat-transfer mechanisms, and evaporation and condensation phenomena.

The greatest portion of weightlessness research up to this time has been devoted to studies of the parameters defining the configuration and position of the liquid-vapor interface under the conditions of no external disturbances. The theoretical background is now extensive and has been verified by experiments. At the present time most of the work in this category is more of a development nature devoted to the application of the principles to systems to provide and maintain proper separation and orientation of liquid and vapor.

With the better understanding of the configuration and position of the interface, more attention has recently been given to the dynamic behavior of the interface. It has been found that a great deal of theoretical work dealing with fluid dynamics is applicable to zero-gravity interface behavior. A sizeable amount of experimental work verifying the theory has been performed, but a great deal (both analytical and experimental) remains to be done--especially that applicable to interface dynamics in response to

acceleration perturbations (attitude controls, docking jolts, etc.) and outflow disturbances.

A great deal of interest has been shown in the change in the heat-transfer mechanism with reduction in gravity or acceleration level. The resulting studies have approached the problem in several ways by studying the fundamental bubble mechanics, by measuring the heat flux as a function of differential temperature input, and by measuring the pressure rise in a closed system. Attempts have been made to correlate the results with existing heat-transfer theory. Although some understanding has been gained, a great deal of work remains in the area of understanding fundamental bubble mechanics.

Solutions for some of the evaporator and condenser liquid-vapor interface problems have become evident from the interface configuration and dynamics studies. The most work at the present time is concentrated on studies of the pressure drop in condensers because it is important to the efficiency of the system and to the tube-to-tube stability. Very little experimental results are available at the present time.

APPENDIX

SYMBOLS

A	area
A_a	annulus area
A_t	capillary tube area
a	acceleration
Bo	Bond number
C,K	constants
D	diameter
F	force
F_a	acceleration force
F_c	capillary force
F_i	inertia force
Fr	Froude number
L	characteristic length
l_a	initial height of liquid in annulus
l_c	length of connecting passage between capillary tube and annulus
l_t	initial height of liquid in capillary tube
M	mass
P	pressure
q	heat flux
R	radius
R_c	radius of capillary tube
R_t	radius of tank
T	time

V	velocity
We	Weber number
Z	liquid rise in capillary tube
θ	contact angle
ν	viscosity
ρ	liquid density
σ_{ls}	surface energy of liquid-solid interface
σ_{vl}	surface energy of vapor-liquid interface
σ_{vs}	surface energy of vapor-solid interface

REFERENCES

1. Reynolds, William C.: Hydrodynamic Considerations for the Design of Systems for Very Low Gravity Environments. Rep. LG-1, Stanford Univ., Sept. 1961.
2. Benedikt, E. T.: Epihydrostatics of Liquids in Vertical Tanks. Rep. ASG-TM-61-48, Norair Div., Northrop Corp., June 1961.
3. Li, Ta: Hydrostatics in Various Gravitational Fields. Jour. Chem. Phys., vol. 36, no. 9, May 1, 1962, pp. 2369-2375.
4. Petrash, Donald A., Zappa, Robert F., and Otto, Edward W.:, Experimental Study of the Effects of Weightlessness on the Configuration of Mercury and Alcohol in Spherical Tanks. NASA TN D-1197, 1962.
5. Petrash, Donald A., Nussle, Ralph C., and Otto, Edward W.: Effect of Contact Angle and Tank Geometry on the Configuration of the Liquid-Vapor Interface During Weightlessness. NASA TN D-2075, 1963.
6. Clodfelter, Robert G.: Fluid Mechanics and Tankage Design for Low-Gravity Environment. Rep. ASD-TDR-63-506, Air Force System Command, Wright-Patterson Air Force Base, Sept. 1963.
7. Evans, David G.: Visual Study of Swirling and Nonswirling Two-Phase Two-Component Flow at 1 and 0 Gravity. NASA TM X-725, 1963.
8. Petrash, Donald A., Nelson, Thomas M., and Otto, Edward W.: Effect of Surface Energy on the Liquid-Vapor Interface Configuration During Weightlessness. NASA TN D-1582, 1963.
9. Petrash, Donald A., and Otto, Edward W.: Controlling the Liquid-Vapor Interface Under Weightlessness. AIAA Jour., vol. 2, no. 3, Mar. 1964, pp. 56-61.

10. Petrash, Donald A., Nussle, Ralph C., and Otto, Edward W.: Effect of the Acceleration Disturbance Encountered in the MA-7 Spacecraft on the Liquid-Vapor Interface in a Baffled Tank During Weightlessness. NASA TN D-1577, Jan. 1963.

11. Chipchak, D., et al.: Development of Expulsion and Orientation Systems for Advanced Liquid Rocket Propulsion Systems. Rep. RTD-TDR-63-1048, Bell Aerosystems Co., July 1963.

12. Blackmon, J. B.: Propellant Orientation in Zero Gravity with Electric Fields. Paper presented at IAS meeting, New York (N.Y.), Jan. 21-23, 1963.

13. Young, N. O., Goldstein, J. S., and Block, M. J.: The Motion of Bubbles in a Vertical Temperature Gradient. Jour. Fluid Mech., vol. 6, pt. 3, Oct. 1959, pp. 350-356.

14. Benedikt, E. T.: General Behavior of a Liquid in a Zero and Near Zero Gravity Environment. Rep. ASG-TM-60-9Z6, Norair Div., Northrop Corp., May 1960.

15. Rayleigh: On the Capillary Phenomena of Jets. Proc. Roy. Soc. (London), vol. 29, no. 196, May 15, 1879, pp. 71-97.

16. Siegert, Clifford E., Petrash, Donald A., and Otto, Edward W.: Time Response of Liquid-Vapor Interface After Entering Weightlessness. NASA TN D-2458, Aug. 1964.

17. Langhaar, H. L.: Steady Flow in the Transition Length of a Straight Tube. Jour. Appl. Mech., vol. 9, no. 2, June 1942, pp. A-55 - A-58.

18. Povitskii, A. S., and Lyubin, L. Ya.: Emptying and Filling Vessels in Conditions of Weightlessness. Planetary and Space Sci., vol. 11, no. 11, Nov. 1963, pp. 1343-1359.

19. Nussle, Ralph C., Derdul, Joseph D., and Petrash, Donald A.: Photographic Study of Propellant Outflow from a Cylindrical Tank During Weightlessness. NASA TN D-2572, Jan. 1965.

20. Masica, William J., Petrash, Donald A., and Otto, Edward W.: Hydrostatic Stability of the Liquid-Vapor Interface in a Gravitational Field. NASA TN D-2267, 1964.

21. Bretherton, F. P.: Motion of Long Bubbles in Tubes. Jour. Fluid Mech., vol. 10, pt. 2, Mar. 1961, pp. 166-188.

22. Hattori, Sin-Iti: On the Motion of a Cylindrical Bubble in a Tube and Its Application to the Measurement of the Surface Tension of a Liquid. Rep. 115, Aero. Res. Inst., Tokyo Imperial Univ., 1935.

23. Maisa, William J., Derdul, Joseph D., and Petrash, Donald A.: Hydrostatic Stability of the Liquid-Vapor Interface in a Low-Acceleration Field. NASA TN D-2444, Aug. 1964.

24. Satterlee, H. M., and Reynolds, W. C.: Dynamics of the Free Liquid Surface in Cylindrical Containers Under Strong Capillary and Weak Gravity Conditions. Rep. LG-2, Stanford Univ., May 1, 1964.

25. Davies, R. M., and Taylor, Geoffrey: The Mechanics of Large Bubbles Rising Through Extended Liquids and Through Liquids in Tubes. Proc. Roy. Soc. (London), ser, A, vol. 200, no. 1062, Feb. 1950, pp. 375-390.

26. Goldsmith, H. L., and Mason, S. G.: Movement of Single Large Bubbles in Closed Vertical Tubes. J. Fluid Mech., vol. 14, Sept.-Dec. 1962, pp. 42-58.

27. Rohsenow, W. M.: A Method of Correlating Heat-Transfer Data for Surface Boiling Liquids. Trans. ASME, vol. 74, no. 6, Aug. 1952, p. 969

28. Forster, H. K., and Zuber, N.: Growth of a Vapor Bubble in a Superheated Liquid. Jour. Appl. Phys., vol. 25, no. 4, Apr. 1954, pp. 474-478.

29. Siegel, R., and Usiskin, C. M.: A Photographic Study of Boiling in the Absence of Gravity. Jour. Heat Transfer (Trans. ASME), ser. C, vol. 81, no. 3, Aug. 1959, pp. 230-236.

30. Usiskin, C. M., and Siegel, R.: An Experimental Study of Boiling in Reduced and Zero Gravity Fields. Jour. Heat Transfer (Trans. ASME), ser. C, vol. 83, no. 3, Aug. 1961, pp. 243-251; discussion, pp. 251-253.

31. Sherley, J. E., and Merino, F.: Zero-G Program. Final Rep. AY62-0031, from May 1960 to Mar. 1962, General Dynamics/ Astronautics, Aug. 15, 1962.

32. Merte, H. Jr., and Clark, J. A.: Pool Boiling in an Accelerating System. Jour. Heat Transfer (Trans. ASME), ser. C, vol. 83, no. 3, Aug. 1961, pp. 233-242.

33. Clodfelter, Robert G.: Low-Gravity Pool-Boiling Heat Transfer. Rep. APL-TDR-64-19, Air Force Systems Command, Wright-Patterson Air Force Base, March 1964.

34. Knoll, Richard H., Smolak, George R., and Nunamaker, Robert R.: Weightlessness Experiments with Liquid Hydrogen in Aerobee Sounding Rockets; Uniform Radiant Heat Addition - Flight I. NASA TM X-484, June 1962.

35. McArdle, Jack G., Dillon, Richard C., and Altmos, Donald A.: Weightlessness Experiments With Liquid Hydrogen in Aerobee Sounding Rockets; Uniform Radiant Heat Addition - Flight 2. NASA TM X-718, Dec. 1962.

36. Nunamaker, Robert R., Corpas, Elias L., and McArdle, Jack G.: Weightlessness Experiments With Liquid Hydrogen in Aerobee Sounding Rockets; Uniform Radiant Heat Addition - Flight 3. NASA TM X-872, Dec. 1963.

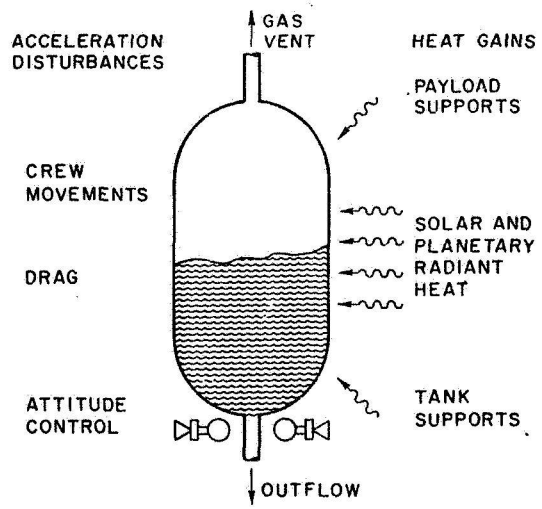
37. Regetz, John D., Jr., Conroy, Martin J., and Jackson, Robert G.: Weightlessness Experiments With Liquid Hydrogen in Aerobee Sounding Rockets; Nonuniform Radiant Heat Addition - Flight 4. NASA TM X-873, Feb. 1964.

38. Abdalla, Kaleel L., Flage, Richard A., and Jackson, Robert G.: Zero-Gravity Performance of Ullage Control Surface With Liquid Hydrogen While Subjected to Unsymmetrical Radiant Heating. NASA TM X-1001. Aug. 1964.

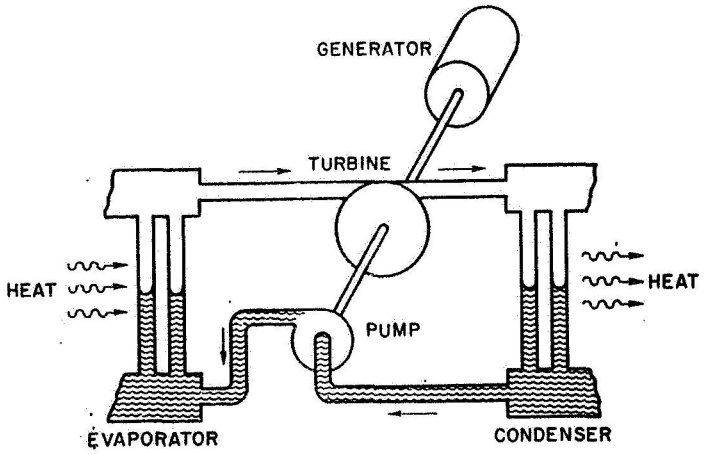
39. Aydelott, John C., Corpas, Elias L., and Gruber, Robert P.: Comparison of Pressure Rise In A Hydrogen Dewar For Homogeneous, Normal-Gravity Quiescent, and Zero-Gravity Conditions - Flight 7. NASA TM X-1006, Sept. 1964.

40. Aydelott, John C., Corpas, Elias L., and Gruber, Robert P.: Comparison of Pressure Rise in a Hydrogen Dewar for Homogeneous, Normal-Gravity Quiescent, and Zero-Gravity Conditions - Flight 9. NASA TM X-1052, 1965.

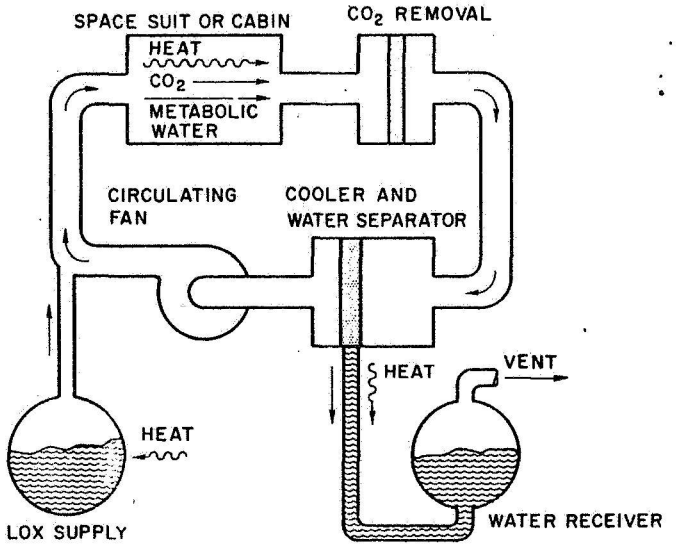
41. Lockhart, R. W., and Martinelli, R. C.: Proposed Correlation of Data for Isothermal Two-Phase, Two-Component Flow in Pipes. Chem. Eng. Prog., vol. 45, no. 1, Jan. 1949, pp. 39-45; discussion, pp. 45-48.



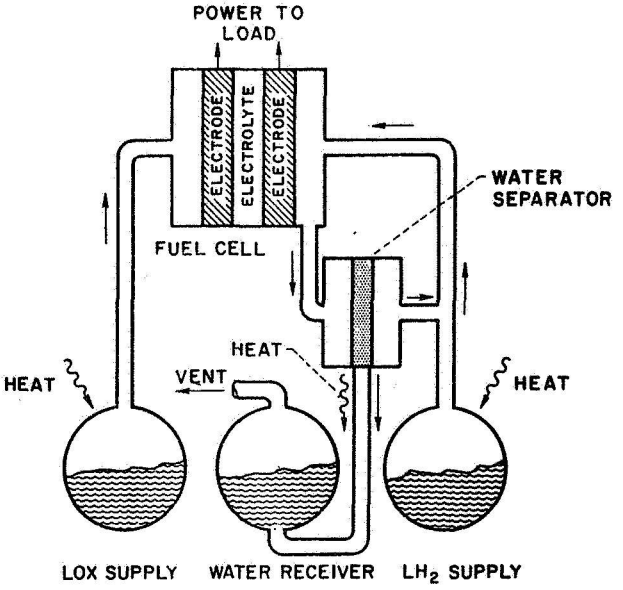
(a) Propellant tank system.



(b) Space power systems.



(c) Life support systems.



(d) Fuel cell systems.

Figure 1. - Fluid management problems in space vehicle systems.

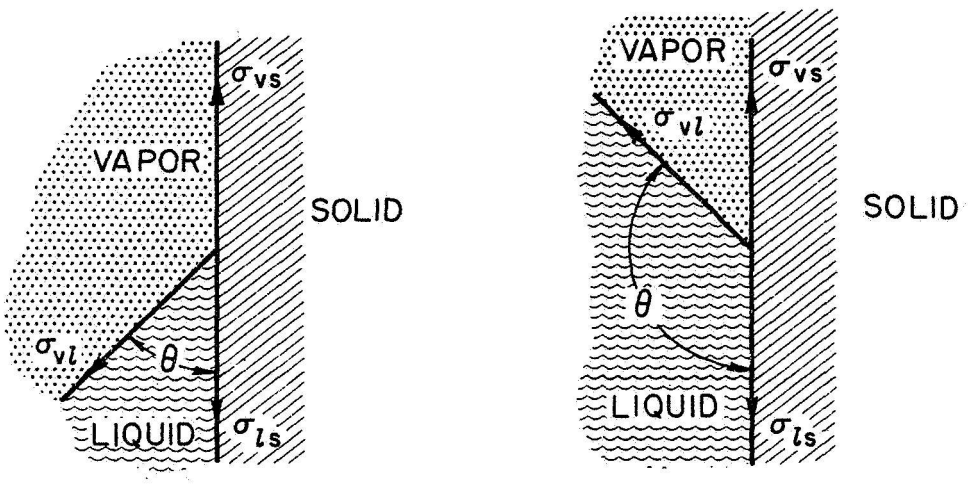


Figure 2. - Surface energy and contact angle relationship.

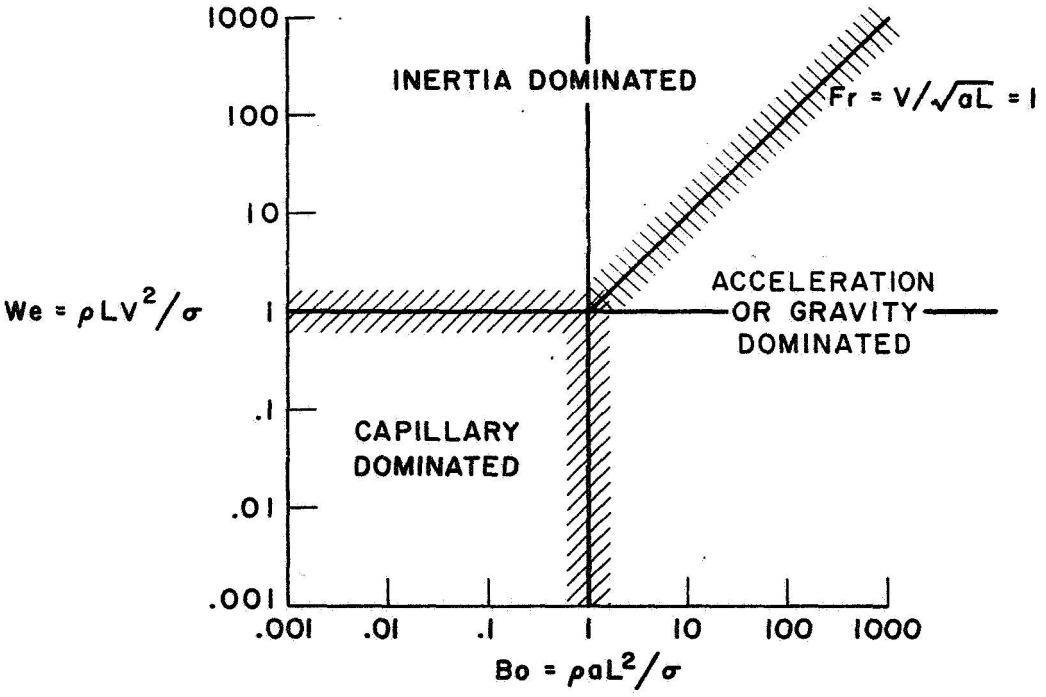


Figure 3. - Hydrodynamic regimes.

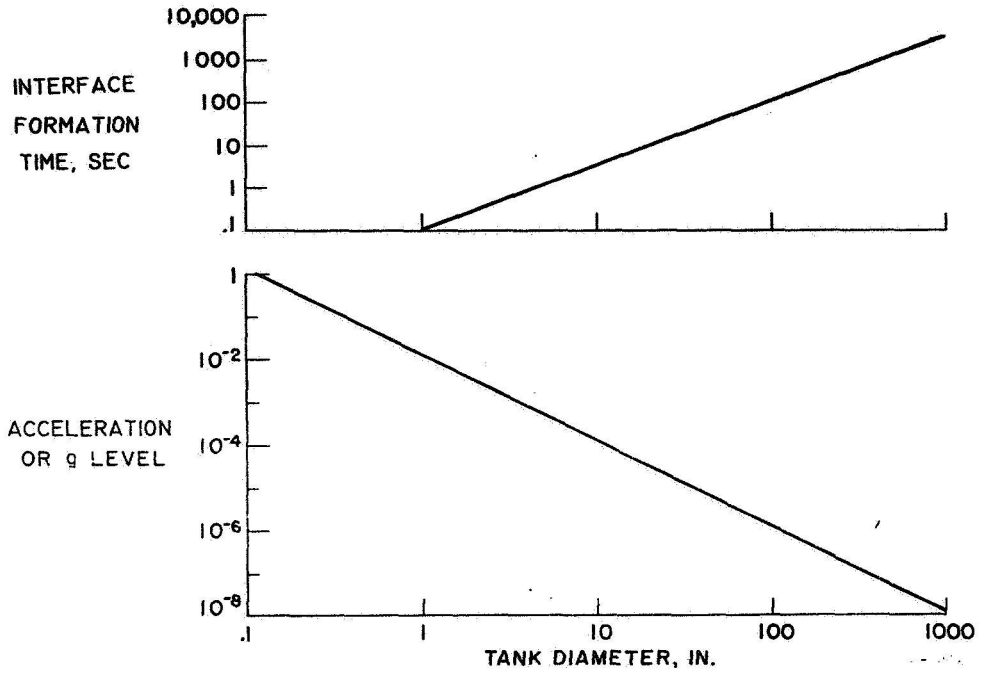
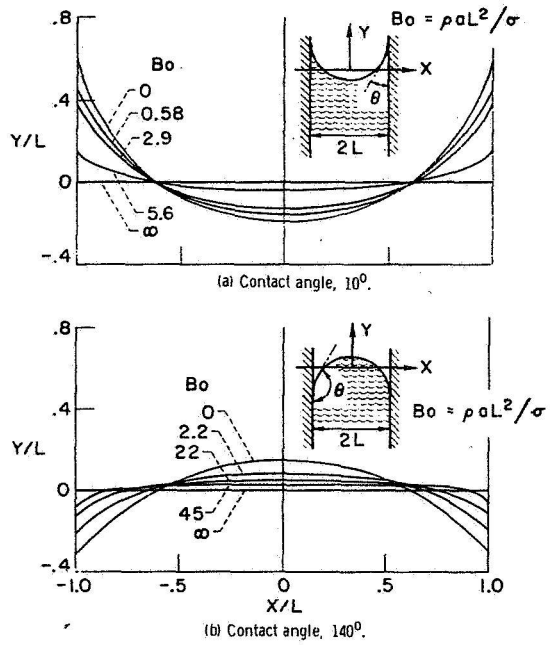


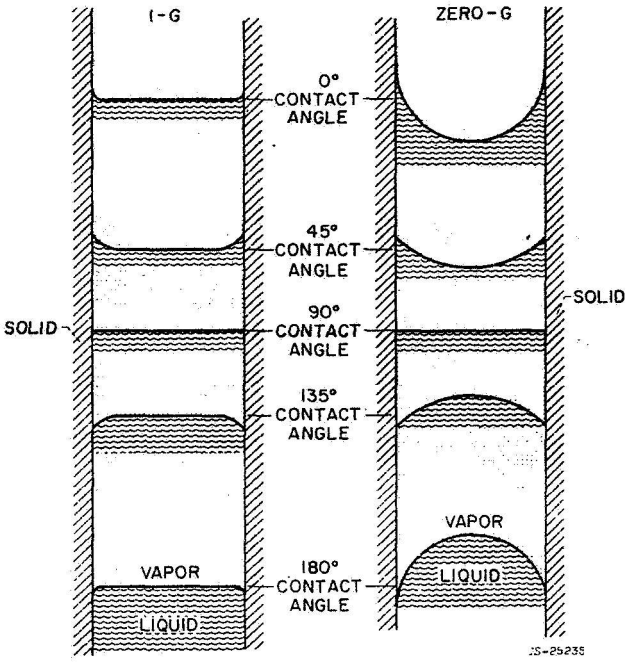
Figure 4. - Effect of model size on facility and g-level requirements.



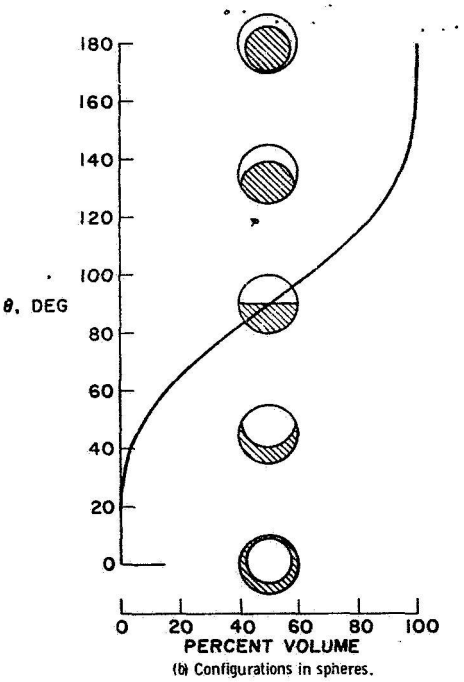
(a) Contact angle, 10^0.

(b) Contact angle, 140^0.

Figure 5. - Calculated configuration of liquid-vapor interface between parallel plates for various Bond numbers and contact angles.

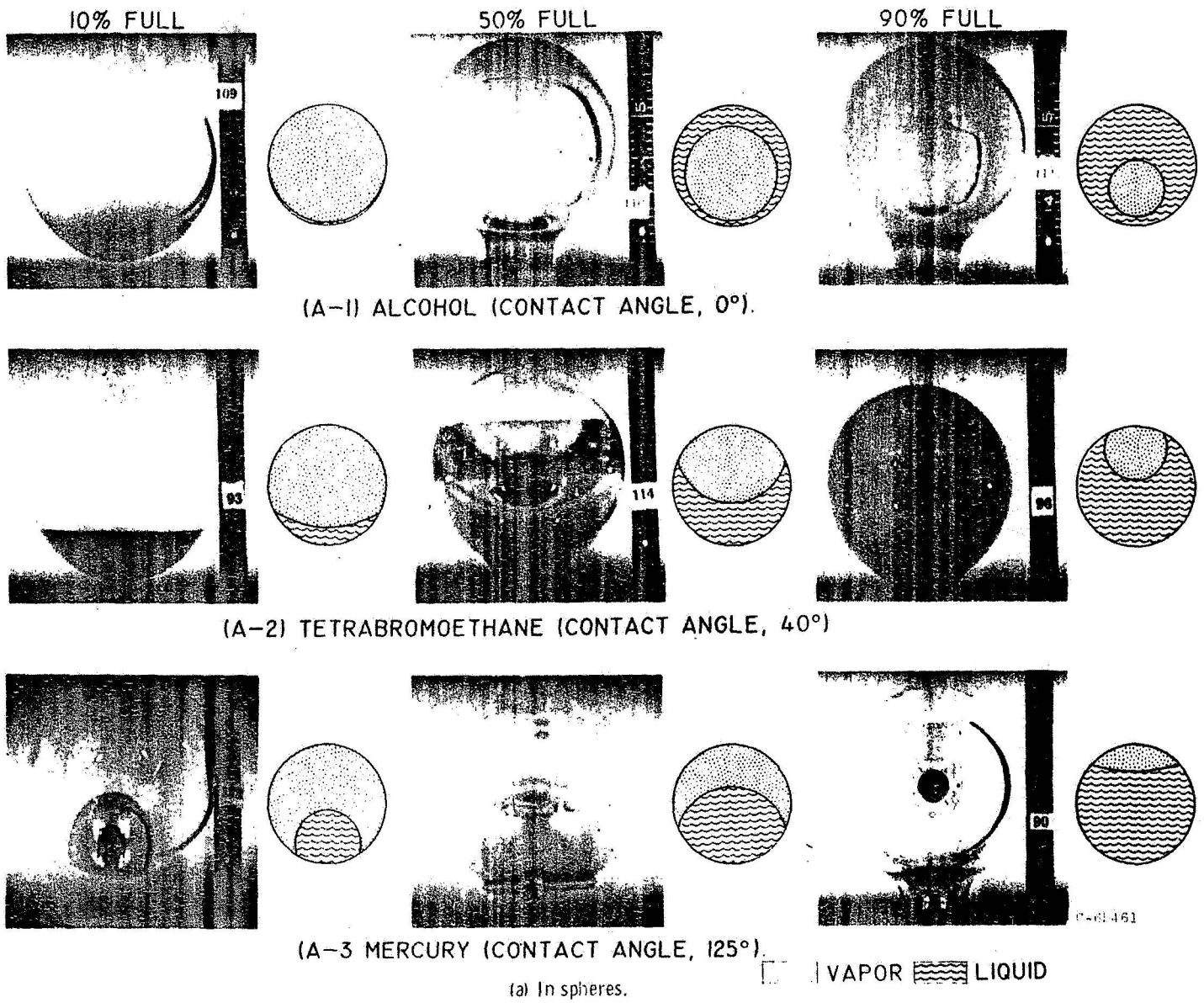


(a) Configurations in cylinders.



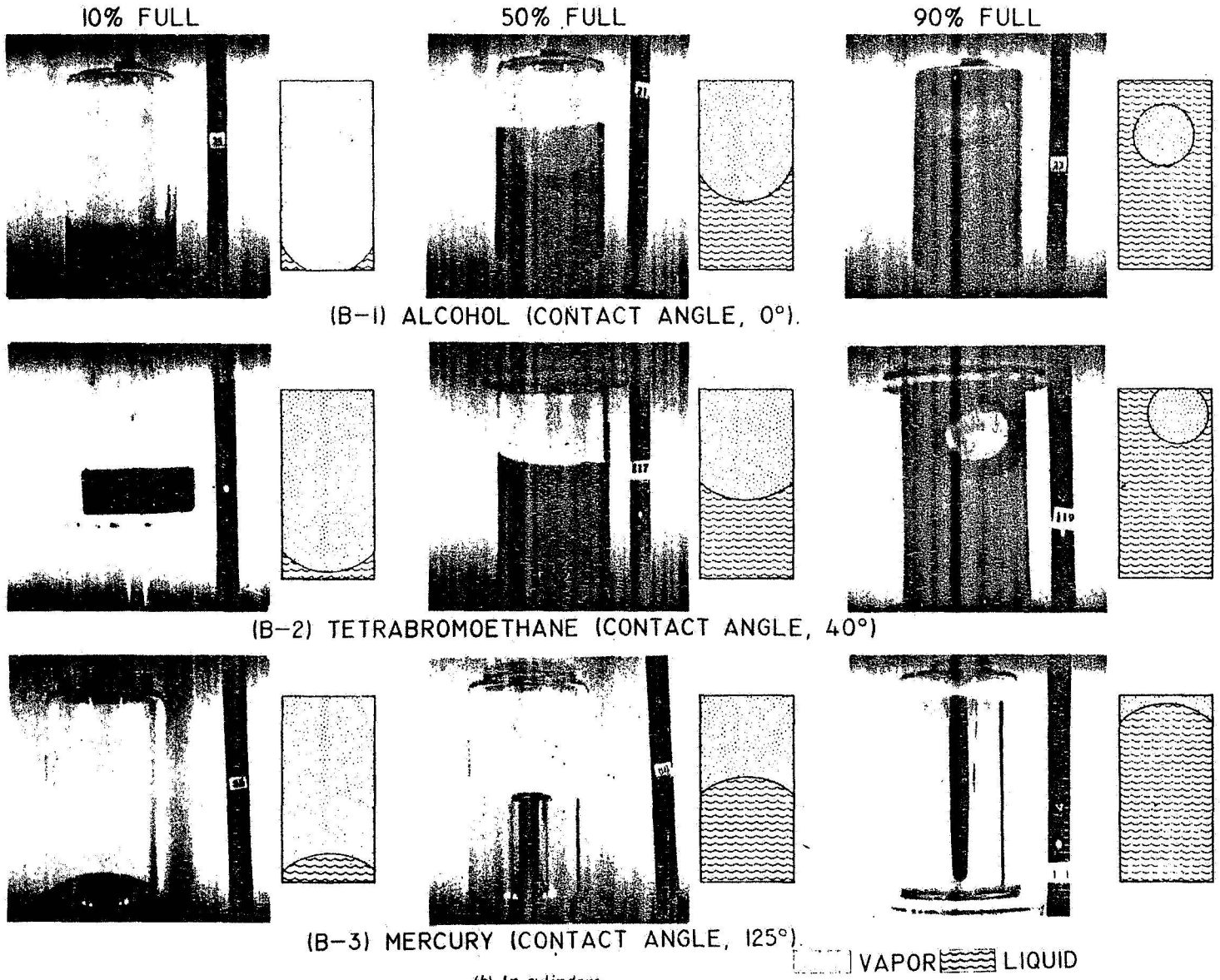
(b) Configurations in spheres.

Figure 6. - Weightlessness configuration in cylinder and spheres.



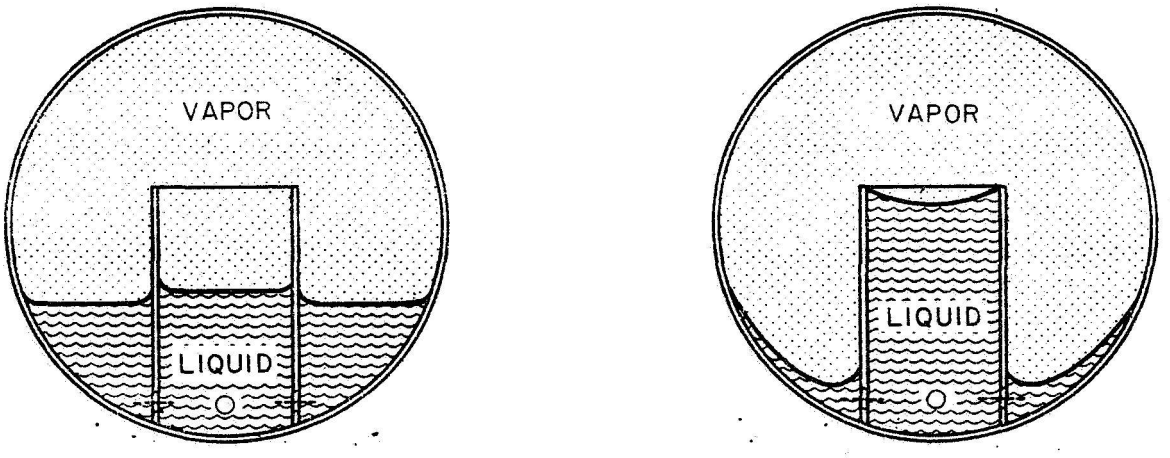
(a) In spheres.

Figure 7. - Configuration of liquid-vapor interface during weightlessness.



(b) In cylinders.

Figure 7. - Continued. Configuration of liquid-vapor interface during weightlessness.



(a) 1-g configuration.

(b) Zero-g configuration.

Figure 8. - Capillary-type ullage control surface.



1–G CONFIGURATION ZERO–G CONFIGURATION

(a) Initial mounting angle, 0^{o}.



1–G CONFIGURATION ZERO–G CONFIGURATION

(b) Initial mounting angle, 45^{o}.



1–G CONFIGURATION ZERO–G CONFIGURATION

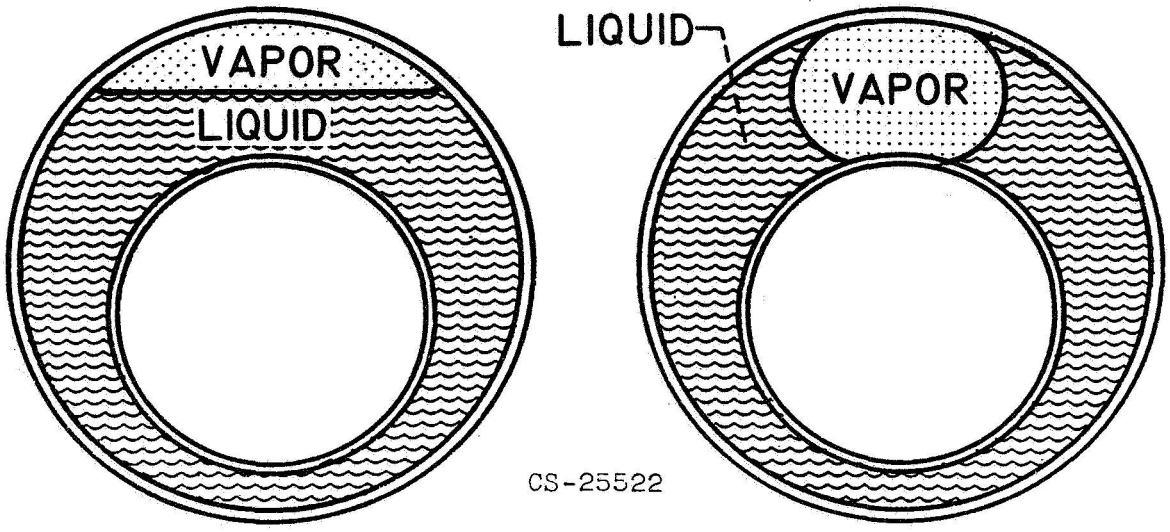
(c) Initial mounting angle, 75^{o}.



1–G CONFIGURATION APPROACHING STEADY–STATE ZERO–G CONFIGURATION

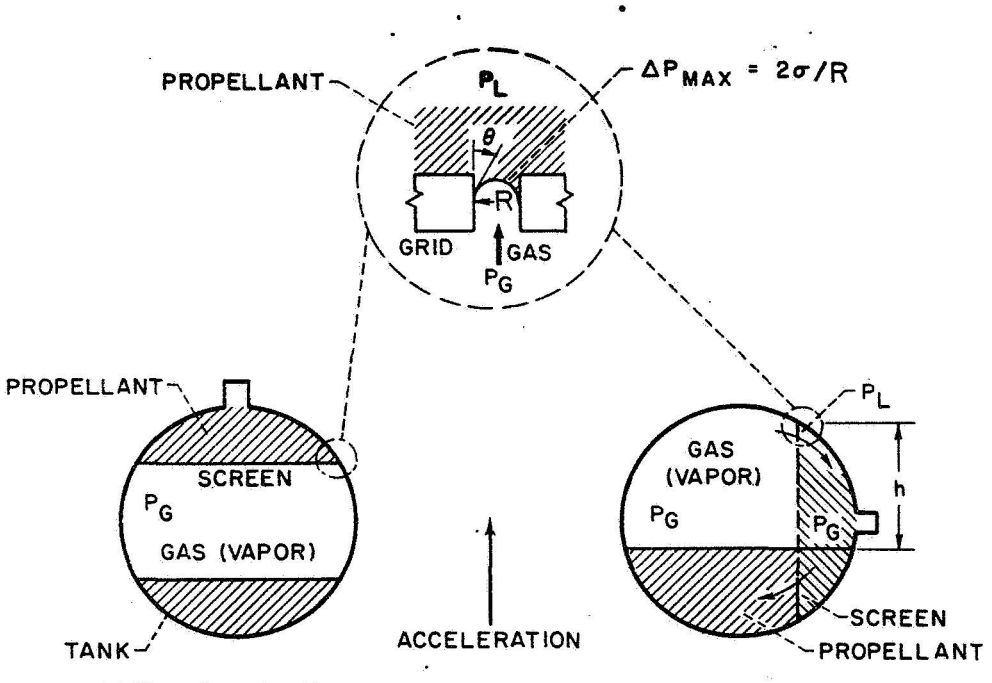
(d) Initial mounting angle, 90^{o}.

Figure 9. - Photographs from preliminary drop-tower tests for range on initial mounting angles.



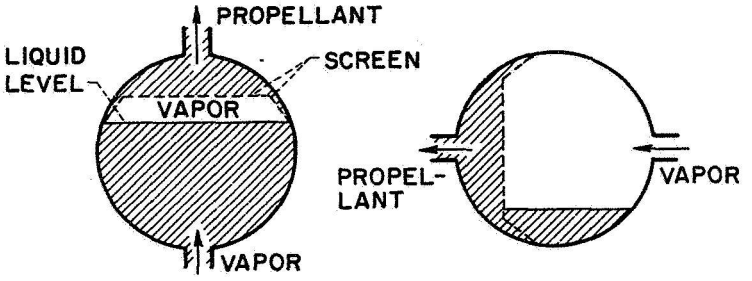
(a) 1-g configuration. (b) zero-g configuration.

Figure 10. - Application of tapered section principle to spherical tank.

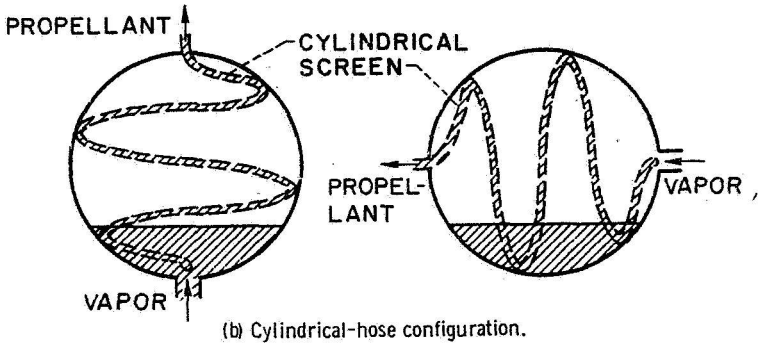


(a) Normal acceleration. (b) Transverse acceleration.

Figure II. - Effect of acceleration on liquid retention power of screens.

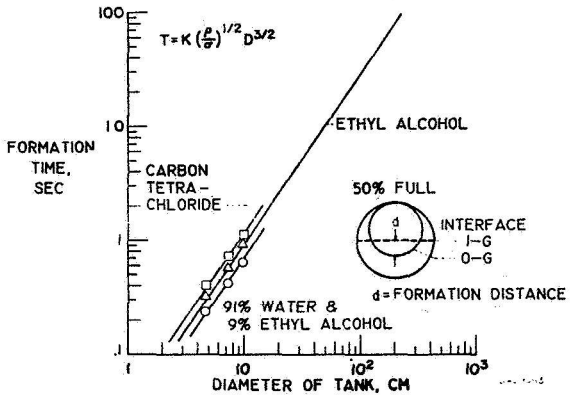


(a) Pie-pan configuration.

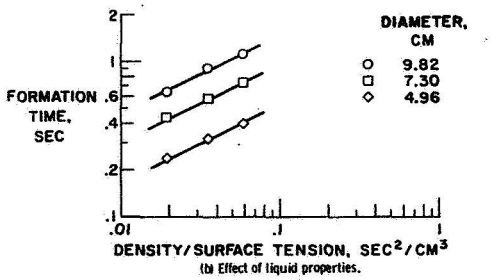


(b) Cylindrical-hose configuration.

Figure 12. - Application of screens to retention of liquid over pump inlet.

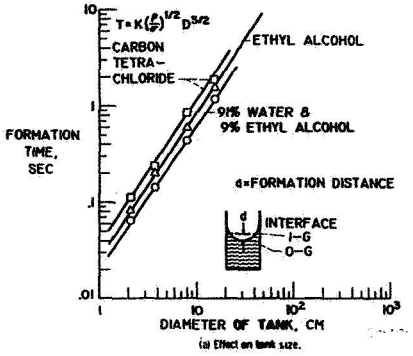


(a) Effect of tank size.

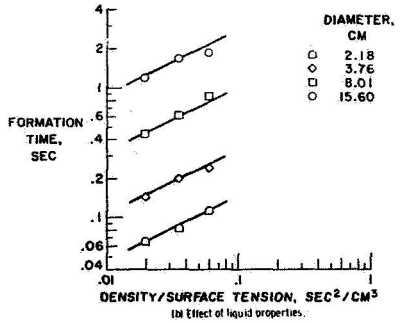


(b) Effect of liquid properties.

Figure 13. - Effect of tank size and liquid properties on interface formation time in spheres after entering zero gravity.

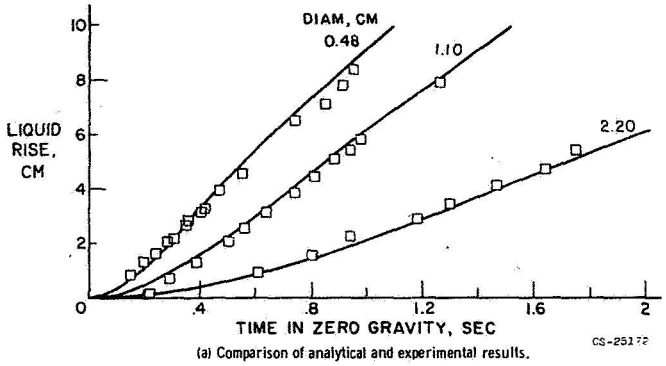


(a) Effect on tank size.

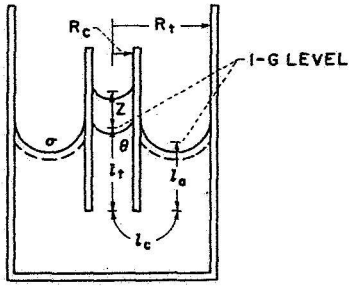


(b) Effect of liquid properties.

Figure 14. - Effect of tank size and liquid properties on interface formation time in cylinders after entering zero gravity.

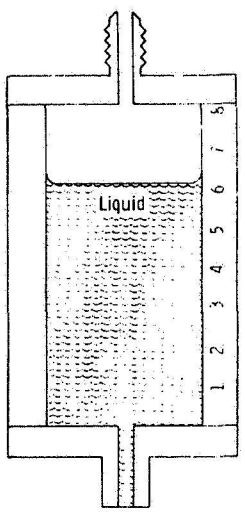


(a) Comparison of analytical and experimental results.

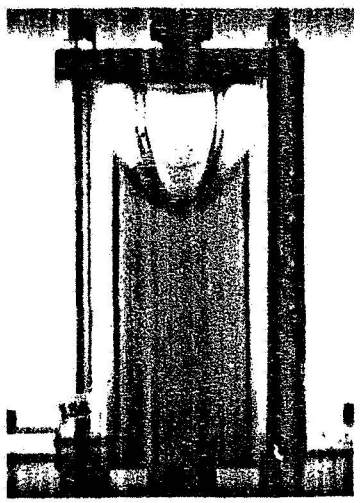


(b) Geometry and nomenclature of capillary system.

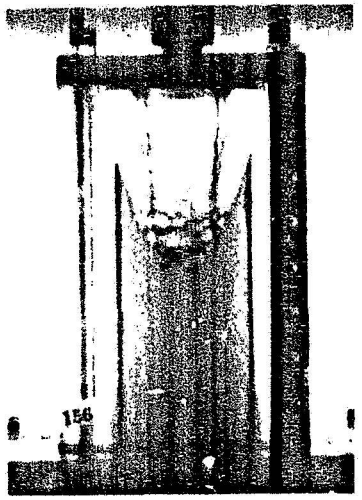
Figure 15. - Variation of liquid rise in a capillary tube with time in zero gravity.



(a) 1-g configuration.

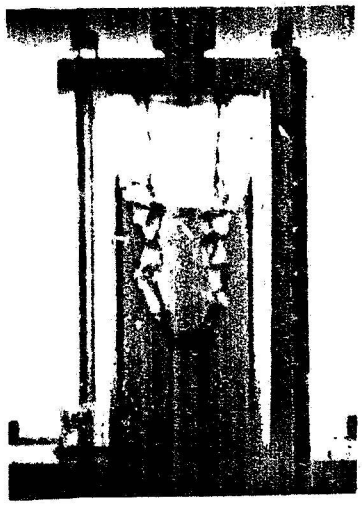


(b) Inception of pumping; time, 0 second.

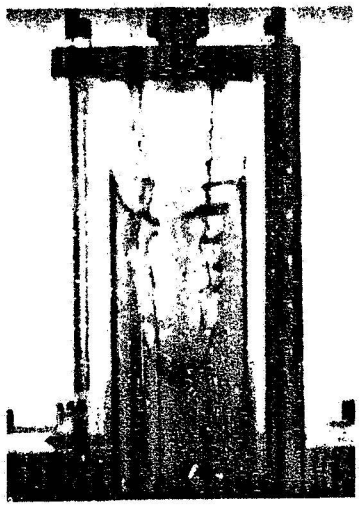


(c) Time, 0.03 second.

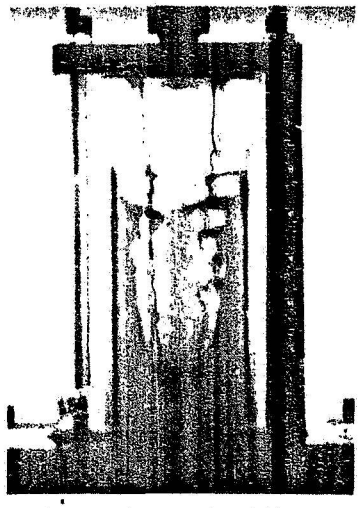
C-71759



(d) Time, 0.07 second.



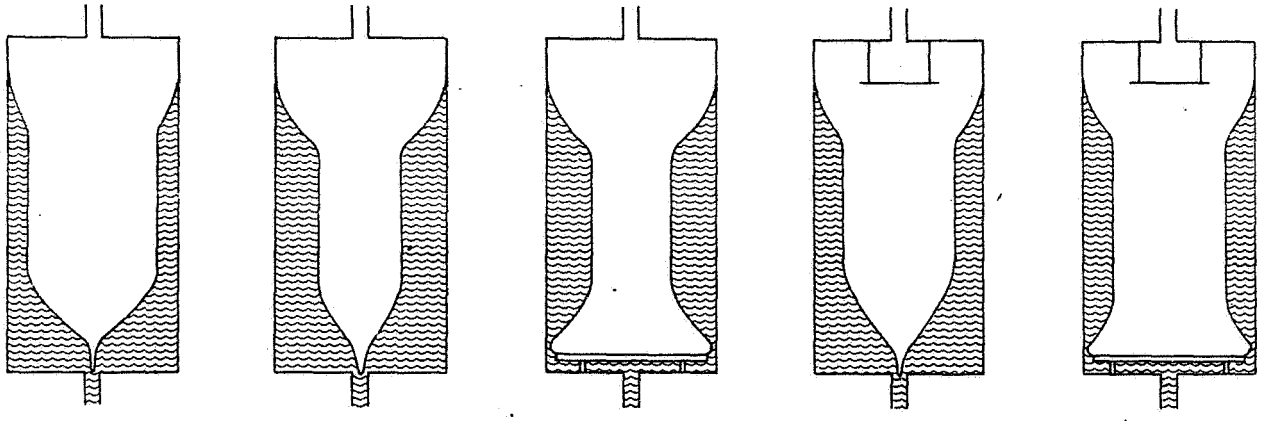
(e) Inception of blowthrough; time 0.09 second.



(f) Vapor blow through; time, 0.10 second.

(a) Configuration at various times in zero-gravity. Outlet velocity 1409 cm/sec.

Figure 16. - Interface configuration during outflow from cylindrical tanks in weightlessness.



Outlet velocity, 291 centimeters per second; expelled liquid, 47 cubic centimeters.

Outlet velocity, 1408 centimeters per second; expelled liquid, 18.7 cubic centimeters.

Outlet velocity, 1330 centimeters per second; expelled liquid, 26 cubic centimeters.

Outlet velocity, 1427 centimeters per second; expelled liquid, 32 cubic centimeters.

Outlet velocity, 1348 centimeters per second; expelled liquid, 45 cubic centimeters.

(b) Configuration at vapor blow-through.

Figure 16. - Interface configurations during outflow from cylindrical tanks in weightlessness.

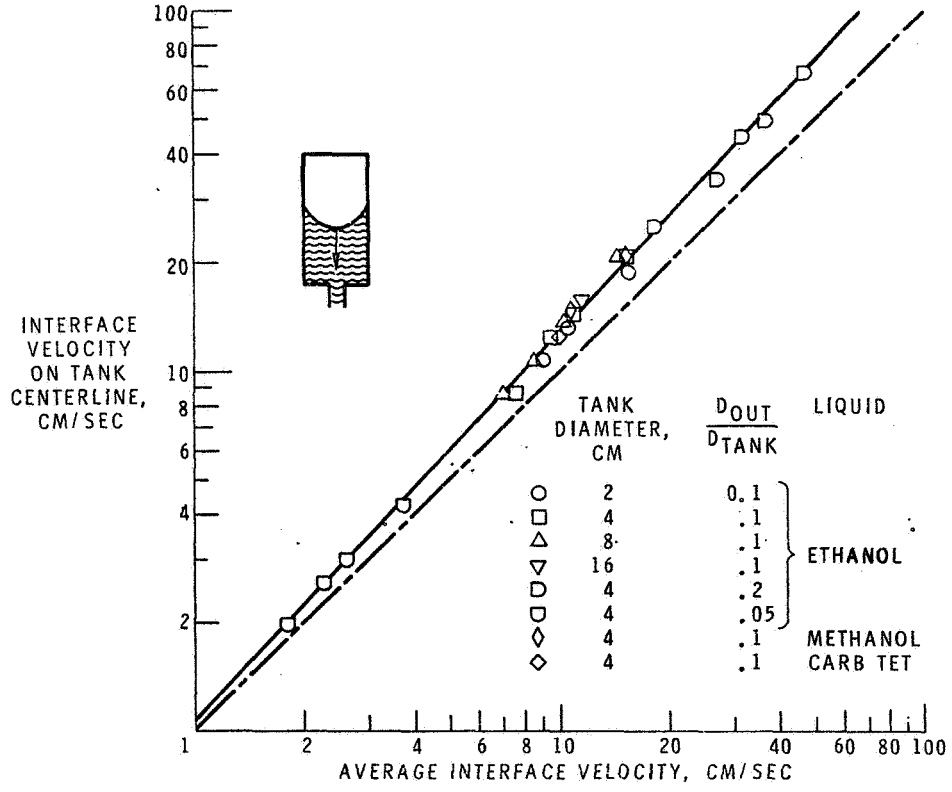


Figure 17. - Liquid-vapor interface velocity during outflow in weightlessness.

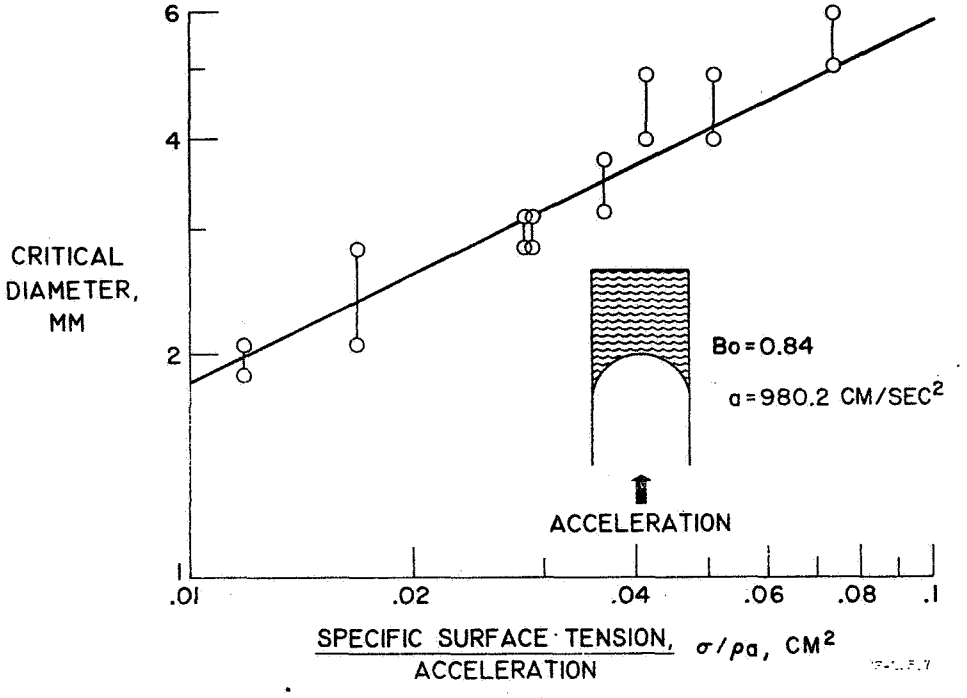


Figure 18. - Stability characteristics in a vertical cylinder.

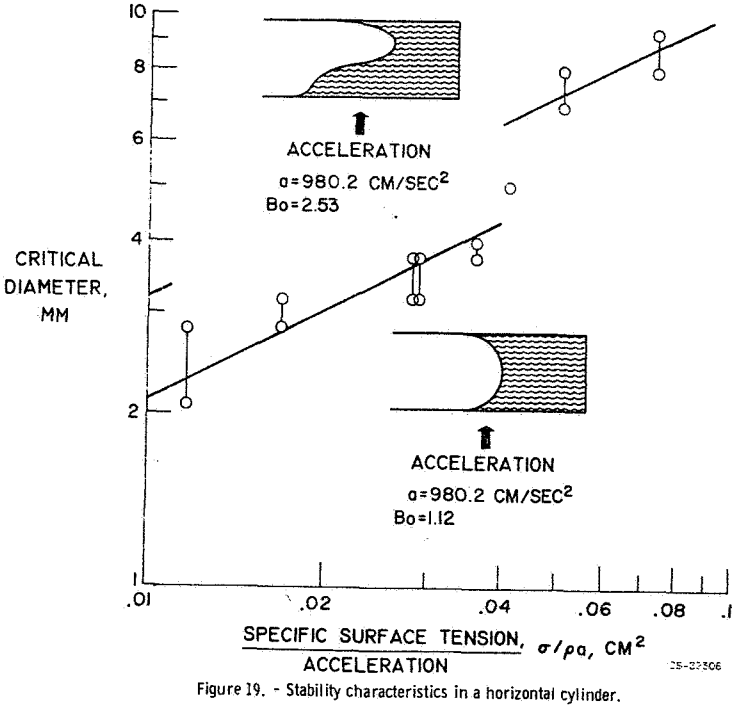


Figure 19. - Stability characteristics in a horizontal cylinder.

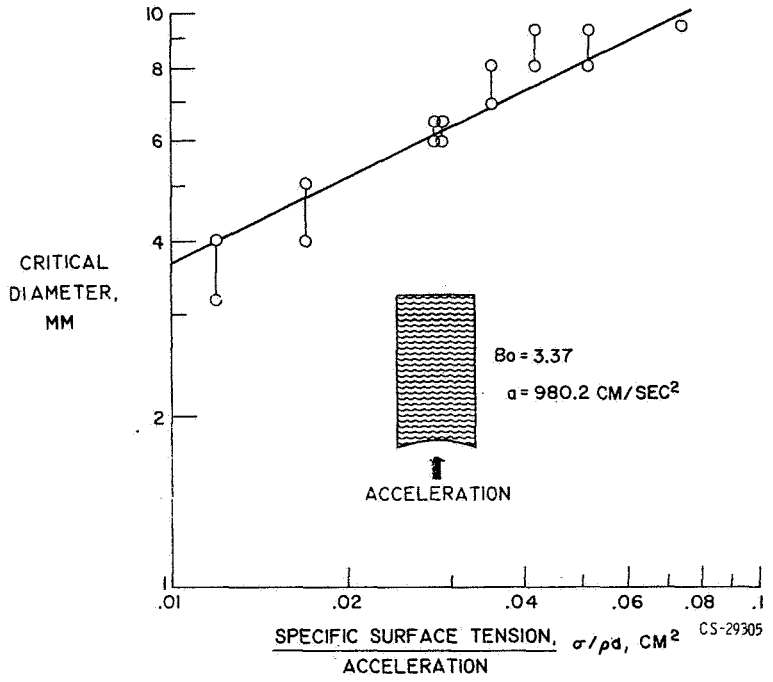


Figure 20. - Stability characteristics at ground edge of a vertical cylinder.

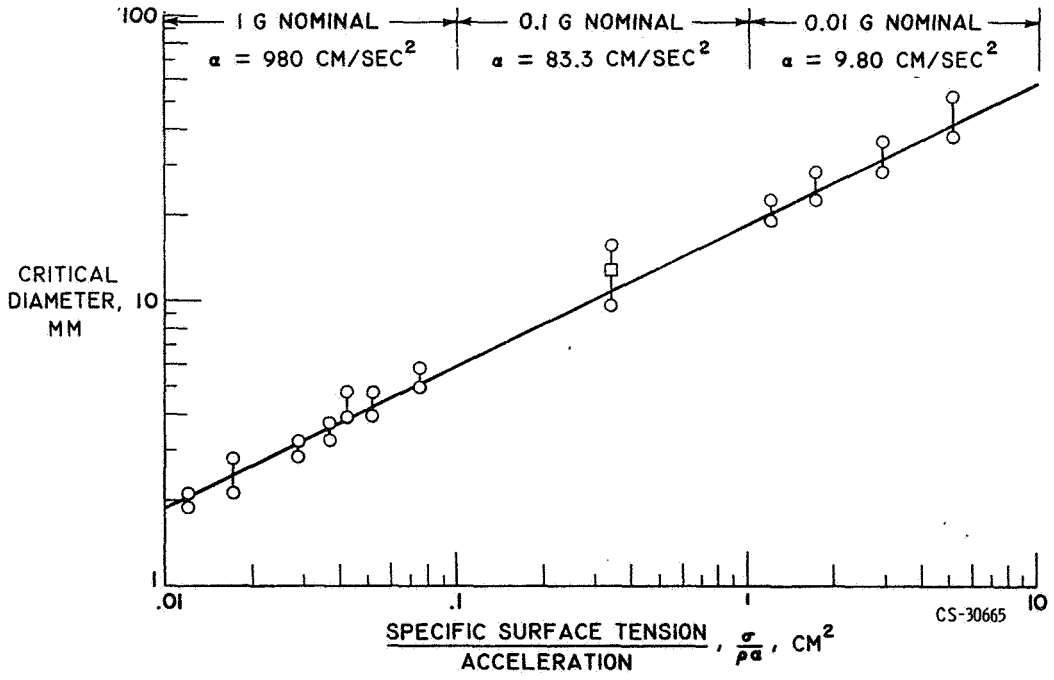


Figure 21. - Stability characteristics in vertical cylinder for several acceleration fields.

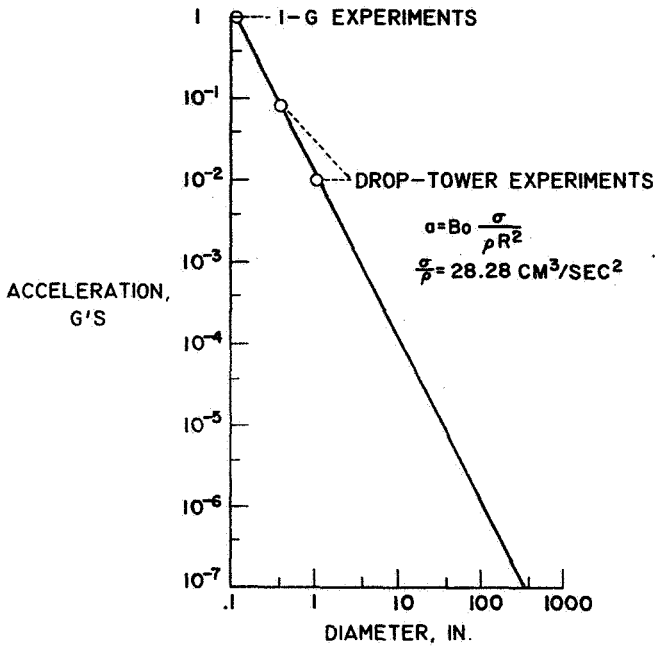


Figure 22. - Interfacial stability as function of acceleration.

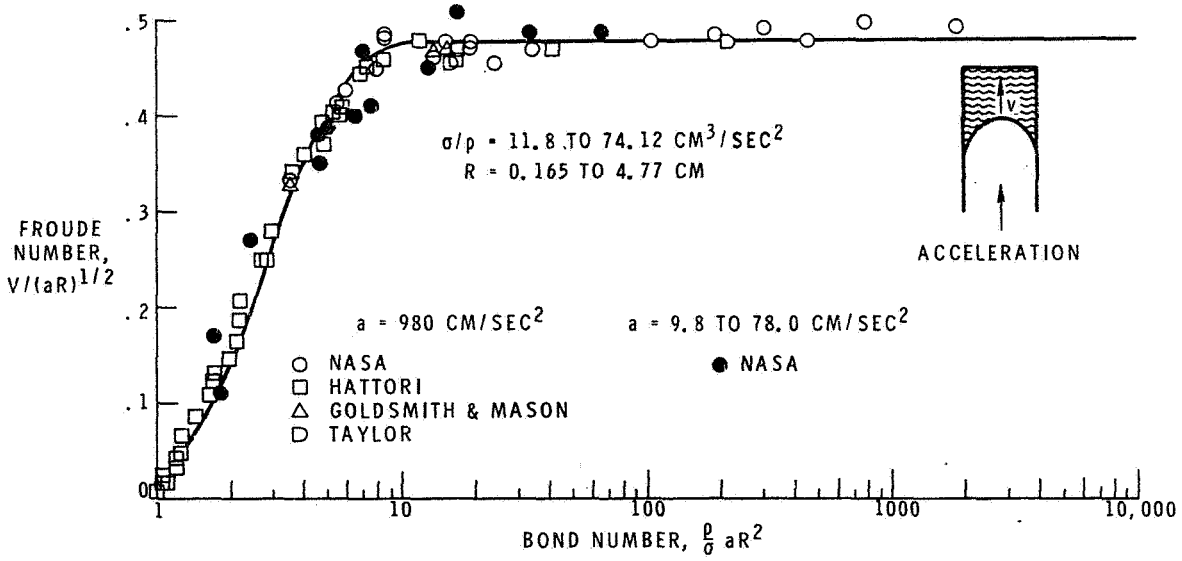


Figure 23. - Penetration velocity of ullage vapor during collection.

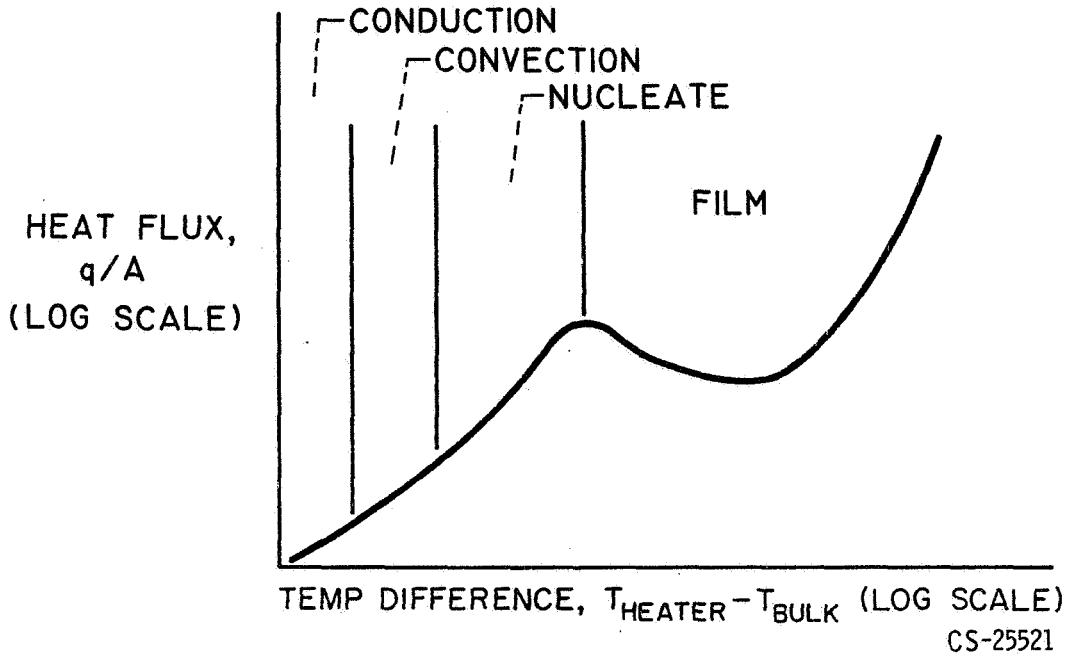


Figure 24. - Typical pool boiling characteristics for 1-g field.

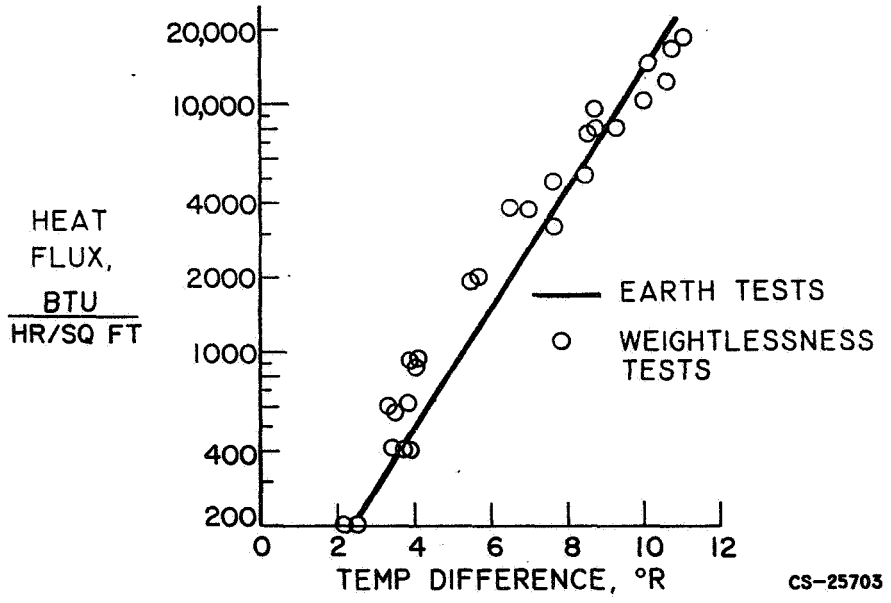


Figure 25. - Comparison of 1-g and zero-g liquid-hydrogen heat-transfer characteristics for nucleate boiling range.

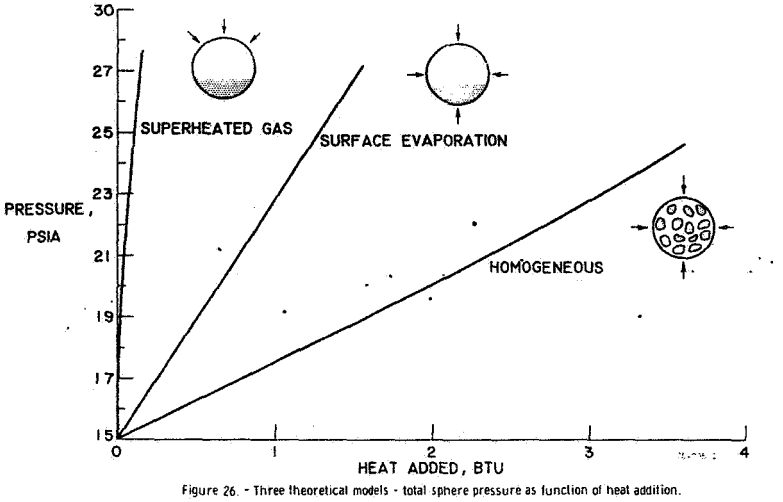


Figure 26. - Three theoretical models - total sphere pressure as function of heat addition.

N63-13093

ZERO GRAVITY LIQUID PROPELLANT CONTROL BY *DIELECTROPHORESIS*

by
J. B. Blackmon
Douglas Aircraft Company, Inc.
Santa Monica, California

ZERO GRAVITY LIQUID PROPELLANT CONTROL BY DIELECTROPHORESIS

J. B. Blackmon*
Douglas Aircraft Company, Inc., Santa Monica, California

A method of collecting liquid propellants in zero gravity by use of electric fields is presented. The method utilizes the concept of dielectrophoresis, which is defined as the induced motion of electrically neutral bodies in a non-uniform electri field. A brief analysis of the field forces is presented, and liquid collection experiments in simulated and actual zero gravity environments are described, including zero-g tests in aircraft flying ballistic trajectories.

A representative dielectrophoretic propellant collection system is described for a 250,000 lb liquid hydrogen-liquid oxygen space vehicle. The system is designed to collect propellant with average forces on the order of 10^{-3}g. The system weighs approximately 400 lbs and can be operated continuously in zero gravity by use of solar cells as the primary power source. In addition, it is shown that propellants such as liquid hydrogen, can be collected off of the tank walls and into the center of the tank to provide an insulating gas layer which decreases the wall to propellant heat transfer and hence boil-off of the propellant. Such a system could decrease the boil-off of the liquid hydrogen from 3300 lbs to approximately 800 lbs. Including the system weight, the total weight savings would be approximately 2100 l

The use of high voltages with space vehicles is discussed, including descriptions of the most promising high voltage generator, electrical breakdown control, and electrode designs which minimize the danger of arcs in the oxidizer tanks.

* Engineer/Scientist - Specialist, Advance Propulsion and Power Department, Research and Development, Missile and Space Systems Division.

THEORY AND ANALYSIS

The effects of electric fields on dielectric liquids are described below, and the equations required for designing a dielectrophoretic collection system are presented.

A continuous, dielectric liquid in a non-uniform electric field experiences forces resulting from free charges and from gradients in the field intensity and liquid dielectric constant. The total volume force on a dielectric liquid with no discontinuities in an electric field is [1]

$$\overline{F}_v = \rho_e \overline{E} - \frac{\epsilon_o}{2} E^2 \nabla K + \frac{\epsilon_o}{2} \nabla \left(E^2 \rho \frac{\partial K}{\partial \rho} \right) \tag{1}$$

The first term is the force exerted on free charges, the second term is the force exerted due to inhomogenity of the liquid, and the last term denotes the dielectrophoretic effect of force on a body in a non-uniform electric field. The last term is also known as the electrostriction force.

A relationship between the dielectric constant, K, and the density, ρ, which holds well for most dielectric liquids, is the Clausius-Masotti equation,

$$C\rho = \frac{K-1}{K+2} , \tag{2}$$

where C is a constant for the liquid. On substituting Eq. (2) into Eq. (1), the volume force becomes

$$\overline{F}_v = \rho_e \overline{E} - \frac{\epsilon_o}{2} E^2 \nabla K + \frac{\epsilon_o}{6} \nabla \left[E^2 (K-1)(K+2) \right]. \tag{3}$$

In our analysis we will be primarily concerned with the ideal case for which the free charge is negligible, $\rho_e = 0$, and the liquid is homogeneous. This condition is met by liquid propellants with high specific restivity, such as liquid oxygen, liquid hydrogen, JP-4, etc. Then, the only electric field force on the liquid is

the dielectrophoretic force,

$$\bar{F}_v = \frac{\epsilon_o(K-1)(K+2)}{6} \nabla E^2, \tag{4}$$

which depends upon the gradient of the square of the electric field intensity, and is in the direction of increasing field strength. Because of the ∇E^2 term, this force is independent of the field polarity and ideally the force vector will be in the same direction for an ac or dc field. H. A. Pohl [2, 3, 4] discussed these effects in studies of dielectrophoretic separation of liquids and suspensions.

There is a pressure difference between a field-free region and the region of a high field, which is given by [5]

$$\Delta P = \frac{\epsilon_o(K-1)}{2} (KE_n^2 + E_t^2) \tag{5}$$

In two concentric, cylindrical electrodes of radii r_1 and r_2, the net pressure difference between the liquid outside the electrodes and inside the electrodes will be given by

$$\Delta P = \frac{\epsilon_o(K-1)\, V^2}{2r^2 \left(\ln \frac{r_2}{r_1}\right)^2} . \tag{6}$$

If the average of the square of the electric field intensity is used,

$$\langle \Delta P \rangle = \frac{\epsilon_o(K-1)\, V^2}{(r_2^2 - r_1^2) \ln \frac{r_2}{r_1}} . \tag{7}$$

This pressure difference will cause the liquid to rise in the electrodes until the field induced hydrostatic pressure rise is balanced by gravity. The average height to which the liquid will rise because of the electric field is then,

$$h_{field} = \frac{\langle \Delta P \rangle}{\rho g} = \frac{\epsilon_o (K-1) V^2}{\rho g (r_2^2 - r_1^2) \ln \frac{r_2}{r_1}} . \tag{8}$$

Surface tension would also cause the liquid to rise between the cylinders to an approximate average height of [6]

$$h_{capillary} = \frac{2\alpha(r_3 - r_2 + r_1)}{\rho g (r_2 - r_1)(r_3 - r_2)} \tag{9}$$

Compared to surface tension effects in the same geometry, the ratio of forces is

$$\frac{\text{Field Force}}{\text{Capillary Force}} = \frac{\epsilon_o (K-1)(r_3 - r_2) V^2}{2\alpha(r_2 + r_1)(r_3 - 2r_2 + r_1) \ln \frac{r_2}{r_1}} \tag{10}$$

For two concentric cylindrical collecting electrodes in liquid hydrogen with the inner radius, $r_1 = .1$ meter, the outer radius, $r_2 = .5$ meter, the voltage, $V = 10^6$ volts, and the surface tension $\alpha = 2.5 \times 10^{-3} \frac{\text{newtons}}{\text{meter}}$, the dielectrophoretic force acting on the liquid hydrogen in the collector is approximately 460 times greater than the average capillary force. Although capillary forces will aid collection in nearly all electrode designs, the effect is usually small compared to the dielectrophoretic forces. In addition, capillary effects result from surface forces, and, because they are essentially passive, are determined only by the design of baffles, screens, standpipes, etc. A capillary system has the disadvantage that vapor bubbles generated within the collected liquid will not be forced out. Also, surface tension decreases as temperature increases and thus collection forces will be decreased in areas of high heat transfer such as are likely at the bottom of propellant tanks close to the rocket engines.

Dielectrophoretic forces, however, are body forces and can be controlled by varying the magnitude of the applied voltage or by varying the electric field configuration used for collection or venting, i.e., by charging or discharging selected electrodes Furthermore, the dielectrophoretic force increases as the temperature of the liquid decreases because of the temperature dependence of the dielectric constant. Thus, free convection currents will be set up within a liquid with variable temperature in zero gravity which will attract the colder liquid into areas of higher field intensity.[7] Any vapor bubbles formed will be displaced by the attracted liquid.

The presence of free charges in the liquid induces disruptive effects such as expulsion of charged globules from the liquid surface and stirring effects or electro-convection at the surface and within the liquid. Discussions of these effects can be found in References 9 & 10. To minimize the free charge effect and provide for stable collection of propellant it has been found that ac voltages above a certain frequency must be used. If the field frequency is large compared to the reciprocal of the relaxation time (σ/ϵ) of the liquid, the interface can be stable. With a propellant such as liquid hydrogen and liquid oxygen, the relaxation time is of the order of 10^{3} seconds and a field frequency as low as 10^{-2} cycles/second should be sufficient. However, experiments on a large scale have yet to be performed to verify this hypothesis.

ELECTRODE CONFIGURATIONS

The collecting forces for particular electrode configurations are difficult to determine, except in the ideal case of perfectly insulating, homogeneous, isotropic liquids with no surface discontinuities and with simple electrode geometries, such as cylinders, spheres, wedges, etc. In the ideal case, the dielectrophoretic force per unit volume acting throughout the liquid, expressed in terms of

the equivalent g level for convenience, is given by

$$\frac{a}{g} = \frac{\epsilon_o(K-1)(K+2)\,\nabla E^2}{6\rho g} \quad . \tag{11}$$

Ignoring end effects, two coaxial cylindrical electrodes have a voltage distribution of

$$V(r) = \frac{V \ln r/r_2}{\ln r_1/r_2} \quad . \tag{12}$$

From Equation (12) the force or "g" level becomes

$$\frac{a}{g} = \frac{\epsilon_o(K-1)(K+2)\,V^2}{3\rho g(\ln \frac{r_2}{r_1})^2\, r^3} \quad , \tag{13}$$

which is the force acting throughout the liquid between the electrodes and radially directed towards the inner electrode. For radii of $r_1 = .1$ and $r_2 = .5$ meter, and an applied voltage of 10^6 volts, the force acting on liquid hydrogen varies from 1.35 g's at the inner cylinder to approximately .01 g at the outer cylinder.

The average integrated collecting force throughout the cylinder is

$$\left\langle \frac{a}{g} \right\rangle = \frac{2\epsilon_o(K-1)(K+2)\,V^2}{3\rho g\,(\ln r_2/r_1)^2\,(r_1+r_2)\,r_1\,r_2} \tag{14}$$

For two concentric spheres of radii r_1 and r_2, the voltage distribution is

$$V(r) = \frac{Vr_1}{(r_2-r_1)}\left(1 - \frac{r_2}{r}\right) \tag{15}$$

The dielectrophoretic force at any point of the liquid is

$$\frac{a}{g} = \frac{2\epsilon_o(K-1)(K+2)\,r_1^2\,r_2^2\,V^2}{3\rho g\,(r_2-r_1)^2\,r^5} \quad , \tag{16}$$

and is directed towards the inner sphere. Again, for radii of r_1 = 0.1 meter, and r_2 = 0.5 meter and V = 10^6 volts, the dielectrophoretic force acting on liquid hydrogen varies from 10.4 g's at the inner electrode to .0033 g's at the outer electrode.

The maximum dielectrophoretic force for the sphere is much greater than for the cylinder because the electric field intensity is more non-uniform. However, break down will occur for the sphere at a lower voltage than for the cylinder, and therefore, the voltage safety factor (ratio of corona discharge voltage to applied voltage) is less for the sphere than for the cylinder.

EXPERIMENTAL WORK

Our first experiments with dielectrophoresis were performed with cylindrical electrodes and demonstrated collection of water drops suspended in an equi-density mixture of carbon tetrachloride and benzene. The experimental collection forces and collection times were compared with theoretical values and were in good agreement. Later experiments with equi-density mixtures of FS-1265* in carbon tetrachloride and benzene demonstrated stable configurations of the collected liquid in complex electrode shapes. Tests were then performed in a catapult tower which provided approximately 1 second of low g. These tests were performed with 250 ml. flasks having a transparent, metallic coating as the outer electrode, and an aluminum rod for the inner electrode, with voltages varied between 35 - 50 kv ac. During the 1 second of low g, the liquid (carbon tetrachloride) flowed up the rod and into the neck of the flask under the influence of the applied field. Figure 1 shows the liquid position at the end of a typical test sequence. Capillary attraction was negligible in these tests compared to the dielectrophoretic forces,

* Dow-Corning Fluorpropyl Silicone Fluid

Reproduced from best available copy.

although the testing periods were too short to study equilibrium configurations. These experiments are described in References 11, 12 and 13.

We have performed tests in an extended period of low g by using an Aerocommander aircraft flying ballistic trajectories. The test periods were of 8-10 seconds duration, and the g level varied between $\pm$ 0.05 g for tests in calm air.

Tests were first performed with a cylindrical electrode 2-1/2 inches in diameter inside a one-gallon jar 6 inches in diameter which formed the outer electrode.[8] The jar was one-quarter full of a dielectric liquid (DC-200*, 5 centistoke). The DC-200 was observed to climb up the inner electrode in low-gravity when the voltage was applied. The tests were designed for an operating voltage of 90,000 volts dc, but because of difficulties with the power supply, only 30,000 volts were obtained. Since the dielectrophoretic force is proportional to the square of the voltage, only one-ninth the force desired was achieved, and hence the inner electrode was covered by a thin sheath of liquid only 3/8 inch thick. Also, stirring effects were not observed because of the low field intensity and also because the test period was shorter than the relaxation time (approximately 100 seconds) necessary for an equilibrium free charge distribution to build up in the DC-200.

In one series of Aerocommander tests, a "standpipe" electrode was used to compare collection with ac and dc fields.[8] The electrode assembly and typical test results are shown in Figures 2 and 3, which are taken from a film of the test. The inner electrode is a 1/2 inch diameter aluminum rod, the outer electrode is a 2-1/2 inch diameter glass tube with a transparent, electrically conducting vacuum deposited coating of nichrome. The assembly is in a 1-gallon jar, 6 inches in diameter, one-quarter full of DC-200.

* Dow-Corning Silicone Oil

The ac voltage tests were limited to 10-12 kv. Figure 2 shows the liquid rising between the electrodes. The field force was approximately twice the capillary force, as obtained from Equation (10), but no collection was achieved when the voltage was not applied. The collection was stable, with no stirring motion, even at the liquid-gas interface.

More liquid was collected in the dc tests because the voltage was higher by a factor of 2 or more (20 kv-25 kv), thus quadrupling the collection force. Free charges in the liquid resulted in a stirring motion, especially at the liquid surface, but the collected liquid was retained between the electrodes for the entire test period, and in fact, liquid was continually collected into the electrode during the test. In Figure 3, the liquid between the electrodes rose 3-5 inches because of the combined surface tension and field forces. From Equation (10), the field forces at 20 kv to 25 kv are 5.6 to 9 times greater than the capillary forces.

Liquid collection in the "standpipe" electrode with dc voltages indicated that even with electrode designs in which the lines of electric field intensity are substantially parallel to the liquid surface initially, and in which the liquid is bounded by electrode surfaces at all other points, there is appreciable stirring of the liquid. Therefore, ac fields must be used for stable collection of liquids and ac fields will be assumed as a primary design requirement.

In the last series of tests a scale model of a high energy upper stage vehicle with spherical tanks was tested for collection with two electrode configurations, (see Figures 4 to 9). The forward tank is 8 inches in diameter and contains 7 disc electrodes each of which has a 1/2 inch diameter hole in the center to allow for passage of gas or liquid during the collection of liquid between the discs. The discs are insulated with cellulose acetate at the edges to resist corona discharge.

The separation distance between the discs is 7/8 inch and the applied voltage was a maximum of 17,000 volts. The aft tank is a sphere 10 inches in diameter with 7 parallel aluminum electrodes 1/2 inch in diameter arranged hexagonally a distance of 2.5 inches from each other, and supported at the bottom of the tank. The voltage on the aft tank was the same as that on the forward tank since they were connected in parallel to the high voltage transformer. The high voltage transformer was connected to a static inverter (28 volt dc to 60 cycle - 120 volt ac). The inverter output for this test was an improperly filtered ac voltage which, when fed into the ignition transformer, resulted in high voltage peaks. The high voltage peaks caused breakdown between the discs of the forward tank at RMS voltages on the order of 17,000 volts, although laboratory tests with 60 cycle - 120 volt ac and the same ignition transformer had indicated no breakdown problem, and breakdown tests had been performed at 35,000 volts dc.

However, the scheduled test was run and the flight test engineer was instructed to start at a low voltage and steadily increase it to the maximum value as the liquid collected between the discs. Two tests were completed without breakdown and eight tests were performed with some breakdown. The results of all tests indicated varying degrees of collection depending on voltage levels and the length of time of the applied voltage. In Figures 4 to 9 results from the first test in which the maximum applied voltage was achieved at the end of the test are compared with a test in which no voltage was applied.

Figures 4 to 8 illustrate collection on the two tanks with approximately 17,000 volts applied; the arrows indicate the liquid interface. In Figure 4 the applied liquid is clearly shown sloshing toward the back of the spheres because of the pitching of the aircraft as it began the zero-g trajectory. In Figure 5 the liquid is beginning to collect between the top three discs in the top sphere. The motion of

the liquid during this collection sequence is primarily towards the camera since the liquid was initially sloshed towards the back of the sphere, away from the camera. In Figure 6 the liquid in the top sphere has collected between the top four discs and partially in the fifth. In Figure 7 an outline of liquid collected between four discs can clearly be seen. The aircraft was completing its zero g trajectory at this point and, therefore, the amount of liquid in the top disc has decreased. In Figure 8 the liquid is shown flowing towards the bottom of the sphere as the aircraft completes the zero g maneuver.

Collection with the rod electrodes in Figures 4 to 8 was not as dramatic as with the discs. The liquid was retained at the bottom of the tank during the test. Collection was expected to occur along the full length of the rods, but instead, a sheath of liquid rose only 1-2 inches along each rod in a truncated cone shape which can partially be seen in Figures 6 and 7. Since there was a slight positive g level induced on the liquid, the liquid collection configuration is the resultant of the small gravitational force and the dielectrophoretic force.

Figure 9 shows liquid collected on the tank wall with no voltage applied, as is expected in zero gravity; there was no tendency for the liquid to collect on the electrodes with no voltage applied. A comparison of Figures 6 and 9 is evidence of the effect of non-uniform electric fields on liquid orientation in zero gravity.

The average dielectrophoretic force achieved with 17,000 volts was on the order of 5×10^{-2} g in both tanks in the radial and longitudinal direction. However, this force was applied for only a fraction of the flight time because of the breakdown problem.

SPACE VEHICLE APPLICATIONS

Engine Restart and Ullage Gas Venting

A dielectrophoretic propellant collection system can be used to collect propellant in zero gravity to the aft end of the propellant tanks to guarantee engine restart without entrapped vapor and ullage gas venting without entrapped liquid. Several different electrode designs are feasible, but only the simplest will be discussed here. The system discussed below is designed for a 250,000 lb liquid hydrogen-liquid oxygen space vehicle approximately half full of propellant. The system, shown in Figure 10 consists of seven cylindrical electrodes with a diameter of approximately 4 inches, positioned in each tank in a hexagonal pattern.

Seven cylindrical electrodes of radius $r_1 = 0.05$ meter are positioned in each tank in a hexagonal pattern. The lengths of the electrodes are approximately one-half the respective tank lengths or 13 feet for the LH_2 electrodes, and 6.5 feet for the LO_2 electrodes. In the liquid hydrogen tank the separation distance between the electrodes is approximately 6.5 feet. Assuming 10^6 volts are applied to the electrodes, the maximum radial force of attraction on the liquid hydrogen will be 3 g's. The minimum radial force will be 3.75×10^{-4}g. The integrated average radial force will be 1.3×10^{-2}g. For the tank half filled with LH_2, the average longitudinal force attracting the liquid to the bottom of the tank will be 2.8×10^{-4}g.

In the liquid oxygen tank, the separation distance between electrodes is 4.5 feet. Assuming 10^6 volts are applied to the electrodes, the maximum radial force will be .55 g, the minimum radial force will be 1.9×10^{-4}g, and the average radial force will be 0.5×10^{-2}g. For the tank half filled with LO_2, the average longitudinal force of attraction will be 1.6×10^{-4}g.

The total weight of the dielectrophoretic system is composed primarily of the electrodes, insulating supports, high voltage generators and batteries or solar cells to power the generators. The LH_2 tank electrodes would be made of a highly polished metal to minimize corona discharge from surface asperities. Aluminum electrodes of .02 inch wall thickness are assumed to calculate the electrode weights for the LH_2 tank. The seven LH_2 electrodes, approximately 13 feet long, would weigh approximately 50 lbs. Internally pressurized teflon electrodes of 1/8 inch thickness are assumed for the LO_2 tank electrodes. A thin film conducting metallic surface is sandwiched inside the teflon walls which will not ignite in case of breakdown between electrodes. The weight of the 7 teflon electrodes would be approximately 120 lbs. The insulating supports in the LH_2 tank are assumed to be made of polypropylene or mylar, both of which have high dielectric strength and relatively low density. The weight of the seven supports is approximately 40-60 lbs for the LH_2 tank electrodes. Teflon insulating supports are used in the liquid oxygen tank, and the seven supports for the one million volt electrodes would weigh approximately 70 lbs. The high voltage generator weight is assumed to be 20 lbs, and two generators are required for each tank. The battery weight and type of primary power source cannot be determined without specifying the number of restarts and vent cycles, the collection time required, and the overall vehicle mission. However, the dielectrophoretic systems should bring about collection in less than one minute and thus for a typical lunar mission requiring 15 vent cycles and one restart, a one-hour total usage time is sufficient. On this basis, and assuming the four Van de Graaff generators will require 0.5 kw, a total of 0.5 kw hr will be required, which can be obtained from the vehicle power supply. Assuming the vehicle power supply consists of space batteries, which typically have power-to-weight ratios of 0.05 kw hr/lb, the battery weight required for the dielectrophoretic systems is only 10 lbs. The total system weight would be made up of 170 lbs for electrodes, 130 lbs for

insulating supports, 80 lbs for high voltage generators, 10 lbs for monofilament supports and 10 lbs for batteries. The system weight would be approximately 400 lbs. If the system were to be operated continuously, approximately 40 lbs of solar cells would be required.

Cryogenic Propellant Boil-off Reduction

A dielectrophoretic system may be used to decrease boil-off losses of cryogenic liquid propellants in zero gravity by collecting the liquid off of the tank walls. The resulting gas layer between the liquid and the tank walls would increase the thermal resistance and decrease the heat flow from the walls to the liquid. A simple electrode configuration, consisting of seven cylindrical rods in the liquid hydrogen tank, is shown in Figure 11; this configuration would collect propellant off of the tank walls and retain the propellant, as shown, against axial disturbances of approximately 10^{-4} - 10^{-3} g.

For the tank shown in Figure 11, half full of liquid hydrogen, the fuel lost by boil-off is given in Figure 12. These curves were obtained from a Douglas Aircraft Company computer program applicable to tanks of the same configuration as that shown in Figure 11. To simplify the analysis, only the heat from solar radiation and the earth's albedo was considered. Heat stored in the space vehicle and conducted to the tank walls was not considered; such heat sources as the liquid oxygen tank, forward and aft section of the vehicle, heat from the rocket motors immediately after cutoff, etc., would increase the total heat input by approximately one half or more. The boil-off rate with fluid collected on the wall (as would be expected in zero g with no field applied) is shown in the top curve of Figure 12. The boil-off rate is found by assuming that all of the heat transferred to the tank vaporizes the liquid and that the amount of liquid vaporized is vented and cannot be recovered.

This approximation is conservative, but the results are approximately the same as results from more generalized analyses used for space vehicle design.

The second curve shows the boil-off rate for fluid collected off of the tank walls and into the center of the tank. Again, all of the heat transferred to the liquid causes boil-off, but because of the increased thermal resistance, only one-fourth as much propellant is lost as in the first case.

In the third curve, the fluid is assumed to be collected on the wall, but completely mixed. Therefore, the heat input to the liquid increases the bulk temperature of the liquid which increases the vapor pressure. The tank pressure increases until it equals the vapor pressure of the hydrogen corresponding to the bulk temperature. The amount of propellant vaporized is less than that for liquid collected off of the tank walls; however, some means of providing complete mixing would be necessary. The possibility exists that mixing could be achieved by using dc fields to produce electro-convection effects which would reduce stratification. The degree of mixing or reduction of stratification which can be achieved by dc fields has not yet been studied.

The fourth curve is found by assuming that liquid is collected off of the tank wall by dielectrophoretic forces and then mixed. It may be possible to adjust ac frequencies low enough to bring about electro-convection effects to reduce stratification, but high enough to retain the propellant on the electrodes. The ac frequency could be increased to provide a completely stable state just prior to restart or venting to ensure completely stable orientation. Collection in this manner would decrease boil-off by a factor of approximately 20.

Either of the two boil-off reduction methods shown will bring about significant weight savings. For example, when liquid is collected off of the tank wall, the boil-off is decreased by a factor of four. Taking into account the effect of heat stored in the vehicle, the total boil-off in 4.5 hours would be 3300 lbs without collection off of the walls. This loss could be decreased to 800 lbs in 4.5 hours by off-wall collection. Assuming a dielectrophoretic system to accomplish this weighs on the order of 400 lbs, a total weight savings of 2100 lbs could be made.

HIGH VOLTAGE PROBLEMS AND CONTROL

Some of the most serious problems associated with a dielectrophoretic system involve the generation and control of the high voltages required for large space vehicle tanks. Voltages on the order of 10^5-10^6 volts are required with large tanks to minimize the system weight. In principle, the electric field intensities required for collection forces on the order of 10^{-3} g could be obtained with low voltages and small separation distances between electrodes. However, the number of electrodes required and the electrode weight would then be prohibitive.

The major problems which arise because of the high voltage requirement are (1) the generation of high ac voltages, and (2) the control of electrical breakdown, especially in oxidizer tanks.

Various high voltage electrostatic generators have been discussed in Reference 8 which appear suitable for a dielectrophoretic system. At this point, the most promising type is a Van de Graaff generator, built by Ion Physics Corp., which supplies 200 μ amperes at 600,000 volts. [14, 15, 16] The generator is approximately 8 inches in diameter and 12 inches in length and can be operated at an ac frequency of 1 cycle/sec with large tanks. Since this frequency is much greater than the

reciprocal of the relaxation time of such propellants as LH_2, LO_2, etc., the device is suitable for advanced space vehicle applications. The power output is orders of magnitude above the resistive power loss in the propellants and the generator weight for a flight application would be on the order of 15-20 lbs. Similar devices can be developed for particular applications. The Van de Graaff generator operated in an ac mode is also suitable from the standpoints of lifetime, structural strength, and reliability.

The electrical breakdown problem is significant for two reasons. First, arcing or electrical breakdown in the tank destroys the electric field and hence the collecting force. Second, arcs in an oxidizer tank striking a metallic surface could cause ignition and destroy the vehicle. Therefore, a dielectrophoretic system must be designed to minimize the occurrence of arcing, and to guarantee that arcs in an oxidizer tank will not initiate combustion of the electrodes or tank walls. Arcing can be eliminated by proper electrode and insulation design, monitoring of the current and the use of suitable voltage safety factors.

In general, the electrodes should be designed such that there are no regions where the electric field intensity is much greater than on the major portion of the electrodes. For instance, with a cylindrical electrode having a hemispherical cap, the field intensity of the cap is much greater than along the length of the cylinder. Therefore, the cap radius should be increased (and joined smoothly to the cylinder) such that the electric field intensity is approximately the same for the entire electrode surface. This maximizes the total electric field energy and collecting force. However, in some applications higher field intensities and hence collecting forces may be

required in certain areas to cause preferential location, as at the bottom of the tank near the pump outlet. In all cases, electrode surfaces should be polished to remove asperities which cause local corona discharge.

Since the dielectric strength of the propellant vapor and pressurizing gas is less than that of the liquid, the electrodes must be designed for voltages well below the gas breakdown voltage. The voltage safety factor (ratio of corona discharge voltage to applied voltage) for breakdown in the gas phase is approximately 3 and 10 for dielectrophoretic systems designed to collect liquid oxygen and liquid hydrogen, respectively, with average forces on the order of 10^{-3}g. The voltage safety factor in the liquid is an order of magnitude higher. Also, in zero gravity, the liquid is collected to the electrode surfaces, where the field intensity is greatest, with forces on the order of 1 g. Therefore, there is an additional safety factor in having the high dielectric strength liquid continuously collected on the electrode surfaces even with very violent disturbing forces caused by attitude control, docking of the vehicle, etc.

The possibility of arcing is also minimized by monitoring the current between electrodes. Because most electrode designs have very highly non-uniform electric fields, corona discharge will occur at electrode surfaces at voltages well below the arcing voltages. Onset of corona discharge can be monitored by measuring the typical exponential current increase, and the voltage can then be automatically lowered below the corona onset voltage. The response time to lower the voltage would be less than the time for a voltage cycle.

Corona discharge or arcing in the fuel tank (such as LH_2) presents no danger since there is no oxidizer present to support combustion. However, in an

oxidizer tank (such as LO_2) the danger of arc-initiated combustion of metallic electrodes is particularly acute. The problem of electrode ignition can be solved by constructing the electrodes of a relatively inert non-combustible dielectric material such as teflon or mylar with a thin film metallic coating sandwiched between the dielectrics. The metallic coating is the conducting surface for the high voltage. The energy of any arcs striking the electrode would be absorbed by the dielectric material. If an arc penetrated the dielectric and ignited the thin film coating, combustion would be prevented because the metallic deposit would be insulated from the oxidizer. Even if the complete metallic coating were to ignite the total energy produced would be negligible because of the small amounts of metal involved.

The possibility of arcs striking the oxidizer tank wall can be minimized by designing the electrodes such that the regions of maximum field intensity are between the electrodes and not between the electrodes and the tank wall. Any arcs which might occur would then pass from one electrode to another, rather than from an electrode to the tank wall. In addition, liquid oxygen tank walls often are internally insulated with materials which are suitable dielectrics and compatible with the liquid oxygen. Arcs which might occur between the electrodes and tank wall would then dissipate energy in penetrating the insulation.

The arcing problem is serious but appears solvable because of the combined solutions of high voltage safety factors, voltage control by corona onset monitoring, and proper electrode design.

CONCLUSIONS

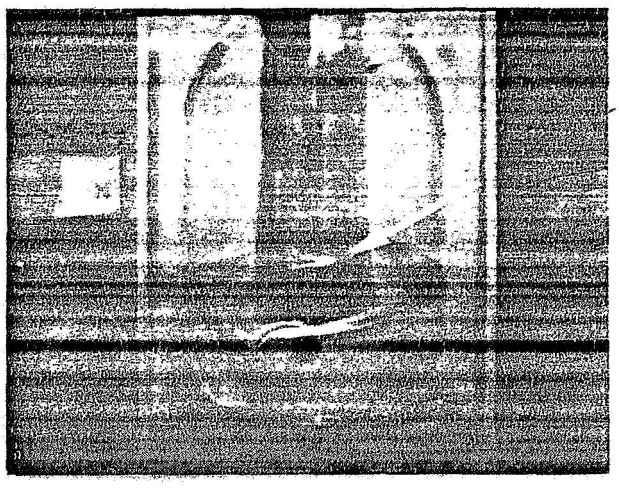
The dielectrophoretic propellant collection system can collect liquid propellant in zero gravity with average forces on the order of 10^{-3} - 10^{-2} g. The system weight and power requirements are low. In addition, the system can be used to decrease propellant boil-off, especially with liquid hydrogen. The system appears most promising for space vehicles requiring five-ten or more engine restarts or ullage gas venting cycles, or for long term storage of cryogenic liquid with minimum boil-off. The generation of the high voltages required for large vehicles is relatively easy to achieve with currently available, light weight Van de Graaff generators. The problem of voltage control and arcing appears solvable.

In view of the advantages offered by a dielectrophoretic system, it is desirable to consider use of this approach in space vehicles and to bear in mind the possible application of the concept in other areas.



1 SECOND ZERO G
CATAPULT TEST SEQUENCE

FIGURE 1



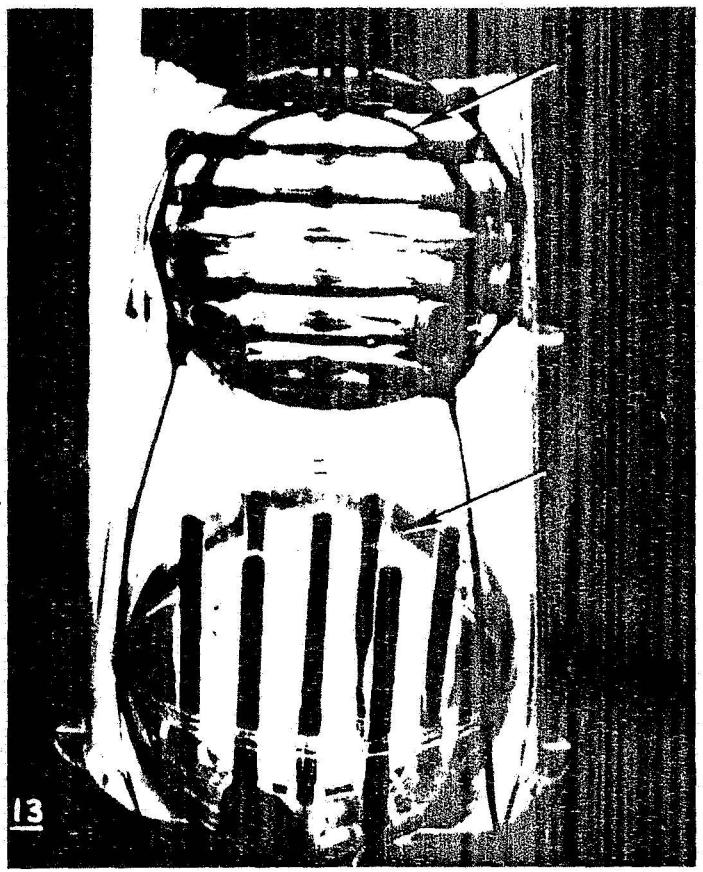
A C COLLECTION V ≈ 10,000 VOLTS

FIGURE 2



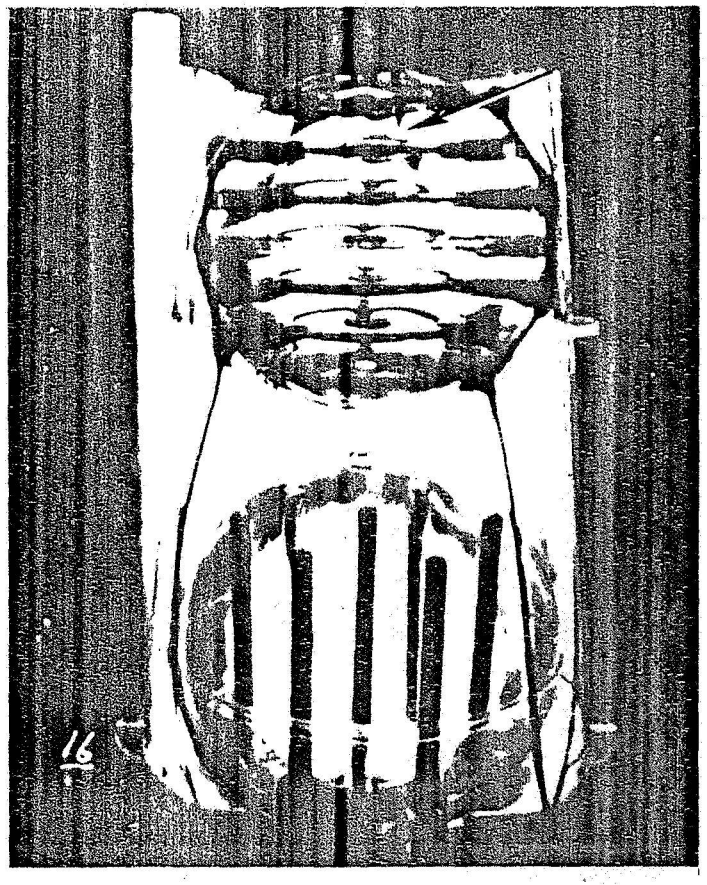
D.C. COLLECTION V ≈ 25,000 VOLTS D.C.

FIGURE 3



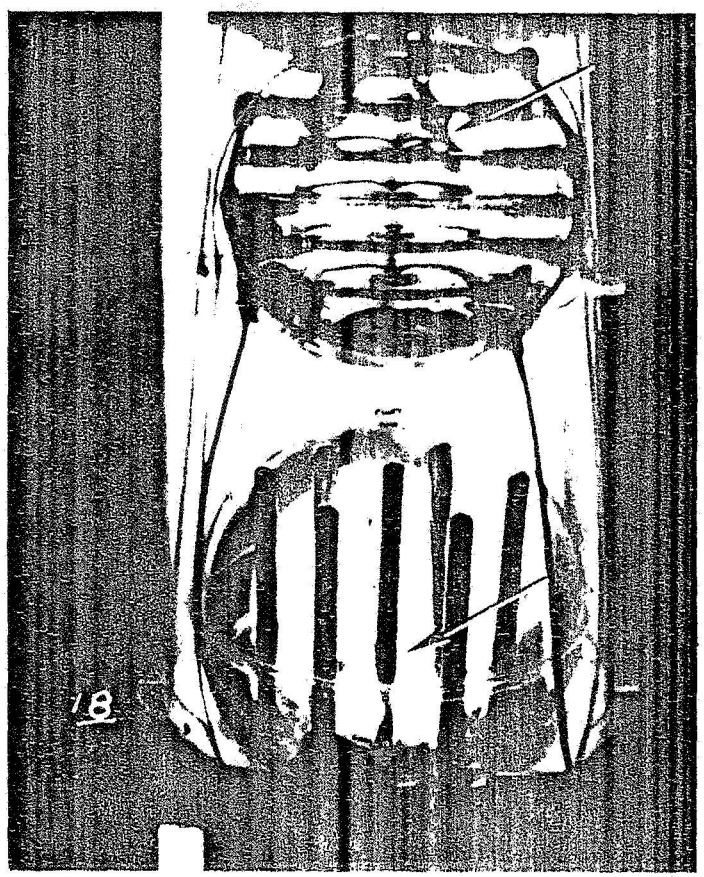
LIQUID SLOSHING TOWARDS BACK OF SPHERES
AWAY FROM CAMERA
NO VOLTAGE APPLIED

FIGURE 4



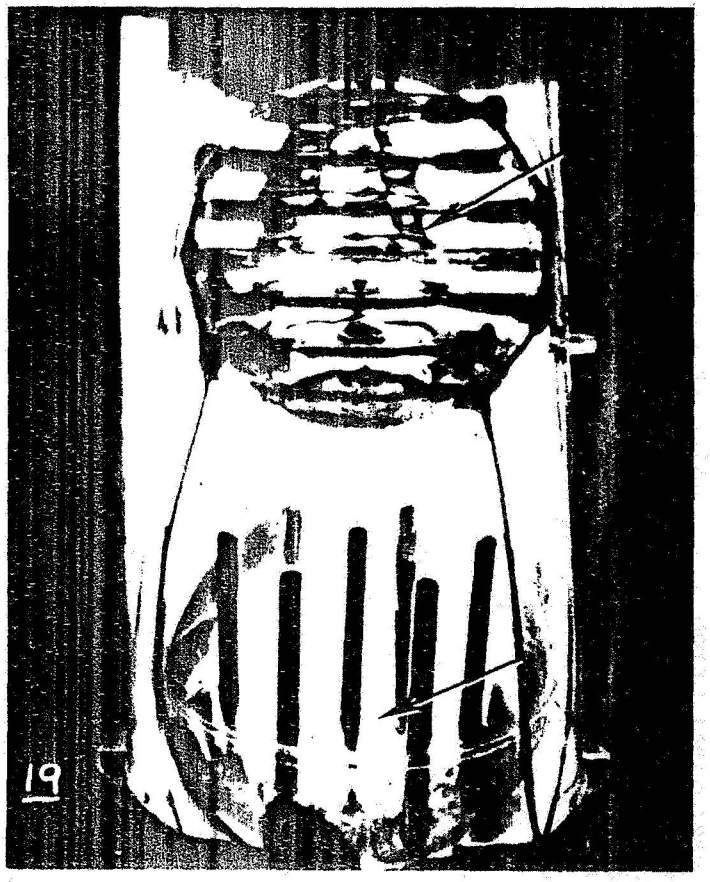
LIQUID COLLECTED IN TOP TWO PAIRS OF DISCS
VOLTAGE LESS THAN 17,000 VOLTS

FIGURE 5



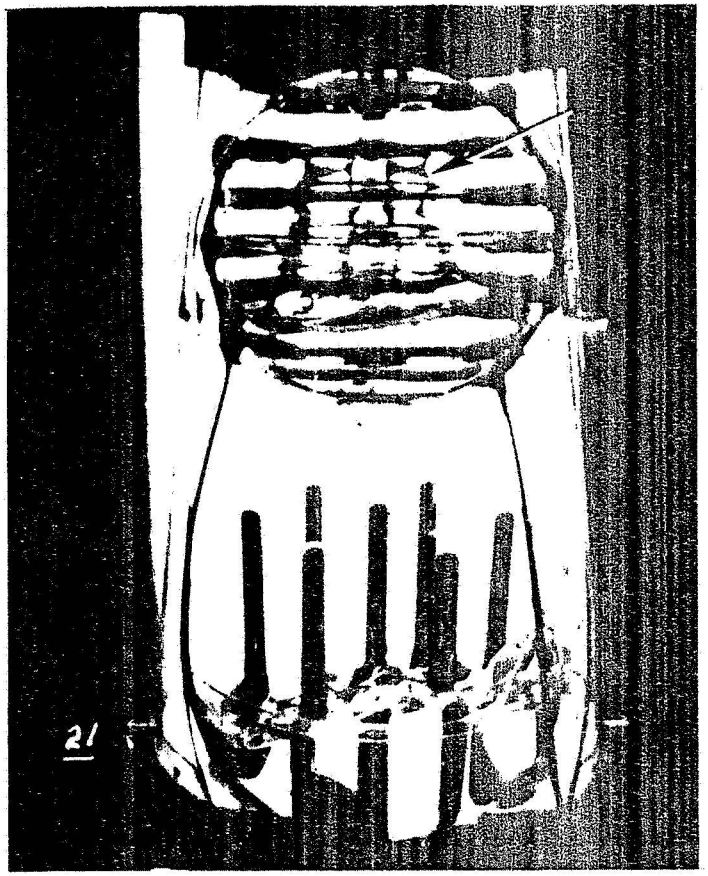
LIQUID COLLECTED BETWEEN TOP THREE PAIRS OF DISCS
LIQUID COLLECTED IN TRUNCATED CONE SHAPES AROUND RODS
17,000 VOLTS

FIGURE 6



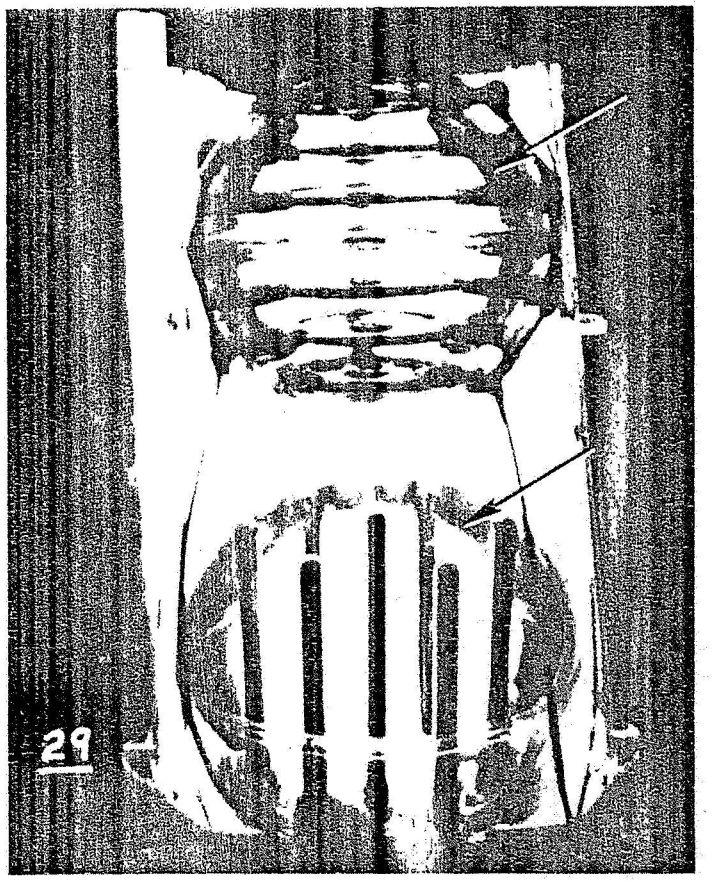
LIQUID COLLECTED BETWEEN TOP FOUR PAIRS OF DISCS
LIQUID COLLECTED IN TRUNCATED CONE SHAPES AROUND RODS
17,000 VOLTS

FIGURE 7



LIQUID IN TOP SPHERE FLOWING DOWN THROUGH
HOLES IN CENTER OF DISCS
17,000 VOLTS APPLIED

FIGURE 8



LIQUID COLECTED ON WALL WITH
NO VOLTAGE APPLIED

FIGURE 9

ELECTRODE CONFIGURATION

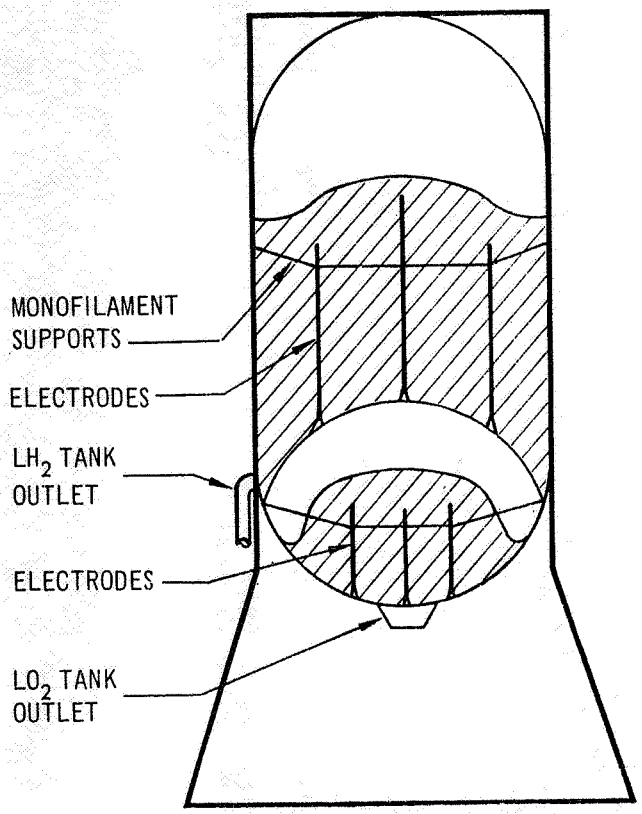


FIGURE 10

PROPELLANT POSITIONING FOR DECREASING BOILOFF LOSS

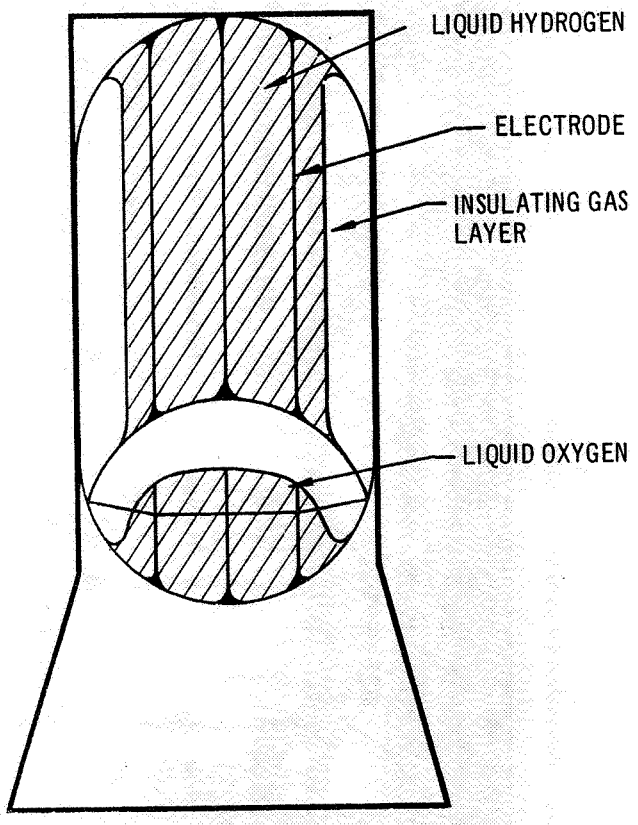


FIGURE 11

M-21023

LH_2 LOST BY BOILOFF ASSUMING ALL HEAT ENTERING TANK VAPORIZES LIQUID

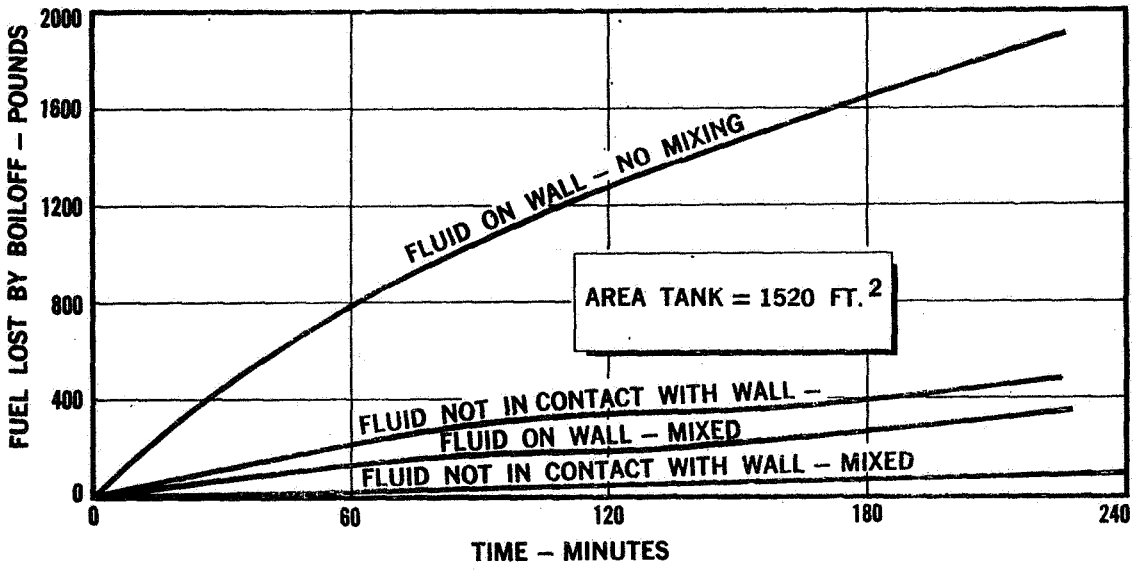


FIGURE 12

NOMENCLATURE

E = Electric Field Intensity $\frac{\text{Volts}}{\text{Meter}}$

F_v = Force per Unit Volume $\frac{\text{Newton}}{\text{Meter}}$

K = Dielectric Constant

P = Pressure $\frac{\text{Newton}}{\text{Meter}^2}$

r_1 = Inner Electrode Radius

r_2 = Outer Electrode Radius

r_3 = Tank radius

ϵ_o = Capacity of Space $\frac{\text{Farads}}{\text{Meter}}$

ρ = Mass Density $\frac{\text{Kilograms}}{\text{Meter}^3}$

ρ_e = Electric Charge Density $\frac{\text{Coulombs}}{\text{Meter}^3}$

σ = Conductivity $\text{ohm}^{-1}\text{m}^{-1}$

α = Surface Tension Dynes/cm or $\frac{\text{Newton}}{\text{Meter}}$

REFERENCES

1. Stratton, J. A., Electromagnetic Theory, McGraw-Hill Book Co., 1941.

2. Pohl, H. A., "Some Effects of Non-Uniform Fields on Dielectrophoresis," J. of Appl. Physics Vol. 29, No. 8, August 1958.

3. Pohl, H. A. and J. P. Schwar, "Factors Affecting Separation of Suspension in Non-Uniform Electric Fields," J. of Appl. Physics Vol. 30, No. 1, January 1959.

4. Pohl, H. A. and C. E. Plymale, "Continuous Separation of Suspensions by Non-Uniform Electric Fields in Liquid Dielectrics," Princeton University Plastics Lab., Technical Report 53B, March 1959.

5. Panofsky, W. K. H., and M. Phillips, Classical Electricity and Magnetism, First Edition, Addison-Wesley Publications, Reading, Mass., 1955.

6. Clodfelter, Robert G., "Fluid Mechanics and Tankage Design for Low Gravity Environment," Tech. Documentary Report No. ASD-TDR-63-506 published by AF Aero-Propulsion Laboratory, AFSC, Wright-Patterson Air Force Base, Ohio, September 1963.

7. Lykoudis, P. S. and C. P. Yu, "The Influence of Electrostrictive Forces in Natural Thermal Convection," Purdue Research Foundation, Project No. 3093, August 1962.

8. Blackmon, J. B., "Collection of Liquid Propellants in Zero Gravity with Electric Fields," Douglas Paper No. 1871, presented at the AIAA First Annual Meeting and Technical Display, Washington D. C., June 29-July 3, 1964.

9. "Zero Gravity Control of Hydrogen and Cesium by Electrical Phenomena," Tech. Documentary Report No. APL-TDR-64-46 published by AF Aero-Propulsion Laboratory, AFSC, Wright-Patterson Air Force Base, Ohio, April 1964.

10. Malkus, W. V. R. and G. Veronis, "Surface Electroconvection," Phys. of Fluids, Vol. 4, No. 1, January, 1961, pp 13-23.

11. Blackmon, J. B., "Dielectrophoretic Propellant Orientation in Zero-Gravity," Douglas Paper No. 1292, presented at the 7th Symposium on Ballistic Missile & Space Technology, Colorado Springs, Colorado, August 13-16, 1962.

12. Blackmon, J. B. and J. F. Crocker, "Experimental Simulation of Propellant Orientation in Zero Gravity with Electrostatic Fields," Douglas Paper No. 1622, presented at AAS 8th Symposium, January 1963, at Los Angeles.

13. Blackmon, J. B., "Propellant Orientation in Zero Gravity with Electric Fields," Douglas Paper No. 1468, presented at IAS 31st Annual Meeting January 1963, New York, N. Y.

14. Denholm, A. S., J. E. Lavelle, F. J. McCoy and C. Coenraads, "Feasibility and Design Study for Electrostatic Generators," Goodrich High Voltage Astronautics, Inc. WADD Tech. Report 61-105, July 1961.

15. McCoy, F. J., C. N. Coenraads and A. S. Denholm, "The Design of Electrostatic Generators for Operation in Space," Goodrich High-Voltage Astronautics, Inc., Papers presented to ARS Space Flight Rpt. to the Nation, New York Coliseum, October 9-15, 1961.

16. Coenraads, C., A. S. Denholm, J. Lavelle and F. McCoy, "Electrostatic Power Generators for Space," ARS Paper presented by Ion Physics Corp., at the Space Power Systems Conf., Sept. 25-28, 1962 in Santa Monica, Calif.

APPROVAL

PROCEEDINGS OF THE CONFERENCE ON PROPELLANT
TANK PRESSURIZATION AND STRATIFICATION
January 20,21, 1965
Volumes I and II

The information in this report has been reviewed for security classification. Review of any information concerning Department of Defense or Atomic Energy Commission programs has been made by the MSFC Security Classification Officer. This report, in its entirety, has been determined to be unclassified.

Max E. Nein

Max E. Nein
Conference Chairman

LIST OF INDUSTRY AND AGENCY ATTENDEES

GOVERNMENT AGENCIES

LOS ALAMOS SCIENTIFIC LABORATORY
Post Office Box 1663
Los Alamos, New Mexico 87544
LIEBENBERG, D. H.

NATIONAL AERONAUTICS AND SPACE ADMINISTRATION
Headquarters
Washington, D. C. 20546
COMPITELLO, FRANK CODE RP

Western Operations Office
Santa Monica, California
WILSON, R. E.

Kennedy Space Center
Huntsville Industrial Center
Huntsville, Alabama
MC CROMBS, W.
MERRIFIELD, D.

Lewis Research Center
21000 Brook Park Road
Cleveland, Ohio 44135.
DEWITT, RICHARD
ELLIOTT, G.
NORED, D. L.
OTTO, E. W.
ROUDEBUSH, W. H.
YEH, FRED

Manned Spacecraft Center
Houston, Texas 77001
CHANDLER, WILLIAM A.
SCOTT, W. R.
SIMKIN, DONALD

NATIONAL BUREAU OF STANDARDS
Boulder Laboratories, Cryogenic Engineering Division
Boulder, Colorado 80301
ARNETT, R. W.
BURGESON, D. A.
MILLHISER, D. R.

INDUSTRIES

ACOUSTICA ASSOCIATES, INC.
5331 West 104th Street
Los Angeles, California 90045
APPLETON,

AEROJET-GENERAL CORPORATION
Department 9620, Building 2019
Post Office Box 1947
Sacramento, California
DEPPE, G.
FLATHERITY, W.
LUEDERITZ, FRANK K.
RANSON, VIC

AIRESEARCH MANUFACTURING DIVISION
Garrett Corporation
9851 Sepulvida Boulevard
Los Angeles, California 9009
LOOS, N. D.
TYLER, J. S.

ARO, INC.
Arnold Air Force Station
Tullahoma, Tennessee 37389
LANDRUM R. G.
SYKES, J. C.
TRIMBLE, M. H.

AUBURN UNIVERSITY
College of Engineering
Auburn, Alabama
TANGER, G. E.
VACHON, R. I.
WHITLEY, H. G.

BEECH AIRCRAFT CORPORATION
Boulder Division
Box 631
Boulder, Colorado 80301
REID, W. H.
ROBINSON,

BELL AEROSYSTEMS
Buffalo, New York
BORASS, STANLEY
PEARSON, W. E.

THE BOEING COMPANY
Post Office Box 1680
Huntsville, Alabama
ALLEN, J.
DOKE, K
FRANKS, H. H. DP-6
GLENN, HOWELL
LESLIE, E.
TORKELSON, B.

Michoud Operations
Post Office Box 26088
New Orleans, Louisiana 70126
BOURASSA, R. J.
DOUGLAS, O. H.
KORNELL, T. J.
MALTHESON, E. R.

BENDIX CORPORATION - PIONEER CENTRAL DIVISION
Post Office Box 508
Davenport, Iowa
CARLSON, WILLIAM
NEWMAN, H.
O'LOUGHLIN, J. R.
UTZ, J. A.
WEBB, D. L.

Post Office Box 3707
Seattle, Washington 98124
FOWLER, J.
LINDOW, C.
ORTON, H.
STRAYER, J.
WHIPPO, H.

BROWN ENGINEERING COMPANY, INC.
300 Sparkman Drive, N. W.
Huntsville, Alabama
BUCKLE, GEORGE
GUINN, G. R.
KNAPINSKE, A. A.
NEUFFER, BRUCE
VOLLO, SAMUEL

THE CHRYSLER CORPORATION-SPACE DIVISION
Post Office Box 857
Huntsville, Alabama 35801
ADAMS, D.
ANDERSON, G. F.
BERRY, J.
GOOLSBY, P. F.
HUETHER, ANN
MC CALLIE, B. G.
MC COMBS, W. M.
OFFIK, W. G.
SCHRENK, A. L.
SNYDER, E. F.
VANN, W.
WRIGHT, W. P.
ZIEMKE, M. C.

Post Office Box 29200
New Orleans, Louisiana 70126
CREWS, C. S.
EHRHARDT, L.
FOX, E.
GREEN, M. Department 2761
LINDEMANN, D.
PISKE, W. E.
WIDOFSKY, BERNARD

CONSOLIDATED SYSTEMS CORPORATION
600 East Bonita
Pomona, California
DAVIES, GEORGE

CURTIS-WRIGHT CORPORATION
Woodridge, New Jersey
BAUGHAN, J.
MC CREA, J.

DOUGLAS AIRCRAFT COMPANY, INC.
Missile and Space Systems Division
300 Ocean Park Boulevard
Santa Monica, California 90405
BLACKMON, J. B.
BURGE, G. W.
CARLSON, C. R.
MC HARRIS, G. A.
NAVICKAS, J.
VAN HORN, P. W.

THE GARRETT CORPORATION
Sahara Office Center
Memorial Parkway, S.
Huntsville, Alabama
STRATTON, ROBERT

GENERAL DYNAMICS/ASTRONAUTICS
Post Office Box 1128
San Diego, California 92112
STARK, JOHN A.
WALBURN, A. B.

GENERAL DYNAMICS/FORT WORTH
Post Office Box 748, Mail Zone E62
Fort Worth, Texas
POTH, L. J.

GENERAL ELECTRIC COMPANY
NSO-ASD
Holiday Office Center
Memorial Parkway, S.
Huntsville, Alabama
SHAW, JOHN.

GIANNINI CONTROLS CORPORATION
2109 West Clinton Avenue
Huntsville, Alabama
GALLAGHER, M. J.

1600 South Mountain Avenue
Duarte, California
GIBSON, A. H. GARRY

GRUMMAN AIRCRAFT ENGINEERING CORPORATION
2109 West Clinton Avenue
Huntsville, Alabama
STEWART, R. J.

Bethpage, L. I., New York 11714
DONNELLY, LAWRENCE A.
FERGUSON, MATT
WALDO, DAN

HEAT TECHNOLOGY LAB
4308 Governors Drive, N. W.
Huntsville, Alabama
DATIS, A.
YOUNGBLOOD, W. W.
USHER, HAROLD

HOFMAN LABORATORIES
6750 Caballero Boulevard
Buena Park, California
CARSE, DAVID B.

INDUSTRIAL NUCLEONICS, INC.
4000 Cherokee Drive, S. E.
Huntsville, Alabama
RUSKIN, W. R.

INDUSTRIAL NUCLEONICS, INC.
605 Ackerman Road
Columbus, Ohio
EVANS, HOWARD

LINDE DIVISION
Union Carbide Company
204 Governors Drive, S. W.
Huntsville, Alabama
LINDQUIST, C. R.

LOCKHEED MISSILES AND SPACE COMPANY
Huntsville Research and Engineering Center
4800 Bradford Boulevard, N. W.
Huntsville, Alabama
WYSOR, ROBERT B.

Post Office Box 504
Sunnyvale, California
BROGAN, J. J.
HARPER, E. Y.
HINES, F. L. Department 5524, Building 102
HURD, S. E. Department 5524, Building 102
LEVY, A. M. Department 5524, Building 102
SATTERLEE, HUGH
SCHALLA, C. A.
VLIET, G. C.

LOCKHEED-GEORGIA COMPANY
Marietta, Georgia 30061
BROWN, W. H.
MOORE, S. B.
TATUM, J. W.

LOCKHEED-CALIFORNIA COMPANY
Box 551
Burbank, California 91503
HIRASAWA, PAUL
WERNER, JERRY

MARTIN COMPANY
Denver Division
Post Office Box 179
Denver, Colorado 80201
FEARN, R. F.
KENNY, RICHARD J. A-130
MC GREW, J. L.
MOSSMAN, EMMETT
MUTH, WAYNE A-130
NEFF, B. D. A-153
PEDREYRA, D. C. A-153

Middle River
Baltimore, Maryland 21203
BUNA, TIBOR
GRAY, WILLIAM A.

THE MARQUARDT CORPORATION
16555 Saticoy Street
Van Nuys, California
SEDGEWICK, THOMAS A.

UNIVERSITY OF MICHIGAN
Department of Mechanical Engineering
Ann Arbor, Michigan
BARAKAT, HUSSEIN Z.
CLARK, JOHN A.

MINNEAPOLIS-HONEYWELL REGULATOR COMPANY
2600 Ridgeway Road
Minneapolis, Minnesota
EXON, JOHN

MISSISSIPPI STATE UNIVERSITY
College of Engineering, Aerophysics Department
Post Office Box 248
State College, Mississippi 39762
BISHOP, E. H.
BOUCHILLON, C. W.
CARLEY, C. T.
FORBES, R. E.

MISSISSIPPI STATE UNIVERSITY (CONTINUED)
HORNER, H. C.
HOUGH, E. W.
MC CAIN, WILLIAM D.
THOMPSON, JOE F., JR.

NORTH AMERICAN AVIATION, INC.
Los Angeles Division
International Airport
Los Angeles, California 90045
KIMMEL, C. C.

OPERATIONS RESEARCH, INC.
225 Santa Monica Boulevard
Santa Monica, California
KRANE, ROBERT J.
WENDORF, GENE

PRATT AND WHITNEY AIRCRAFT DIVISION
United Aircraft Corporation
Florida Research and Development Center
West Palm Beach, Florida 33401
KARRAH, WILEY

ROCKETDYNE DIVISION
North American Aviation, Inc.
6333 Canoga Avenue
Canoga Park, California 91304
ABSALOM, J. G.
BELL, G. S.
BENDERSKY, CHARLES
BOWERS, W. M.
GEORGIUS, H. K.
GOLDSTEIN, S. M.

ROCKET RESEARCH CORPORATION
520 South Portland Street
Seattle, Washington 98108
MC CULLOUGH, FOY

SPACE AND INFORMATION SYSTEMS DIVISION
North American Aviation, Inc.
12214 Lakewood Boulevard
Downey, California 90214
ABSHIER, DORSEY
ANDERSON, J.
ANDERSON, RICHARD E. GB 54, Building 305
GLASSER, SIDNEY BB28, 595-511
HUZEL, DEITER
ISENBERG, LON
KRAFT, L.
LISTON, J.
ROBERTSON, ROBERT G. 595-511
WILLIAMS, K.

SPACE CRAFT, INC.
Astran Division
8310 Whitesburg Drive, S.
Huntsville, Alabama
MOMENTHY, ALBERT M.
WYBRANOWSKI, EDWARDS

TRW SPACE TECHNOLOGY LABORATORIES
One Space Park
Redondo Beach, California 90277
ELIZALDE, J. C.

DISTRIBUTION

DIR	Dr. von Braun
DEP-T	Dr. Rees
EX-DIR	Mr. Maus
I-DIR	Colonel O'Connor
I-SE-CH	Dr. Mrazek
I-I/IB-DIR	Colonel James
I-I/IB-S-IVB	Mr. McDaris
I-V-DIR	Dr. Rudolph
I-V-S-IVB	Mr. Hammer
I-E-DIR	Mr. Belew
R-DIR	Mr. Weidner
R-FP	Dr. Koelle
R-AERO-DIR	Dr. Geissler
R-ASTR-DIR	Dr. Haeussermann
R-COMP-DIR	Dr. Hoelzer
R-ME-DIR	Mr. Kuers
R-PR-DIR	Dr. Stuhlinger
R-QUAL-DIR	Mr. Grau
R-TEST-DIR	Mr. Heimburg
R-TEST-C	Mr. Halbrooks
R-TEST-CTM	Mr. Wise
	Mr. Stone
R-TEST-ID	Mr. Schulzer
	Mr. Lackner
R-TEST-IS	Mr. McNabb
R-TEST-SB	Mr. Reilmann
R-P&VE-DIR	Mr. Cline
R-P&VE-A	Mr. Goerner
R-P&VE-ANP	Mr. Priest
R-P&VE-AUA	Mr. Hethcoat
R-P&VE-XI	Mr. Faulkner
R-P&VE-V	Mr. Aberg
R-P&VE-M	Dr. Lucas
R-P&VE-S	Mr. Kroll
R-P&VE-P	Mr. Paul
	Mr. McCool
	Mr. Isbell
	Mr. Kuberg
(6)	Mr. Neuffer
R-P&VE-PA	Mr. Thomson
R-P&VE-PAS	Mr. Cox
	Mr. Patefield
R-P&VE-PT	Mr. Wood
	Mr. Connell
(2)	Mr. Nein
	Mr. Hargis
	Mr. Stokes
R-P&VE-PTD	Mr. Barnett

R-P&VE-PM	Mr. Fuhrmann
R-P&VE-PMD	Mr. Haas
	Mr. Schaffranke
R-P&VE-PMP	Mr. Edwards
	Mr. L. Smith
R-P&VE-PP	Mr. Heusinger
R-P&VE-PPE	Mr. Gross
R-P&VE-PE	Dr. Head
	Mr. Bergeler
R-P&VE-PEC	Mr. Dickson
	Mr. Campbell
	Mr. Fritz
	Mr. Appleberry
	Mr. Ponder
R-P&VE-PEM	Mr. Mann
	Mr. Nicholson
R-P&VE-PR (30)	Mr. Eby
R-P&VE-RT	Mr. Hofues
V	Dr. Gruene
LO-DF	Mr. von Tiesenhousen
MS-IP	
MS-IPL (8)	
MS-H	
All Conference Attendees (169)	